REGULATORY ROLE OF APLNR SIGNALING IN MIGRATION AND DIFFERENTIATION OF MESODERM TISSUE AND MESENCHYMAL STEM CELLS

by
Hatice Burcu Şişli

Submitted to Graduate School of Natural and Applied Sciences
in Partial Fulfillment of the Requirements
for the Degree of Doctor of Philosophy in
Biotechnology

Yeditepe University
2023

REGULATORY ROLE OF APLNR SIGNALING IN MIGRATION AND DIFFERENTIATION OF MESODERM TISSUE AND MESENCHYMAL STEM CELLS

APPROVED BY:

Assoc. Prof. Dr. Ayşegül Doğan ……
(Thesis Supervisor)
(Yeditepe University)

Prof. Dr. Ahmet Arman ……
(Marmara University)

Prof. Dr. Fikrettin Şahin ……
(Yeditepe University)

Prof. Dr. Ömer Faruk Bayrak ……
(Yeditepe University)

Assist. Prof. Dr. Zeynep Büşra Bolat ……
(University of Health Sciences)

DATE OF APPROVAL: ..../..../20..

I hereby declare that this thesis is my own work and that all information in this thesis has been obtained and presented in accordance with academic rules and ethical conduct. I have fully cited and referenced all material and results as required by these rules and conduct, and this thesis study does not contain any plagiarism. If any material used in the thesis requires copyright, the necessary permissions have been obtained. No material from this thesis has been used for the award of another degree.

I accept all kinds of legal liability that may arise in case contrary to these situations.

Name, Last name	Hatice Burcu Şişli
Signature	…….

ACKNOWLEDGEMENTS

This study was funded by TÜBİTAK 2232 International Fellowship for Outstanding Researchers Program (Project No:118C186). The study was also supported by Yeditepe University.

It is with immense gratitude that I acknowledge the support and help of my supervisor Assoc. Prof. Dr. Ayşegül Doğan. Pursuing my thesis under her supervision has been an experience that broadens the mind and presents an unlimited source of learning. I would like to express my gratitude to my jury members Prof. Dr. Fikrettin Şahin, Prof. Dr. Ahmet ARMAN, Prof. Dr. Ömer Faruk Bayrak and Assist. Prof. Dr. Zeynep Büşra Bolat for their patience during qualifier exam and thesis process. I am also grateful to my colleagues; Selinay Şenkal, Ezgi Bulut and Taha Bartu Hayal, for their help and support during the experiments of the thesis.

Finally, many thanks to my friends, Zeynep İşlek, Ezgi Taşkan, Binnur Kıratlı and Başak Şentürk, and my family members, Asiye Şişli, Halit Yaşar Şişli, Burçin Şişli and Lucky Şişli (my cat), for their immense support, love and patience.

ABSTRACT

REGULATORY ROLE OF APLNR SIGNALING IN MIGRATION AND DIFFERENTIATION OF MESODERM TISSUE AND MESENCHYMAL STEM CELLS

Embryonic morphogenesis is the most complicated cell movement event that is controlled by individual or mass form of cell migration during gastrulation of the embryo. Establishment and maintenance of the cell populations during gastrulation movements in response to cell-to-cell contact and signaling molecules is not only crucial for determination of body plan and tissue patterning but also required for generation of progenitor populations for adult tissue regeneration. Embryonic stem cells (ESCs) as pluripotent stem cells are the most appropriate model to recapitulate early embryonic development, gastrulation and adult tissue morphogenesis of humans. Embryoid bodies (EBs) as ESC aggregates in suspension culture construct a regionalized tissue patterning that is displaying gastrulation and organized germ layer structure and gene expression patterning of germ layers *in vitro*. Wnt signaling pathway is the fundamental regulatory pathway which triggers the morphogenetic events and initiates the gastrulation movements resulting in germ layer formation. Apelin receptor (Aplnr) has been identified as a novel Wnt target gene during hindgut differentiation of ESCs. However, the molecular mechanism and the regulatory role of Aplnr in cell migration and differentiation process in development and adult remain unclear. The main objective of my thesis project is to understand regulatory role of Aplnr signaling in cell migration and differentiation process of mesoderm tissue and mesenchymal stem cells (MSCs), which are very important for gastrulation movements, tissue specification and cell fate decision in adult tissue morphogenesis and adult tissue regeneration. The study was conducted using mouse ESC (mESC) and human ESC (hESC) lines. Peptide and small molecule induced Aplnr signaling activation as well as genetic modifications were applied to activate or inactivate the Aplnr pathway. Overexpression of Aplnr signaling pathway components was provided by 3rd generation lentiviral vector system for hESCs. CRISPR/Cas9 gene editing technique was used to knockout Aplnr pathway components in mESCs and hESCs. siRNA and shRNA strategies were utilized to downregulate Aplnr signaling pathway genes. These genetically modified ESCs were used to form EBs as three dimensional gastruloid models which were used to track cellular movements under the

control of Aplnr signaling and cell fate decision during three germ layers specification. Migration and differentiation of mesodermal population into MSCs were conducted by differentiation experiments. Those cell populations were subjected to gene and protein expression analyses, including antibody array, LC/MS, mRNA and miRNA sequencing, to analyze molecular regulatory pathways. Morphological changes as well as gene and protein expression data revealed that Aplnr signaling promote mesoderm commitment possibly via EGFR, FGF and TGF-beta signaling pathways and enhances migration of ESCs-derived EBs during mesoderm differentiation. Antibody array and LC/MS protein profiling data of mESC-derived mesoderm cells demonstrated that Apelin-13 treatment enhanced cell cycle, EGFR, FGF, Wnt and Integrin signaling pathway proteins. Moreover, Aplnr signaling positively regulates MSCs differentiation from ESCs and increases cell viability, proliferation, survival, MSC characteristics and differentiation capacity of MSCs by regulating various pathways, such as EGFR, TGF-beta, Wnt, PDGF and FGF signaling pathways. Osteogenic, chondrogenic, adipogenic, odontogenic, endothelial and myogenic differentiations were significantly enhanced with Aplnr signaling activity. So, this study also lays an important foundation to generate high potential MSCs from ESCs to be used in personalized cell therapy.

ÖZET

APLNR SİNYALİNİN MESODERM DOKU VE MEZENKİMAL KÖK HÜCRE FARKLILAŞMASINDAKİ VE MİGRASYONUNDAKİ DÜZENLEYİCİ ROLÜ

Embriyonik morfogenez, embriyonun gastrulasyonu sırasında bireysel veya toplu hücre migrasyonu tarafından kontrol edilen en karmaşık hücre hareketi olayıdır. Hücreden hücreye temas ve sinyal moleküllerine yanıt olarak gastrulasyon hareketleri sırasında hücre popülasyonlarının oluşturulması ve sürdürülmesi, yalnızca vücut planının ve doku modelinin belirlenmesi için değil, aynı zamanda yetişkin doku rejenerasyonu için progenitör popülasyonların oluşturulması için de gereklidir. Pluripotent kök hücreler olarak embriyonik kök hücreler (ESC'ler), insanların erken embriyonik gelişimini, gastrulasyonunu ve yetişkin doku morfogenezini özetlemek için en uygun modeldir. Süspansiyon kültüründeki ESC agregaları olarak embriyoid cisimcikleri (EB'ler), gastrulasyon ve organize germ tabakası yapısı ve germ tabakalarının *in vitro* gen anlatımı paternini gösteren bölgeselleştirilmiş bir doku paternini oluşturur. Wnt sinyal yolağı, morfogenetik olayları tetikleyen ve germ tabakası oluşumuyla sonuçlanan gastrulasyon hareketlerini başlatan temel düzenleyici yolaktır. Apelin reseptörü (Aplnr), ESC'lerin arka bağırsak farklılaşması sırasında yeni bir Wnt hedef geni olarak tanımlanmıştır. Bununla birlikte, Aplnr'nin moleküler mekanizması ve gelişim ve yetişkinlikte hücre göçü ve farklılaşma sürecindeki düzenleyici rolü belirsizliğini koruyor. Tez projemin temel amacı, gastrulasyon hareketleri, doku spesifikasyonu ve hücre kaderi kararı için çok önemli olan mezoderm dokusu ve mezenkimal kök hücrelerin (MSC'lerin) hücre göçü ve farklılaşma sürecinde Aplnr sinyalinin düzenleyici rolünü anlamaktır. yetişkin doku morfogenezinde ve yetişkin doku rejenerasyonunda. Çalışma, fare ESC (mESC) ve insan ESC (hESC) hatları kullanılarak gerçekleştirildi. Aplnr yolunu etkinleştirmek veya etkisiz hale getirmek için peptid ve küçük molekül kaynaklı Aplnr sinyal aktivasyonunun yanı sıra genetik modifikasyonlar uygulandı. Aplnr sinyal yolu bileşenlerinin aşırı gen ifadeleri hESC'ler için 3. nesil lentiviral vektör sistemi tarafından sağlandı. mESC ve hESC'lerinde Aplnr yolu bileşenlerini devre dışı bırakmak için CRISPR/Cas9 gen düzenleme tekniği kullanıldı. Aplnr sinyal yolu genlerini baskılamak için siRNA ve shRNA stratejileri kullanıldı. Genetiği değiştirilmiş bu ESC'ler, üç germ tabakası spesifikasyonu sırasında Aplnr sinyalinin kontrolü ve hücre kaderi kararı altındaki hücresel hareketleri izlemek için kullanılan üç boyutlu gastruloid modeller olan EBleri oluşturmak için kullanıldı. Mezodermal popülasyonun göçü ve MSC'lere farklılaşması, farklılaşma deneyleri ile gerçekleştirildi. Bu hücre popülasyonları, moleküler

düzenleyici yolakları analiz etmek için antikor dizisi, LC/MS, mRNA ve miRNA sekanslamaları dahil olmak üzere gen ve protein ekspresyon analizlerine tabi tutuldu. Morfolojik değişikliklerin yanı sıra gen ve protein ekspresyon verileri, Aplnr sinyalinin, muhtemelen EGFR, FGF ve TGF-beta sinyal yolakları yoluyla mezoderm taahhüdünü desteklediğini ve mezoderm farklılaşması sırasında ESC'lerden türetilen EB'lerin göçünü arttırdığını ortaya koydu. mESC'den türetilen mezoderm hücrelerinin antikor dizisi ve LC/MS protein profilleme verileri, Apelin-13 uygulamasının hücre döngüsü, EGFR, FGF, Wnt ve Integrin sinyal yolu proteinlerini arttırdığını gösterdi. Ayrıca, Aplnr sinyali, MSC'lerin ESC'lerden farklılaşmasını pozitif olarak düzenler ve EGFR, TGF-beta, Wnt, PDGF ve FGF sinyal yolları gibi çeşitli yolakları düzenleyerek MSC'lerin hücre canlılığını, çoğalmasını, hayatta kalmasını, MSC özelliklerini ve farklılaşma kapasitelerini artırır. Osteojenik, kondrojenik, adipojenik, odontojenik, endotel ve miyojenik farklılaşmalar Aplnr sinyal aktivitesi ile önemli ölçüde arttırıldı. Dolayısıyla, bu çalışma aynı zamanda kişiselleştirilmiş hücre tedavisinde kullanılmak üzere ESC'lerden yüksek potansiyelli MSC'ler üretmek için önemli bir temel oluşturmaktadır.

TABLE OF CONTENTS

ACKNOWLEDGEMENTS iv

ABSTRACT v

ÖZET vii

LIST OF FIGURES xiii

LIST OF TABLES xviii

LIST OF SYMBOLS/ABBREVIATIONS xx

1. INTRODUCTION 1

1.1. CELL THERAPY 1

1.2. EPIDEMIOLOGY OF CELL BASED THERAPY 2

1.3. FORMATION OF THREE GERM LAYER BY GASTRULATION 2

1.4. MESODERM 4

1.5. MOLECULAR PATHWAYS IN MESODERM DEVELOPMENT 5

1.6. PROTOCOLS FOR EMBRYONIC STEM CELLS AND MESODERM DIFFERENTIATION 6

1.7. DEVELOPMENT OF MSCS FROM PLURIPOTENT STEM CELLS 8

1.8. APELIN RECEPTOR 9

1.9. APELIN RECEPTOR IN DEVELOPMENT 11

1.10. APELIN RECEPTOR SINALING IN MSCS 12

1.11. AIM 13

2. MATERIALS AND METHODS 14

2.1. MOUSE ESC-DERIVED MESODERM AND MSCS 14

2.1.1. Cell Culture 14

2.1.2. Preparation of Culture Well Plates 14

2.1.3. Preparation of Small Molecule and Peptide ……..……14
2.1.4. Activation of Aplnr ……15
2.1.5. Generation of CRISPR/Cas9 KO Cell Lines ……15
2.1.6. Inhibition of Aplnr Activity ……...17
2.1.6.1. siRNA ……..17
2.1.6.2. shRNA ……17
2.1.7. Migration and Differentiation Protocol of Mesoderm and MSCs ……18
2.1.8. Live Cell Imaging ……..19
2.1.9. Immunofluorescence (IF) Analysis ……19
2.1.10. Gene Expression Analysis ……20
2.1.11. Antibody Array ……..22
2.1.12. Liquid Chromotography Mass Spectrometry (LC-MS) Analysis ……..……22
2.1.13. Characterization of MSCs ……..……23
2.1.13.1. Surface Marker Analysis ……...……...……...23
2.1.13.2. Trilineage Differentiation ……...……23
2.1.13.3. Differentiation Staining ……..……..23
2.1.13.4. Cell Viability Assay ……..……..24
2.1.13.5. Cell Doubling Analysis ……...……24
2.1.14. Statistical Analysis ……24
2.2. HUMAN ESC-DERIVED MESODERM AND MSCS ……..……..25
2.2.1. Cell Culture ……25
2.2.2. Preparation of Culture Well Plates for Migration……...25
2.2.3. Preparation of Small Molecule and Peptide ……...25
2.2.4. Activation of Aplnr……26
2.2.5. Generation of CRISPR/Cas9 KO Cell Lines ……..26
2.2.6. Inhibition of Aplnr Activity ……27
2.2.6.1. siRNA ……..27
2.2.6.2. shRNA ……27
2.2.7. Migration and Differentiation Protocol of Mesoderm and MSCs ……..28
2.2.8. Live Cell Imaging ……...29
2.2.9. Antibody Array ……...29
2.2.10. Characterization of MSCs ……..……43
2.2.10.1. Differentiation of MSCs ……..…….....43

2.2.10.2. Surface Marker Analysis …….……45
2.2.10.3. Staining Analysis ……48
2.2.11. Immunofluorescence (IF) Analysis ..……...48
2.2.12. Quantitative Real Time PCR (qPCR) Analysis ……...49
2.2.13. Cell Viability Assay ……..……50
2.2.14. Cell Doubling Analysis ……..……51
2.2.15. Liquid Chromotography Mas Spectrometry (LC-MS) Analysis …….51
2.2.16. RNA Sequencing Analysis ……..…….....51
2.2.17. Statistical Analysis ……...……..52
3. RESULTS 53

3.1. EFFECT OF APLNR SIGNALING ON MESODERM AND MSC DIFFERENTIATION OF MOUSE ESCS.....53
3.1.1. Aplnr Signaling Improves Migration Potential of EBs During Mesoderm Differentiation…….53
3.1.2. Selection of Mesoderm Differentiation Media to Generate Aplnr Positive and Aplnr Negative Cells……...61
3.1.3. Activation of Aplnr Enhances Paraxial Mesoderm Differentiation of mESCs…….....63
3.1.4. Suppression of Aplnr Signaling Activity Hinders Mesoderm Differentiation of mESCs.……...……76
3.1.5. Effect of Aplnr Signaling Activity on Protein Profile of mESC-derived Mesoderm Cells ..……92
3.1.6. Aplnr Signaling Acts on MSC differentiation of mESC-derived Mesoderm Cells ……97

3.2. EFFECT OF APLNR SIGNALING ON MESODERM AND MSC DIFFERENTIATION OF HUMAN ESCS……106
3.2.1. Activation of Aplnr Signaling Enhances Cell Migration during Mesoderm Differentiation……...……106
3.2.2. Activation of Aplnr Signaling Promotes Mesoderm Commitment of hESC-derived EBs ……...114
3.2.3. Aplnr Signaling Activity Enhances MSC Differentiation from hESC-derived mesoderm progenitors ...……...134

3.2.4. Aplnr Signaling is Require for Modulation of Migration Rate During Mesoderm Differentiation and Cell Survival During MSC Differentiation of hESC-derived EBs ...……...…..241
4. DISCUSSION……..... 244
4.1. MOUSE ESC-DERIVED MESODERM AND MSCS…….....244
4.2. HUMAN ESC-DERIVED MESODERM AND MSCS……...247
5. CONCLUSION ……..…. 251

REFERENCES 252

LIST OF FIGURES

Figure 1.1. Derivation of three germ layers, namely endoderm, mesoderm and ectoderm, to contribute formation of different tissues and organs 4

Figure 1.2. Molecular mechanism of Aplnr signaling……..10

Figure 2.1. Design of CRISPR/Cas9 constructs.....16

Figure 3.1. Effect of knocking out Apelin, Aplnr and Elabela on migration of EBs during mesoderm differentiation of mESCs…….56

Figure 3.2. Effect of shRNA and siRNA mediated silencing of Aplnr signaling on migration of EBs during mesoderm differentiation of mESCs……..59

Figure 3.3. Effect of medium ingredients on Aplnr expression and migration of mESCs-derived EBs during mesoderm differentiation……..62

Figure 3.4. Effect of Aplnr signaling on mesoderm differentiation of mESCs…….65

Figure 3.5. Antibody array profile of mESC derived EBs treated with Apelin-13……66

Figure 3.6. Effect of silencing Aplnr signaling components, via shRNA delivery on mesoderm commitment of mESC-derived EBs during mesoderm differentiation……78

Figure 3.7. Antibody array profile of mESC derived EBs when Aplnr was silenced…….79

Figure 3.8. Effect of silencing Aplnr signaling components, via siRNA delivery on mesoderm commitment of mESC-derived EBs during mesoderm differentiation……88

Figure 3.9. Effect of CRISPR-Cas9 mediated KO of Aplnr signaling components on mesoderm commitment of mESC-derived EBs during mesoderm differentiation...…….91

Figure 3.10. Protein profile of mESC derived EBs treated with Apelin-13. …….93

Figure 3.11. Optimization of MSC differentiation protocol from mESCs…….98

Figure 3.12. Optimization of Apelin-13 addition to the MSC differentiation media..…….100

Figure 3.13. Effect of Aplnr activity on MSC differentiation from mESCs……101

Figure 3.14. Effect of shRNA mediated silencing of Aplnr signaling components on MSC differentiation of R1 cells……...102

Figure 3.15. Effect of siRNA mediated silencing of Aplnr signaling components on MSC differentiation of R1 cells……...103

Figure 3.16. Effect of CRISPR-Cas9 mediated KO of Aplnr signaling components on MSC differentiation of R1 cells……...105

Figure 3.17. Effect of Aplnr signaling on migration of EBs during mesoderm differentiation of hESCs…….107

Figure 3.18. Effect of activation of Aplnr by Apelin-13 and ML233 on migration of EBs during mesoderm differentiation of hESCs……109

Figure 3.19. Effect of CRISPR-Cas9 mediated KO of Aplnr Signaling Components on migration of EBs during mesoderm differentiation of hESCs……110

Figure 3.20. Effect of silencing Aplnr signaling by Apelin siRNA and Aplnr siRNA on migration of EBs during mesoderm differentiation of hESCs…….112

Figure 3.21. Effect of overexpressing Aplnr signaling components on migration of EBs during mesoderm differentiation of hESCs…….113

Figure 3.22. Effect of Aplnr activity on mesoderm differentiation of hESCs……117

Figure 3.23. Antibody array analysis of hESC derived EBs treated with Apelin-13……118

Figure 3.24. Effect of activation of Aplnr by Apelin-13 and ML233 on mesoderm differentiation of hESCs…….119

Figure 3.25. Differential expression analysis for mRNA seq and small RNA seq analyses of hESC derived mesodermal cells in the presence of Apelin-13 at day 6……..120

Figure 3.26. Differential expression analysis for mRNA seq analysis of hESC derived mesodermal cells in the presence of Apelin-13 at day 6..…….....121

Figure 3.27. miRNA seq analysis of hESC derived mesodermal cells in the presence of Apelin-13 at day 6……...122

Figure 3.28. Functional enrichment analysis of significantly upregulated miRNAs in Apelin-13 treated mesoderm cells…….....123

Figure 3.29. Functional enrichment analysis of significantly downregulated miRNAs in Apelin-13 treated mesoderm cells……...124

Figure 3.30. Protein profile of hESC derived EBs treated with Apelin-13……..125

Figure 3.31. Effect of downregulation of Aplnr signaling components on mesoderm differentiation of hESCs. ……...129

Figure 3.32. Effect of shRNA mediated downregulation of Aplnr signaling components on mesoderm differentiation of hESCs. ……..130

Figure 3.33. Effect of CRISPR-Cas9 mediated knock out of Aplnr signaling components on mesoderm differentiation of hESCs. ……..……131

Figure 3.34. Effect of siRNA mediated downregulation of Aplnr signaling components on mesoderm differentiation of hESCs. ..……132

Figure 3.35. Effect of overexpression of Aplnr signaling components on mesoderm differentiation of hESCs……..…….……..133

Figure 3.36. Aplnr activity supports MSC differentiation from hESCs. ……137

Figure 3.37. Optimization of Apelin-13 administration during MSC differentiation of hESCs.……....138

Figure 3.38. Characterization of hESC derived MSCs in the presence of Apelin-13……...139

Figure 3.39. Differentiation of hESC derived MSCs and characterized MSCs into multiple cell types in the presence of Apelin-13……..……140

Figure 3.40. Morphology of multiple cell type differentiation from MSC and hESC derived MSCs ...…….……141

Figure 3.41. Differential expression analysis for mRNA seq of DPSC and hESC derived MSCs…….……142

Figure 3.42. Differential expression analysis for mRNA seq of hESC-derived MSCs and DPSC…….…….143

Figure 3.43. Differential expression analysis for mRNA seq of hESC-derived MSCs, in the presence of Apelin-13, and DPSCs. ……..144

Figure 3.44. Protein profile of hESC derived MSCs treated with Apelin-13…….145

Figure 3.45. Knock out of Aplnr signaling components hinders MSC differentiation from hESCs……...…….191

Figure 3.46. Characterization of hESC derived MSCs when Aplnr signaling pathway components were knocked out…...…….……192

Figure 3.47. Differentiation of hESC derived MSCs into ostegenic, adipogenic, chondrogenic and odontogenic cell types when Aplnr signaling pathway components were knocked out……...…..……193

Figure 3.48. Differentiation of hESC derived MSCs into epithelial, endothelial, myogenic and neurogenic cell types when Aplnr signaling pathway components were knocked out…….……..194

Figure 3.49. Morphology of multiple cell type differentiation from hESC derived MSCs when Aplnr signaling pathway components were knocked out…….195

Figure 3.50. Knock down of Aplnr signaling components by shRNA hinders MSC differentiation from hESCs. ……...……198

Figure 3.51. Characterization of hESC derived MSCs when Aplnr signaling pathway components were knocked down via shRNA……..……...199

Figure 3.52. Differentiation of hESC derived MSCs into multiple cell types when Aplnr signaling pathway components were knocked down via shRNA…….……...200

Figure 3.53. Morphology of multiple cell type differentiation from hESC derived MSCs when Aplnr signaling pathway components were knocked down via shRNA……...201

Figure 3.54. Gene expression verification of multiple differentiation from hESC-derived MSCs when Aplnr signaling components were overexpressed or silenced via shRNA…..202

Figure 3.55. Protein profile of hESC derived MSCs when Aplnr components were silenced by shRNA…..…….……204

Figure 3.56. Silencing Aplnr signaling components by siRNA treatment hinders MSC differentiation from hESCs…….230

Figure 3.57. Characterization of hESC derived MSCs when Aplnr signaling pathway components were silenced via siRNA...……..231

Figure 3.58. Differentiation of hESC derived MSCs into multiple cell types when Aplnr signaling pathway components were silenced via siRNA…….……..232

Figure 3.59. Morphology of multiple cell type differentiation from hESC derived MSCs when Aplnr signaling pathway components were silenced via siRNA……..…….234

Figure 3.60. Overexpression of Aplnr signaling components enhances MSC differentiation from hESCs…….……236

Figure 3.61. Characterization of hESC derived MSCs when Aplnr signaling pathway components were overexpressed…….……...237

Figure 3.62. Differentiation of hESC derived MSCs into ostegenic, adipogenic, chondrogenic and odontogenic cell types when Aplnr signaling pathway components were overexpressed…….…….……...238

Figure 3.63. Differentiation of hESC derived MSCs into epithelial, endothelial, myogenic and neurogenic cell types when Aplnr signaling pathway components were overexpressed…….…….……...239

Figure 3.64. Morphology of multiple cell type differentiation from hESC derived MSCs when Aplnr signaling pathway components were overexpressed……...……240

Figure 3.65. Selection of high and low Aplnr positive populations and their effect on migration of hESCs-derived EBs during mesoderm differentiation……242

Figure 3.66. Reducing Aplnr expression in hESC via media formulation caused loss of viability during MSC differentiation..…….243

LIST OF TABLES

Table 2.1. gRNAs for generation of mouse CRISPR/Cas9 KO cell lines. 17

Table 2.2. Antibody list for mESC-derived mesoderm and MSCs……..……..19

Table 2.3. List of primers for qPCR analysis of mESC-derived cells. 21

Table 2.4. gRNAs for generation of human CRISPR/Cas9 KO cell lines……..27

Table 2.5. Protein list screened by human antibody array for control group and Apelin-13 treated group at day 6……...29

Table 2.6. Media supplements for differentiation of MSCs……..44

Table 2.7. Antibody list for hESC derived mesoderm and MSCs……46

Table 2.8. Primer list for qPCR analysis of hESC-derived cells. DSPP: Dentinsialophospho protein, α-sma: α-Smooth muscle actin……49

Table 3.1. Protein list screened by antibody array for Control and Apelin-13 treated groups at day 6. Significantly increased (red) and decreased (black) proteins in Apelin-13 treated group compared to control group were highlighted on the table.....67

Table 3.2. Protein list screened by antibody array for shControl and shAplnr groups at day 6. Significantly increased (red) and decreased (black) proteins in shAplnr group compared to shControl group were highlighted on the table.....80

Table 3.3. Protein profiling data of day 6 mesoderm cells, differentiated from R1 mESCs. Apelin-13 was added to the media between day 3 and day 6. Significantly increased (red) and decreased (black) proteins in Apelin-13 treated group compared to control group were highlighted on the table……94

Table 3.4. Protein profiling data of control group and Apelin-13 treated group at day 6. Apelin-13 was added to the media between day 2 and day 6. Significantly increased (red) and decreased (black) proteins in Apelin-13 treated group compared to control group were listed on the table……126

Table 3.5. Protein profiling data of DPSC, Control MSC and Apelin-13 MSC groups at day 24. Significantly increased and decreased proteins in Control MSC compared to DPSC (increased: red, decreased: black) and Apelin MSC compared to Control MSC (increased: red, decreased: black) were listed on the table…….146

Table 3.6. Protein profiling data of shControl MSC, shApelin MSC and shAplnr MSC groups at day 24. Significantly increased and decreased proteins in shApelin MSC compared to shControl MSC (increased: red, decreased: blue) and shAplnr MSC compared to shControl MSC (increased: pink, decreased: purple) were listed on the table…….206

LIST OF SYMBOLS/ABBREVIATIONS

Aplnr	Apelin receptor
BMP4	Bone Morphogenic Protein 4
Bra	Brachyury
EB	Embryoid bodies
Ela	Elabela
EMT	Epithelial to Mesenchymal Transition
EpiSC	Epiblast Stem Cells
Erk	Extracellular signal regulated kinase
ESCs	Embryonic Stem Cells
G	Guanine nucleotide binding
hESCs	human Embryonic Stem Cells
HSCs	Hematopoietic Stem Cells
iPSCs	induced Pluripotent Stem Cells
mESCs	mouse Embryonic Stem Cells
MSCs	Mesenchymal Stem Cells
JAK	Janus Kinase
Klf4	Krueppel-like factor 4
LIF	Leukemia Inhibitory Factor
MEF	Mouse Embryonic Fibroblast
Oct4	Octamer-binding transcription factor 4
PSCs	Pluripotent Stem Cells
PSM	Presomitic Mesoderm
Sox2	Sex determining region Y box 2
STAT3	Signal Transducer and Activator of Transcription 3
TFs	Transcription Factors
TGFβ	Transforming Growth Factor beta

INTRODUCTION

1.1. CELL THERAPY

Discovery of stem cell, with the potential of self-renewal and differentiation capacity, made it a worthy candidate of cell-based therapies for a wide range of diseases. Stem cells can be obtained from four different sources, which are listed as embryonic tissues, fetal tissues, adult tissues and somatic cells via reprogramming [1]. Unlimited self-renewal and differentiation capacity of pluripotent stem cells (PSCs) into the cells derived from all three germ layers, endoderm, mesoderm and ectoderm, marked them as the most promising candidate for stem cell-based therapies [2]. Embryonic Stem Cells (ESCs) are the most common PSCs isolated from inner cell mass of blastocysts in human and mouse. Although they provide a source for cell-based therapies with their unlimited differentiation capacity, their use has always caused ethical conflicts [3–6]. Yamanaka and Takahashi overcame this ethical limitation by inducing expression of four transcription factors (TFs), Octamer-binding transcription factor 4 (Oct4), Krueppel-like factor 4 (Klf4), Sex determining region Y box 2 (Sox2) and c-myc, in adult somatic cells to reprogram pluripotent state for the first time [7,8]. However, these induced pluripotent stem cells (iPSCs) had higher teratoma formation rate than ESCs [9,10]. These concerns can be overcome with both ethical and safer alternatives, adult stem cells, for stem cell-based therapies. Adult stem cells, also called as postnatal stem cells, can be obtained from nearly all along the body, yet have relatively limited differentiation and proliferation capacity compared to pluripotent stem cells. They are used as an emergency cell source by the body to maintain integrity of tissue, to regenerate, to restore damaged tissue, etc. [11].

Mesenchymal stem cells (MSCs), which can be obtained easily, hold a high growth capacity and a multi-lineage differentiation potential to adipose, bone, cartilage and connective tissues [12–14]. Although these properties make them considered as a promising tool for clinical applications, there are still abundance of issues need to be addressed. Some of which are limited differentiation capacity, efficient delivery system, management of optimal growth and conditions for differentiation and heterogeneity of the population [15,16]. Hematopoietic stem cells (HSCs) is another adult stem cell, which is the best characterized

multipotent stem cell isolated from bone marrow and possess ability to differentiate blood cells aside from self-renewal properties [17].

1.2. EPIDEMIOLOGY OF CELL BASED THERAPY

Stem cells have always been a popular target to be manipulated for therapeutic approaches due to their pluripotency and self-renewal properties. Owing to emergence of gene editing and reprograming technologies, utilization of stem cells has finally found its potential in cell therapy for tissue regeneration and disease treatment. Previously we reported that while HSCs, 47.23 percent, and MSCs, 44.26 percent, are prioritized in clinical use of stem cell therapy, use of PSCs in clinical trials are insufficient according to data obtained from Clinical Trials webpage of U.S. National Institute of Health. The data indicates that only 1.16 percent of stem cells used in clinal trials are consist of iPSCs and 2.32 percent of the stem cells consist of ESCs, while the remaining 2.84 percent and 2.19 percent are neural stem cells and limbal stem cells, respectively. Moreover, the data revealed that clinical stem cells and PSC therapies are primarily performed in U.S., which is followed by China and Germany for stem cell therapies and by China and France for PSC therapies [18]. Considering the limited number of clinical research in the field of stem cell therapy, there is an urgent need to overcome challenges for therapeutic use of PSCs. Understanding the molecular mechanism in cell fate decision of mesodermal cell population, stem cell migration and developmental origin of MSCs might aid to surpass the limitations and enable generation of fully specified cells from PSCs for clinical applications of cell therapy and regenerative medicine.

1.3. FORMATION OF THREE GERM LAYER BY GASTRULATION

During mammalian embryonic development, gastrulation, which gives rise to the three germ layers, in terms of ectoderm, mesoderm and endoderm, through migration of cells, is counted as the main determinant of lineage specification and early cell fate decision [19]. Gastrulation begins with primitive streak formation, which is a transient structure formed at the caudal part of the epiblast layer [20,21]. At primitive streak, epiblast cells, which undergo epithelial to mesenchymal transition (EMT), migrate towards the primitive groove and

replace the hypoblast cells to form endoderm cells. The cells migrated to the space between hypoblast and epiblast give rise to mesoderm cells, that spread laterally as a layer, and the epiblast cells on the surface form ectoderm layer [22–24].

Various subpopulations of lineage progenitors are induced at the different parts of primitive streak at specified times [25,26]. At the stage of neurulation, ectoderm give rise to surface ectoderm and neuroectoderm, which is further subdivided to neural tube and neural crest. Surface ectoderm differentiates to tissues found on the body surface, such as nail, teeth enamel, eye lens, hair, epidermis, and external glands including mammary and cutaneous glands. Neural crest cells contribute to formation of cranial and sensory ganglia and nerves, pigment cells, head mesenchyme and connective tissue, while neural tube forms retina, central nervous system, pituitary gland and pineal body [27] (Figure 1.1). Some of endoderm precursors that draw apart from inner cell mass form visceral endoderm which contribute to formation of extra-embryonic tissues and gut tube, definitive endoderm, on the other hand, constitute epithelial lining of gastrointestinal tract, thyroid and parathyroid glands and several organs [27–30] (Figure 1.1). Subpopulations of mesoderm include chordamesoderm, lateral mesoderm, intermediate mesoderm, paraxial mesoderm and head mesenchyme [31]. Notochord is originated from Chordamesoderm, while head mesenchyme forms the skull. Mesoderm cells located at the cranial region make the cardiogenic mesoderm [32]. Mesoderm cells settled at the sides of notochord are the source of paraxial mesoderm, which differentiates to axial skeleton, somites and dermis. Mesoderm cells next to paraxial mesoderm give rise to intermediate mesoderm, which forms genital and urinary system [33]. Lateral mesoderm differentiates into extra embryonic mesoderm, somatic mesoderm and splanchnic mesoderm, which gives rise to myocardium, hemangioblast and mesenchyme [32] (Figure 1.1).

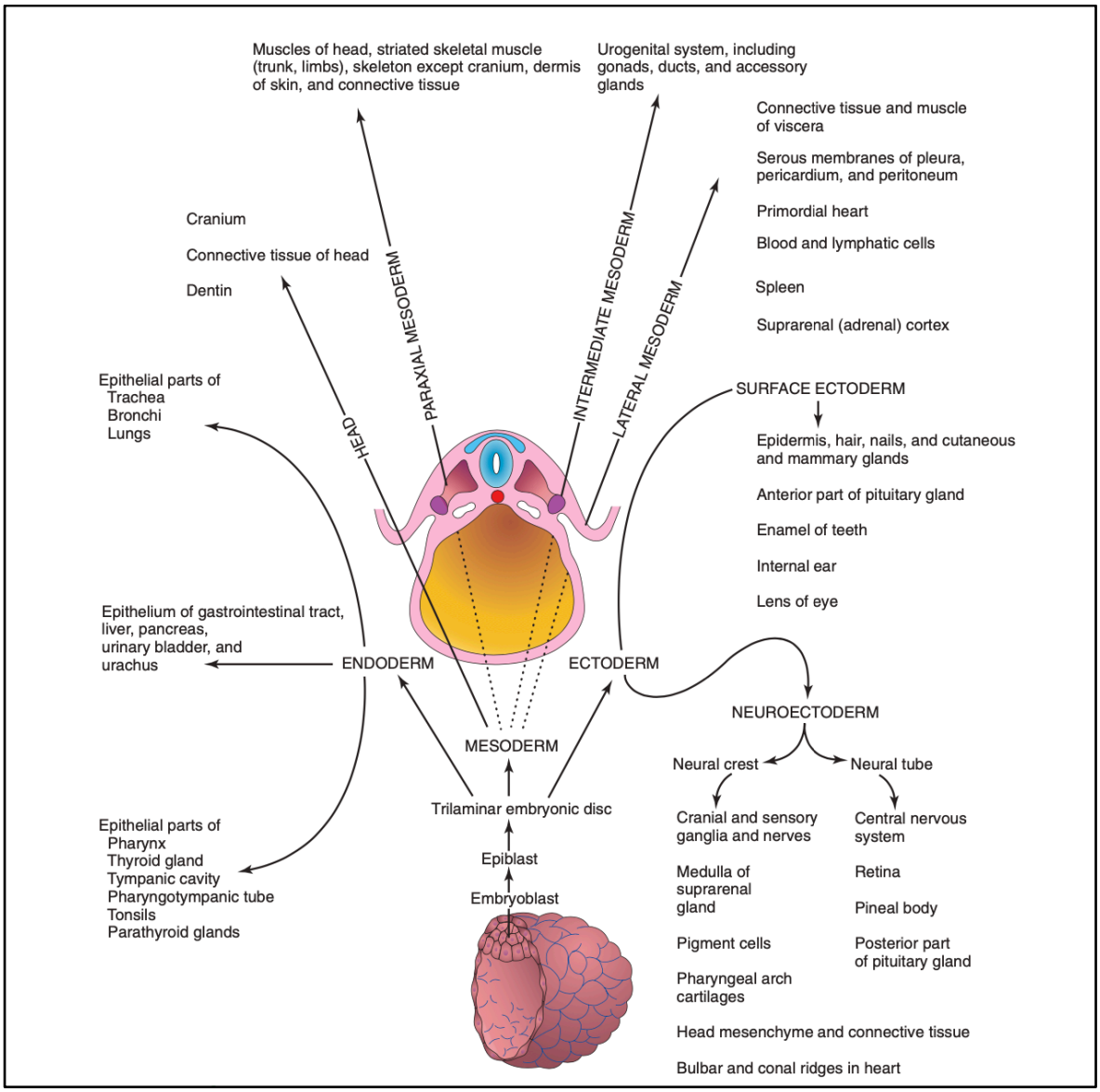


Figure 1.1. Derivation of three germ layers, namely endoderm, mesoderm and ectoderm, to contribute formation of different tissues and organs [27].

1.4. MESODERM

Mesoderm layer emanates upon migration of epiblast cells, which underwent EMT by loosening adherent junctions due to down regulation of E-cadherin expression, to primitive groove to form a new layer between the epiblast and visceral endoderm. Formation of mesoderm requires BMP signaling, Nodal/SMAD2 and SMAD3 signalings and Wnt signaling in epiblast [34–36]. First, the mesoderm subpopulation, patterned under the regulation of BMP4, at the posterior end makes up extraembryonic mesoderm tissues, such

as visceral yolk sac mesoderm, chorion and allantois [34,37,38]. After that, intermediate mesoderm emerges and followed by formation of paraxial mesoderm, cardiac mesoderm and lateral mesoderm. Lastly, midline axial mesoderm tissue arises from the epiblast cells at the most anterior end of primitive streak and give rise to notochord, prechordal plate and definitive endoderm [29,34].

After gastrulation reaches the end, organogenesis takes the rise. The three germ layers, endoderm, mesoderm and ectoderm, generate specific tissues. The tissues and systems originate from ectoderm cells are mainly consist of central nervous system, peripheral nervous system, cornea and epidermis [39,40]. Endoderm cells arise to form internal organs, such as liver, bladder, and pancreas, epithelial lining of gastrointestinal tract and respiratory system, and glands, such as thyroid and parathyroid glands [41]. The tissues of mesodermal lineage are connective tissue, smooth muscle cells, mesenchymal stem cells, skeleton, bone marrow cells, blood cells and cardiovascular system [42]. Since the major source of MSCs, which has a great potential at cell-based therapies, are mesoderm cells, it is crucial to understand the signaling pathways involving mesoderm differentiation from pluripotent stem cells and MSCs differentiation.

1.5. MOLECULAR PATHWAYS IN MESODERM DEVELOPMENT

Initiation of primitive streak in mouse and human embryos is conducted by Wnt/B-catenin signaling, transforming growth factor beta (TGFβ)/Activin/Nodal signaling and bone morphogenic protein 4 (BMP4)/SMAD signaling [24,34,43,44]. As a major player and initiator of primitive streak, Brachyury (Bra) gene expression is essential for migration of the cells towards the primitive streak to give rise to mesoderm cells [45]. Bra expression regulates Wnt signaling pathway [46]. TGFβ/Activin/Nodal signaling controls the expression of primitive streak lineage genes including Mix1, Lhx1, Cripto (Tdgf1), Foxh1 and Eomes, which are necessary for a proper EMT process and so the formation of primitive streak [47].

According to the previous researches, Wnt/B-catenin signaling, TGFβ/Activin/Nodal signaling, FGF signaling and BMP signaling work together for induction of mesoderm [48,49]. Wnt/B-catenin signaling pathway is crucial for formation of mesoderm. It induces expression of genes related to mesoderm fate [50]. Bra is not only involved in primitive

streak formation but also is necessary for generation of mesoderm [51–53]. Wnt signaling and FGF signaling target Bra, which controls mesoderm development by inducing TBX6 [54–56]. It was also reported that interaction between Bra and effectors of TGFβ/Activin/Nodal signaling and BMP4/SMAD signaling indicated the importance of Bra expression in mesoderm differentiation [57]. BMP4 was reported another important player for differentiation to mesoderm [36,38]. During the differentiation induced by BMP4/activin, the cell fate decision between mesoderm and extra embryonic lineages is regulated by FGF2, whose presence directs cells to mesodermal fate marked by expression of Bra gene [58–60]. Furthermore, FGF2 acts in cooperation with BMP4 and interferes with the differentiation to endoderm [59].

1.6. PROTOCOLS FOR EMBRYONIC STEM CELLS AND MESODERM DIFFERENTIATION

Differentiation of pluripotent stem cells can be performed on three main systems, which are monolayer differentiation, co-culture-based differentiation and embryoid bodies (EB)-based differentiation. Monolayer differentiation is simplified system, executing differentiation of adherent hPSCs to the desired lineage through differentiation media supplemented with specific factors. Differentiation based on co-culture system takes advantage of the feeder cells that secrete the specific factors needed for differentiation of hPSCs to the lineage of interest. However, using feeder layer hinders our control over the differentiation process and cell fate. EB-based differentiation system involves differentiation of three-dimensional assembly of hPSCs as a suspension culture to the germ lineages to mimic embryogenesis [6,61,62].

Various signaling pathways in human and mouse regulate Sox2, Nanog, Oct4 in nucleus to maintain pluripotency and self-renewal properties of stem cells. In mESCs, pluripotency is preserved at naïve state by four major signaling pathways including Leukemia inhibitory factor (LIF)/Janus Kinase (JAK)/Signal transducer and activator of transcription 3 (STAT3) pathway, BMP4/SMAD pathway, FGF4/Extracellular signal regulated kinase (Erk) pathway and Wnt/b-Catenin pathway. JAK/STAT3 pathway is activated upon LIF binding to its receptor, LIFR, and subsequent activation of Klf4 regulates expression of Oct4 to maintain pluripotency. In hESCs, primed state of pluripotency is maintained by FGF2/ERK pathway,

TGFβ/Activin/Nodal pathway, IGF2/PI3K/AKT pathway, Wnt/b-Catenin pathway and BMP4/SMAD pathway [2]. It was also reported that keeping the balance of the signaling between mesoendodermal lineage and neural lineage is required to maintain pluripotency [63].

In vitro cell culture, researchers take great advantage of small molecules to maintain pluripotency properties [64] of pluripotent stem cells, to promote their proliferation [65,66] and differentiation [67,68]. As a Wnt pathway activator by inhibiting glycogen synthase kinase 3 beta (GSK3β) and so preventing degradation of B-catenin, CHIR99021 is used to maintain self-renewal properties of PSCs [69] and their differentiation [70]. CHIR99021 was also reported to direct pluripotent stem cells to mesoderm lineage differentiation by activating Wnt signaling pathway, indicating its role in fate decision at early embryogenesis [71,72].

In literature, abundance of protocols has been developed to induce differentiation of pluripotent stem cells to mesoderm. One of the methods demonstrated presomitic mesoderm (PSM) differentiation of mESCs via Epiblast Stem Cells (EpiSCs) [73]. The protocol involves the activation of Wnt signaling using CHIR99021, which inhibits GSK3β, and various concentration of FGF2 ligand, which can determine the PSM cell state. Low concentration of FGF led to formation of anterior PSM, while its high concentration generated posterior PSM. Furthermore, they demonstrated that Activin/Nodal signaling interferes with PSM differentiation induced by CHIR99021 in EpiSCs, but not affects Bra expression. However, inhibition of Activin/ Nodal led to enhanced induction of PSM through Wnt signaling and FGF signaling. The protocol proceeds as following; mouse ESCs (mESCs) maintained on mitotically inactivated mouse embryonic fibroblast (MEF) cells in ESC medium supplemented with LIF were transferred to fibronectin coated plates and were cultured in ESC medium supplemented LIF, 1uM PD0325901 and 3uM CHIR99021. The EBs, brought to the naïve pluripotent state at day2, were cultured with EpiSC medium, which is composed of N2B27 medium supplemented with 20ng/ml Activin A and 10ng/ml FGF2, for 3 days to express EpiSC markers. Then, the EpiSCs were maintained in N2B27 medium supplemented with 3uM CHIR99021 and different concentrations (0/10/250 ng/ml) of FGF2 to induce PSM [73]. Another study demonstrated mesodermal differentiation of hESCs. hESCs were cultured overnight in mTESR1 medium, supplemented with 1uM thiazovivin, on wells coated with Geltrex. Then, differentiation of hESCs to anterior primitive streak, to

give rise to paraxial mesoderm, was induced by 4uM CHIR99021, 20ng/ml FGF2, 30ng/ml Activin and 100nM PIK90 for 24 hours. Also, differentiation of hESCs to mid primitive streak, to develop downstream lateral mesoderm, was directed by 6uM CHIR99021, 20ng/ml FGF2, 30ng/ml Activin and 40ng/ml BMP4 for 24 hours. Next day, paraxial mesoderm differentiation of anterior primitive streak cells was induced by 3uM CHIR99021, 20ng/ml FGF2, 1uM A8301 and 250nM LDN193189 for a day. For lateral mesoderm differentiation of mid primitive streak cells were provided by 30ng/ml BMP4, 1uM A8301 and 1uM C59 for a day [74].

There are also methods directing differentiation of pluripotent stem cells to MSCs. According to one of the protocols, human ESCs (hESCs) colonies cultured on MEF feeder cell layer, which was inactivated mitotically, were transferred to plates coated with Matrigel and cultured in mTESR1 medium [75–77] supplemented with 10uM GSK126, which is a small molecule inhibitor of EZH2 methyl transferase epigenetic modifier acting on hESCs, for 3 days. Then, the cells were detached to make single cell suspension and cultured for 5 more days to proceed further differentiation. The article also stated that GSK126 enhanced mesodermal marker expressions, including Bra, Msx1, Gata4, Foxf1 and KDR, and downregulated TUBB3 ectoderm marker gene expression and Sox17 endoderm marker gene expression. In addition, with multiple other analysis, they demonstrated the inhibitory role of EZH2 in mesoderm lineage commitment [77].

1.7. DEVELOPMENT OF MSCS FROM PLURIPOTENT STEM CELLS

Mesenchymal tissue is an embryonic connective tissue, derived basically from mesoderm layer and migrate through the embryo during embryonic development. Hence, MSCs can be obtained from tissues derived from mesoderm during embryonic development [78,79]. However, ontogenesis of MSCs can’t be clearly stated and the origin sets the function of MSCs in adult body. There are also reports relating MSCs to ectoderm-derived cells [78,80]. It was reported two types of MSC population in bone marrow of mouse embryo. No nestin expression and high proliferation are characteristics of mesoderm-derived MSCs, which contribute to skeleton formation, while nestin expressing but nondividing neural crest-derived MSCs contribute to formation of not bone but hematopoietic cell niche [78,81].

MSCs can be isolated from various sources, including bone marrow, dental pulp, adipose tissue, placenta, umbilical cord [78,82–86]. However, MSCs acquired from fetal origin exhibit higher proliferation and later senescence compared to MSCs isolated from adult tissue [78,87]. Also, bone marrow derived MSCs have higher self-renewal and stemness, which were supported by greater colony formation capacity and Sox2 gene expression [78,88].

In the last decade, researches were focused on derivation of MSCs from PSCs. The first attempt in 2005 demonstrated that MSCs can also be obtained from PSCs *in vitro*. They co-cultured hESCs with murine OP9 stromal cells, and finally CD73+ sorted cells were revealed to attain the expression of some MSCs marker genes [89]. Later, Stavropoulos et al. obtained MSCs from PSCs by using insulin transferrin selenite for hESCs culture [90]. By the time, hESCs, cultured with medium supplemented with bFGF and FBS and detached with trypsin during passages, were also demonstrated to differentiate to MSCs [91]. Compared to these methods with random differentiation signals, recently more specified methods with specific inhibitors or growth factors were used to differentiate PSCs to MSCs. One of the methods required preparation of a medium, supplemented with N2 and B27 neural stem cell supplements and Y-27632 inhibitor, to differentiate PSCs to MSCs [92,93].

1.8. APELIN RECEPTOR

Discovery of Apelin receptor (Aplnr), which is a guanine nucleotide binding (G) protein coupled receptor consisting of 377 amino acids, was made in 1993 for the first time and until the identification of its ligand, the receptor was regarded as an orphan G protein coupled receptor [94]. The first ligand of Aplnr, namely Apelin, was isolated from bovine stomach extract and identified in 1998 [95]. This peptide, endogenously binding to Aplnr, was reported to consist of 77 amino acids as a prepropeptide with a signal peptide at the N-terminal. The preproapelin produce active apelin, including 36 amino acids apelin (apelin-36), 17 amino acids apelin (apelin-17) and 13 amino acids apelin (apelin-13), which is the most active apelin among 46 characterized apelin isoforms [95,96]. Apelin expression was detected in a broad range of organs including nervous system, heart, kidney, lung, gastrointestinal system, placenta and adipose tissue [97–105].

In 2013, another endogenous ligand of Aplnr, called Elabela (Ela) or Apela or Toddler, was identified in human as a circulated peptide hormone. The peptide consists of 54 amino acid with its signal peptide and generates functionally active 32 amino acid Elabela (Ela-32), 21 amino acid Elabela (Ela-21) and 11 amino acid Elabela (Ela-11) [106,107]. Ela was reported to be expressed in kidney, prostate and pluripotent stem cells [106,108]. The studies also revealed that Ela is highly expressed in late blastula and gastrulation and later its expression becomes limited to notochord, mesoderm and endoderm [107].

Apelin/Aplnr signaling involves in various physiological events, such as angiogenesis, fluid homeostasis, cardiovascular system regulation, energy metabolism and myocardial contractility [109–118]. Aplnr defective mice embryo was demonstrated to lack in vascular development which caused lethality of the embryo [119]. Recently, Apelin/Aplnr signaling was shown to regulate development of early placenta by inducing cell proliferation of trophoblast through ERK, STAT3, APJ and AMPK signaling [103]. Ela/Aplnr signaling is also involved in crucial biological events such as placental angiogenesis [120,121]. In zebrafish model system, Ela/Aplnr signaling was demonstrated to regulate development of heart and vasculature [106,108]. It was also reported to take part in mESCs renewal [122,123]. Another study reported that gastrulation movements are promoted by Ela/Aplnr signaling in zebrafish [107].

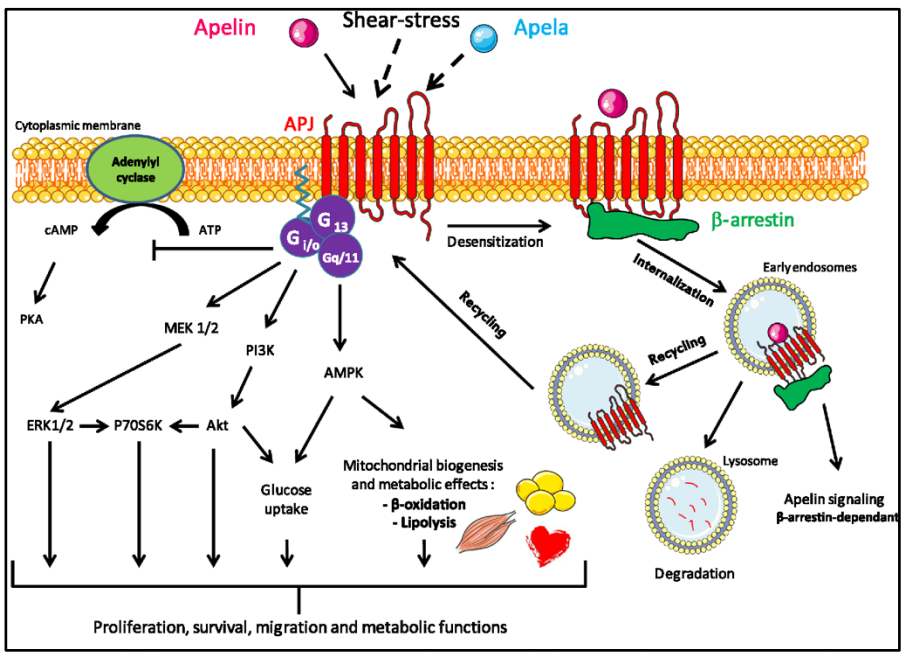


Figure 1.2. Molecular mechanism of Aplnr signaling [124].

Aplnr activation shows its effect mainly through PI3K/AKT and MAPK/ERK pathways [115]. Upon activation of Aplnr by Apelin, Akt and Erk are activated while PKA is inactivated due to cAMP suppression [125,126]. Ela also activates Aplnr, which leads to inhibition of cAMP production and phosphorylation and action of Erk1/2 [108]. Recently, Aplnr expression was revealed to be targeted by Wnt signaling pathway during differentiation of ESCs to hindgut [127].

1.9. APELIN RECEPTOR IN DEVELOPMENT

During mouse embryogenesis, transcription of Apelin was reported to initiate at gastrulation stage, which made Apelin one of the earliest expressed peptide hormones [128]. Besides, Aplnr defective mouse embryo was demonstrated to lack in vascular development which caused lethality of the embryo [119]. Another study reported that gastrulation movements are promoted by Ela/Aplnr signaling in zebrafish [107]. In addition, during zebrafish gastrulation, mesodermal cell migration was reported to be promoted by Aplnr signaling, under the regulation of Nodal signaling, and endodermal cell migration was also reported to be affected indirectly by Aplnr signaling [129]. In literature, role of Aplnr in germ layer specification and mesoderm cell fate determination showed that Aplnr signaling regulates the cardiac development and hematopoiesis. Apelin deficient or overexpressing zebrafish embryos failed to form normal cardiac morphology and gastrulation indicating the role Apelin/Aplnr axis in gastrulation and cardiac mesoderm specification [130]. Supporting this data, in zebrafish model system, Ela/Aplnr signaling was demonstrated to regulate development of heart and vasculature [106,108]. Loss of Aplnr disrupted the Nodal/TGFβ pathway which is required for cardiac development, and interrupted cardiac progenitor development in zebrafish [131]. Molecular mechanism of cardiac progenitor specification has been studied in mouse ES cells and demonstrated the control of Aplnr signaling under the Cripto pathway for cardiac cell specification [128]. In addition to cardiac progenitor specification, hematopoiesis of anterior mesendoderm cell population is regulated by Apelin/Aplnr signaling. Aplnr signaling positively regulated the hematopoietic and endothelial growth and differentiation of human ES cell derived hemangioblast populations [132].

Aplnr expression was revealed to be targeted by Wnt signaling pathway during differentiation of ESCs to hindgut [85,127]. Furthermore, recently, Apelin/Aplnr signaling was shown to regulate development of early placenta by inducing cell proliferation of trophoblast through ERK, STAT3, APJ and AMPK signaling [103].

1.10. APELIN RECEPTOR SIGNALING IN MSCS

Utilization of stem cells for cell-based therapy became one of the major purposes of regenerative medicine. Stem cells have been used for treatment of various diseases and conditions, such as Parkinson's Disease, Muscular degeneration, cartilage defect and heart failure [133–135]. MSCs, which have high growth capacity and multi-lineage differentiation potential into mesoderm-derived cells, such as adipocytes, osteoblasts and chondrocytes [12,13,136], are preferred as a safer and ethical option compared to PSCs. Availability, absence of ethical constraints, controlled differentiation potential, immunomodulatory and paracrine mechanisms of MSCs pave the way for clinical utilization [137]. MSCs were used in approximately 1600 clinical trials, which are available on ClinicalTrials.gov (https://clinicaltrials.gov/) [18,138,139]. However, there are some limitations, including limited lifespan, rapid senescence, insufficient cell number for treatment, functional decline and heterogeneity, need to be addressed to bring out its optimum potential in clinical trials [140,141]. A solution to these challenges might be the generation of MSCs, with high proliferation potential, from PSCs [139,141].

Various effects of Aplnr signaling on MSC survival, proliferation and differentiation were reported up to date. Vodyanik and colleagues reported that hESC-derived Aplnr+ precursor cells give rise to MSCs [142,143]. Another report stated that viability of adipose-derived MSCs increased by Apelin induced autophagy during hypoxia in mouse hindlimb ischemia model [144]. It was also reported that Apelin pre-treatment of MSCs improved survival of MSCs and enhanced their cardioprotective effect in myocardial infraction [145]. Hang and colleagues also revealed that Aplnr signaling improved osteogenic differentiation of MSCs via Wnt signaling pathway *in vitro* [146]. Another report stated that Apelin contributes proliferation and neural differentiation of neural stem cell [147].

1.11. AIM

The aim of my thesis is to reveal regulatory role of Aplnr signaling in migration and differentiation of mesoderm tissue using pluripotent stem cells as a model system. The role of Aplnr signaling in mesoderm layer during gastrulation movements, tissue specification and cell fate decision was explored to understand developmental role. Furthermore, the role of Aplnr signaling in adult tissue morphogenesis and adult tissue regeneration was studied in terms of MSCs differentiation. Embryonic stem cell based *in vitro* culture system was established to examine cell migration and differentiation patterns under Aplnr signaling control.

2. MATERIALS AND METHODS

2.1. MOUSE ESC-DERIVED MESODERM AND MSCS

2.1.1. Cell Culture

R1/E (ATCC, SCRC1036), mESCs, were cultured and maintained in Dulbecco's Modified Eagle's Medium (DMEM, Thermo Fisher, Gibco, UK), supplemented with 1% Penicillin, Streptomycin, and Amphotericin B (PSA, Gibco, UK), 1000u/ml Leukemia inhibitory factor (LIF, Sigma Aldrich, UK), 1% non-essential amino acids(Thermo, UK), 1%L-Glutamine(Sigma Aldrich, UK) and 15% ES Cell Qualified FBS (ATCC, USA), and were grown on mitomycin c treated MEF feeder cells, which were isolated and stored in our laboratory [148]. The media was replenished daily, and the cells were incubated at 37^{o}C and 5% CO_2 conditions.

2.1.2. Preparation of Culture Well Plates

All mESC derived EBs were plated on Matrigel (Gibco, USA) - 0.1% Gelatin (Sigma Aldrich, UK) (1:200) coated 6- or 12-well plates (TPP, Switzerland) at day 2 [139,149]. Feeder-free mESC for siRNA treatment were also seeded on Matrigel-Gelatin coated plates.

2.1.3. Preparation of Small Molecule and Peptide

ML233 (#15187, Cayman, USA), a small molecule which induces Aplnr, and Apelin-13 (#13523, Cayman, USA), a peptide activator of Aplnr, were dissolved in DMSO to prepare 1mM and 10mM stock solutions, respectively. 1μM ML233 and 0.5μM Apelin-13 were prepared freshly in complete growth medium to treat the cells.

2.1.4. Activation of Aplnr

Aplnr was activated by ML233 and Apelin-13 as following. EBs, which were formed at day 2, were transferred to Matrigel-Gelatin coated plates in N2B27 media supplemented with 3μM CHIR99021 and either 0.5μM Apelin-13 or 1μM ML233 and were incubated at 37ºC and 5% CO_2 conditions until day 6.

2.1.5. Generation of CRISPR/Cas9 KO Cell Lines

KO of Aplnr, Apelin and Elabela genes were conducted by using Multiplex CRISPR/Cas9 Assembly System as previously described [150]. The CRISPR kit, which was needed to construct multiplex CRISPR/Cas9 vectors, was provided by Takashi Yamamoto (Addgene, #1000000055) [150]. Two guides for each gene were selected through Deskgen website (Figure 2.1, Table 2.1). The guides were cloned into the px330A 1x2 and px330S-2 vectors by Bpi digestion and the subsequent ligation. Eventually, two guides were assembled into one expression cassette and sequenced. R1 cells, which were grown on mitomycin treated MEF cells, were separated from MEF cells. The cells were grown on matrigel-gelatin coated plates in 2i+LIF medium, which consist of N2B27 medium supplemented with 3μM CHIR99021, 1uM PD0325901 and 1000u/ml LIF, and maintained at 37ºC and 5% CO_2 conditions. Next day, the cells were trypsinized and the CRISPR vectors were transferred to the cells via electroporation.

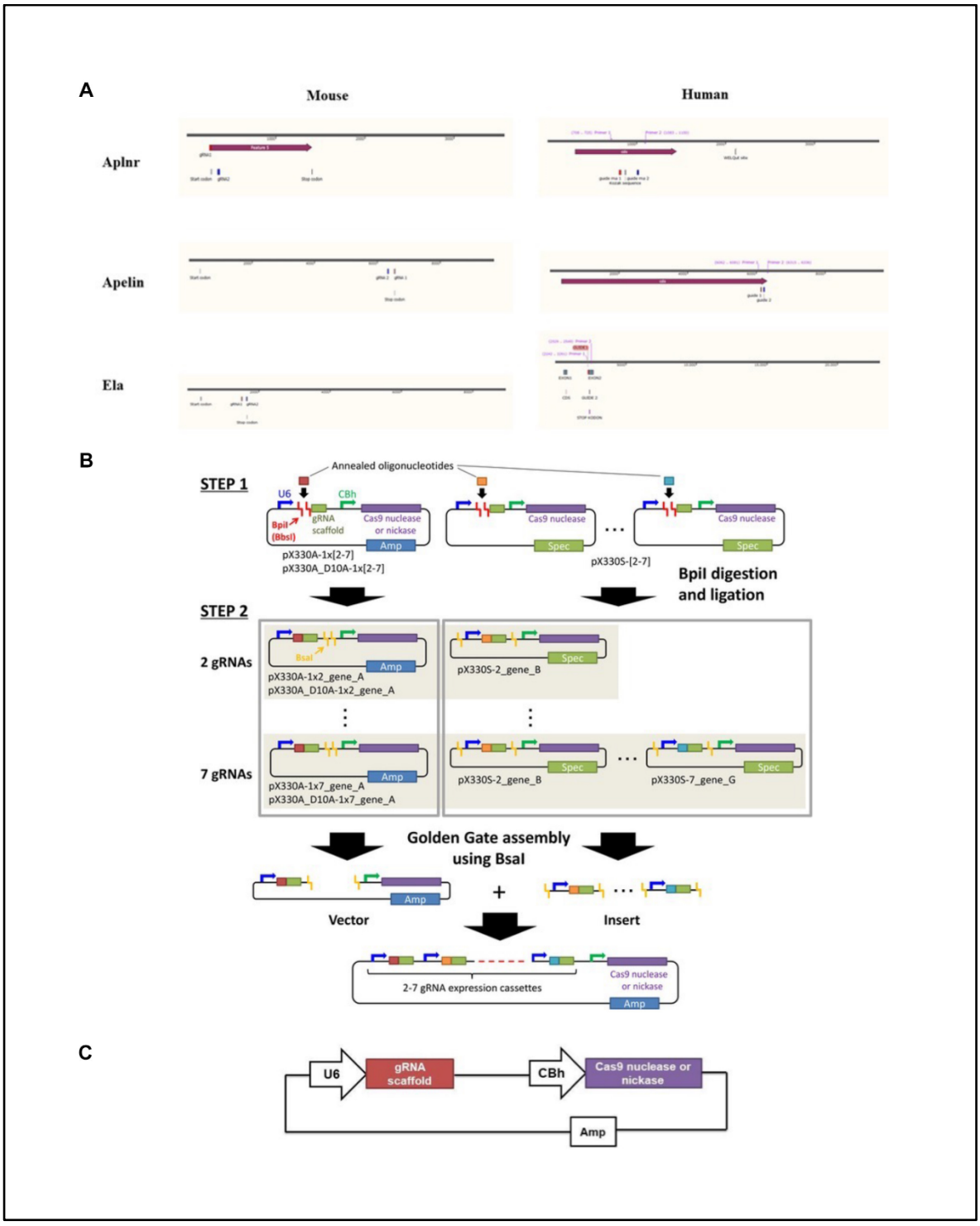


Figure 2.1. Design of CRISPR/Cas9 constructs. A. Guide RNA targeting Ela, Apelin and Aplnr gene regions on human and mouse DNA regions were shown. B. Multiplex CRISPR/Cas9 Assembly System, which allows the generation of 7 knockouts at a time by using one plasmid vector system. Guides were introduced into Px330A and Px330S vectors [150]. C. Final expression cassette containing the gRNA scaffold, which was

inserted into Cas9 carrying plasmid by the two-step protocol, and Cas9 nuclease (or nickase) driven by U6 and CBh promoters respectively. Expression cassette has ampicillin resistant gene for bacterial selection.

Table 2.1. gRNAs for generation of mouse CRISPR/Cas9 KO cell lines.

gRNA Names	**Forward (5'->3')**	**Reverse (5'->3')**
Apelin gRNA_1	CACCGACCTGCTTTAGAAAGGCATG	AAACCATGCCTTTCTAAAGCAGGTC
Apelin gRNA_2	CACCGTGGATTGAGAGAGACCGTAG	AAACCTACGGTCTCTCTCAATCCAC
Aplnr gRNA_1	CACCGTGCTGAATGAAGTGAAGCT	AAACAGCTTCACTTCATTCAGCAC
Aplnr gRNA_2	CACCGGCAGGAATGAGCGCTCCAG	AAACCTGGAGCGCTCATTCCTGCC
Elabela gRNA_1	CACCGTGCACAGCAAAACCGTTCTG	AAACCAGAACGGTTTTGCTGTGCAC
Elabela gRNA_2	CACCGTCTCGAGTGCCCTTCCCATG	AAACCATGGGAAGGGCACTCGAGAC

2.1.6. Inhibition of Aplnr Activity

2.1.6.1. siRNA

Downregulation of Aplnr signaling components was performed by siRNA and shRNA applications. For siRNA application, R1 cells were separated from MEF cells and were grown on matrigel-gelatin coated plates in 2i+LIF medium Next day, the cells were treated with Control siRNA (#AM4611, ThermoFisher, USA), Apelin siRNA (#AM16708, ThermoFisher, USA) and Aplnr siRNA (#AM16708, ThermoFisher, USA) at a concentration of 20pmol using Lipofectamine RNAimax (Invitrogen, USA) according to instructions of the manufacturer. After 48 hours of incubation at 37^{o}C with 5% CO_2, the cells were used for further analysis.

2.1.6.2. shRNA

Lentiviral Apelin shRNA (#sc-44742-SH, SantaCruz, USA), Aplnr shRNA (#sc-44733-SH, SantaCruz, USA) and Control shRNA (#sc-108060, SantaCruz, USA) plasmids were used to produce and package the lentiviruses in HEK293T (ATCC, CRL11268) cells according to the protocol as described previously [151].

For shRNA application, R1 cells were separated from MEF feeder layer. The concentrated viruses of mouse shApelin, shAplnr and shControl were added to the mESC media in 3:1 ratio (virus:media) and 10µg/ml polybrene were added to the final volume. 1x105 cells/infection were incubated with the media as suspension in the tubes in 5% CO_2 incubator at 37ºC for 12-16 hours. The cell suspension was transferred onto the MEF feeder layer. Next day, the media was changed with fresh mESC media and individual colonies were picked after a week.

2.1.7. Migration and Differentiation Protocol of Mesoderm and MSCs

mESCs cells were separated from MEF feeder layer and were seeded to a polypropylene 96 well qPCR plate (Biorad, USA) at the density of 4000cells/well in N2B27 medium (DMEM F12 (Thermo Fisher, Gibco, UK)/ Neurobasal Medium (Thermo Fisher, Gibco, UK) (1:1), 0.5% of 10% Bovine Serum Albumin (BSA, Sigma Aldrich, UK), 0.5% 100x N2 supplement (Thermo Fisher, Gibco, UK), 1% 50x B27 supplement (Thermo Fisher, Gibco, UK), 1% 100x L-glutamine, 1% PSA medium), supplemented with 12ng/ml bFGF (Peprotech, UK) and the plate was incubated at 37ºC and 5% CO_2 conditions for 48 hours to form EBs. At day 2, the EBs were transferred to Matrigel-Gelatin coated plates in N2B27 medium supplemented with 3µM CHIR99021 and were incubated at 37ºC and 5% CO_2 conditions until day 6 to differentiate cells to mesoderm layer cells. During the mesoderm differentiation, core and total area and intensity of the EBs were measured with Image J (NIH, Bethesda, USA) [152] and migration area and intensity were calculated.

The mesoderm cells, which were obtained at day 6, were further differentiated into MSCs by using 10 days of protocol. 1g/L Glucose DMEM medium, supplemented with 10ng/ml bFGF, were administered to the cells between day 6 and day 8. At day 8, the medium was replaced with complete 1g/L Glucose DMEM medium, supplemented with 8ng/ml bFGF and the cells until day 10.

2.1.8. Live Cell Imaging

mESCs-derived EBs were transferred to Matrigel-Gelatin coated plates in N2B27 medium supplemented with 3μM CHIR99021 at day 2 and the plate was placed in Live Cell Imaging platform, which provide 37ºC and 5% CO_2 conditions. Migration and differentiation of the EBs were continuously imaged with Zeiss Axio Observer Live Cell Microscope (Zeiss, Germany) every hour for 72 hours using ZEN 3.3 Blue Software (Zeiss, Germany).

2.1.9. Immunofluorescence (IF) Analysis

mESC-derived EBs were transferred to Matrigel-Gelatin coated plates in N2B27 medium supplemented with 3μM CHIR99021 at day 2 and were incubated at 37ºC and 5% CO_2 conditions. Next day, the cells were fixed with 4% paraformaldehyde (PFA) and permeabilized in a PBS solution containing 0.1% Triton-X 100. Then, cells were rinsed with PBS and blocked with 1% bovine serum albumin (BSA, Santa Cruz, CA, USA). Cells were incubated with the primary antibodies: Aplnr, Apelin, Flk1, Pdgfrα, Sox2, mTOR, MyoD, Erk1/2, Mek1/2 and Akt (Table 2.2) overnight at 4 °C. Cells were rinsed and incubated with secondary antibodies including AlexaFluor 488, AlexaFluor 594 and DAPI (0.5 lg/mL; Applichem, Darmstadt, Germany) for 30 minutes at room temperature. The images were taken with a confocal microscope (LSM 700; Zeiss, Heidelberg, Germany) and the intensities were analyzed with ZEN 3.2 Blue software (Zeiss, Germany).

Table 2.2. Antibody List for mESC-derived mesoderm and MSCs.

Antibody Name	Catalog Number	Brand Name	Country	Application
Apelin Receptor (Aplnr)	702069	Cell Signalling Technology	USA	ICC
Apelin	BS-2425R	Bioss	China	ICC
FLK1	Sc-6251	SantaCruz Biotechnology	USA	ICC
Pdgfr-α	Sc-398206	SantaCruz Biotechnology	USA	ICC
Sox2	MAB2018	R&D Systems	USA	ICC
mTOR	2983S	Cell Signalling Technology	USA	ICC

MyoD	554130	BD Biosciences	USA	ICC
Akt	9272S	Cell Signalling Technology	USA	ICC
Erk1/2	4695P	Cell Signalling Technology	USA	ICC
Mek1/2	4694S	Cell Signalling Technology	USA	ICC
Alexa Fluor 488 (Anti-mouse)	A28175	Invitrogen	USA	ICC
Alexa Fluor 488 (Anti-rabbit)	A27034	Invitrogen	USA	ICC
Alexa Fluor 594 (Anti-mouse)	A21125	Invitrogen	USA	ICC
Alexa Fluor 594 (Anti-rabbit)	A11037	Invitrogen	USA	ICC
Mouse Mesenchymal Stem Cell Marker Antibody Panel (Sca-1, CD106, CD73, CD29, CD105, CD44, CD11b, CD45)	SC-018	R&D Systems		Flow Cytometry
CD90/Thy1	Ab3105	Abcam	USA	Flow Cytometry
Alexa Fluor 488, IgG1 Cross-Absorbed Antibody (anti-mouse)	A21121	Invitrogen	USA	Flow Cytometry

2.1.10. Gene Expression Analysis

For mesoderm differentiation samples at day 6, cores were scraped off to eliminate unmigrated cells and cell pellet was collected after washing with PBS. Total RNAs were isolated using RNeasy plus mini kit (Qiagen, Hilden, Germany) following the manufacturer's instructions. iScprit cDNA synthesis kit (Bio-Rad, USA) was utilized for cDNA synthesis. SYBR Green (Applied Biosystems, Thermo Scientific, USA) and CFX96 RT-PCR system (Bio-Rad, USA) were used for qPCR experiment, which was described previously [153]. The primers were designed using Primer-BLAST software from the National Center for Biotechnology (Bethesda, MD, USA) and synthesized by Sentegen. The primer list was provided in Table 2.3. GAPDH was used as a housekeeping gene.

Table 2.3. List of primers for qPCR analysis of mESC-derived cells.

Gene Name	Forward Primer (5'->3')	Reverse Primer (5'->3')
GAPDH	TGGTGAAGCAGGCATCTGAG	TGAAGTCGCAGGAGACAACC
Bra	GCTTCAAGGAGCTAACTAACGAG	CCAGCAAGAAAGAGTACATGGC
CD 73	AGTTCGAGGTGTGGACATCGTG	ATCATCTGCGGTGACTATGAATGG
CD 90	CCTTACCCTAGCCAACTTCAC	AGGATGTGTTCTGAACCAGC
CD 105	CTGGAGCAGGGACGTTGT	GCTCCACGCCTTTGACC
CD 31	ACGCTGGTGCTCTATGCAAG	TCAGTTGCTGCCCATTCATCA
Apelin	AGTGAGTGGTCGACTTGTCC	AGAGCTACCAACTGACAAGGG
Aplnr	TGGAAGGACTCTAAGCACCC	TGGTTCGAAACACGGTCCAG
Elabela	ACCTGCGTGTCTGTGTAGCC	AAGGGGAGGGGGAAGGCGCG
CD 44	TCGATTTGAATGTAACCTGCCG	CAGTCCGGGAGATACTGTAGC
CD 45	ACTGAATCCACACCCCCAAG	AGCTTGGCTGCTGAATGTCT
CD 166	CTGATTGTGGGAATTGTCGTT	TCCTTGTTTACATGTTTTGATGC
Meox1	GACAGCAGCATACCCCGAC	CGTTGAAGATTCGCTCAGTCC
Pax1	CCGCCTACGAATCGTGGAG	CCCGCAGTTGCCTACTGATG
Nestin	CCCTGAAGTCGAGGAGCTG	CTGCTGCACCTCTAAGCGA
Cxcr4	GACTGGCATAGTCGGCAATG	AGAAGGGGAGTGTGATGACAAA
Sox2	TACAGCATGTCCTACTCGCAG	GAGGAAGAGGTAACCACGGG
Sox17	GATGCGGGATACGCCAGTG	CCACCACCTCGCCTTTCAC
Flk1	TTTGGCAAATACAACCCTTCAGA	GCAGAAGATACTGTCACCACC
Foxa2	ATGCACTCGGCTTCCAGTATG	TGTTGCTCACGGAAGAGTAGC
Pdgfra	CCTGGCATGATGGTCGATTCTAC	GGTCTCTTCTCGGGCTCACT
Pdgfrb	AGGAGTGATACCAGCTTTAGTCC	CCGAGCAGGTCAGAACAAAGG
Pax3	CCGGGGCAGAATTACCCAC	GCCGTTGATAAATACTCCTCCG
OTX1	ATGTCTTACCTCAAACAACCCCC	GTAGCGAGTCTTTGCGAACAG
ZBTB16	CTGGGACTTTGTGCGATGTG	CGGTGGAAGAGGATCTCAAACA
Osteonectin	TGGGAGAATTTGAGGACGGTG	GAGTCGAAGGTCTTGTTGTCAT
Col1A1	GTGGAAACCCGAGGTATGC	TTGGGTCCCXCGACTCCTAC
Col2A1	GGGAATGTCCTCTGCGATGAC	GAAGGGGATCTCGGGGTTG
Aggrecan	CCTGCTACTTCATCGACCCC	AGATGCTGTTGACTCGAACCT
FABP4	AAGGTGAAGAGCATCATAACCCT	TCACGCCTTTCATAACACATTCC
Adiponectin	TGTTCCTCTTAATCCTGCCCA	CCAACCTGCACAAGTTCCCTT
Bax	CTCAAGGCCCTGTGCACTAA	CACGCAGGAAGTCCAGTGTC

2.1.11. Antibody Array

mESC-derived EBs were transferred to Matrigel-Gelatin coated plates in N2B27 medium supplemented with 3μM CHIR99021 at day 2 and were incubated at 37ºC and 5% CO_2 conditions until day 6. 0.5μM Apelin-13 was added to the media between day2 and day6. The cell pellets were collected at day 6 after the cores were scraped off to eliminate unmigrated cells, the lysates were prepared and Mouse L-308 Array Kit was used according to instructions of the manufacturer (Raybiotech, USA). Briefly, after dialysis of the lysates, protein concentrations were measured and 90μg protein for each sample were biotinylated. Biotinylation was stopped and unbound biotin was removed by spin filter. After the array membranes were incubated with blocking buffer for 1 hour, the membranes were incubated with the extracted proteins, diluted with 1x blocking buffer, overnight at 4ºC. Next day, the membranes were washed with the washing buffers and were incubated with HRP-Conjugated Streptavidin for 2 hours at room temperature. After the membranes were washed, the signals were detected using a chemiluminescence imaging system (Bio-Rad, USA). Image Lab software (Bio-Rad, Hercules, CA, USA) was used to measure dot intensities and the results were analyzed using the analysis tool of the kit (Raybiotech, USA) (Table 3.1 and 3.2).

2.1.12. Liquid Chromotography Mass Spectrometry (LC-MS) Analysis

R1 cells and Apelin-13 treated cells at day 6 were underwent to LC/MS analysis according to the previously published protocol [154]. Briefly, mESC-derived EBs were incubated in Matrigel-Gelatin coated plates in N2B27 medium supplemented with 3μM CHIR99021 between day 2 and day 6. 0.5μM Apelin-13 was added to the media between day2 and day6 to activate Aplnr signaling. At day 6, the pellets were collected after the cores were scraped off and their protein were run on SDS-PAGE. The protein band were excised after fixation and staining with colloidal Coomassie Blue G-250. Following in-gel tryptic digestion, the peptides were analyzed by LC-MS/MS using Ultimate 3000 RSCL nanosystem (Dionex, Thermo Fisher Scientific, USA). Xcalibur 4.0 software (Thermo Fisher Scientific, USA) was used. High Performance Liquid Chromatography (HPLC) was performed using A and B mobile phases and full-scan MS spectra were acquired. MS/MS was performed with the top

ten precursor ions and protein identification analysis were done using Proteome Discoverer 2.2 software (Thermo Fisher Scientific, USA) and searched against the database of Uniprot/Swissprot (Table 3.3).

2.1.13. Characterization of MSCs

2.1.13.1. Surface Marker Analysis

MSCs, which were obtained at day 10, were fixed with 4% PFA at 4°C for 30 minuntes. The cells were washed with PBS and primary antibodies, including CD45, CD73, CD90 and 105 were used for labelling of cells according to instructions of the manufacturer (#SC018, R&D Systems, USA). Secondary antibody, Alexa Fluor 488, IgG1 Cross Absorbed Antibody (Table 2.2), was used in 1:500 dilution. Non-stained MSC was used as negative control to determine the gate of cells in flow cytometry device (Bio-Rad, USA).

2.1.13.2. Trilineage Differentiation

MSCs, which were obtained at day 10, were differentiated into osteocyte, adipocyte and chondrocyte according to the literature with some modifications [155]. Briefly, the cells were seed at density of 104 cells/well in growth medium to 12-well-plates (TPP, Switzerland). Next day, differentiation medium prepared in DMEM was given to the cells. MSCs cells were maintained in adipogenic, chondrogenic and osteogenic media for 6 days to complete differentiation. Adipogenic differentiation media was prepared in DMEM medium with the supplements including 10%FBS, 0.5 mM 3-Isobutyl-1-Methylxanthine, 100 nM Dexamethasone, 5 µg/ml Insulin and 60µM Indomethacin. DMEM medium, supplemented with 10% FBS, 100 ng/ml TGF-B, 100 nM Dexamethasone, 1X ITS, 14 µg/ml Ascorbic Acid and 1mg/ml BSA, was used to induce chondrogenic differentiation. For osteogenic differentiation, 10% FBS, 100 nM Dexamethasone, 10 mM B-Glycerophosphate and 0.2 mM Ascorbic Acid were dissolved in DMEM media. After the incubation periods were completed in 5% CO_2 incubator at 37^{o}C, the cells were confirmed for differentiation by qPCR and staining techniques.

2.1.13.3. Differentiation Stainings

Osteogenic differentiation was visualized using Alizarin Red staining (Millipore, USA). The cells, which were fixed with 4 % PFA, were stained with Alizarin Red following

manufacturer's instructions. Calcium depositions were observed by using light microscope (Axio Vert.A1; Zeiss, Heidelberg, Germany).

Lipid droplets were detected with Oil red staining (Sigma-Aldrich, UK) at the end of adipogenic differeniation. The PFA fixed cells were stained with Oil red O according to instructions of the manufacturer. Lipid particles were observed under light microscope.

Alcian blue staining (Sigma-Aldrich, UK) was used to demonstrate chondrogenic differentiation. Cells were fixed with 4 % PFA and stained with Alcian blue solution according to instructions of the manufacturer. Differentiated chondrocytes were observed under light microscope.

2.1.13.4. Cell Viability Assay

Cell viability analysis was performed by the 3-(4,5-di-methyl-thiazol-2-yl)-5-(3-carboxy-methoxy-phenyl)-2-(4-sulfo-phenyl)-2H tetrazolium (MTS) assay (CellTiter96 AqueousOne Solution; Promega, Southampton, UK) as previously described according to instructions of the manufacturer [156]. Briefly, MSCs were seeded at a density of 5x103 cells/well in a 96-well plate. Next day, media of positive control was replenished with 20% DMSO in culture media. Following day, 10% MTS reagent was applied to the cells and incubated for 2 hours at 37°C and 5% CO_2 conditions in a humidified incubator. Cell viability was determined by absorbance measurement at 490 nm using an ELISA plate reader (Biotek, Winooski, VT).

2.1.13.5. Cell Doubling Analysis

MSCs were seeded at the density of 1x104 cells/well to 12-well plates and counted every day to determine the cell doubling time. Cell doubling of the MSCs were calculated according to the protocol as described previously [139].

2.1.14. Statistical Analysis

Experiments were conducted as triplicates and statistical analysis were performed by using, one-way analysis of variance (ANOVA) post hoc Tukey test. The P values less than 0.05 were considered as statistically significant. All statistical analysis and correlation matrix analysis were performed by using the GraphPad Prism 8.0.0 statistical program for Windows (GraphPad Software, SanDiego, California, USA, www.graphpad.com). ClustVis online

tool (https://biit.cs.ut.ee/clustvis/) was used for hierarchical clustering with heat map and principal component analysis (PCA) [157]. Hierarchical clustering with heat map, protein distribution histogram and profile plot for protein profiling with LC/MS were generated by using Perseus software package (version: 1.5.5.3) (https://maxquant.net/perseus/) [158]. String database (https://string-db.org) was used to indicate network of protein interactions [159]. Protein Analysis Through Evolutionary Relationships (PANTHER) (version: 17.0) online tool (http://www.pantherdb.org) was used for gene ontology and pathway analysis of LC/MS data [160–162].

2.2. HUMAN ESC-DERIVED MESODERM AND MSCS

2.2.1. Cell Culture

H9 cell line of human ESCs (hESCs) (WA09, Wicell, USA) was cultured in mTESR medium (Stemcell Technologies, USA), on Matrigel (Corning, USA) coated plates under feeder-free culture conditions [148] and the medium was refreshed daily. Dental Pulp Stem Cells (DPSCs), which were isolated and characterized by our laboratory [163], and ASC-Telo cells (ASC52telo, ATCC-SCRC-4000) were cultured with Dulbecco's modified essential medium (DMEM) (1 g/L glucose) (Gibco, USA) supplemented with 10 % FBS and 1 % PSA. The cells were maintained in 5% CO_2 incubator at 37^{o}C.

2.2.2. Preparation of Culture Well Plates for Migration

All hESC derived EBs were plated on Matrigel (Gibco, USA) - 0.1% Gelatin (Sigma Aldrich, UK) (1:200) coated 6- or 12-well plates (TPP, Switzerland) at day 2.

2.2.3. Preparation of Small Molecule and Peptide

Both ML233 ((E)-4-Methyl-5-(((phenylsulfonyl) oxy) imino)-[1,1′-bi(cyclohexane)]-3,6-dien-2-one, #15187, Cayman, USA), a synthetic Aplnr agonist, and Apelin-13 (#13523, Cayman, USA), a peptide activator of Aplnr, were dissolved in DMSO to prepare 10mM

stock solutions. 1μM ML233 and 0.5μM Apelin-13 were prepared in culture medium as working concentrations.

2.2.4. Activation of Aplnr

Aplnr was activated by ML233 and Apelin-13 as following. EBs, which were formed at day 2, were transferred to Matrigel-Gelatin coated plates in N2B27 media supplemented with 3μM CHIR99021 and either 0.5μM Apelin-13 or 1μM ML233 and were incubated at 37ºC and 5% CO_2 conditions until day 6.

2.2.5. Generation of CRISPR/Cas9 KO Cell Lines

Knockout of Apelin, Aplnr and Elabela genes were carried out with Multiplex CRISPR/Cas9 Assembly System (#1000000055, Addgene, USA) as previously described [150]. The CRISPR kit, which was used for construction of multiplex CRISPR/Cas9 vectors, was a gift from Takashi Yamamoto. Two guides for each gene were designed (Figure 2.1, Table 2.4) and the guides were cloned into the px330A 1x2 and px330S-2 vectors by Bpi digestion and the subsequent ligation. Eventually, two guides were assembled into one expression cassette and sequenced. H9 cells were detached from the plate using Versene (Gibco, USA) and CRISPR vectors were transferred to the cells via electroporation. Cells were plated onto Matrigel coated plates after electroporation and clones were selected for further experiments.

Table 2.4. gRNAs for generation of human CRISPR/Cas9 KO cell lines.

gRNA Names	Forward (5'-> 3')	Reverse (5'-> 3')
Apelin gRNA_1	CACCGAAGGAGAAAGCCTGTTAGTG	AAACCACTAACAGGCTTTCTCCTTC
Apelin gRNA_2	CACCGACCCTCTGGGCTGCACCAGG	AAACCCTGGTGCAGCCCAGAGGGTC
Aplnr gRNA_1	CACCGCATGGTGTTACGCACCACCG	AAACCGGTGGTGCGTAACACCATGC
Aplnr gRNA_2	CACCGTTCCGCAAGGAACGCATCGA	AAACTCGATGCGTTCCTTGCGGAAC
Ela gRNA_1	CACCGTATTAGGAGCATTTTTCAG	AAACCTGAAAAATGCTCCTAATAC
Ela gRNA_2	CACCGTCACGAGTACCCTTTCCCTG	AAACCAGGGAAAGGGTACTCGTGAC

2.2.6. Inhibition of Aplnr Activity

2.2.6.1. siRNA

H9 cells, which were grown on Matrigel coated plates, were treated with control siRNA (#sc-37007, Santa Cruz Biotech Inc., USA), Apelin siRNA (#AM16708A, ThermoFisher, USA) and Aplnr siRNA (#AM16708A, ThermoFisher, USA) at the concentration of 20pmol using Lipofectamine RNAimax (Invitrogen, USA) according to instructions of the manufacturer. After 48 hours of incubation at 37^{o}C with 5% CO_2, the cells were used for further analysis.

2.2.6.2. shRNA

Lentiviral shApelin (#sc-44741-SH, SantaCruz, USA), shAplnr(#sc-44732-SH, SantaCruz, USA) and shControl (#sc-108060, SantaCruz, USA) plasmids were used to produce the lentiviruses in HEK293T cell line [151]. HEK293T cells were transfected with shRNA, pCI-VSVG (Addgene,USA) and pCMV-dR8.2 dvpr (Addgene USA) to produce viruses and the viruses were collected with the media. H9 cells, which were grown on Matrigel coated plates, were detached from the plate using a scraper. After the cell clusters were resuspended in 1ml

mTESR, 1 ml virus and 10ug/ml polybrene were added and the tubes were incubated in humidified incubator at 37°C with 5% CO_2 for 3 hours. Then, the cells with the viruses were transferred to Matrigel coated plates and incubated in humidified incubator at 37°C with 5% CO_2. Next day, the media was changed with fresh mTESR.

2.2.7. Migration and Differentiation Protocol of Mesoderm and MSCs

H9 cells were treated with TrypLE and single cell suspension were seeded to a low attachment plate (Corning, USA) in N2B27 medium (DMEM F12 (Thermo Fisher, Gibco, UK)/ Neurobasal Medium (Thermo Fisher, Gibco, UK) (1:1), 0.5% of 10% Bovine Serum Albumin (BSA, Sigma Aldrich), 0.5% 100x N2 supplement (Thermo Fisher, Gibco, UK), 1% 50x B27 supplement (Thermo Fisher, Gibco, UK), 1% 100x L-glutamine, 1% PSA medium), supplemented with 12ng/ml bFGF (FGF basic, Peprotech, UK) and 3uM CHIR99021 (Stemcell Technologies, USA) and the plate was incubated in humidified incubator at 37°C with 5% CO_2 for 48 hours to form EBs. At day 2, the EBs were transferred to 1:200 Matrigel-Gelatin coated plates in N2B27 medium supplemented with 3μM CHIR99021 and were incubated in the incubator until day 6 to observe migration of mesoderm cells. For small molecule group, 1μM ML233 was added to the media between day 2 and day 6. For peptide group, 0.5μM Apelin-13 was added to the media between day 2 and day 6 (Figure 1A). Image J (NIH, Bethesda, USA) [152] was used to measure area and intensity of core EB and total EBs (core and migrated area). Migration area and intensity were calculated.

EBs, which were generated from hESCs at day 3, were differentiated to MSCs for 24 days. Medium of mesoderm cells were replenished with N2B27 medium supplemented with 10ng/ml bFGF at day 3, N2B27 medium supplemented with 8ng/ml bFGF at day 5 and DMEM (1 g/L glucose) supplemented with 10 % FBS and 1 % PSA at day 8. For peptide group, 0.5μM Apelin-13 was added to the media at various time points; Option 1 (Control), Option 2 (Apelin-13 administration between day 3 and day 5), Option 3 (Apelin-13 administration between day 5 and day 8), Option 4 (Apelin-13 administration between day 8 and day 10), Option 5 (Apelin-13 administration between day 10 and day 24) and Option 6 (Apelin-13 administration between day 3 and day 24) (Figure 3.36A and 3.37A).

2.2.8. Live Cell Imaging

EBs derived from hESCs were transferred to Matrigel-Gelatin coated plates in N2B27 medium supplemented with 3μM CHIR99021 at day 2 and the plate was placed in Live Cell Imaging platform. Migration and differentiation of the EBs were continuously imaged at 37ºC and 5% CO_2 conditions with Zeiss Axio Observer Live Cell Microscope (Zeiss, Germany) every hour for 72 hours using ZEN 3.3 Blue Software (Zeiss, Germany).

2.2.9. Antibody Array

Protein expression profile of mesoderm cells and MSCs were determined by membrane-based antibody array analysis (#AAH-BLM-1000B-4, Raybiotech, USA). Table 2.5 demonstrates the protein panel. Pellets were obtained from day 6 control mesoderm, day 6 peptide treated mesoderm, Option 1 MSC and Option 6 MSC and experiment was conducted according to instructions of the manufacturer. Briefly, proteins were isolated by Lysis Buffer of the kit and protein concentrations were measured by BCA assay (ThermoScientific, USA). Membranes were incubated in blocking buffer for 1 hour and then treated with Biotin-labeled protein samples overnight at 4°C on a rocking platform. Protein samples were removed, and membranes were washed. Membranes were washed and treated with HRP for 2 hours. Membranes were washed, protein expression was detected and visualized by a chemiluminescent system (Bio-Rad Biotechnology Inc., USA). Protein spot intensity measurements were conducted by Image Lab software (Bio-Rad Laboratories Inc., Hercules, CA, USA) and results were analyzed by the analysis tool of the kit (Raybiotech, USA).

Table 2.5. Protein list screened by human antibody array for control group and Apelin-13 treated group at day 6.

Protein Name	**Protein Name**	**Protein Name**
6Ckine	MCP-2	Defensin
Activin A	MCP-3	Desmin
Activin B	MCP-4 / CCL13	DLL1

Activin C	M-CSF	DLL4
Activin RIA / ALK-2	M-CSF R	DMP-1
Activin RIB / ALK-4	MDC	DPPIV
Activin RII A/B	MFG-E8	E-Cadherin
Activin RIIA	MFRP	Endorphin Beta
Adiponectin / Acrp30	MIF	Endothelin Receptor A
AgRP	MIG	Enolase 2
ALCAM	MIP-1a	ENPP2
Angiogenin	MIP-1b	EpCAM
Angiopoietin-1	MIP-1d	EphA1
Angiopoietin-2	MIP 2	EphA2
Angiopoietin-4	MIP-3 alpha	EphA3
Angiopoietin-like 1	MIP-3 beta	EphA4
Angiopoietin-like 2	MMP-1	EphA5
Angiopoietin-like Factor	MMP-2	EphA6
Angiostatin	MMP-3	EphA7
APJ	MMP-7	EphA8
AR (Amphiregulin)	MMP-8	EphB1
APRIL	MMP-9	EphB2
Artemin	MMP-10	EphB3
Axl	MMP-11 /Stromelysin-3	EphB4
B7-1 /CD80	MMP-12	EphB6
BAFF R / TNFRSF13C	MMP-13	ERRa
BCMA / TNFRSF17	MMP-14	Erythropoietin R

BD-1	MMP-15	ESAM
BDNF	MMP-16 / MT3-MMP	EV15L
beta-Catenin	MMP-19	EXTL2
BAX	MMP-20	FABP1
beta-NGF	MMP-24 / MT5-MMP	FABP2
BIK	MMP-25 / MT6-MMP	FABP3
BLC / BCA-1 / CXCL13	Musk	FABP4
BMP-2	MSP alpha Chain	Factor XIII A
BMP-3	MICA	Factor XIII B
BMP-3b / GDF-10	NAP-2	FAK
BMP-4	NCAM-1 / CD56	FAP
BMP-5	Neuritin	Fc RIIB/C
BMP-6	NeuroD1	Fen 1
BMP-7	Neuropilin-2	FER
BMP-8	Neurturin	Ferritin
BMP-15	NGF R	Fetuin A
BMPR-IA / ALK-3	NOV / CCN3	Fetuin B
BMPR-IB / ALK-6	NRG1 Isoform GGF2	FGFR1
BMPR-II	Nidogen-1	FGFR1 alpha
BTC	NrCam	FGFR2
Cardiotrophin-1 / CT-1	NRG2	Fibrinogen
CCL14 / HCC-1 / HCC-3	NRG3	Fibrinopeptide A
CCL28 / VIC	NT-3	Fibronectin
CCR1	NT-4	Ficolin-3

CCR2	Orexin A	FIH
CCR3	Orexin B	FOLR1
CCR4	OSM	FOXN3
CCR5	Osteoactivin / GPNMB	FoxO1
CCR6	Osteocrin	FoxP3
CCR7	Osteoprotegerin / TNFRSF11B	FRK
CCR8	OX40 Ligand / TNFSF4	FSH
CCR9	PARC / CCL18	Furin
CD14	PD-ECGF	Fyn
CD27 / TNFRSF7	PDGF R alpha	GADD45A
CD30 / TNFRSF8	PDGF R beta	Galanin
CD30 Ligand / TNFSF8	PDGF-AA	Galectin-1
CD40 / TNFRSF5	PDGF-AB	Galectin-3BP
CD40 Ligand / TNFSF5 /CD154	PDGF-BB	Galectin-7
CD 163	PDGF-C	gamma-Thrombin
Cerberus 1	PDGF-D	Gas1
Chem R23	PECAM-1 /CD31	Gastrin
Chordin-Like 1	Pentraxin3 / TSG-14	GATA-3
Chordin-Like 2	Persephin	GATA-4
Csk	PF4 / CXCL4	Gelsolin
CLC	PlGF	Ghrelin
CNTF	PLUNC	GLP-1
CNTF R alpha	Pref-1	GMNN
Coagulation Factor III / Tissue Factor	Progranulin	GPBB

CRIM 1	Prolactin	GPI
Cripto-1	P-selectin	GPR-39
CRTH-2	RAGE	GPX1
Cryptic	RANK / TNFRSF11A	GPX3
CTACK / CCL27	RANTES	GRP
CTGF / CCN2	RELM beta	GRP75
CTLA-4 /CD152	RELT / TNFRSF19L	GRP78
CV-2 / Crossveinless-2	ROBO4	GSR
CXCL14 / BRAK	S100 A8/A9	GST
CXCL16	S100A10	HADHA
CXCR1 / IL-8 RA	SAA	HAI-1
CXCR2 / IL-8 RB	SCF	HAI-2
CXCR3	SCF R /CD117	Haptoglobin
CXCR4 (fusin)	SDF-1 / CXCL12	hCG alpha
CXCR5 /BLR-1	sFRP-1	hCGb
CXCR6	sFRP-3	Hck
D6	sFRP-4	HE4
DAN	sgp130	Hemopexin
DANCE	SIGIRR	Hepcidin
DcR3 / TNFRSF6B	Siglec-5/CD170	HOXA10
Decorin	Siglec-9	HSP10
Dkk-1	SLPI	HSP20
Dkk-3	Smad 1	HSP27
Dkk-4	Smad 4	HSP32

DR3 / TNFRSF25	Smad 5	HSP40
DR6 / TNFRSF21	Smad 7	HSP60
Dtk	Smad 8	HSP70
EDA-A2	Prdx	HSP90
EDAR	Soggy-1	HSPA8
EDG-1	Sonic Hedgehog (Shh N-terminal)	HTRA2
EGF	SPARC	IBSP
EGF R / ErbB1	Spinesin	IGF2BP1
EG-VEGF / PK1	TACI / TNFRSF13B	IGFBP-5
EMAP-II	Tarc	IL-23p19
ENA-78	TCCR / WSX-1	IL-33
Endocan	TECK / CCL25	IL-34
Endoglin / CD105	TFPI	IL36RN
Endostatin	TGF-alpha	INSL3
EN-RAGE	TGF-beta 1	INSRR
Eotaxin / CCL11	TGF-beta 2	Integrin alpha V
Eotaxin-2 / MPIF-2	TGF-beta 3	Itk
Eotaxin-3 / CCL26	TGF-beta 5	ITM2B
Epiregulin	TGF-beta RI / ALK-5	Kallikrein 2
ErbB2	TGF-beta RII	Kallikrein 5
ErbB3	Grb2	Kallikrein 6
ErbB4	TGF-beta RIII	Kallikrein 7
Erythropoietin	Thrombopoietin (TPO)	Kallikrein 8
E-Selectin	TPX	Kallikrein 10

Endothelin	Thrombospondin-1	Kallikrein 11
FADD	Thrombospondin-2	Kallikrein 14
FAM3B	Thrombospondin-4	KCC3
Fas / TNFRSF6	Thymopoietin	KCTD10
Fas Ligand	Tie-1	KIF3B
FGF Basic	Tie-2	KLF4
FGF-BP	TIMP-1	LAG-3
FGF R3	TIMP-2	Layilin
FGF R4	TIMP-3	LDL R
FGF R5	TIMP-4	Legumain
FGF-4	TL1A / TNFSF15	LH
FGF-5	TLR1	LIMPII
FGF-6	TLR2	LIN41
FGF-7 / KGF	TLR3	Livin
FGF-8	TLR4	LOX-1
FGF-9	TMEFF1 / Tomoregulin-1	LPS
FGF-10 / KGF-2	TMEFF2	LRG1
FGF-11	TNF-alpha	LTF
FGF-12	TNF-beta	LTK
FGF-13 1B	TNF RI / TNFRSF1A	Lumican
FGF-16	TNF RII / TNFRSF1B	Lyn
FGF-17	TRADD	LYRIC
FGF-18	TRAIL / TNFSF10	LYVE-1
FGF-19	TRAIL R1 / DR4 / TNFRSF10A	LZTS1

FGF-20	TRAIL R2 / DR5 / TNFRSF10B	Mammaglobin A
FGF-21	TRAIL R3 / TNFRSF10C	Marapsin
FGF-23	TRAIL R4 / TNFRSF10D	MATK
FLRG	TRANCE	MBL
Flt-3 Ligand	TREM-1	MBL-2
Follistatin	TROY / TNFRSF19	Mer
Follistatin-like 1	TSG-6	Mesothelin
Fractalkine	TSLP R	MICB
Frizzled-1	TWEAK / TNFSF12	Midkine
Frizzled-3	TWEAK R / TNFRSF12	MINA
Frizzled-4	Ubiquitin+1	MSHa
Frizzled-5	uPA	MTUS1
Frizzled-6	uPAR	Myoglobin
Frizzled-7	Vasorin	NAIP
Galectin-3	VCAM-1 (CD106)	Nanog
GASP-1 / WFIKKNRP	VE-Cadherin	NELL2
GASP-2 / WFIKKN	VEGF	NEP
GCP-2 / CXCL6	VEGF R2 (KDR)	Nesfatin
GCSF	VEGF R3	Nestin
G-CSF R / CD 114	VEGF-B	NET1
GDF1	VEGF-C	Netrin G2
GDF3	VEGF-D	Netrin-4
GDF5	VEGI / TNFSF15	Neurokinin-A
GDF8	WIF-1	Neuropeptide Y

GDF9	WISP-1 / CCN4	NF1
GDF11	XEDAR	NM23-H1/H2
GDF-15	11b-HSD1	Notch-1
GDNF	2B4	NPTX1
GFR alpha-1	4-1BB	NPTXR
GFR alpha-2	A1BG	NR3C3
GFR alpha-3	A2M	Ntn1
GFR alpha-4	ABL1	OCT3/4
GITR / TNFRF18	ACE	Omentin
GITR Ligand / TNFSF18	ACE-2	Osteocalcin
Glucagon	ACK1	Osteopontin
Glut1	ACPP	OX40
Glut2	ACTH	p21
Glut3	ADAM-9	p27
Glut5	ADAMTS-1	p53
Glypican 3	ADAMTS-10	PAI-1
Glypican 5	ADAMTS-13	PAK7
GM-CSF	ADAMTS-15	Pancreastatin
GM-CSF R alpha	ADAMTS-17	Pancreatic Polypeptide
Granzyme A	ADAMTS-18	Pappalysin-1
GREMLIN	ADAMTS-19	PARK7
GRO	ADAMTS-4	P-Cadherin
GRO-a	ADAMTS-5	PCAF
Growth Hormone (GH)	ADAMTS-L2	PD-1

Growth Hormone R (GHR)	Adipsin	PDX-1
HB-EGF	Afamin	PEDF
HCC-4 / CCL16	AFP	PEPSINOGEN I
HCR / CRAM-A/B	ALBUMIN	PEPSINOGEN II
Hepassocin	Aldolase A	PGRP-S
GLO-1	Aldolase B	PI 16
HGF	Aldolase C	PI 3Kinase p85 beta
HGFR	ALK	PIM2
HRG-alpha / NRG1-alpha	Alpha 1 AG	PKM2
HRG-beta 1 / NRG1-beta 1	Alpha 1 Microglobulin	Plasminogen
HVEM / TNFRSF14	Alpha Lactalbumin	Podocalyxin
I-309	ALPP	POMC
ICAM-1	AMICA	PON1
ICAM-2	AMPKa1	PON2
ICAM-3 (CD50)	Amylin	PPARg2
ICAM-5	ANGPTL3	PPP2R5C
IFN-alpha / beta R1	ANGPTL4	Presenilin 1
IFN-alpha / beta R2	Annexin A7	Presenilin 2
IFN-beta	APC	Pro-BDNF
IFN-gamma	APCS	Procalcitonin
IFN-gamma R1	Apelin	Pro-Cathepsin B
IGFBP-1	Apex1	Progesterone
IGFBP-2	APN	pro-Glucagon
IGFBP-3	ApoA1	Prohibitin

IGFBP-4	ApoA2	Pro-MMP-7
IGFBP-6	ApoA4	Pro-MMP-9
IGFBP-rp1 / IGFBP-7	ApoB	Pro-MMP-13
IGF-I	ApoB100	ProSAAS
IGF-I SR	ApoC1	Prostasin
IGF-II	ApoC2	Protein p65
IGF-II R	ApoC3	PSA-Free
IL-1 alpha	ApoD	PSA-total
IL-1 beta	ApoE	PSP
IL-1 F5 / FIL1delta	ApoE3	PTH
IL-1 F6 / FIL1 epsilon	ApoH	PTHLP
IL-1 F7 / FIL1 zeta	ApoM	PTN
IL-1 F8 / FIL1 eta	APP	PTPRD
IL-1 F9 / IL-1 H1	ASPH	PYK2
IL-1 F10 / IL-1HY2	Attractin	PYY
IL-1 R3 / IL-1 R AcP	B3GNT1	Ras
IL-1 R4 /ST2	BAF57	RBP4
IL-1 R6 / IL-1 Rrp2	BAFF	RECK
IL-1 R8	BAI-1	RELM alpha
IL-1 R9	BCAM	Resistin
IL-1 ra	Beta 2M	RET
IL-1 sRI	Beta Defensin 4	RIP1
IL-1 sRII	Beta IG-H3	ROCK1
IL-2	Biglycan	ROCK2

IL-2 R alpha	BLAME	ROR1
IL-2 R beta /CD122	BMP-9	ROR2
IL-2 R gamma	BMX	ROS
IL-3	BNIP2	RYK
IL-3 R alpha	BNP	S100A4
IL-4	Btk	S100A6
IL-4 R	C2	S100A8
IL-5	C3a	S-100b
IL-5 R alpha	C5/C5a	SART1
IL-6	C7	SART3
IL-6 R	C8B	SCG3
IL-7	C9	Selenoprotein P
IL-7 R alpha	CA9	SEMA3A
IL-8	CA15-3	Serotonin
IL-9	CA19-9	Serping 1
IL-10	CA125	Serpin A1
IL-10 R alpha	Cadherin-13	Serpin A3
IL-10 R beta	Calbindin	Serpin A4
IL-11	Calbindin D	Serpin A5
IL-12 p40	Calcitonin	Serpin A8
IL-12 p70	Calreticulin	Serpin A9
IL-12 R beta 1	Calsyntenin-1	Serpin A12
IL-12 R beta 2	CART	Serpin B5
IL-13	Caspase-3	Serpin D1

IL-13 R alpha 1	Caspase-8	Serpin I1
IL-13 R alpha 2	Cathepsin B	SERTAD2
IL-15	Cathepsin D	SHBG
IL-15 R alpha	Cathepsin L	SMAC
IL-16	Cathepsin S	SNCG
IL-17	CBP	Somatotropin
IL-17B	CCK	SOST
IL-17B R	CD23	SOX17
IL-17C	CD24	SOX2
IL-17D	CD36	SPARCL1
IL-17E	CD38	SPINK1
IL-17F	CD44	SRMS
IL-17R	CD45	SSEA-1
IL-17RC	CD46	SSEA-4
IL-17RD	CD47	SSTR2
IL-18 BPa	CD55	SSTR5
IL-18 R alpha /IL-1 R5	CD59	Survivin
IL-18 R beta /AcPL	CD61	SYK
IL-19	CD71	Syndecan-1
IL-20	CD74	Syndecan-3
IL-20 R alpha	CD79 alpha	TACE
IL-20 R beta	CD90	TAF4
IL-21	CD97	Tec
IL-21 R	CD200	TFF1

IL-22	CEA	TFF3
IL-22 BP	CEACAM-1	Thrombin
IL-22 R	Ceruloplasmin	Thrombomodulin
IL-23	CFHR2	Thymidine Kinase-1
IL-23 R	Chemerin	Thyroglobulin
IL-24	CHI3L1	TIM-1
IL-26	Chromogranin A	TNK1
IL-27	Chymase	TOPORS
IL-28A	cIAP-2	TPA
IL-29	Ck beta 8-1	TPM1
IL-31	CK-MB	TRA-1-60
IL-31 RA	Claudin-3	TRA-1-81
BACE-1	Claudin-4	Transferrin
FACX	CLEC3B	Trappin-2
Insulin	Clusterin	TRKB
Insulin R	CNDP1	Troponin I
Insulysin / IDE	COCO	Troponin C
IP-10	Complement factor H	TRPC1
I-TAC / CXCL11	Contactin-1	TRPC6
Kininostatin / kininogen	Contactin-2	TRPM7
Kremen-1	Corticosteroid-binding globulin	Trypsin 1
Kremen-2	COX-2	TSH
Lck	C-peptide	TSLP
Latent TGF-beta bp1	CPN2	TXK

LBP	Creatinine	Tyk2
LECT2	CRP	TYRO10
Lefty - A	CRTAM	Uromodulin
Leptin R	CSH1	Vasopressin
Leptin (OB)	cTnT	VDUP-1
LFA-1 alpha	CutA	VEGF R1
LIF	Cyclin D1	VGF
LIF R alpha	Cystatin A	VIP Receptor 2
LIGHT / TNFSF14	Cystatin B	Visfatin
Lipocalin-1	Cystatin C	Vitamin D Receptor
LRP-1	Cytochrome C	Vitamin D-BP
LRP-6	Cytokeratin 8	Vitamin K-dependent protein S
L-Selectin (CD62L)	Cytokeratin18	Vitronectin
Lipocalin-2	Cytokeratin19	VWF
Lymphotactin / XCL1	DBI	Wilms Tumor 1
Lymphotoxin beta / TNFSF3	DCBLD2	XIAP
Lymphotoxin beta R / TNFRSF3	D-Dimer	ZAG
MAC-1	DEFA1/3	ZAP70
MCP-1		

2.2.10. Characterization of MSCs

2.2.10.1. Differentiation of MSCs

Confirmation of MSC characteristics was done with osteogenic, chondrogenic, adipogenic, odontogenic, myogenic, neurogenic, epithelial and endothelial differentiation of MSCs,

derived from mesoderm, according to the literature [139,155,164,165]. The cells were seed at density of 104 cells/well in growth medium to 12-well-plates (TPP, Switzerland). Next day, differentiation medium (Table 2.6) prepared in DMEM was given to the cells. After the differentiations were completed, confirmations were done by real time PCR, staining and immunofluorescence analysis.

Table 2.6. Media supplements for differentiation of MSCs

Type of Differentiation	**Supplements of Media**	**Incubation Time**
Adipogenic Differentiation	10% FBS	14 days
	0.5 mM 3-Isobutyl-1-Methylxanthine	
	100 nM Dexamethasone	
	5 µg/ml Insulin	
	60µM Indomethacin	
Chondrogenic Differentiation	10% FBS	14 days
	100 ng/ml TGF-B	
	100 nM Dexamethasone	
	1X Insulin–Transferrin–Selenium (ITS)	
	14 µg/ml Ascorbic Acid	
	1 mg/ml Bovine Serum Albumin (BSA)	
Osteogenic Differentiation	10% FBS	14 days
	100 nM Dexamethasone	
	10 mM B-Glycerophosphate	
	0.2 mM Ascorbic Acid	
Odontogenic Differentiation	10% FBS	14 days
	10 nM Dexamethasone	

	10 mM B-Glycerophosphate	
	0.5mM Ascorbic Acid	
Endothelial Differentiation	2% FBS	7 days
	50ng/ml VEGF	
	10ng/ml bFGF	
Epithelial Differentiation	10% FBS	3 days
	10ng/ml Keratinocyte Growth Factor (KGF)	
	30ng/ml Epidermal Growth Factor (EGF)	
	10ng/ml Hepatocyte Growth Factor (HGF)	7 days
	60ng/ml Insulin-like Growth Factor-2 (IGF-2)	
Myogenic Medium	10% FBS	18 days
	5% Horse Serum	
	100 nM Dexamethasone	
	50µM Hydrocortisone	
Neurogenic Growth Factor	10% FBS	14 days
	200µM Butylated Hydroxyanisole	
	5mM KCl	
	10ng/ml Neurogenic Growth Factor (NGF)	
	5µM Insulin	
	2µM Valproic Acid	

2.2.10.2. Surface Marker Analysis

MSCs, which were obtained at day 24, were fixed with 4% PFA at 4 °C for 30 minutes. The cells were washed with PBS and primary antibodies, including CD29, CD31, CD34, CD44, CD45, CD73, CD90, CD105, and CD166 were applied according to instructions of the manufacturer (#SC018, R&D Systems, USA). Secondary antibody, Alexa Fluor 488, IgG1

Cross Absorbed Antibody (Table 2.7), was used in 1:500 dilution. Non-stained MSC was used to determine gate of flow cytometry. S3e Cell Sorter (Bio-rad, USA) was used for flow cytometry analysis.

Table 2.7. Antibody List for hESC derived mesoderm and MSCs.

Antibody Name	**Catalog Number**	**Brand Name**	**Country**	**Application**
Apelin Receptor (Aplnr)	702069	Cell Signalling Technology	USA	IF
Apelin	BS-2425R	Bioss	China	IF
Flk1	sc-6251	SantaCruz Biotechnology	USA	IF
PDGFR-α	sc-398206	SantaCruz Biotechnology	USA	IF
Sox2	MAB2018	R&D Systems	USA	IF
mTOR	2983S	Cell Signalling Technology	USA	IF
MyoD	554130	BD Biosciences	USA	IF
Akt	9272S	Cell Signalling Technology	USA	IF
Erk1/2	4695P	Cell Signalling Technology	USA	IF
MEK1/2	4694S	Cell Signalling Technology	USA	IF
Collagen I (Col1)	ab34710	Abcam	USA	IF
Collagen II (Col2)	ab34712	Abcam	USA	IF
A-FABP	sc-271529	SantaCruz Biotechnology	USA	IF
Desmin	sc-14026	SantaCruz Biotechnology	USA	IF

MYH	sc-20641	SantaCruz Biotechnology	USA	IF
MyoD	sc-760	SantaCruz Biotechnology	USA	IF
Dentin Matrix Protein I (DMP1)	Ab103203	Abcam	USA	IF
Vimentin		Cell Signalling Technology	USA	IF
Cytokeratin 19	sc-33119	SantaCruz Biotechnology	USA	IF
VEGF	sc-152	SantaCruz Biotechnology	USA	IF
Tyrosine Hydroxylase (TH)	sc-14007	SantaCruz Biotechnology	USA	IF
Microtubule Associated Protein 2 (MAP2)	4542S	Cell Signalling Technology	USA	IF
Alexa Fluor 488 (Anti-mouse)	A28175	Invitrogen	USA	IF
Alexa Fluor 488 (Anti-rabbit)	A27034	Invitrogen	USA	IF
Alexa Fluor 594 (Anti-mouse)	A21125	Invitrogen	USA	IF
Alexa Fluor 594 (Anti-rabbit)	A11037	Invitrogen	USA	IF
CD29	Ab27314	Abcam	USA	Flow Cytometry
CD31 (PECAM-1)	sc-53411	SantaCruz Biotechnology	USA	Flow Cytometry
Human Mesenchymal Stem Cell Marker Antibody Panel	SC-017	R&D Systems		Flow Cytometry

(CD34/Stro-1, CD44, CD45, CD90, CD105, CD166)				
CD73	Ab157335	Abcam	USA	Flow Cytometry
Alexa Fluor 488, IgG1 Cross-Absorbed Antibody (anti-mouse)	A21121	Invitrogen	USA	Flow Cytometry

2.2.10.3. Staining Analysis

Calcium deposition after osteogenic differentiation was visualized using von Kossa staining (Abcam, UK) and alizarin red staining (Sciencell, USA). The cells, which were fixed with 4 % PFA, were stained with von Kossa kit following manufacturer's instructions. Calcium depositions were observed by using light microscope (Axio Vert.A1; Zeiss, Heidelberg, Germany).

Oil red O staining (Sigma-Aldrich, UK) was performed to demonstrate lipid vesicles at the end of adipogenic differeniation. The PFA fixed cells were stained with oil red O according to instructions of the manufacturer. Lipid particles were observed under light microscope.

Chondrogenic differentiation was observed using alcian blue staining (Sigma-Aldrich, UK). Cells were fixed with 4 % PFA and stained with alcian blue solution according to instructions of the manufacturer. Differentiated chondrocytes were observed under light microscope.

2.2.11. Immunofluorescence (IF) Analysis

For mesoderm cells, H9-derived EBs were transferred to 1:200 Matrigel-Gelatin coated plates in N2B27 medium supplemented with 3μM CHIR99021 at day 2 and were incubated in the humidified incubator at 37°C and 5% CO_2 conditions. The cells were fixed at day 3 and day 6 with 4% paraformaldehyde (PFA, ThermoScientific, USA). For multiple differentiation from MSCs, the cells were fixed with PFA at the end of differentiation. The cells were permeabilized in a PBS solution containing 0.1% Triton-X 100. Then, cells were rinsed with PBS and blocked with 1% bovine serum albumin (BSA, Santa Cruz, CA, USA). Cells were incubated with the primary antibodies: Aplnr, Apelin, Flk1, PDGFRα, Sox2, mTOR, MyoD, Erk1/2, Mek1/2, Akt, Col1, Col2, A-FABP, Desmin, MYH, DMP1,

Vimentin, EpCAM, VEGF, TH and MAP2 (Table 2.7) overnight at 4 °C. Cells were rinsed and incubated with secondary antibodies including AlexaFluor 488, AlexaFluor 594 and DAPI (0.5 lg/mL; Applichem, Darmstadt, Germany) for 30 minutes at room temperature. The images were taken with a confocal microscope (LSM 700; Zeiss, Heidelberg, Germany) and intensities were calculated with ZEN 3.2 Blue software (Zeiss, Germany).

2.2.12. Quantitative Real Time PCR (qPCR) Analysis

Total RNAs were isolated using RNeasy plus mini kit (Qiagen, Hilden, Germany) according to instructions of the manufacturer and iScprit cDNA synthesis kit (Bio-Rad, USA) was used for cDNA synthesis. The primers were designed using Primer-BLAST software from the National Center for Biotechnology (Bethesda, MD, USA) and synthesized by Sentegen (Ankara, Turkey). B-actin was used as a housekeeping gene and list of the primers was provided in Table 2.8. qPCR was performed using SYBR Green (Applied Biosystems, Thermo Scientific, USA) as described previously [166] and CFX96 RT-PCR system (Bio-Rad, USA) were used for qPCR experiment.

Table 2.8. Primer List for qPCR analysis of hESC-derived cells. DSPP: Dentinsialophosphoprotein, α-sma: α-Smooth muscle actin.

Gene Name	Forward (5'->3')	Reverse Primer (5'->3')
β-Actin	CACCATTGGCAATGAGCGGTTC	AGGTCTTTGCGGATGTCCACGT
T/Bra	TATGAGCCTCGAATCCACATAG	CCTCGTTCTGATAAGCAGTCAC
CD31	GGTTCTGAGGGTGAAGGTGA	CTGCTTGGTCCAAAATGCCT
CD44	CCAGAAGGAACAGTGGTTTGGC	ACTGTCCTCTGGGCTTGGTG
CD45	CACTGCAGGGATGGATCTCA	ACTCGTGGGTTCAGAACCTTCA
CD90	AGAGACTTGGATGAGGAG	CTGAGAATGCTGGAGATG
CD73	CAGCGAGGACTCCAGCAAG	TATCCAACGATTCCCACAACT
CD105	ACGCTCCCTCTGGCTGTTG	GCCCTTCGAGACCTGGCTAG
CD166	TGGCAATATCACATGGTACAGGAA	CCAGGGTGGAGGTCATGGTATAGAG

Apelin	GCTGGAAGACGGCAATGT	ATGGGTCCCTTATGGGAGAG
Aplnr	GGCCAGTGGCCAATGCTC	AGGGCATCCAGCACAGGG
Ela	AGCGGACAGAGACCAGTTA	CTCGTGAATGGAGAGGCATAC
PDGFR-α	TGGCAGTACCCCATGTCTGAA	CCAAGACCGTCACAAAAAGGC
Bax	TGCAGAGGATGATTGCCGCCG	ACCCAACCACCCTGGTGTTGG
TERT	GACGTGGAAGATGAGCGTG	GAGGACGTACACACTCATC
α-sma	AGACATCAGGGGGTGATGGT	ATCTTTTCCATGTCGTCCCAGTTG
DSPP	CAGTAAGGATGAGTTAAATGCC	TACTTCTGCCCACTTAGAGCC
Osteocalcin	GTGCAGAGTCCAGCAAAGGT	TCAGCCAACTCGTCACAGTC
Aggrecan	ACTGCTGCAGACCAGGAGGT	TCCTCGGGGGTGACGATGCT
Flk1	CGTGTCTTTGTGGTGCACTG	TCTAGGACTGTGAGCTGCCT
Adiponectin	TATCCCCAACATGCCCATTCG	TGGTAGGCAAAGTAGTACAGCC
E-Cadherin	GGTTTTCTACAGCATCACCG	GCTTCCCCATTTGATGACAC
VE-Cadherin	AATGCGTCCGTGCCTGAGTCGT	GTGGTCTCCCACAGTGGGGTCG
B-Tubulin	GCAACTACGTGGGCGACT	CGAGGCACGTACTTGTGAGA

2.2.13. Cell Viability Assay

Cell viability analysis was performed by the 3-(4,5-di-methyl-thiazol-2-yl)-5-(3-carboxy-methoxy-phenyl)-2-(4-sulfo-phenyl)-2H tetrazolium (MTS) assay (CellTiter96 AqueousOne Solution; Promega, Southampton, UK) as previously described according to instructions of the manufacturer [156]. Briefly, MSCs were seeded at a density of 5x103 cells/well in a 96-well plate. Next day, media of positive control was replenished with 20% DMSO in culture media. Following day, 10% MTS reagent was applied to the cells and incubated for 2 hours at 37°C and 5% CO_2 conditions in a humidified incubator. Cell viability was determined by absorbance measurement at 490 nm using an ELISA plate reader (Biotek, Winooski, VT).

2.2.14. Cell Doubling Analysis

MSCs were seeded at the density of 1x104 cells/well to 12-well plates and counted every day to determine the cell doubling time. Cell doubling of the MSCs were calculated according to the protocol as described previously [139].

2.2.15. Liquid Chromotography Mas Spectrometry (LC-MS) Analysis

EBs derived from H9 cells with and without Apelin-13 treatment, shControl, shApelin and shAplnr at day 6 were underwent to LC/MS analysis according to the previously published protocol [154]. Briefly, EBs of control shRNA, Apelin shRNA and Aplnr shRNA administered H9 cells as well as H9 cells with/without Apelin-13 were harvested at day 6. Their proteins were run on SDS-PAGE and bands were excised after fixation and staining with colloidal Coomassie Blue G-250. Following in-gel tryptic digestion, the peptides were analyzed by LC-MS/MS using Ultimate 3000 RSCL nanosystem (Dionex, Thermo Fisher Scientific, USA). Xcalibur 4.0 software (Thermo Fisher Scientific, USA) was used. High Performance Liquid Chromatography (HPLC) was performed using A and B mobile phases and full-scan MS spectra were acquired. MS/MS was performed with the top ten precursor ions and protein identification analysis were done using Proteome Discoverer 2.2 software (Thermo Fisher Scientific, USA) and searched against the database of Uniprot/Swissprot.

2.2.16. RNA Sequencing Analysis

EB-derived mesoderm cells, control (H) and Apelin-13 treated (HApln) groups at day 6, EB-derived MSCs at cells, Option 1 (HM) and Option 6 (HMApln) groups at day 24, and DPSCs were collected. After total RNA isolation of the samples using Qiagen RNeasy Kit (Qiagen, Germany) according to instructions of the manufacturer, the RNA samples were received by Genoks Company to perform mRNA sequencing to all the samples and miRNA sequencing to the mesoderm samples. The samples with OD values between 1.8-2.2 and RIN>9.7 were selected for mRNA and miRNA sequencing.

For miRNA sequencing, small RNAs were enriched and purified from total RNA of mesoderm samples (H and HApln) and was ligated to 5’- and 3’- RNA adaptors. cDNA

library was prepared by reverse transcription and the samples were amplified with PCR. Sequencing was performed on DNBSEQ library with 10million reads. Bowtie2 program (version 2.4.5) was used to align the reads to refence human sequences. Differential gene expression analysis based on the negative binomial distribution was performed using DEseq2 program (version 4.1) and functional enrichment analysis was visualized by gprofiler2 program (version 0.2.1). Effective miRNA target sites in human mRNAs were predicted by Targetscan2 (version 8.0).

mRNA sequencing was performed with 5.5gb reads for the mesoderm (H and HApln) and MSC samples (HM, HMApln and DPSC). The sequencing reads were mapped to human reference sequences with Hisat2 alignment program (version 2.2.1). Differential gene expression analysis based on the negative binomial distribution was performed using DEseq2 program (version 4.1) and functional enrichment analysis was visualized by gprofiler2 program (version 0.2.1).

2.2.17. Statistical Analysis

Experiments were conducted as triplicates and one way analysis of variance (ANOVA) with Tukey's post hoc test was utilized for statistical analysis. All statistical analysis and correlation matrix analysis were performed by GraphPad Prism version 8.0.0 for Windows (GraphPad Software, SanDiego, California USA, www.graphpad.com). The p values less than 0.05 were accepted as statistically significant. Hierarchical clustering with heat map an principal component analysis (PCA) were generated by using ClustVis online tool (https://biit.cs.ut.ee/clustvis/) [157]. Hierarchical clustering with heat map, protein distribution histogram and profile plot for protein profiling with LC/MS were generated by using Perseus software package (version: 1.5.5.3) (https://maxquant.net/perseus/) [158]. Network of protein interactions were formed using String database (https://string-db.org) [159]. Gene ontology and pathway analysis of LC/MS data were done using Protein Analysis Through Evolutionary Relationships (PANTHER) (version: 17.0) online tool (http://www.pantherdb.org) [160–162].

3. RESULTS

3.1. EFFECT OF APLNR SIGNALING ON MESODERM AND MSC DIFFERENTIATION OF MOUSE ESCS

3.1.1. Aplnr Signaling Improves Migration Potential of EBs During Mesoderm Differentiation

To investigate the role Aplnr signaling on migration of EBs during mesoderm differentiation, Aplnr signaling was either activated by Apelin-13 and ML233 (Figure 3.1) or suppressed by shRNA, siRNA and CRISPR-Cas9 mediated gene KO (Figure 3.1 and 3.2). Figure 3.1B represents the protocol for mesoderm differentiation by Aplnr activation via Apelin-13 or ML233 administration. EBs, which were brought to Epi-stem cell state at day 2 using N2B27 media supplemented with bFGF, were transferred to matrigel-gelatin coated plates. Apelin-13 or ML233 was added to the N2B27 media, supplemented with CHIR, at day 2 and migration of the EBs were observed until day 6 (Figure 3.1B). Morphological images of the EBs were taken at day 2, day 3 and day 6 during migration and differentiation of EBs into mesoderm cells. Core area, total area and migration area of the EBs as well as their intensities were measured at day 2, day 3 and day 6 as schematically indicated in Figure 3.1C (Figure 3.1C and 3.1D). Although core area of Apelin-13 or ML233 treated EBs at day 3 and day 6 were not significantly different than core area of Control group at day 3 and day 6, total area of Apelin-13 treated EBs at day 3 and day 6 were 1.2-fold larger and ML233 treated EBs at day 3 and day 6 were 1.3-fold and 1.5-fold larger than total area of Control EBs. Also, migration area of Apelin-13 treated EBs at day 3 and day 6 were 1.2-fold and 1.5-fold higher while ML233 treated EBs at day 3 and day 6 were 2-fold higher than migration of Control group (Figure 3.1E and 3.1F). Total migration area, which indicates the total area change between day 6 and day2, increased 1.2-fold in Apelin-13 group and 1.5-fold in ML233 group compared to Control group (Figure 3.1F). Furthermore, intensity measurements at day 6 demonstrated that core intensity was upregulated approximately 2.5-fold in the presence of Apelin-13 and 2.8-fold in the presence of ML233. Migration intensity was upregulated 1.2-fold at day 3, 2-fold at day 6 with Apelin-13 treatment and about 3.6-fold at day 3 and day 6 with ML233 treatment (Figure 3.1E and 3.1F). Total migration intensity, which indicates

the total intensity change between day 6 and day2, increased 1.6-fold in Apelin-13 group and 2-fold in ML233 group compared to Control group (Figure 3.1F).

CRISPR-Cas9 gene editing technology was used to KO Apelin, Aplnr and Elabela genes in R1 cells. Selection of targeted region has been conducted based on coding region localization. Guides were selected to disrupt open reading frame and resulted in a knockout gene. DNA sequences of selected genes, Ela, apelin and Aplnr, were derived from USCS genome browser (https://genome.ucsc.edu/), in which 5'UTR, CDS, 3'UTR, exon and intron localizations were detected. This is required to identify guide targeting region to disrupt CDS which results in knockout of the gene. Guide selection was made through the Deskgen website (https://www.deskgen.com/landing/#/) and off target effects were calculated. Deskgen website allows to select guide RNAs which are in the target range with minimized off target effect. mRNA sequence of the Ela, Apelin and Aplnr were derived from the NCBI web browser (https://www.ncbi.nlm.nih.gov/) and paste into the Snap gene software to mark guide regions. Selected guides were marked in the SnapGene software for further analysis (Figure 2.1A, Table 2.1). PCR primers to confirm gene knockout were selected at least 100 bp upstream and downstream of the targeted region on the genomic DNA to analyze successful knockout. Knock out strategy has been carried out by CRISPR/Cas9 gene editing technology. Multiplex CRISPR/Cas9 Assembly Systems from Yamamoto Lab protocol has been used for generation of knockout clones [167]. This system allows the generation of multiple knockout gene combinations in one vector system (Figure 2.1B). Two guides were generated for each knockout and guides were cloned into Px330A and Px330S followed by a golden date assembly reaction for generation of expression cassette containing plasmid (Figure 2.1C). One gene knockout each time were generated and therefore Px330A-1x2 and Px330S-2 were used for cloning and subcloning purposes. Designed gRNA oligos (forward and reverse) were diluted and ligated by using T4 polynucleotide kinase (STEP 1). Then a phosphorylation (To enhance 5'binding to the target) and annealing reaction were made for each gRNA pair. Annealed gRNAs were diluted (1:250) and subjected to a digestion and ligation reaction (STEP 2). After ligation and additional exonuclease digestion plasmids were transformed into competent E.coli DH5α bacteria and clones were picked up. Selected clones were propagated and digested with BpsI restriction enzyme followed by gel load and colony PCR. This method allowed confirmation of knockout lines. Cell transfection was performed using electroporation technique. Biorad Gene Pulser II device was used for

electroporation of the plasmid constructs. Because human ES Cell line is still in the order/transport process, CRISPR/Cas9 based knockout of selected Aplnr signaling genes have been conducted with the mouse ES Cell line. A2lox Cre mouse ES cells has been propagated on mitomycin C treated mouse embryonic fibroblast cell line and were prepared for electroporation experiment. Cells were separated from mouse embryonic fibroblast cells and plated on matrigel-gelatin coated tissue culture well plates in 2i+LIF medium. Next day, cells were trypsinized and electroporated with 10 of each construct+pmax GFP under appropriate electroporation conditions (0,4cm cuvettes, 0.32V /250 F/ 4.9sec). Cells were immediately cultured on coated well plates and after two days sorted for GFP positive cells for clonal expansion. Figure 3.1A represents the final CRISPR constructs to produce KO cell lines. Figure 3.1B represents the protocol for mesoderm differentiation of Apelin KO, Aplnr KO and Elabela KO mESCs. EBs, formed from the KO cells in low attachment plates, were transferred to matrigel-gelatin coated plates at day 2 and migration of the EBs were observed until day 6. Apelin-13 or ML233 was added to the media between day 2 and day 6 (Figure 3.1B). Morphological pictures of the EBs were taken at day 2, day 3 and day 6 during migration and mesoderm differentiation of EBs (Figure 1D, 1G, 1J, 1M). While there was no noticeable difference at the core area and total area of Aplnr KO and Ela KO EBs at day 3 and day 6 with Apelin-13 or ML233 treatment compared to non-treated EBs, core area of Apelin KO group with Apelin-13 treatment reduced 1.4-fold and the total area decreased 1.2-fold compared to the non-treated ones at day 6. Additionally, only migration area of Apelin KO EBs, among the other KO groups, increased with Apelin-13 (1.4-fold) or ML233 (2.3-fold) treatments at day 6 (Figure 3.1H, 3.1I, 3.1K, 3.1L, 3.1N and 3.1O). Migration intensity Apelin KO EBs decreased 3.7-fold at day 3 and core intensity of Apelin KO EB decreased 1.9-fold at day 6 when Apelin-13 was added to the media. Core intensity and migration intensity of Apelin KO EB increased 1.4-fold and 2.2-fold, respectively at day 6 when ML233 was administered to the media (Figure 3.1H and 3.1I). Migration intensity increased 1.5-fold at day 6 for Aplnr KO EBs in the presence of Apelin-13 but decreased about 1.6-fold at day 6 for Elabela KO EBs, treated with Apelin-13 or ML233, compared to the intensity of their non-treated control EBs (Figure 3.1K, 3.1L, 3.1N and 3.1O). Neither total migration area nor total migration intensity changed significantly for Aplnr KO and Ela KO EBs in the presence of Apelin-13 or ML233. On the other hand, both total migration area and total migration intensity of non-treated Apelin KO EBs were 1.5-fold higher than the Apelin-13 treated group. Although total migration area of ML233 treated Apelin KO

EBs were not significantly different than the non-treated ones, total migration intensity of ML233 treated Apelin KO EBs was 1.4-fold higher than the non-treated EBs (Figure 3.1I, 3.1L, and 3.1O). Moreover, total migration area of all the EBs reduced more than 1.2-fold compared to R1 control EBs, except for Apelin-13 and ML233 treated R1 EBs, which increased 1.2-fold and 1.5-fold respectively. Total migration area of Elabela KO EBs, treated or non-treated, decreased about 1.9-fold, while total migration area of Aplnr KO EBs, treated or non-treated, decreased at least 1.2-fold and Apelin KO EB area reduced at least 1.5-fold, treated or non-treated, compared to the area of R1 control EBs (Figure 3.1P). Total migration intensity of Elabela KO EBs, treated or non-treated, decreased about 3-fold, while total migration intensity of Aplnr KO EBs, treated or non-treated, decreased at least 2-fold and total migration intensity of Apelin KO EBs reduced at least 2-fold, treated or non-treated, compared to the area of R1 control EBs. Additionally, total migration intensity of R1 increased 1.6-fold and 2-fold when Apelin-13 and ML233, respectively, was administered to the media (Figure 3.1R).

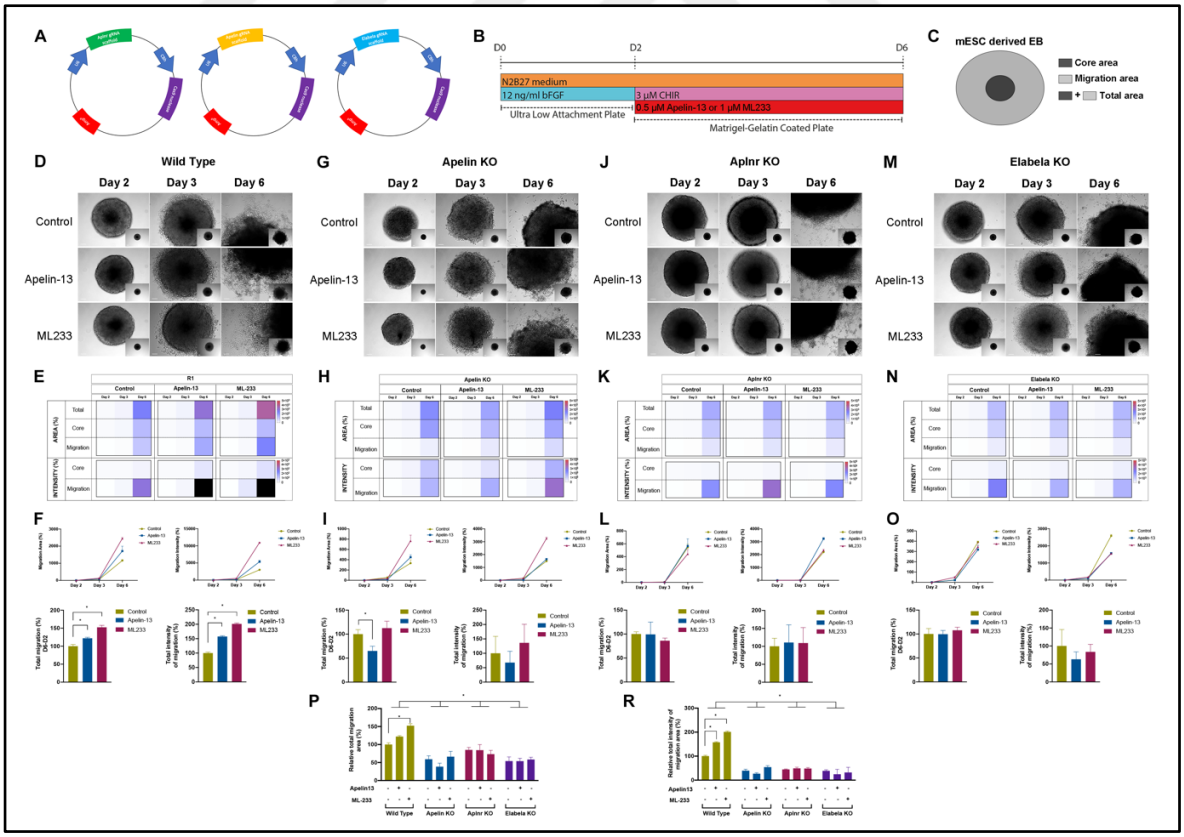


Figure 3.1. Effect of knocking out Apelin, Aplnr and Elabela on migration of EBs during mesoderm differentiation of mESCs. A. CRISPR constructs, carrying the gRNA scaffolds of Aplnr signaling components, to generate Apelin KO, Aplnr KO and Elabela KO cell

lines. B. The protocol for mesoderm differentiation of mESC. EBs, formed from mESCs, were transferred to matrigel-gelatin coated surface at day 2 and migration of the EBs were observed until day 6. Apelin-13 or ML233 was optionally added at day 2 to activate Aplnr signaling. C. Graphical illustration which represents total area, core area and migration area of EBs. D. Morphological pictures of the EBs were taken at day 2, day 3 and day 6 for wild type cells. E. Total area, core area and migration area (total area-core area) as well as core intensity and migration intensity were measured at day 2, day 3 and day 6 and visualized as a heat map for Control, Apelin-13 and ML233 treated wild type EBs and F. scattered line graphs of migration area and migration intensity as well as total migration area and total migration intensity between day 6 and day 2 were drawn. G. Morphological pictures of the EBs were taken at day 2, day 3 and day 6 for Apelin KO cells. H. Total area, core area and migration area (total area-core area) as well as core intensity and migration intensity were measured at day 2, day 3 and day 6 and visualized as a heat map for Control, Apelin-13 and ML233 treated Apelin KO EBs and I. scattered line graphs of migration area and migration intensity as well as total migration area and total migration intensity between day 6 and day 2 were drawn. J. Morphological pictures of the EBs were taken at day 2, day 3 and day 6 for Elabela KO cells. K. Total area, core area and migration area (total area-core area) as well as core intensity and migration intensity were measured at day 2, day 3 and day 6 and visualized as a heat map for Control, Apelin-13 and ML233 treated Elabela KO EBs and L. scattered line graphs of migration area and migration intensity as well as total migration area and total migration intensity between day 6 and day 2 were drawn. M. Morphological pictures of the EBs were taken at day 2, day 3 and day 6 for Aplnr KO cells. N. Total area, core area and migration area (total area-core area) as well as core intensity and migration intensity were measured at day 2, day 3 and day 6 and visualized as a heat map for Control, Apelin-13 and ML233 treated Aplnr KO EBs and O. scattered line graphs of migration area and migration intensity as well as total migration area and total migration intensity between day 6 and day 2 were drawn. P. Bar graphs of total migration area (day 6 Area - day 2 Area) and R. total migration intensity (day 6 Intensity - day 2 Intensity) compared to the ones of R1 were drawn. Scale bar: 50μm, 100μm. *P<0.05

The protocol for mesoderm differentiation of shRNA lentivirus treated mESCs was schematically displayed in Figure 3.2A. After the lentiviral transduction of mESCs, the

selected colonies were used to generate EBs. The EBs were transferred onto matrigel-gelatin coated plate at day 2 and migration of the EBs were observed until day 6 (Figure 3.2A). Reduced expression of Apelin and Aplnr genes in shApelin and shAplnr treated cells were demonstrated (Figure 3.2B). Morphological images of the EBs were taken at day 2, day 3 and day 6 during migration and differentiation of EBs into mesoderm cells (Figure 3.2C). Total area of shAplnr EB reduced 1.5-fold at day3 and day 6, while its migration area decreased 8-fold at day 3 and 10-fold at day 6 compared to shControl EB. Migration area of shApelin EB also reduced 1.3-fold at day 6 compared to shControl EB. On the other hand, core area of both shApelin EB and shAplnr EB increased 2-fold at day 6 compared to core area of shControl EB (Figure 3.2D, 3.2E and 3.2F). Moreover, core intensity shApelin EB was upregulated 1.4-fold and 2-fold at day 3 and day 6, respectively, while core intensity shAplnr EB was upregulated approximately 3-fold and 4-fold at day 3 and day 6, respectively, compared to the intensity of shControl EB. On the other hand, migration intensity of shAplnr reduced 8.4-fold and 11-fold at day 3 and day 6, respectively, and migration intensity of shApelin decreased 1.3-fold at day 3 compared to the intensity of shControl EB (Figure 3.2D, 3.2E and 3.2F).

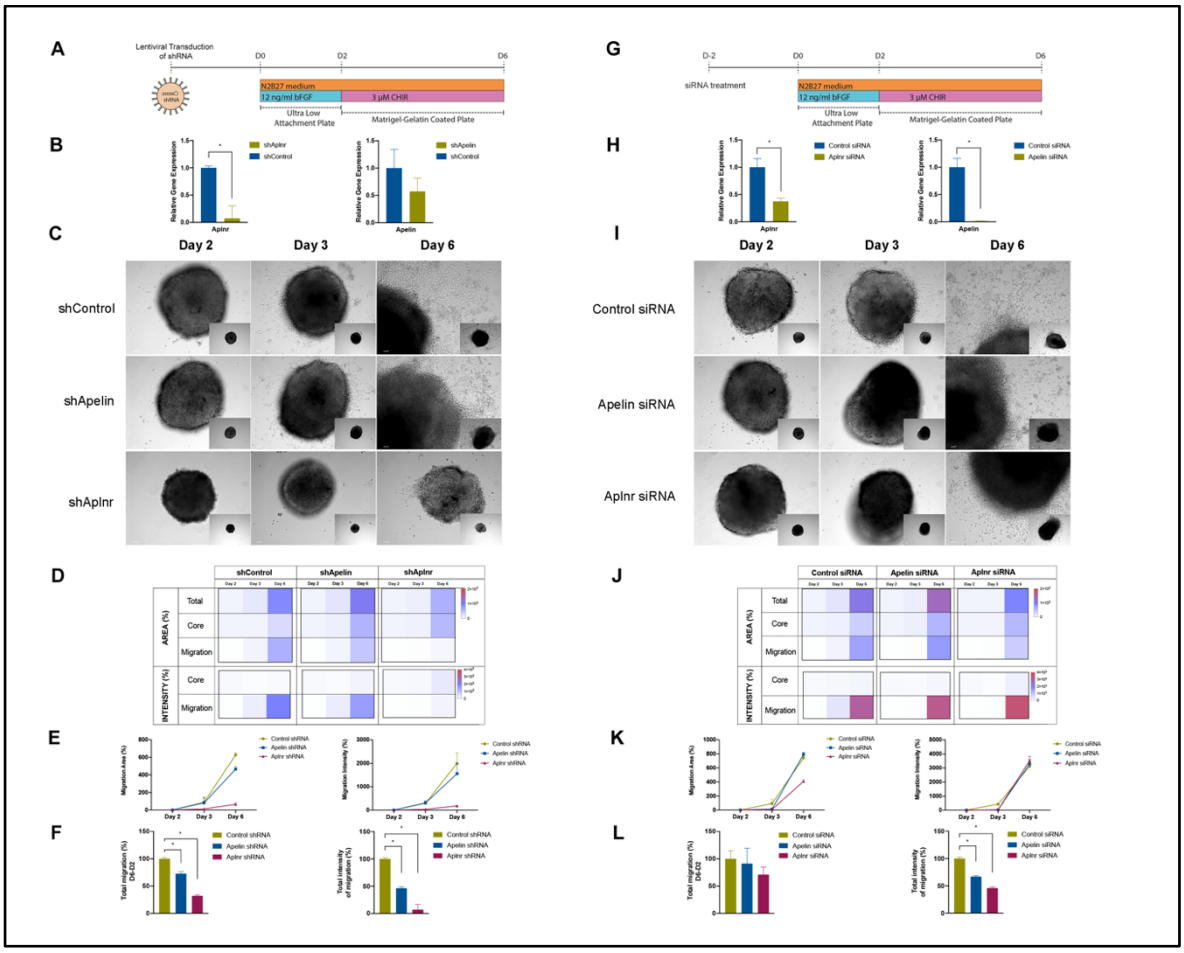


Figure 3.2. Effect of shRNA and siRNA mediated silencing of Aplnr signaling on migration of EBs during mesoderm differentiation of mESCs. A. Protocol for mesoderm differentiation of mESCs after lentiviral transduction of shApelin, shAplnr and shControl lentiviruses. EBs, formed from mESCs, were transferred to matrigel-gelatin coated surface at day 2 and incubated until day 6. B. Bar graph representation of qPCR analysis indicates relative gene expression of Apelin and Aplnr in the cells administered with the shRNA viruses. C. Morphological pictures of the EBs were taken at day 2, day 3 and day 6. D. Total area, core area and migration area (total area-core area) as well as core intensity and migration intensity were measured at day 2, day 3 and day 6 and visualized as a heat map. E. Scattered line graphs of migration area and migration intensity at day 2, day 3 and day 6 as well as F. bar graphs of total migration area and total migration intensity between day 6 and day 2 were drawn. G. Protocol for mesoderm differentiation of mESCs after siRNA treatment. H. Bar graph representation of qPCR analysis indicates relative gene expression of Apelin and Aplnr in the cells treated with Apelin siRNA, Aplnr siRNA and Control siRNA. I. Morphological pictures of the EBs were taken at day 2, day 3 and day 6. J. Total area, core area and migration area (total area-core area) as well as core intensity and

migration intensity were measured at day 2, day 3 and day 6 and visualized as a heat map. K. Scattered line graphs of migration area and migration intensity at day 2, day 3 and day 6 as well as L. bar graphs of total migration area and total migration intensity between day 6 and day 2 were drawn for the siRNA treated EBs. Scale bar: 50µm, 100µm. *P<0.05

The protocol for mesoderm differentiation of siRNA treated mESCs was schematically displayed in Figure 3.2G. siRNA treated mESCs were used to form EBs. The EBs were transferred onto matrigel-gelatin coated plate at day 2 and migration of the EBs were observed until day 6 (Figure 3.2G). Significantly reduced expression of Apelin and Aplnr in Apelin siRNA and Aplnr siRNA treated cells were demonstrated before the cells were used to generate EBs (Figure 3.2H). Morphological images of the EBs were taken at day 2, day 3 and day 6 during migration and differentiation of EBs into mesoderm cells (Figure 3.2I). Core area, total area and migration area of the EBs as well as their intensities were measured at day 2, day 3 and day 6 as schematically indicated in Figure 3.2J. Total area and migration area were 1,5-fold and 7.5-fold, respectively, smaller for Apelin siRNA treated EBs at day 3 compared to the ones of Control siRNA treated EBs, yet, their total area and core area became 1.2-fold and 1.5-fold, respectively, larger at day 6 compared to the control EBs. Similarly, total area and migration area of Aplnr siRNA treated EBs decreased 2-fold and 15-fold, respectively, at day 3 and reduced 1.2-fold and 1.8-fold, respectively at day 6 compared to the control siRNA administered EBs. Core and migration intensity were 1.5-fold and 18-fold, respectively, lower for Apelin siRNA treated EBs and 2.3-fold and 16-fold, respectively, lower for Aplnr siRNA treated EBs at day 3 compared to Control EBs. However, their intensities became like the intensities of Control EB at day 6 (Figure 3.2J, 3.2K and 3.2L). The overall data showed that KO or silence of any component of Aplnr signaling lead to significant reduction at migration area and migration intensity of the EBs during mesoderm differentiation. However, small molecule and peptide induced activation of functional Aplnr enhances migration area and migration intensity. These results indicate importance of Aplnr signaling activity in promotion of cell movement during mesoderm differentiation of mESCs.

3.1.2. Selection of Mesoderm Differentiation Media to Generate Aplnr Positive and Aplnr Negative Cells

Various protocols were tested by changing the media ingredients for mesoderm differentiation to determine the highest number of positive cells for Aplnr (Figure 3.3A). Morphological images of the EBs were taken at day 2, day 3 and day 6 during migration and differentiation of EBs. Option I and Option III formed neural rosettes like structures and with neurites growing out from the EBs. A branched morphology was observed at Option I and Option III at day 6 (Figure 3.3B). Total area and migration area increased significantly for the EBs of Option I, III and V at day 3, compared to other groups. On the other hand, whereas EBs of Option V demonstrated the most significant enlargement at total area and migration area, core area of Option IV EBs increased the most at day 6 compared to the others. Furthermore, although Option I, III and V had higher core and migration intensity at day 3, Option III and IV had significantly higher core and migration intensity at day 6 compared to others (Figure 3.3C and 3.3D). The groups were investigated for expression of neural rosette markers, OTX1, Pax3 and ZBTB16, and compared to day 0 R1 cells. Option I and Option III expressed all the markers at least 15-fold higher than R1 cells. Option II expressed ZBTB16 approximately 30-fold higher than R1. While ZBTB16 was expressed in Option IV at the same level with R1, its expression in Option V and Option VI was 15-fold and 20-fold higher than the expression in R1. Expression of Pax3, a paraxial mesoderm marker, was enhanced 6-fold in Option IV and reduced 100-fold in Option V compared to R1, while it wasn't expressed in Option VI. Also, OTX1 wasn't expressed in Option IV, Option V and Option VI (Figure 3.3E). In addition, amount of Aplnr positive cells were detected with flow cytometry for each option set at day 2, day 3 and day 6 during mesoderm differentiation. Option III and Option IV had significantly higher Aplnr positive cells at day 2, day 3 and day 6 compared to other groups. On the other hand, Option V and Option VI had lower Aplnr positive cells compared to other groups at day 2, day 3 and day 6 (Figure 3.3F and 3.3G). By considering the data, FGF basic and CHIR have a significant effect on Aplnr expression during mesoderm differentiation of EBs and Option IV media led to generation of more Aplnr positive cells with mesoderm-like morphology. Moreover, Option IV media not only led to significantly increased core area and intensity but also caused higher migration intensity compared to the other groups. Thus, Option IV media was selected for the further experiments.

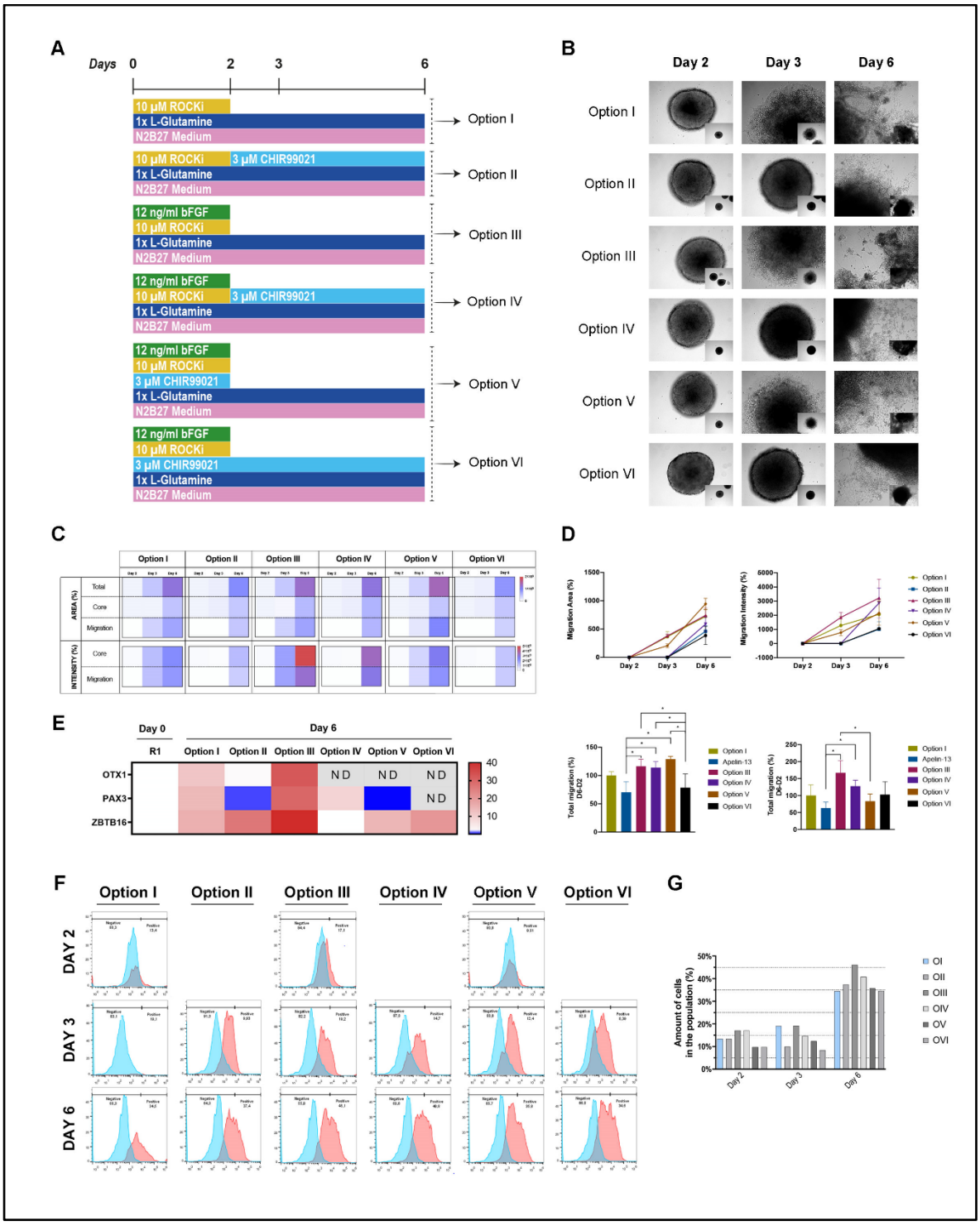


Figure 3.3. Effect of medium ingredients on Aplnr expression and migration of mESCs-derived EBs during mesoderm differentiation. A. Medium supplements for each media options and timeline for mesoderm differentiation of R1 mESCs were shown. mESCs were used at day 0 to form EBs. The EBs were transferred to matrigel-gelatin coated surface at day 2 and their migration were observed until day 6. B. Morphological pictures of the EBs were taken at day 2, day 3 and day 6. C. Total area, core area and migration area (total

area-core area) as well as core intensity and migration intensity were measured at day 2, day 3 and day 6 and visualized as a heat map. D. Scattered line graphs of migration area and migration intensity at day 2, day 3 and day 6 as well as bar graphs of total migration area and total migration intensity between day 6 and day 2 were drawn. E. Heatmap of relative gene expression for neural rosette markers. ND: not detected. F. Detection of Aplnr expression by flow cytometry at day 2, day 3 and day 6 EBs. G. Percentage of Aplnr positive cells in the populations were shown in the graph. Scale bar: 50μm, 100μm. *P<0.05

3.1.3. Activation of Aplnr Enhances Paraxial Mesoderm Differentiation of mESCs

To investigate the role of Aplnr on mesoderm differentiation of mESCs, Aplnr was activated with Apelin-13 or ML233. The protocol for mesoderm differentiation of mESCs was schematically represented in Figure 3.4A. Briefly, mESCs-derived EBs were transferred to matrigel-gelatin coated wells at day 2 and 0.5uM Apelin-13 peptide or 1uM ML233 were added to the media. Expression of Apelin and Aplnr genes at day 3, next day of Apelin-13 administration to the media, were presented in Figure 3.4B. IF data of EBs at day 3 shows that although Flk1, a lateral mesoderm marker, didn't show a noticeable change with addition of Apelin-13 or ML233, expression level of Pdgfrα, a paraxial mesoderm marker, increased 1.3-fold in Apelin-13 treated group and almost 2-fold in ML233 treated group compared to the expression level in Control. Apelin expression level increased 1.3-fold and 2.5-fold in the presence of Apelin-13 and ML233, respectively. Also, Aplnr expression level increased 1.3-fold with ML233 treatment compared to the control EBs. Furthermore, Apelin-13 and ML233 led to 2-fold downregulation of ectoderm marker, Sox2, and Akt. Also, MyoD expression was not significantly changed whereas Mek, mTOR and Erk1/2 expressions were enhanced about 1.3-fold, 1.4-fold and 1.2-fold, respectively, with Apelin-13 and ML233 treatments compared to non-treated R1 EBs (Figure 4C and 4D). Furthermore, according to the mRNA expression levels at day 6, addition of Apelin-13 enhanced gene expression level of Pdgfrα and Brachyury (Bra), which are paraxial mesoderm markers, up to 10-fold and 2-fold, Flk1 up to 3-fold and Aplnr up to 2-fold. Meox1 and Pax1, somitic markers of paraxial mesoderm, were also expressed in both groups. Endoderm markers, Sox17 and Cxcr4, were expressed at very low level, while Sox2 and Nestin expression were not observed in neither of the groups. Foxa2, early mesoderm

and endoderm marker, was expressed at low level only in Apelin-13 treated group. Interestingly, Apelin expression level significantly downregulated and Bax expression level increased 1.4-fold in the presence of Apelin-13 at day 6 (Figure 3.4E).

Moreover, antibody array was performed for Control and Apelin-13 treated cells at day 6 (Table 3.1) and the membranes were shown in Figure 3.5A. Hierarchical cluster analysis and heat map analysis showed that the repeats of Control and repeats of Apelin-13 are highly correlated, 0.95 and 0.93 correlation coefficient values, respectively, while control and Apelin groups were not grouped closely, the correlation coefficient values between 0.55 and 0.65 (Figure 3.5B, 3.5C and 3.5D). The results indicated that LIF expression, which inhibits differentiation of mESC to mesoderm and endoderm cells and maintains the self-renew and pluripotency of mouse PSCs [168,169], significantly increased in Apelin-13 treated cells compared to control cells. Also, Frizzled 1 and Frizzled 7 expressions significantly reduced in Apelin-13 treated group compared to control group (Figure 3.5E). Taken together, the data indicates that activation of Aplnr signaling improves paraxial mesoderm commitment of mESCs.

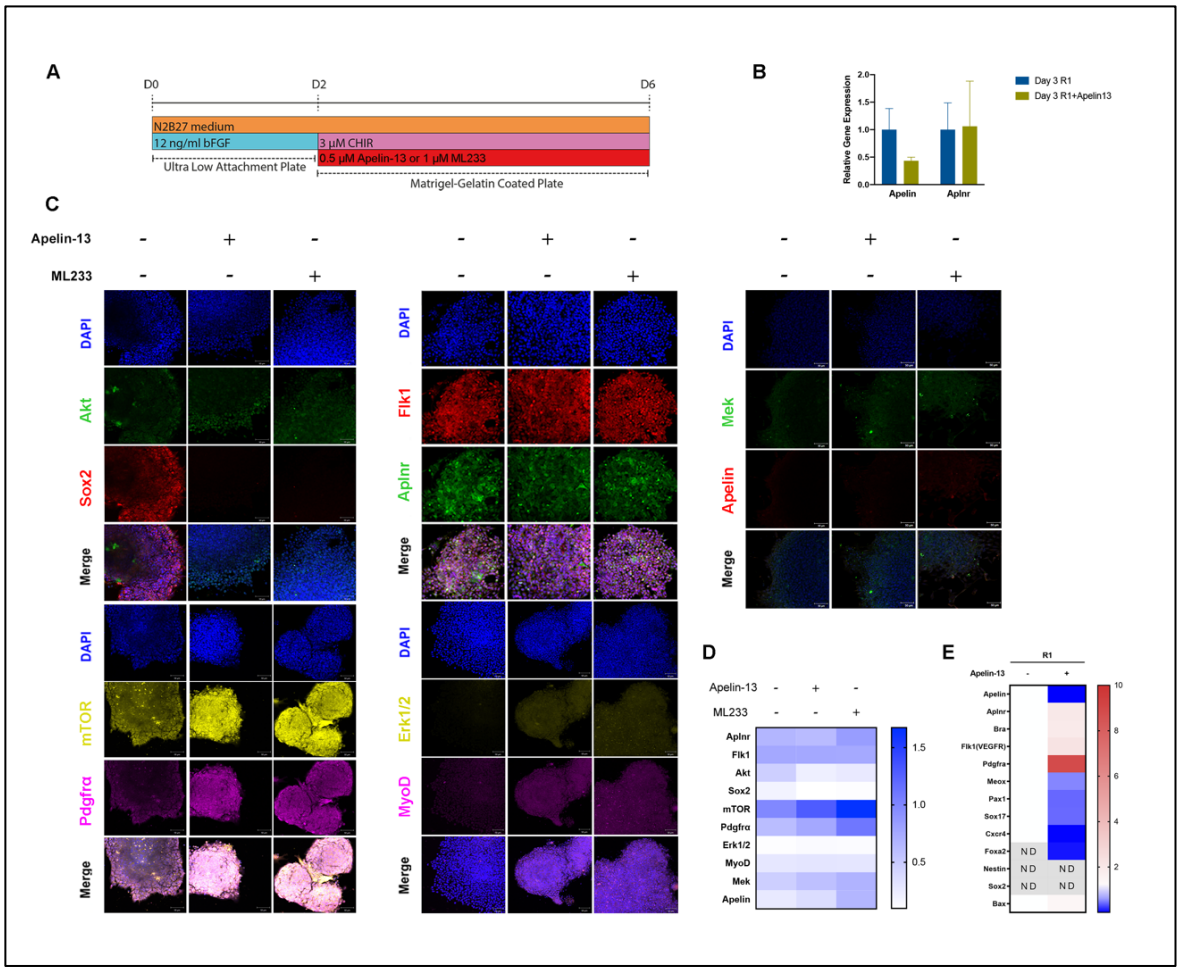


Figure 3.4. Effect of Aplnr signaling on Mesoderm Differentiation of mESCs. A. The protocol for mesoderm differentiation of mESC. EBs, formed from mESCs, were transferred to matrigel-gelatin coated surface at day 2 and migration of the EBs were observed until day 6. Apelin-13 or ML233 was optionally added at day 2 to activate Aplnr signaling. B. Bar graph representation of qPCR analysis indicates relative Apelin and Aplnr gene expressions in Control and Apelin-13 treated EBs at day 3 and day6. C. The EBs were fixed using 4% paraformaldehyde at the end of day3 and they were analyzed for protein expression of the Apelin, Aplnr, ectoderm marker protein, Sox2, the related pathway proteins, Akt and mTOR, MAPK pathway proteins involved in mesoderm commitment, Mek and Erk1/2, Pdgfrα, which guides migration of mesoderm cells, and mesoderm markers, Flk1 and MyoD. DAPI was used to stain nuclei of the cells. D. Immunofluorescence analysis and the intensity of the expression as a heat map were shown. E. Relative gene expression levels of the EBs at day 6 were shown as a heatmap. ND: not detected. Scale bar: 50μm.

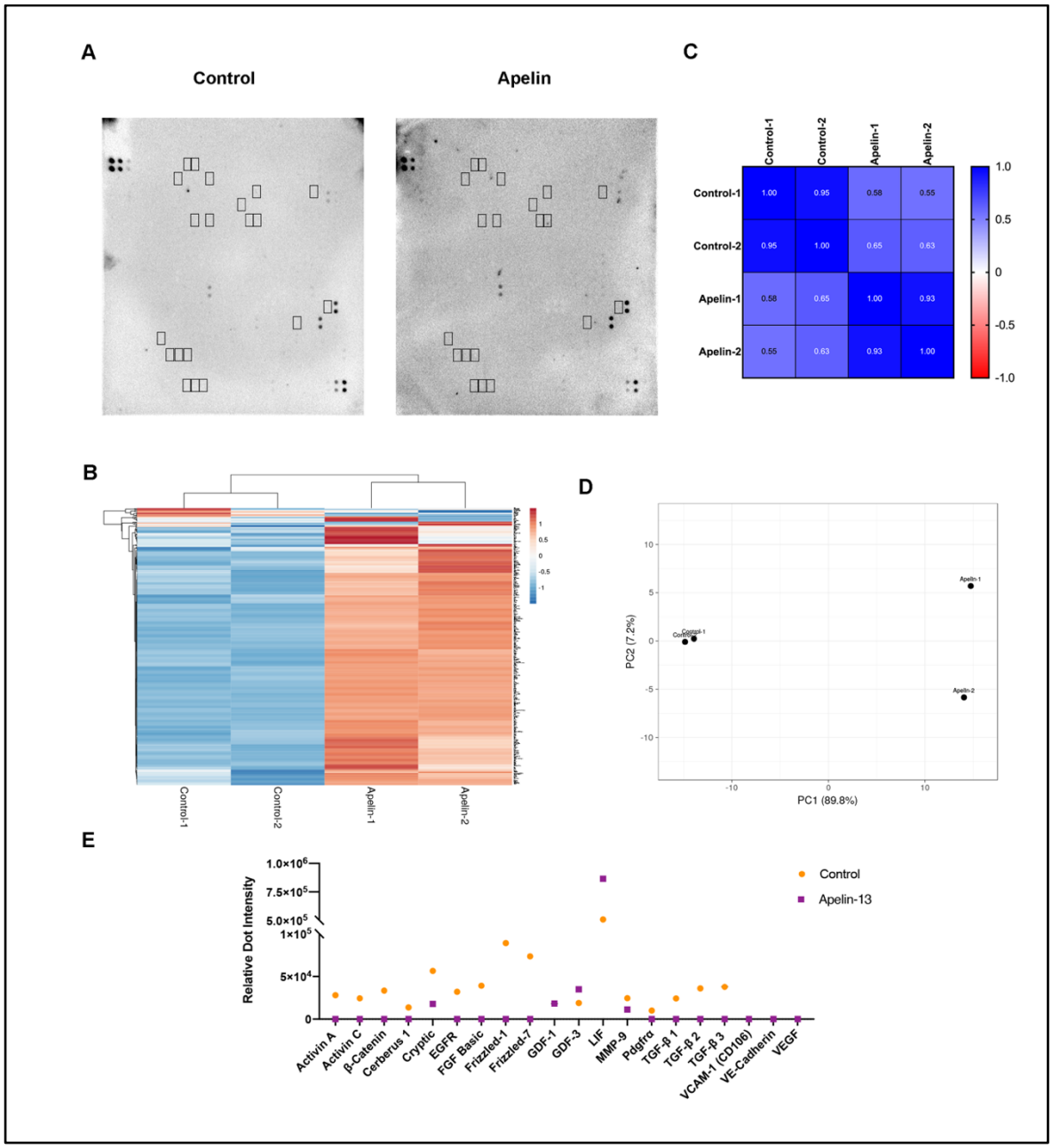


Figure 3.5. Antibody array profile of mESC derived EBs treated with Apelin-13. A. Membranes of the antibody array. Mesoderm related proteins were selected with black boxes on the membranes. B. Hierarchical cluster analysis and heat map representation of proteins from Control and Apelin-13 treated EBs at day 6. C. Correlation coefficient matrix of the proteins. D. Principal component analysis (PCA) of the cells. E. A scattered graph indicating relative dot intensity for Control and Apelin-13 treated groups.

Table 3.1. Protein list screened by antibody array for Control and Apelin-13 treated groups at day 6. Significantly increased (red) and decreased (black) proteins in Apelin-13 treated group compared to control group were highlighted on the table.

Description	**Control**	**Apelin**	**Abundance Ration: Apelin/ Control**
CRP	219589,7	1,1	**0,00001**
CCL7 / MCP-3 / MARC	151849,7	1,1	**0,00001**
CXCL14 / BRAK	137639,7	1,1	**0,00001**
Fas / TNFRSF6	119719,7	1,1	**0,00001**
IL-21 R	117199,7	1,1	**0,00001**
FAM3B	115137,7	1,1	**0,00001**
M-CSF	107891,7	1,1	**0,00001**
IL-22BP	106587,7	1,1	**0,00001**
Progranulin	104465,7	1,1	**0,00001**
IL-21	103339,7	1,1	**0,00001**
IL-23	101417,7	1,1	**0,00001**
IL-23 R	101031,7	1,1	**0,00001**
FLRG (Follistatin)	96565,7	1,1	**0,00001**
Fit-3 Ligand	96111,7	1,1	**0,00001**
ICAM-1	95899,7	1,1	**0,00001**
IL-13	94449,7	1,1	**0,00001**
MDC	94329,7	1,1	**0,00001**
PlGF-2	94179,7	1,1	**0,00001**
IL-24	92529,7	1,1	**0,00001**
Prolactin	92303,7	1,1	**0,00001**

Frizzled-1	89063,7	1,1	**0,00001**
Dkk-3	88805,7	1,1	**0,00001**
DKK-1	88575,7	1,1	**0,00001**
Granzyme B	88535,7	1,1	**0,00001**
IL-22	87741,7	1,1	**0,00001**
FADD	86203,7	1,1	**0,00001**
IL-15	85073,7	1,1	**0,00001**
HVEM / TNFRSF14	84767,7	1,1	**0,00001**
MFG-E8	84069,7	1,1	**0,00001**
MFRP	84059,7	1,1	**0,00001**
IL-13 R alpha 2	82987,7	1,1	**0,00001**
GM-CSF	82075,7	1,1	**0,00001**
HGF	82031,7	1,1	**0,00001**
Fractalkine	81739,7	1,1	**0,00001**
ICAM-5	81619,7	1,1	**0,00001**
HGF R	80379,7	1,1	**0,00001**
FGF-21	80239,7	1,1	**0,00001**
MCP-5	80065,7	1,1	**0,00001**
Glut2	79733,7	1,1	**0,00001**
Follistatin-like 1	78717,7	1,1	**0,00001**
TGF-beta RII	77915,7	1,1	**0,00001**
Frizzled-6	76863,7	1,1	**0,00001**
Epiregulin	76431,7	1,1	**0,00001**
Dkk-4	75603,7	1,1	**0,00001**

PF-4	75359,7	1,1	**0,00001**
CD14	74817,7	1,1	**0,00001**
Frizzled-7	73547,7	1,1	**0,00002**
P-Selectin	73111,7	1,1	**0,00002**
MIG	73069,7	1,1	**0,00002**
IL-7	72545,7	1,1	**0,00002**
FGF R5 beta	72523,7	1,1	**0,00002**
Thrombospondin	70287,7	1,1	**0,00002**
Dtk	69871,7	1,1	**0,00002**
CD27 / TNFRSF7	68399,7	1,1	**0,00002**
GITR	65727,7	1,1	**0,00002**
IL-1 R4 / ST2	65119,7	1,1	**0,00002**
DPPIV / CD26	65061,7	1,1	**0,00002**
IFN-alpha / beta R1	62683,7	1,1	**0,00002**
CD27 Ligand / TNFSF7	61975,7	1,1	**0,00002**
MCP-1	61111,7	1,1	**0,00002**
TGF-beta RI / ALK-5	60745,7	1,1	**0,00002**
DR3 / TNFRSF25	60285,7	1,1	**0,00002**
GFR alpha-4 / GDNF R alpha-4	59527,7	1,1	**0,00002**
GITR Ligand / TNFSF18	58887,7	1,1	**0,00002**
TLR2	57769,7	1,1	**0,00002**
IL-20 R alpha	57425,7	1,1	**0,00002**
Pentraxin3 / TSG-14	57257,7	1,1	**0,00002**
IL-1 alpha	56603,7	1,1	**0,00002**

B7-1/CD80	55115,7	1,1	**0,00002**
IL-1 beta	52389,7	1,1	**0,00002**
RAGE	52171,7	1,1	**0,00002**
Tie-2	51955,7	1,1	**0,00002**
Thymus Chemokine-1	51179,7	1,1	**0,00002**
IL-5 R alpha	50017,7	1,1	**0,00002**
MAdCAM-1	49331,7	1,1	**0,00002**
Activin RIB / ALK-4	47879,7	1,1	**0,00002**
TIMP-1	45189,7	1,1	**0,00002**
Galectin-3	42519,7	1,1	**0,00003**
PDGFR beta	41555,7	1,1	**0,00003**
EDAR	40609,7	1,1	**0,00003**
BAFF R / TNFRSF13C	40515,7	1,1	**0,00003**
CD30 L	40241,7	1,1	**0,00003**
bFGF	39239,7	1,1	**0,00003**
MIP-1 alpha	38113,7	1,1	**0,00003**
TGF-beta 3	37897,7	1,1	**0,00003**
Adiponectin / Acrp30	37817,7	1,1	**0,00003**
IL-27	37151,7	1,1	**0,00003**
S100A10	36845,7	1,1	**0,00003**
IL-10 R alpha	36345,7	1,1	**0,00003**
TLR1	36211,7	1,1	**0,00003**
TGF-beta 2	36015,7	1,1	**0,00003**
SCF R / c-kit	35123,7	1,1	**0,00003**

B-Catenin	33397,7	1,1	**0,00003**
IGF-II	33097,7	1,1	**0,00003**
TLR3	32443,7	1,1	**0,00003**
EGFR	32009,7	1,1	**0,00003**
IL-10	31669,7	1,1	**0,00004**
TLR4	30667,7	1,1	**0,00004**
SIGIRR	30651,7	1,1	**0,00004**
IL-3 R beta	30233,7	1,1	**0,00004**
Resistin	28887,7	1,1	**0,00004**
Shh-N	28443,7	1,1	**0,00004**
Activin A	28107,7	1,1	**0,00004**
GFR alpha-3 / GDNF R alpha-3	28049,7	1,1	**0,00004**
TL1A / TNFSF15	27353,7	1,1	**0,00004**
FGF R3	27225,7	1,1	**0,00004**
IGF-I	27135,7	1,1	**0,00004**
RANTES	25205,7	1,1	**0,00004**
SLPI	24553,7	1,1	**0,00005**
Activin C	24413,7	1,1	**0,00005**
CRG-2	24343,7	1,1	**0,00005**
TGF-beta 1	24259,7	1,1	**0,00005**
TMEFF1 / Tomoregulin-1	23843,7	1,1	**0,00005**
Serum Amyloid A1	22061,7	1,1	**0,00005**
IL-4	21877,7	1,1	**0,00005**
Neuregulin-3 / NRG3	21663,7	1,1	**0,00005**

CXCL16	21537,7	1,1	**0,00005**
G-CSF	21413,7	1,1	**0,00005**
TIMP-2	20841,7	1,1	**0,00005**
IL-28 / IFN-lambda	20671,7	1,1	**0,00005**
IL-2	20413,7	1,1	**0,00005**
Eotaxin-2	19325,7	1,1	**0,00006**
FCrRIIB / CD32b	19249,7	1,1	**0,00006**
EG-VEGF / PK1	19095,7	1,1	**0,00006**
GFR alpha-2 / GDNF R alpha-2	18393,7	1,1	**0,00006**
GDF-1	18265,7	1,1	**0,00006**
CD30	18137,7	1,1	**0,00006**
TIMP-4	16681,7	1,1	**0,00007**
IL-31	14669,7	1,1	**0,00008**
Cerberus 1	13805,7	1,1	**0,00008**
Granzyme D	13147,7	1,1	**0,00008**
IL-2 R beta	12769,7	1,1	**0,00009**
Endocan	11947,7	1,1	**0,00009**
RELM beta	10339,7	1,1	**0,00011**
PDGFR alpha	10179,7	1,1	**0,00011**
GDF-9	9775,7	1,1	**0,00011**
Fas Ligand	9205,7	1,1	**0,00012**
CD40 Ligand / TNFSF5	8387,7	1,1	**0,00013**
TROY	8365,7	1,1	**0,00013**
Gremlin	8069,7	1,1	**0,00014**

CD40	7317,7	1,1	**0,00015**
TSLP	7253,7	1,1	**0,00015**
TPO	5845,7	1,1	**0,00019**
Soggy-1	3693,7	1,1	**0,00030**
TSLP R	3407,7	1,1	**0,00033**
GDF-8	2671,7	1,1	**0,00042**
Granzyme G	2633,7	1,1	**0,00042**
I-TAC	1381,7	1,1	**0,00080**
TREM-1	953,7	1,1	**0,00116**
Neurturin	217,7	1,1	**0,00510**
Axl	178009,7	4548,2	**0,02555**
Growth Hormone R	57233,7	1886,9	**0,03297**
E-Selectin	98023,7	4699,2	**0,04794**
Erythropoietin (EPO)	84837,7	4266,1	**0,05028**
ICAM-2 / CD102	77071,7	5485,6	**0,07118**
IL-12 R beta 1	87555,7	6267,6	**0,07158**
Cripto	45377,7	3473,0	**0,07654**
IGFBP-2	11817,7	1093,9	**0,09256**
FGF R4	36449,7	3715,1	**0,10193**
IGFBP-rp1 / IGFBP-7	19583,7	2195,7	**0,11212**
CCL4 / MIP-1 beta	126413,7	14677,9	**0,11611**
MIP-1 gamma	13921,7	2177,9	**0,15644**
IL-6	77237,7	12123,2	**0,15696**
MIP-3 alpha	24233,7	4175,0	**0,17228**

ICK	71655,7	12423,1	**0,17337**
Artemin	169107,7	30969,8	**0,18314**
Epigen	63397,7	11950,0	**0,18849**
Common gamma Chain / IL-2 R gamma	5839,7	1105,0	**0,18922**
Angiopoietin-like 3	118779,7	22504,0	**0,18946**
CTLA-4 / CD152	145147,7	31287,5	**0,21556**
Crossveinless-2	57727,7	13271,7	**0,22990**
IL-1 R9	75571,7	19425,1	**0,25704**
CD11b	67941,7	19338,4	**0,28463**
MIP-2	48697,7	13929,3	**0,28604**
AR (Amphiregulin)	139643,7	41419,4	**0,29661**
CCL1 / I-309 / TCA-3	112645,7	34919,5	**0,30999**
Cryptic	56585,7	17819,0	**0,31490**
IL-1 RI	69855,7	22857,2	**0,32721**
Decorin	87951,7	29465,9	**0,33502**
SCF	28761,7	9728,5	**0,33825**
IL-1 RII	66013,7	22552,8	**0,34164**
CCR9	82455,7	30912,0	**0,37489**
IL-3	29053,7	10970,3	**0,37759**
Cardiotrophin-1	57673,7	22039,7	**0,38214**
ALCAM	47793,7	18927,5	**0,39602**
DAN	71563,7	28568,4	**0,39920**
IGFBP-6	17539,7	7014,0	**0,39989**
BTC (Betacellulin)	45461,7	18556,5	**0,40818**

IFN-alpha / beta R2	37365,7	15286,5	**0,40911**
Angiopoietin-like 2	68817,7	28646,2	**0,41626**
SDF-1	42635,7	18016,7	**0,42257**
Csk	87079,7	37194,2	**0,42713**
IL-6 R	70699,7	32473,7	**0,45932**
MMP-9	24517,7	11274,7	**0,45986**
6Ckine	30243,7	45455,7	**1,50298**
IGFBP-1	11469,7	17623,5	**1,53653**
CCR6	68647,7	114379,8	**1,66619**
LIF	507025,7	864588,1	**1,70522**
CXCR3	44617,7	77764,1	**1,74290**
GDF-3	18919,7	34939,5	**1,84673**
CXCR4	48189,7	90801,6	**1,88426**
MMP-24 / MT5-MMP	428683,7	836953,6	**1,95238**
MMP-14 / LEM-2	22145,7	50240,7	**2,26864**
MMP-12	21671,7	61059,0	**2,81746**
IL-7 R alpha	60315,7	180140,7	**2,98663**
CCR4	33811,7	154212,2	**4,56092**
Leptin R	4815,7	22001,9	**4,56882**
Kremen-2	6175,7	30983,1	**5,01697**
CCL8 / MCP-2	20413,7	107882,2	**5,28480**
CCR3	50583,7	281482,0	**5,56468**
IL-16	12697,7	78466,1	**6,17957**
CCR10	3183,7	235962,8	**74,11669**

Coagulation Factor III / Tissue Factor	1,0	3808,4	**3808,44658**
IFN-gamma	1,0	3897,3	**3897,30355**
KC	1,0	5232,4	**5232,37946**
Lefty-1	1,0	8811,1	**8811,09376**
IFN-gamma R1	1,0	9011,0	**9011,02194**
TACI / TNFRSF13B	1,0	10930,3	**10930,33240**
IFN-beta	1,0	11736,7	**11736,70937**
LEPTIN(OB)	1,0	12047,7	**12047,70875**
IL-17	1,0	17017,0	**17017,03456**
TECK	1,0	24163,4	**24163,35605**
TCCR / WSX-1	1,0	27988,6	**27988,64843**
TARC	1,0	43749,7	**43749,65276**
TCA-3	1,0	47443,9	**47443,88112**

3.1.4. Suppression of Aplnr Signaling Activity Hinders Mesoderm Differentiation of mESCs

To investigate the effect of downregulation of Aplnr signaling components on mesoderm differentiation of mESCs, Aplnr and Apelin genes were silenced with shRNA (Figure 3.6) and siRNA (Figure 3.8). Furthermore, Apelin, Aplnr and Elabela genes were knocked out using CRISPR Cas9 technology (Figure 3.9).

The protocol for mesoderm differentiation of shRNA lentivirus-treated mESCs was schematically represented in Figure 3.6A. IF data of the EBs at day 3 showed that Flk1 and Aplnr expression levels were downregulated 1.7-fold and almost 1.2-fold, respectively, in shApelin EBs, and 1.5-fold and 1.3-fold, respectively, in shAplnr EBs compared to the expression levels in shControl EBs. Both Apelin and MyoD expressions increased almost 2-fold and 1.5-fold for shApelin and shAplnr cells, respectively, while Erk1/2 expression was

upregulated 2.6-fold in shApelin and 2.2-fold in shAplnr cells. Expression of Sox2 and Akt were upregulated 3.2-fold and 1.9-fold, respectively for shApelin and 2.6-fold and 1.3-fold, respectively, for shAplnr cells. mTOR and Pdgfrα expressions were not significantly changed in shApelin cells, but both increased approximately 1.4-fold in shAplnr cells (Figure 3.6B and 3.6C). Furthermore, Bra expression was downregulated 10-fold shApelin group but was enhanced 5-fold in shAplnr group compared to shControl group at day 6. Apelin expression was very low at both shApelin and shAplnr EBs, Aplnr expression was not detected in shAplnr EBs and its expression decreased 5-fold in shApelin EBs compared to Control EBs at day 6. In addition to those, Bax expression reduced 2-fold in shApelin EBs yet, increased 5-fold in shAplnr EBs (Figure 3.6D). Moreover, antibody array was performed for shControl and shAplnr cells at day 6 (Table 3.2) and the membranes was shown in Figure 3.7A. Hierarchical cluster analysis and heat map analysis showed that the repeats of shControl and repeats of shAplnr are correlated strongly, with 0.8 and 0.94 correlation coefficient values, respectively, while shControl and shAplnr groups were not correlated, the correlation coefficient values between 0.07 and 0.09 (Figure 3.7B, 3.7C and 3.7D). The results indicated that LIF expression significantly reduced in shAplnr cells compared to shControl cells, while Activin A, Activin B, Activin C, EGFR, FGF basic, Frizzled 1, Frizzled 7, VCAM1, VE-Cadherin and VEGF significantly increased in shAplnr group (Figure 3.7E).

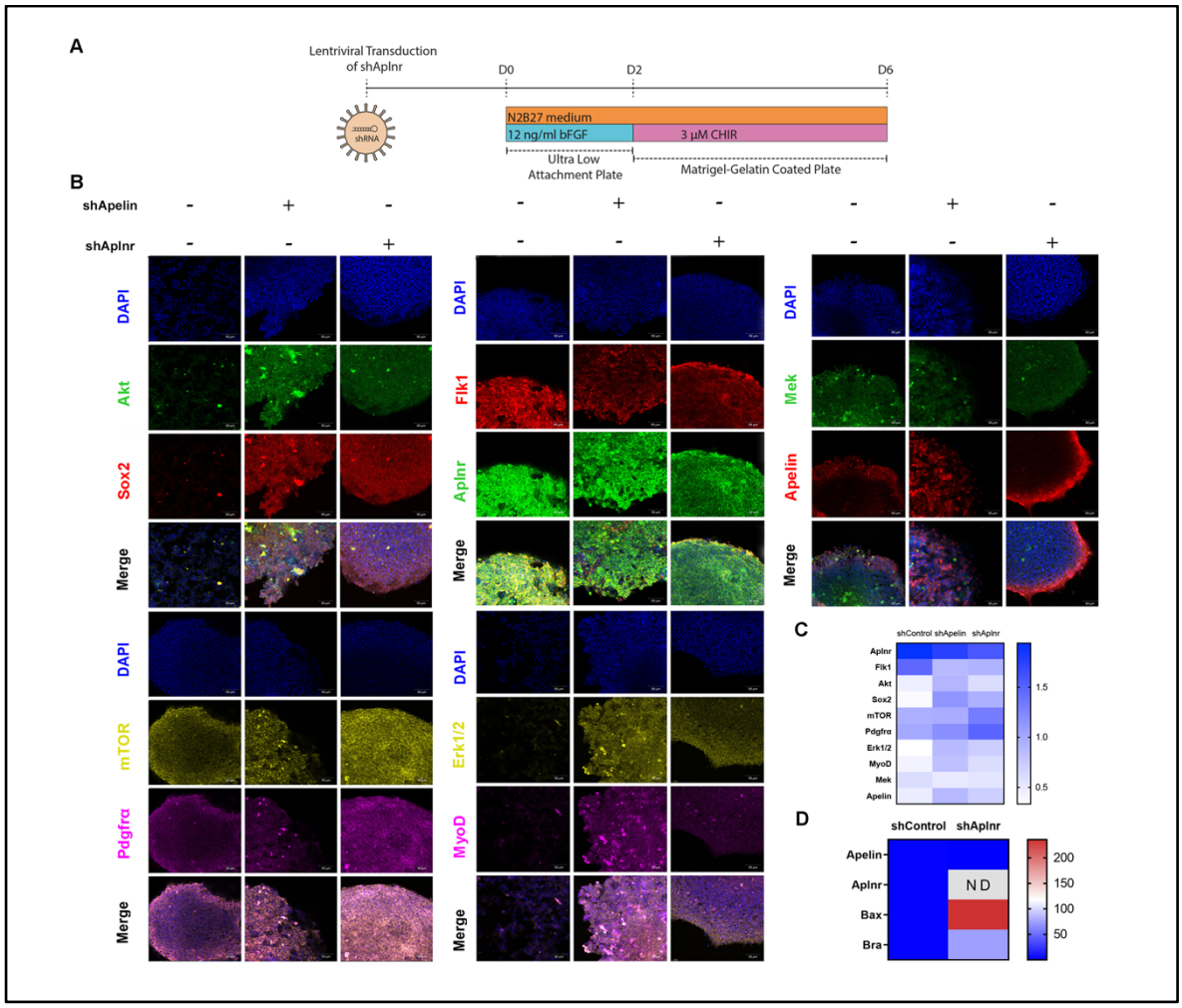


Figure 3.6. Effect of silencing Aplnr signaling components, via shRNA delivery on mesoderm commitment of mESC-derived EBs during mesoderm differentiation. A. Protocol for mesoderm differentiation of mESCs after lentiviral transduction of shApelin, shAplnr and shControl lentiviruses. EBs, formed from mESCs, were transferred to matrigel-gelatin coated surface at day 2 and incubated until day 6. B. The EBs were fixed using 4% paraformaldehyde at the end of day 3 and they were analyzed for protein expression of the Apelin, Aplnr, ectoderm marker protein, Sox2, the related pathway proteins, Akt and mTOR, MAPK pathway proteins involved in mesoderm commitment, Mek and Erk1/2, Pdgfrα, which guides migration of mesoderm cells, and mesoderm markers, Flk1 and MyoD. DAPI was used to stain nuclei of the cells. C. Immunofluorescence analysis and the intensity of the expression as a heat map were shown. D. Heatmap of relative gene expressions. ND: not detected. Scale bar: 50μm.

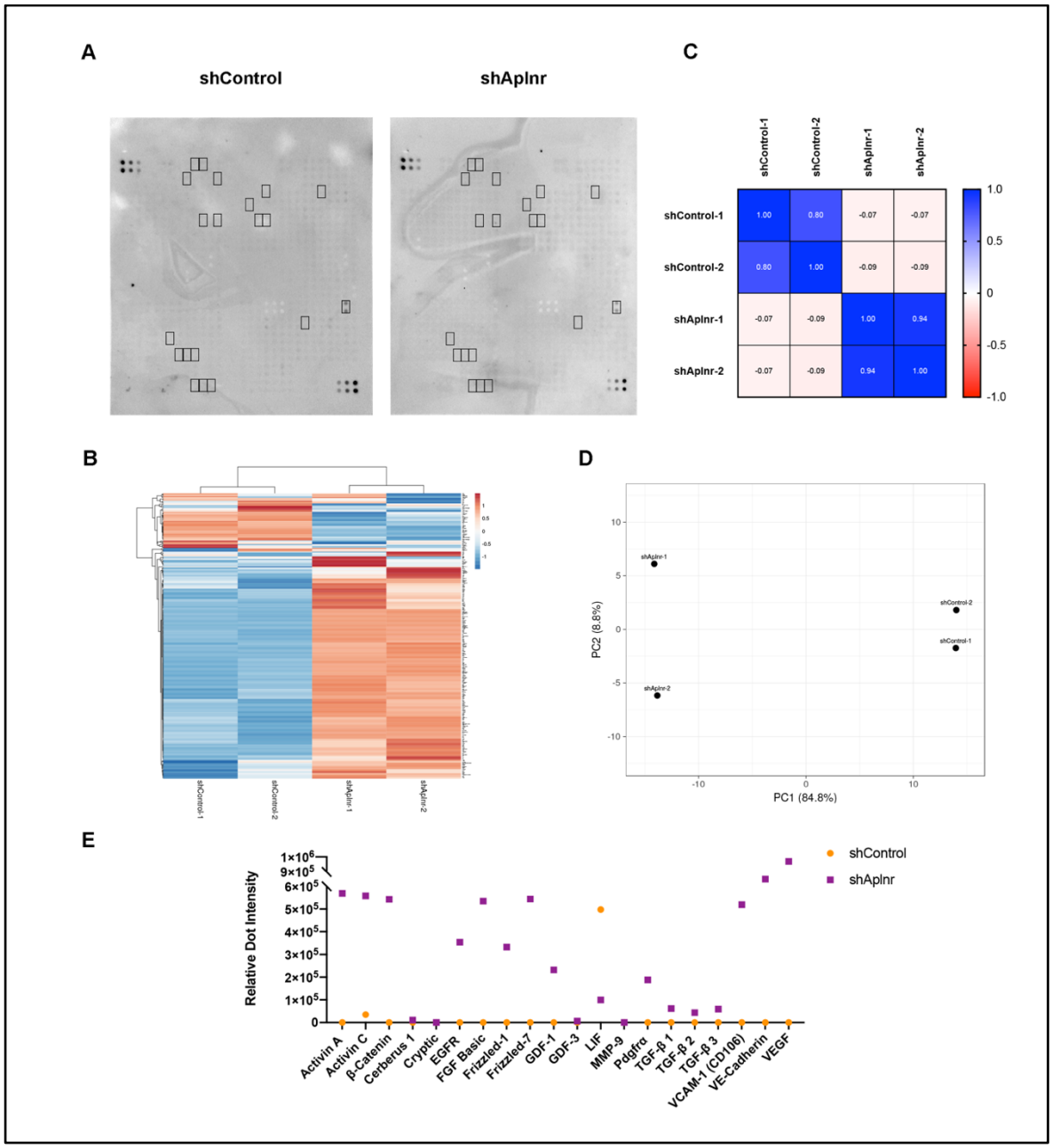


Figure 3.7. Antibody array profile of mESC derived EBs when Aplnr was silenced. A. Membranes of the antibody array. Mesoderm related proteins were selected with black boxes on the membranes. B. Hierarchical cluster analysis and heat map representation of proteins from shControl and shAplnr EBs at day 6. C. Correlation coefficient matrix of the proteins. D. Principal component analysis (PCA) of the cells. E. A scattered graph indicating relative dot intensity for shControl and shAplnr groups.

Table 3.2. Protein list screened by antibody array for shControl and shAplnr groups at day 6. Significantly increased (red) and decreased (black) proteins in shAplnr group compared to shControl group were highlighted on the table.

Description	**shControl**	**shAplnr**	**Abundance Ratio: shAplnr/ Control**
IGFBP-rp1 / IGFBP-7	111181,7	1,3	**0,00001**
GFRa-3 / GDNFRa-3	110821,7	1,3	**0,00001**
IGFBP-6	80179,7	1,3	**0,00002**
IGF-I	55639,7	1,3	**0,00002**
IGFBP-3	52323,7	1,3	**0,00002**
IGFBP-5	51107,7	1,3	**0,00002**
GFRa-2 / GDNFRa-2	47745,7	1,3	**0,00003**
IL-3	46257,7	1,3	**0,00003**
IL-2 R beta	44279,7	1,3	**0,00003**
AgRP	35789,7	1,3	**0,00004**
CTLA-4 / CD152	28145,7	1,3	**0,00005**
GFRa-4 / GDNFRa-4	19101,7	1,3	**0,00007**
IL-9	11495,7	1,3	**0,00011**
LIF	498027,7	99899,5	**0,20059**
IGFBP-1	105375,7	27384,1	**0,25987**
I-TAC	32943,7	62902,8	**1,90941**
HVEM / TNFRSF14	27585,7	58486,4	**2,12017**
IL-13	26917,7	71902,9	**2,67122**
IFN-gamma R1	105013,7	363817,6	**3,46448**
Fit-3 Ligand	47431,7	223304,7	**4,70792**

IFN-gamma	131633,7	628100,8	**4,77158**
IL-13 R alpha 2	38447,7	184832,5	**4,80738**
CCR7	61135,7	400104,5	**6,54453**
Dkk-3	32447,7	214215,9	**6,60189**
IL-12 R beta 1	12147,7	88971,4	**7,32415**
IFN-beta	112199,7	904352,9	**8,06021**
IL-2 R alpha	56771,7	555195,0	**9,77944**
IL-7 R alpha	47971,7	573182,5	**11,94836**
Galectin-3	33517,7	418865,2	**12,49685**
CCR9	33727,7	450271,7	**13,35022**
IL-7	20741,7	301030,0	**14,51330**
Activin C	34999,7	557945,8	**15,94146**
DAN	19047,7	359327,7	**18,86466**
CCR6	20917,7	414311,9	**19,80680**
Decorin	11709,7	246012,8	**21,00938**
IFN-alpha / beta R1	17151,7	398631,5	**23,24156**
IFN-alpha / beta R2	20645,7	544382,2	**26,36787**
CXCR6	17393,7	484398,6	**27,84913**
DKK-1	5841,7	194681,9	**33,32643**
Follistatin-like 1	5649,7	209695,5	**37,11644**
IL-15 R alpha	7363,7	755983,2	**102,66397**
IL-15	1637,7	342486,2	**209,13056**
Adiponectin / Acrp30	325,7	666753,0	**2047,34814**
GDF-3	1,0	6255,5	**6255,48479**

Gremlin	1,0	7343,1	**7343,10124**
Cerberus 1	1,0	10570,5	**10570,45731**
TWEAK / TNFSF12	1,0	19347,4	**19347,44606**
RELM beta	1,0	26641,3	**26641,32146**
TIMP-1	1,0	27424,7	**27424,70954**
TGF-beta 2	1,0	43784,6	**43784,59066**
IL-17R	1,0	58309,0	**58308,96055**
TGF-beta 3	1,0	59675,5	**59675,45302**
TGF-beta 1	1,0	61685,9	**61685,89556**
TFPI	1,0	73964,0	**73964,04592**
TPO	1,0	74818,4	**74818,42062**
IL-23	1,0	76986,0	**76986,04783**
IL-17RC	1,0	80847,2	**80847,21301**
KC	1,0	82026,1	**82026,09798**
IL-22BP	1,0	90321,4	**90321,39180**
IL-20	1,0	91794,4	**91794,36421**
Osteoactivin / GPNMB	1,0	97267,9	**97267,93980**
IL-20 R alpha	1,0	103808,8	**103808,84997**
IL-2	1,0	104052,2	**104052,23267**
Lymphotoxin beta R / TNFRSF3	1,0	122780,0	**122780,02468**
HGF	1,0	122891,6	**122891,57508**
Kremen-1	1,0	123763,7	**123763,69644**
ICAM-5	1,0	127967,1	**127967,11855**
TCCR / WSX-1	1,0	130598,7	**130598,69403**

IL-6 R	1,0	131810,5	**131810,53708**
IL-6	1,0	131985,5	**131985,46840**
Osteoporotegerin	1,0	133225,2	**133225,19904**
MIP-3 alpha	1,0	136224,4	**136224,38382**
OX40 Ligand / TNFSF4	1,0	137666,9	**137666,93339**
Osteopontin	1,0	138120,7	**138120,74072**
TECK	1,0	142260,8	**142260,78192**
L-Selectin	1,0	143203,9	**143203,88990**
MMP-3	1,0	145802,5	**145802,50731**
MCP-1	1,0	149278,3	**149278,31655**
PDGFR beta	1,0	151347,1	**151347,06953**
LRP-6	1,0	152325,7	**152325,67081**
Lymphotactin	1,0	153872,2	**153872,16508**
M-CSF	1,0	161368,9	**161368,85940**
MCP-5	1,0	161480,4	**161480,40981**
CD40 Ligand / TNFSF5	1,0	162464,1	**162464,08157**
RANTES	1,0	163108,0	**163108,03164**
EG-VEGF / PK1	1,0	167298,8	**167298,77757**
Lungkine	1,0	179782,3	**179782,28208**
TSLP R	1,0	180710,2	**180710,17864**
TGF-beta RI / ALK-5	1,0	182264,3	**182264,27861**
MAdCAM-1	1,0	182571,0	**182571,04223**
MIP-2	1,0	183078,1	**183078,08953**
FLRG (Follistatin)	1,0	184961,8	**184961,77024**

PF-4	1,0	185917,6	**185917,55440**
MFG-E8	1,0	186008,8	**186008,82292**
PDGFRa	1,0	188090,3	**188090,25208**
MDC	1,0	188949,7	**188949,69725**
Thymus Chemokine-1	1,0	189350,3	**189350,26462**
HGF R	1,0	189403,5	**189403,50459**
TCA-3	1,0	190164,1	**190164,07554**
MIP-3 beta	1,0	190764,9	**190764,92659**
Tie-2	1,0	193538,5	**193538,47531**
Thrombospondin	1,0	197463,0	**197463,02141**
CD40	1,0	198226,1	**198226,12760**
TARC	1,0	199219,9	**199219,94031**
IL-31	1,0	200908,4	**200908,40781**
RAGE	1,0	201395,2	**201395,17322**
IL-23 R	1,0	205560,6	**205560,56678**
Granzyme G	1,0	206724,2	**206724,24034**
MMP-2	1,0	209462,3	**209462,29575**
Pentraxin3 / TSG-14	1,0	211082,3	**211082,31188**
CCL8 / MCP-2	1,0	216451,9	**216451,94278**
NOV / CCN3	1,0	219220,4	**219220,42103**
Urokinase	1,0	219955,6	**219955,63962**
IL-1 RII	1,0	222739,3	**222739,32929**
GDF-1	1,0	232124,8	**232124,77480**
PDGF C	1,0	237851,9	**237851,87405**

TACI / TNFRSF13B	1,0	240044,9	**240044,85362**
CD14	1,0	241378,4	**241378,38802**
IL-17RD	1,0	243315,3	**243315,30870**
TRAIL / TNFSF10	1,0	244263,5	**244263,48715**
Growth Hormone R	1,0	248750,9	**248750,85575**
MIP-1 gamma	1,0	250132,6	**250132,55964**
FGF-21	1,0	260798,3	**260798,29959**
IL-18 R alpha/IL-1 R5	1,0	265724,3	**265724,26410**
TSLP	1,0	267998,4	**267998,37124**
IL-1 RI	1,0	273449,1	**273449,12971**
LIX	1,0	274572,2	**274572,23948**
VEGF-B	1,0	278245,8	**278245,79716**
PlGF-2	1,0	278380,2	**278380,16470**
CRP	1,0	285159,4	**285159,38709**
Fractalkine	1,0	285940,2	**285940,23993**
P-Selectin	1,0	289489,6	**289489,57103**
Dkk-4	1,0	290280,6	**290280,56481**
MFRP	1,0	292737,2	**292737,20898**
TGF-beta RII	1,0	295249,6	**295249,62835**
FCrRIIB / CD32b	1,0	296362,6	**296362,59717**
IL-24	1,0	298319,8	**298319,79975**
DPPIV / CD26	1,0	303192,5	**303192,52430**
CD11b	1,0	303897,3	**303897,32004**
G-CSF	1,0	304467,7	**304467,74825**

ICK	1,0	317057,7	**317057,73270**
IL-27	1,0	330547,7	**330547,72610**
Spinesin Ectodomain	1,0	330687,2	**330687,16411**
Frizzled-1	1,0	332763,5	**332763,52280**
FGF R5 beta	1,0	333516,5	**333516,48804**
IL-28 / IFN-lambda	1,0	344311,5	**344311,52504**
MIP-1 alpha	1,0	347774,7	**347774,65810**
TROY	1,0	348591,0	**348591,00425**
Prolactin	1,0	353078,4	**353078,37285**
EGFR	1,0	354034,2	**354034,15701**
DR3 / TNFRSF25	1,0	354523,5	**354523,45766**
IL-1 R9	1,0	358587,4	**358587,44176**
CCR10	1,0	369993,5	**369993,47076**
CD27 / TNFRSF7	1,0	384586,3	**384586,29204**
FGF R4	1,0	387641,3	**387641,25202**
Dtk	1,0	390838,2	**390838,18524**
Frizzled-6	1,0	396775,7	**396775,70912**
Progranulin	1,0	397176,3	**397176,27649**
FGF R3	1,0	401336,6	**401336,59958**
CXCL16	1,0	405671,9	**405671,85399**
MIG	1,0	415171,4	**415171,38514**
CD27 Ligand / TNFSF7	1,0	426455,7	**426455,72279**
Granzyme D	1,0	435293,6	**435293,55722**
EDAR	1,0	440627,7	**440627,69481**

CD30	1,0	442808,0	**442807,99820**
BCMA / TNFRSF17	1,0	453341,9	**453341,90585**
CXCR4	1,0	455048,1	**455048,12001**
CD30 L	1,0	455894,9	**455894,88900**
B7-1/CD80	1,0	457238,6	**457238,56434**
BAFF R / TNFRSF13C	1,0	457261,4	**457261,38147**
CXCR2 / IL-8 RB	1,0	465227,1	**465227,09455**
Fas Ligand	1,0	470551,1	**470551,09119**
CXCR3	1,0	472399,3	**472399,27860**
CCR4	1,0	502211,1	**502211,12457**
VCAM-1 (CD106)	1,0	519062,8	**519062,84157**
6Ckine	1,0	525220,9	**525220,93102**
CCR3	1,0	532002,7	**532002,68865**
Activin RIB / ALK-4	1,0	534355,4	**534355,38812**
bFGF	1,0	535354,3	**535354,27130**
VEGF R3	1,0	539707,3	**539707,27236**
B-Catenin	1,0	543010,7	**543010,68552**
Frizzled-7	1,0	544260,6	**544260,55711**
Activin A	1,0	569316,3	**569316,29942**
VE-Cadherin	1,0	659365,4	**659365,36456**
VEGF R2	1,0	676681,0	**676681,02984**
TRAIL R2 / TNFRSF10B	1,0	680014,9	**680014,86583**
TREM-1	1,0	799977,2	**799977,18641**
VEGF R1	1,0	967675,5	**967675,47500**

VEGF	1,0	969843,1	**969843,10220**
TRANCE / TNFSF11	1,0	994237,1	**994237,14778**

The protocol for mesoderm differentiation of siRNA treated mESCs was schematically displayed in Figure 3.8A. Immunofluorescence data of the EBs at day 3 demonstrated that while Aplnr expression was reduced 1.2-fold, Akt, Sox2, mTOR, Erk1/2 and MyoD expressions increased 1.2-fold, 1.3-fold, 1.2-fold, 2.5-fold and 2-fold, respectively, for Aplnr siRNA treated cells compared to the Control siRNA treated cells. On the other hand, Erk1/2 and MyoD expressions were upregulated 3.7-fold but Apelin expression was downregulated 1.3-fold in Apelin siRNA treated cells compared to the expression levels in Control EBs (Figure 3.8B and 3.8C). Furthermore, according to the mRNA expression levels, Bra expression was upregulated approximately 5-fold and 1.8-fold in Apelin siRNA and Aplnr siRNA treated groups, respectively, compared to Control group at day 6. While Aplnr expression was upregulated 1.5-fold in Apelin siRNA treated cells, it was downregulated 50-fold in Aplnr siRNA treated cells. Apelin expression was also reduced 1.3-fold in Apelin siRNA treated EBs. Bax expression increased 1.5-fold in Apelin siRNA treated EBs but, reduced 1.7-fold at Aplnr siRNA treated EBs. (Figure 3.8D).

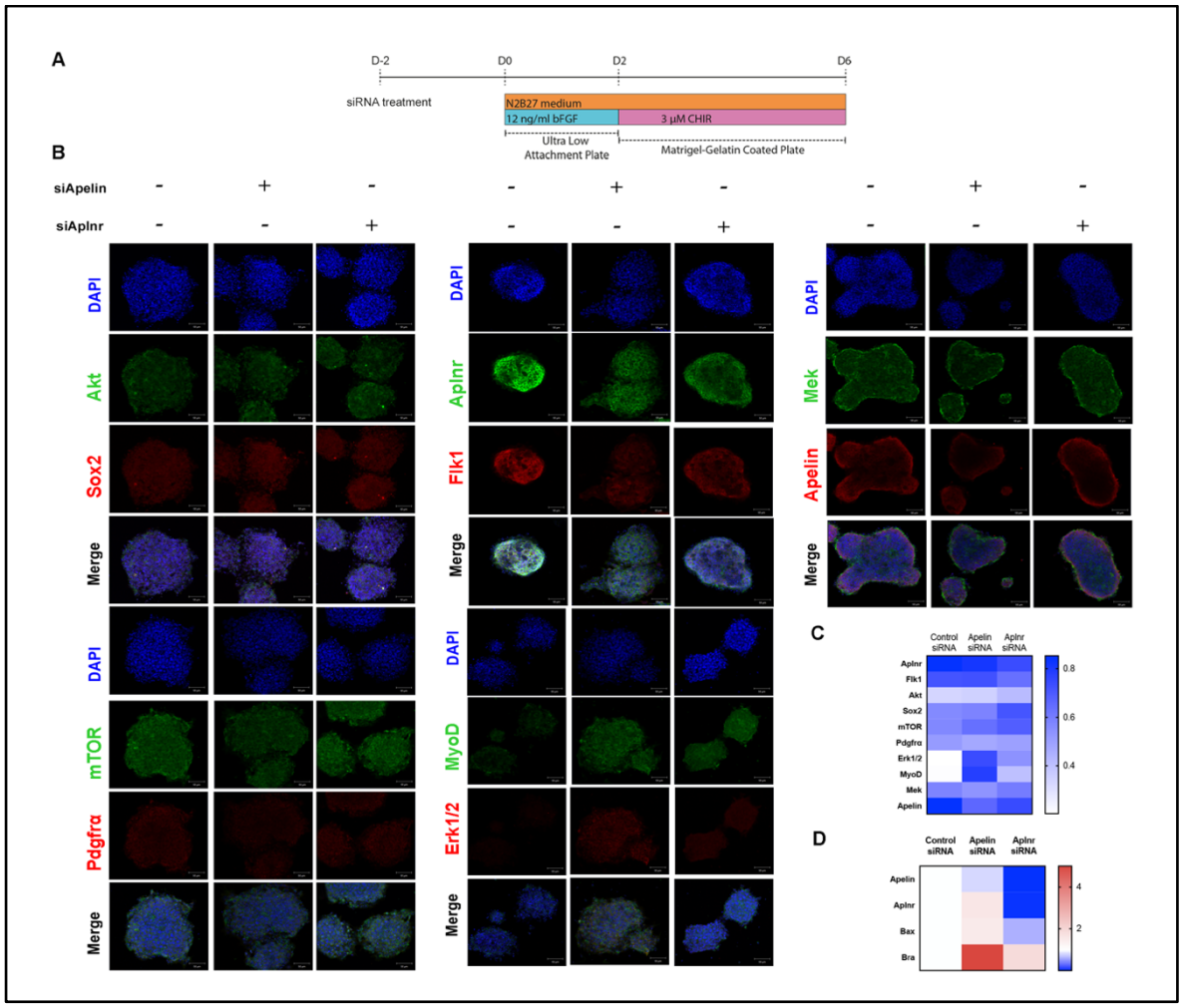


Figure 3.8. Effect of silencing Aplnr signaling components, via siRNA delivery on mesoderm commitment of mESC-derived EBs during mesoderm differentiation. A. Protocol for mesoderm differentiation of mESCs after siRNA treatment. B. The EBs were fixed using 4% paraformaldehyde at the end of day 3 and they were analyzed for protein expression of the Apelin, Aplnr, ectoderm marker protein, Sox2, the related pathway proteins, Akt and mTOR, MAPK pathway proteins involved in mesoderm commitment, Mek and Erk1/2, Pdgfrα, which guides migration of mesoderm cells, and mesoderm markers, Flk1 and MyoD. DAPI was used to stain nuclei of the cells. C. Immunofluorescence analysis and the intensity of the expression as a heat map were shown. D. Heatmap of relative gene expressions. Scale bar: 50μm.

For KO mESC lines, IF data of EBs at day 3 showed that addition of Apelin-13 or ML233 didn't significantly affect expression of Aplnr or Flk1 in Apelin KO and Aplnr KO cells compared to the non-treated ones. However, Apelin-13 treatment increased Aplnr expression in Elabela KO cells. Akt and Sox2 expression increased approximately 1.3-fold in the

presence of Apelin-13 or ML233 in Apelin KO EBs compared to their control, but not in Aplnr KO EBs. ML233 treatment enhanced expression of mTOR and Pdgfrα approximately 1.4-fold in Apelin KO and Elabela KO EBs, but not in Aplnr KO EBs. Apelin expression was 2.2-fold and 1.6-fold higher in Apelin-13 treated and ML22 treated EBs, respectively, in Aplnr KO EBs and the expression level was 1.2-fold and 1.5-fold higher in Apelin-13 treated and ML233 treated EBs, respectively, in Elabela KO EBs. Mek expression was 1.2-fold and 1.8-fold higher in Apelin-13 treated and ML233 treated EBs, respectively, in Aplnr KO EBs and the expression level was 1.3-fold higher in ML233 treated Elabela KO EBs compared to the non-treated control EBs. Apelin-13 and ML233 expression also led to 1.6-fold and 1.3-fold, respectively, downregulation of Erk1/2 and 1.7-fold and 1.5-fold downregulation of MyoD in Apelin KO EBs. On the other hand, Apelin-13 and ML233 enhanced Erk1/2 expression 2.4-fold and 2-fold, respectively, in Aplnr KO EBs and 7-fold and 8-fold in Elabela KO EBs. MyoD expression also increased 1.5-fold and 1.4-fold, respectively, in Aplnr KO EBs (Figure 3.9B and 3.9C). Furthermore, according to the mRNA expression levels of the EBs, Bra expression was upregulated approximately 1.2-fold, 1.8-fold and 2-fold in non-treated and Apelin-13 treated Elabela KO EBs and non-treated Apelin KO EBs, respectively, compared to control R1 EBs at day 6. On the other hand, Bra expression was reduced 1.4-fold, 2.1-fold and 3.3-fold in non-treated and Apelin-13 treated Aplnr KO EBs and Apelin-13 treated Apelin KO EBs, respectively, compared to the non-treated R1 EBs. Also, Bax expression reduced 2.8-fold in Apelin-13 treated Aplnr KO cells but increased 1.9-fold and 2.2-fold in non-treated and Apelin-13 treated Elabela KO EBs, respectively, compared to R1 EBs. Apelin expression was almost none in Apelin KO, Aplnr KO and Elabela KO cells in the presence or absence of the Apelin-13 peptide, except non-treated Elabela EBs, which expressed 2-fold higher Apelin compared to R1 EBs. Aplnr expression, which was reduced 2-fold and 1.2-fold in Aplnr KO and Elabela KO EBs, respectively, increased 1.4-fold, 1.7-fold and 2-fold in Apelin-13 treated Aplnr KO, Elabela KO and Apelin KO EBs, respectively, compared to R1 (Figure 3.9D). Overall, the data indicates that blocking Aplnr signaling, obstruct mesoderm commitment of mESCs. Despite activating Aplnr signaling via Apelin-13 peptide or ML233 improves mesoderm differentiation in R1 cells, Apelin KO cells or Elabela KO cells, it doesn't have a significant effect on Aplnr KO EBs.

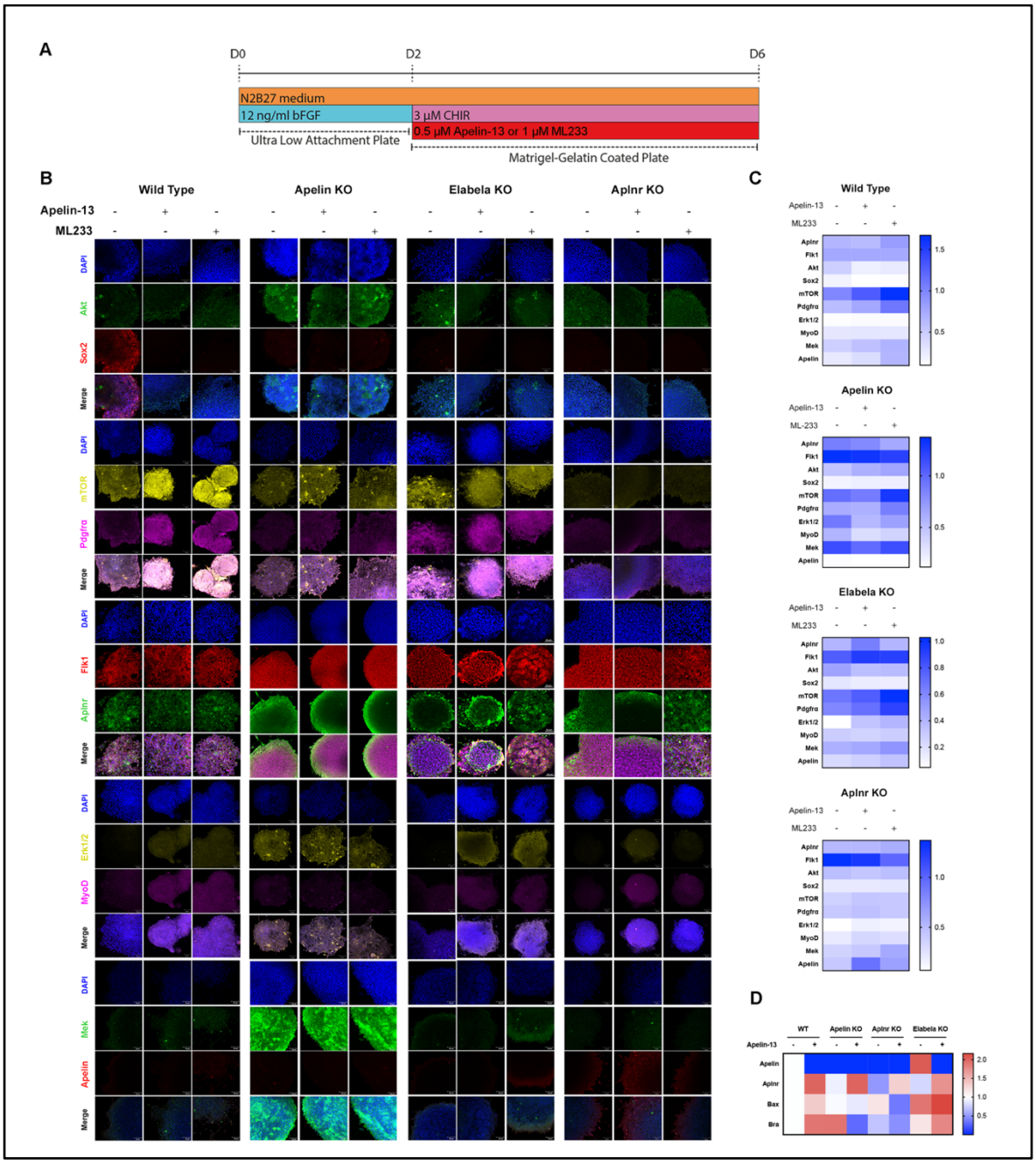


Figure 3.9. Effect of CRISPR-Cas9 mediated KO of Aplnr signaling components on mesoderm commitment of mESC-derived EBs during mesoderm differentiation. A. The protocol for mesoderm differentiation of mESC. EBs, formed from mESCs, were transferred to matrigel-gelatin coated surface at day 2 and migration of the EBs were observed until day 6. Apelin-13 or ML233 was optionally added at day 2 to activate Aplnr signaling. B. Bar graph representation of qPCR analysis indicates relative Apelin and Aplnr gene expressions in Control and Apelin-13 treated EBs at day 3 and day 6. C. The EBs were fixed using 4% paraformaldehyde at the end of day3 and they were analyzed for

protein expression of the Apelin, Aplnr, ectoderm marker protein, Sox2, the related pathway proteins, Akt and mTOR, MAPK pathway proteins involved in mesoderm commitment, Mek and Erk1/2, Pdgfrα, which guides migration of mesoderm cells, and mesoderm markers, Flk1 and MyoD. DAPI was used to stain nuclei of the cells. D. Immunofluorescence analysis and the intensity of the expression as a heat map were shown. E. Heatmap of relative gene expressions. Scale bar: 50µm.

3.1.5. Effect of Aplnr Signaling Activity on Protein Profile of mESC-derived Mesoderm Cells

To investigate the effect of Aplnr signaling activity on protein expression of mESCs-derived mesoderm cells, Aplnr signaling was induced with Apelin-13 during mesoderm differentiation and protein profile of the cells were analyzed with LC/MS analysis (Table 3.3). Briefly, R1 cells-derived EBs at day 2 were grown on matrigel gelation surface during mesoderm differentiation until day 6 and the pellet was collected. To activate Aplnr signaling, Apelin-13 was administered to the media between day 2 and day 6 (Figure 3.1B). Hierarchical cluster analysis and heat map analysis showed that both samples are closely correlated, with 0.99 correlation coefficient value (Figure 3.10A and 3.10B). Distribution of protein quantification for significantly increased and decreased expressions with Apelin-13 treatment were demonstrated on the histogram (Figure 3.10C) and profile plot (Figure 3.10D). According to the gene ontology analysis cellular and developmental processes, biological regulation and signaling related proteins were significantly enhanced with Apelin-13 treatment regarding biological processes (Figure 3.10E). Apelin-13 treatment also enhanced proteins related to some molecular functions, including ATP-dependent activity, binding, catalytic activity, molecular function regulator, structural molecule activity and transporter activity (Figure 3.10F). Furthermore, proteins related to pathways, in terms of cell cycle, EGFR signaling pathway, Wnt signaling pathway, FGF signaling pathway, ubiquitin proteosome pathway and integrin signaling pathway, were upregulated with Apelin-13 administration compared to the control cells (Figure 3.10G). Furthermore, according to the protein-protein interaction network, generated using string, clustered network with clustering coefficient 0.436 contained 53 nodes and 84 edges with 46 expected edges for significantly enhanced proteins in Apelin-13 group compared to control group. Clustered network with clustering coefficient 0.6 contained 28 nodes and 90 edges with 22

expected edges for significantly enhanced proteins in control group compared to Apelin-13 group. These indicate much more interaction than the expected values (Figure 3.10H). Taken together, these results revealed that Apelin-13 treatment during mESC-derived mesoderm differentiation affects expression of proteins associated with various signaling pathways, including EGFR, Wnt and FGF signaling, and acts on different processes such as survival, proliferation, migration, differentiation and adherence.

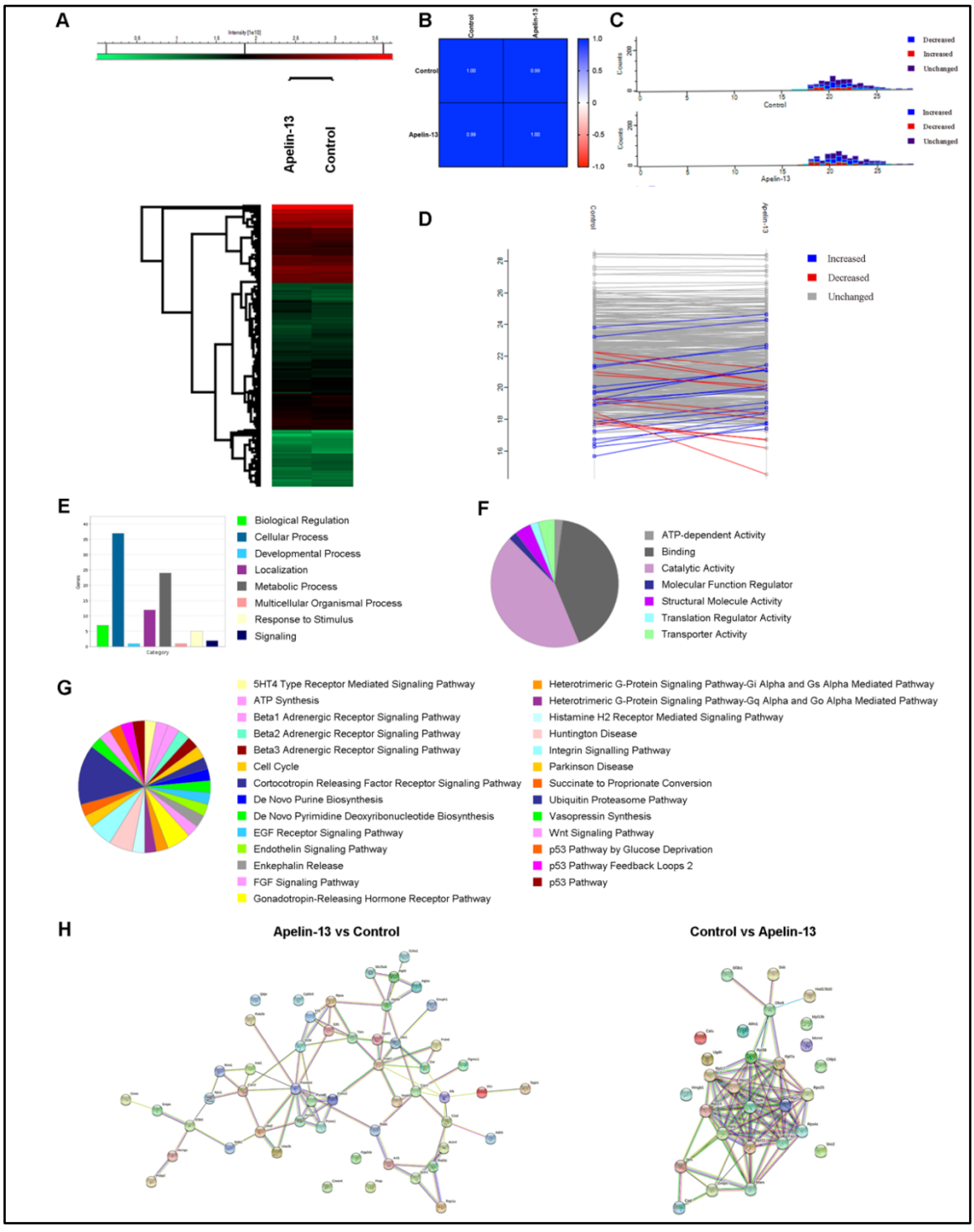


Figure 3.10. Protein profile of mESC derived EBs treated with Apelin-13. A. Hierarchical cluster analysis and heat map representation of proteins from Control and Apelin-13 treated EBs at day 6. B. Correlation coefficient matrix of the proteins. C. Histogram indicating the distribution of the protein quantification. D. Profile plot indicating the proteins, which were significantly upregulated (blue) and downregulated (red) after Apelin-13 treatment. The graphs demonstrating E. biological processes, F. molecular functions and G. related pathways of the upregulated proteins in Apelin-13 treated EBs. H. Protein interaction network for the upregulated proteins in Control and Apelin-13 treated EBs.

Table 3.3. Protein profiling data of day 6 mesoderm cells, differentiated from R1 mESCs. Apelin-13 was added to the media between day 3 and day 6. Significantly increased (red) and decreased (black) proteins in Apelin-13 treated group compared to control group were highlighted on the table.

Accession	**Description**	**Abundance Ratio: Apelin-13 / Control**
Q9DCN2	NADH-cytochrome b5 reductase 3	**4,236**
Q91WQ3	Tyrosine--tRNA ligase, cytoplasmic	**3,736**
P20152	Vimentin	**3,028**
Q9CPQ8	ATP synthase subunit g, mitochondrial	**2,71**
Q921M3	Splicing factor 3B subunit 3	**2,65**
Q9Z1F9	SUMO-activating enzyme subunit 2	**2,402**
P63163	Small nuclear ribonucleoprotein-associated protein N	**2,304**
P35564	Calnexin	**2,301**
P56382	ATP synthase subunit epsilon, mitochondrial	**2,28**
Q8BGB7	Enolase-phosphatase E1	**2,232**
P07742	Ribonucleoside-diphosphate reductase large subunit	**2,22**

P28474	Alcohol dehydrogenase class-3	**2,156**
P18242	Cathepsin D	**2,117**
Q8BVI4	Dihydropteridine reductase	**2,108**
Q99JY9	Actin-related protein 3	**2,069**
P51881	ADP/ATP translocase 2	**2,064**
P07724	Albumin	**2,017**
P62835	Ras-related protein Rap-1A	**2,003**
Q3U1J4	DNA damage-binding protein 1	**1,984**
Q9QUR6	Prolyl endopeptidase	**1,944**
Q8QZY1	Eukaryotic translation initiation factor 3 subunit L	**1,922**
P61205	ADP-ribosylation factor 3	**1,889**
P63168	Dynein light chain 1, cytoplasmic	**1,887**
O55022	Membrane-associated progesterone receptor component 1	**1,863**
P59279	Ras-related protein Rab-2B	**1,847**
P97371	Proteasome activator complex subunit 1	**1,84**
Q99LX0	Parkinson disease protein 7 homolog	**1,822**
P35278	Ras-related protein Rab-5C	**1,775**
Q6R0H7	Guanine nucleotide-binding protein G(s) subunit alpha isoforms	**1,672**
P57780	Alpha-actinin-4	**1,671**
Q9CX56	26S proteasome non-ATPase regulatory subunit 8	**1,668**
O35593	26S proteasome non-ATPase regulatory subunit 14	**1,659**
Q61699	Heat shock protein 105 kDa	**1,635**
Q6P5F9	Exportin-1	**1,627**
P46471	26S proteasome regulatory subunit 7	**1,627**

Q8BH95	Enoyl-CoA hydratase, mitochondrial	**1,618**
Q61990	Poly(rC)-binding protein 2	**1,611**
Q8BY71	Histone acetyltransferase type B catalytic subunit	**1,594**
Q9ERK4	Exportin-2	**1,59**
P14206	40S ribosomal protein SA	**1,58**
Q8BWY3	Eukaryotic peptide chain release factor subunit 1	**1,579**
Q69ZF7	Metal transporter CNNM4	**1,578**
P48024	Eukaryotic translation initiation factor 1	**1,573**
Q9WVA4	Transgelin-2	**1,57**
P61087	Ubiquitin-conjugating enzyme E2 K	**1,567**
Q9Z204	Heterogeneous nuclear ribonucleoproteins C1/C2	**1,565**
O08709	Peroxiredoxin-6	**1,556**
P62821	Ras-related protein Rab-1A	**1,556**
Q9CPU0	Lactoylglutathione lyase	**1,552**
Q9R1P0	Proteasome subunit alpha type-4	**1,539**
P56480	ATP synthase subunit beta, mitochondrial	**1,537**
P47791	Glutathione reductase, mitochondrial	**1,534**
P62715	Serine/threonine-protein phosphatase 2A catalytic subunit B isoform	**1,505**
P49717	DNA replication licensing factor MCM4	**0,505**
Q3THE2	Myosin regulatory light chain 12B	**0,489**
Q9CPR4	60S ribosomal protein L17	**0,478**
P27659	60S ribosomal protein L3	**0,475**
P62852	40S ribosomal protein S25	**0,463**
B2RQC6	CAD protein	**0,349**

Q9CWK8	Sorting nexin-2	**0,312**
P32067	Lupus La protein homolog	**0,262**
Q9Z0X1	Apoptosis-inducing factor 1, mitochondrial	**0,261**
O08756	3-hydroxyacyl-CoA dehydrogenase type-2	**0,101**
O88271	Craniofacial development protein 1	**0,066**
O35887	Calumenin	**0,001**
P62843	40S ribosomal protein S15	**0,001**
Q99NB9	Splicing factor 3B subunit 1	**0,001**

3.1.6. Aplnr Signaling Acts on MSC differentiation of mESC-derived Mesoderm Cells

To understand how Aplnr signaling affects differentiation of mesoderm to MSCs, either Aplnr signaling was induced or repressed with various methods. First, the best media formulation was selected to obtain MSCs from R1-derived mesoderm cells via EB method. Three different media, as indicated in standard protocol, mESC protocol and FCS protocol, were tested from day 6 to day 10 for R1 cells, which were differentiated to mesoderm cells at day 6 (Figure 3.11A). Media of standard protocol was selected for MSC differentiation of R1 cells, as the cells, grown with standard protocol, at day 10 demonstrated better MSC phenotype and plastic adherence capacity (Figure 3.11B) as well as the highest gene expression levels for positive markers of MSCs compared to the other protocols (Figure 3.11C).

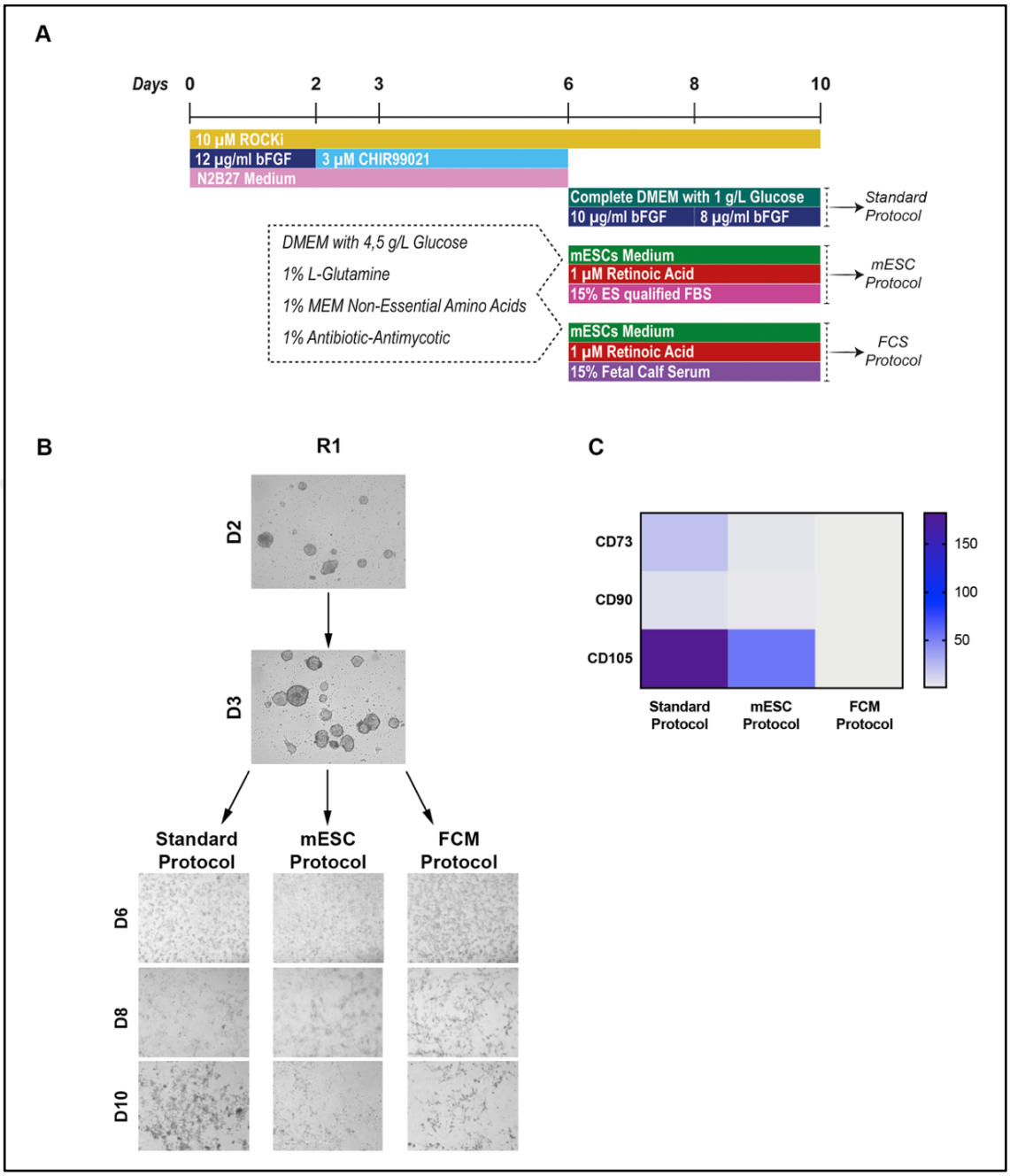


Figure 3.11. Optimization of MSC differentiation protocol from mESCs. A. Protocols and timeline for MSC differentiation from mESCs. Standard protocol, mESC protocol and FCS protocol were applied. B. Morphological pictures of R1 EBs at day 2, day 3, day 6, day 8 and day 10. C. Heatmap of relative gene expression analysis. Scale Bar: 200µm.

Apelin-13 peptide was used to activate Aplnr during MSC differentiation. To optimize time of Apelin-13 addition to the standard protocol to activate Aplnr signaling during MSC differentiation, 0.5uM Apelin-13 was added to the media at various periods (Figure 3.12A and 3.13A). Among the time intervals, addition of Apelin-13 between day2 and day3, Option

IV, increased plastic adherence capacity and MSC morphology of the cells at day 10 (Figure 3.12B and 3.13B). Also, option IV media led the cells at day 10 to express positive surface markers of MSC, CD 73, CD90, CD105, CD29, Sca-1 and CD106 higher than the control, Option I. CD31, which was expressed by endothelial and some immune cells, was negative for both Option I and Option IV cells. On the other hand, CD45, a hematopoietic marker, was also found to be expressed higher than the control cells, Option I, in Option IV and the other options with Apelin-13 addition during flow cytometry analysis (Figure 3.12C, 3.12D, 3.13C and 3.13D). Gene expression analysis indicated that MSC markers, CD73, CD90, CD105, were overexpressed in Option IV group compared to other groups. CD73 was expressed 2.5-fold, CD90 was expressed 4-fold and CD105 was expressed 60-fold more in Apelin administered MSCs, Option IV, compared to Control MSCs, Option I (Figure 3.12E and Figure 3.13E). Option I and Option IV were further analyzed for mRNA expression of MSC markers. While expression of CD31 and CD 45 reduced 2.5-fold and 9-fold, respectively, CD166 and Pdgfrb expressions increased 18-fold and 4-fold in Apelin-13 treated MSC, Option IV, compared to Control MSC, Option I. Pdgfrα was also reduced 2-fold with Apelin-13 treatment (Figure 3.13E). Moreover, the results of MTS assay (Figure 3.13F) and cell counting with trypan blue staining (Figure 3.13G) showed increased cell viability and proliferation in the presence of Apelin, compared to control group. Apelin-13 treatment also reduced the MSC doubling time significantly (Figure 3.13H). Furthermore, trilineage potential of Option I and Option IV derived MSCs were compared. Osteogenic, chondrogenic and adipogenic differentiation were evaluated by alizarin red, alcian blue and oil red O stainings, respectively as well as gene expression analysis. Both the stainings (Figure 3.13I) and gene expression analysis (Figure 3.13J) indicated positive effect of Apelin-13 treatment on trilineage differentiation capacity of the MSCs. Col1A1 expression was enhanced 40-fold in Option IV MSC derived Osteocytes, Col2A expression increased almost 1.5-fold in Option IV MSC derived Chondrocytes, FABP4 and Adiponectin expression levels increased 6-fold and 3.5-fold, respectively, in Option IV MSC derived Adipocytes compared to ones differentiated from Option I MSCs (Figure 3.13J).

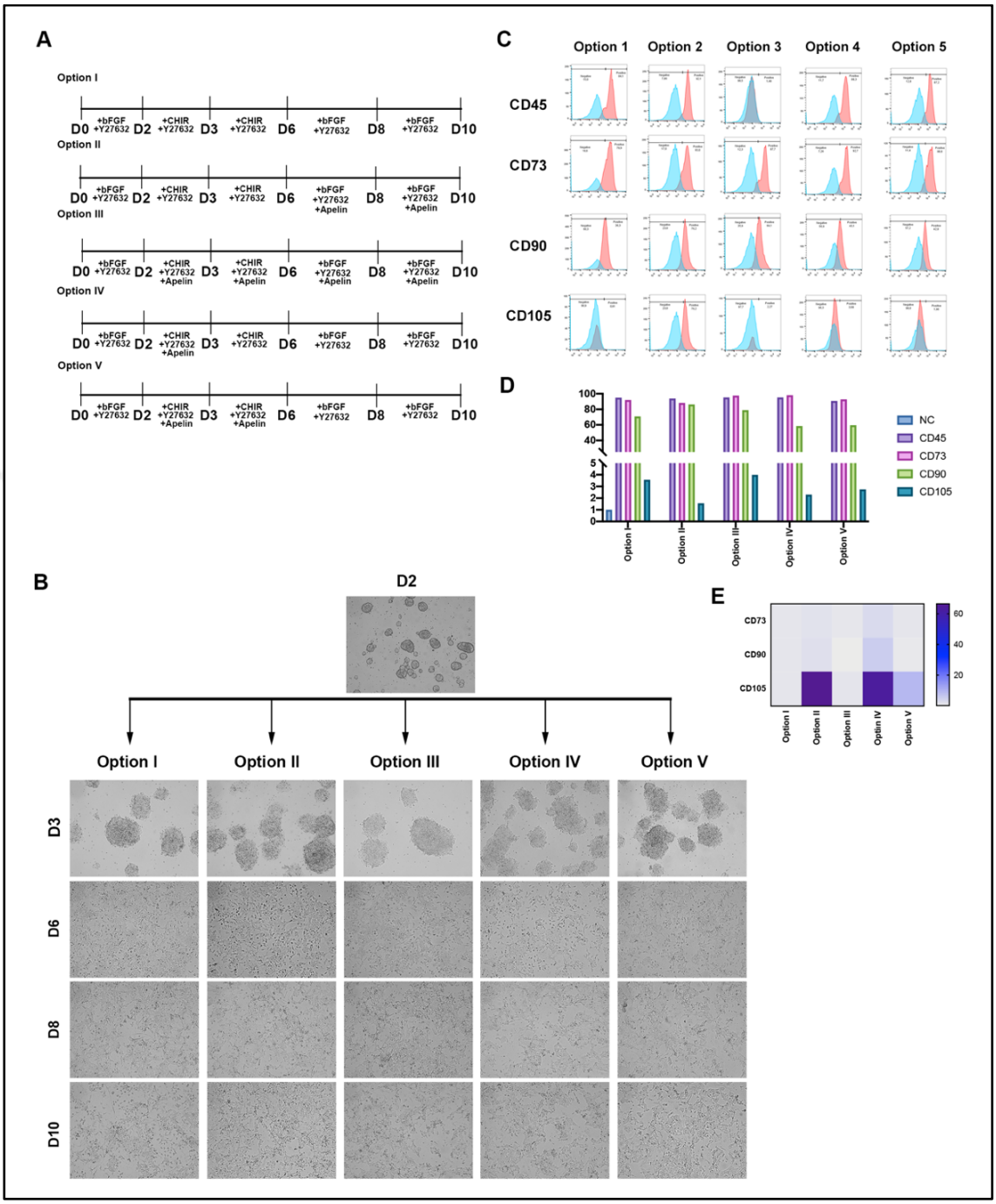


Figure 3.12. Optimization of Apelin-13 addition to the MSC differentiation media. A. Protocols and timelines for Apelin-13 addition to MSC differentiation protocol. B. Morphological pictures of R1 EBs treated with the media options at day 2, day 3, day 6, day 8 and day 10. C. Flow cytometry analysis of R1 EBs at day 10 for MSC markers and D. its graphic representation indicating the positive cells for the markers. E. A heat map representation of relative gene expressions for R1 EBs at day 10. Scale Bar: 200µm.

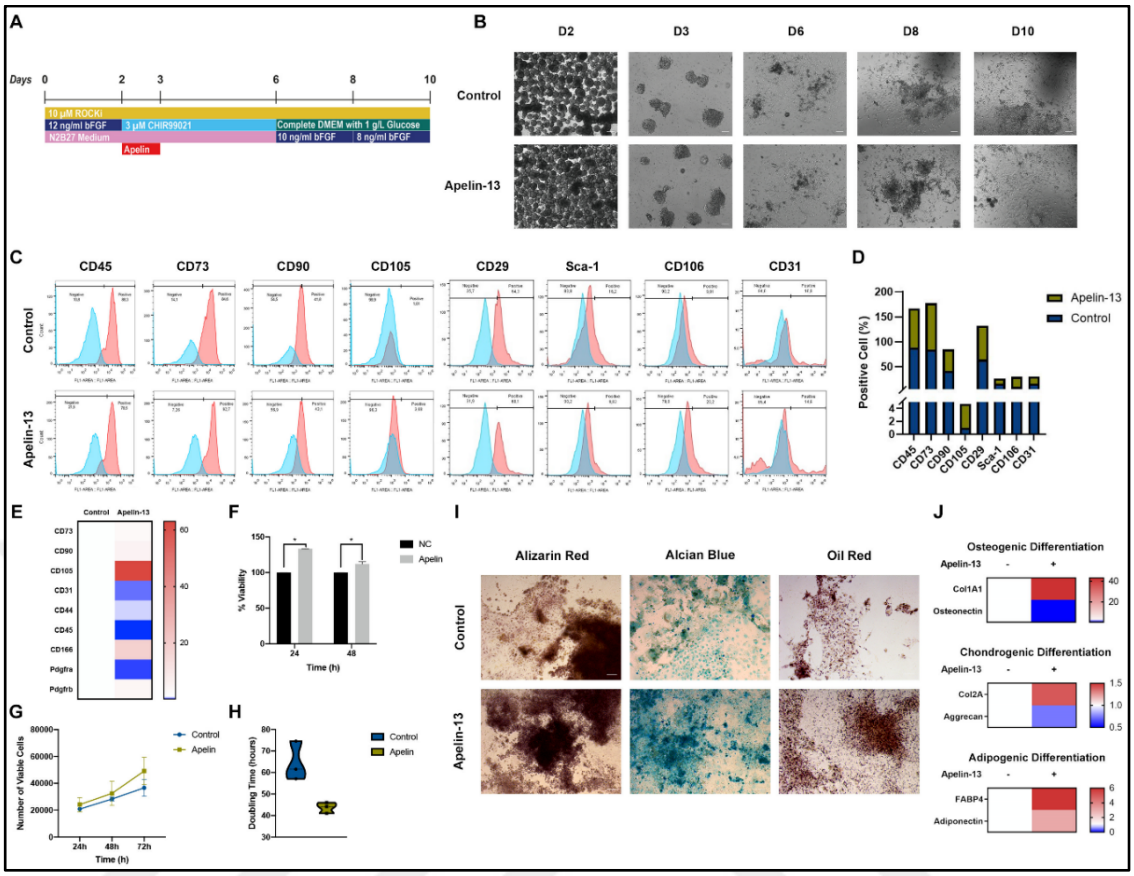


Figure 3.13. Effect of Aplnr activity on MSC differentiation from mESCs. A. A protocol for MSC differentiation from mESC. EBs, formed from mESCs, were transferred to matrigel-gelatin coated surface at day2 and at day6 mesoderm cells were obtained. Mesoderm cells were differentiated to MSC finally at day 10. B. Morphological pictures were taken at day2, day3, day6, day8 and day10 during MSC differentiation from mesoderm cells. Scale bar: 200μm. C. MSC markers were detected with flow cytometry analysis and D. a graphic was drown showing the positive cells for the markers. E. Relative gene expression analysis for MSC markers were shown as a heatmap. F. Cell viability was measured for Control MSCs, and Apelin-13 treated MSCs and was represented with a bar graph. G. Viable cells were counted with Trypan Blue staining and H. cell duplication time was calculated for Control and Apelin-13 treated MSCs. I. Morpholohical picture of alizarin red, alcian blue and oil red O stainings (Scale bar: 50μm) and J. relative gene expression analysis after osteogenic, chondrogenic and adipogenic differentiation of MSCs. *P<0.0001

Suppression of Aplnr signaling components was realized by shRNA, siRNA or CRISPR-Cas9 mediated KO. When Aplnr signaling components were suppressed via lentiviral

transduction of Apelin shRNA and Aplnr shRNA viruses and the cells were differentiated to MSCs according to the protocol (Figure 3.14A), increased cell death and loss of plastic adherence were observed both in shApelin and shAplnr groups compared to shControl cells. Also, MSC phenotype, observed at shControl MSCs, were not observed in shApelin and shAplnr MSCs (Figure 3.14B). Moreover, although gene expression of CD44 and CD166 were upregulated in shApelin-derived cells, CD73, CD90 and CD 105, as well as hematopoietic markers, CD31 and CD45, were downregulated significantly compared to shControl-derived MSCs. In shAplnr MSCs, CD73, CD90, CD105, CD31, CD44 and CD166 expressions decreased at a significant degree yet, expression of CD45 increased significantly compared to shControl-derived MSCs (Figure 3.14C).

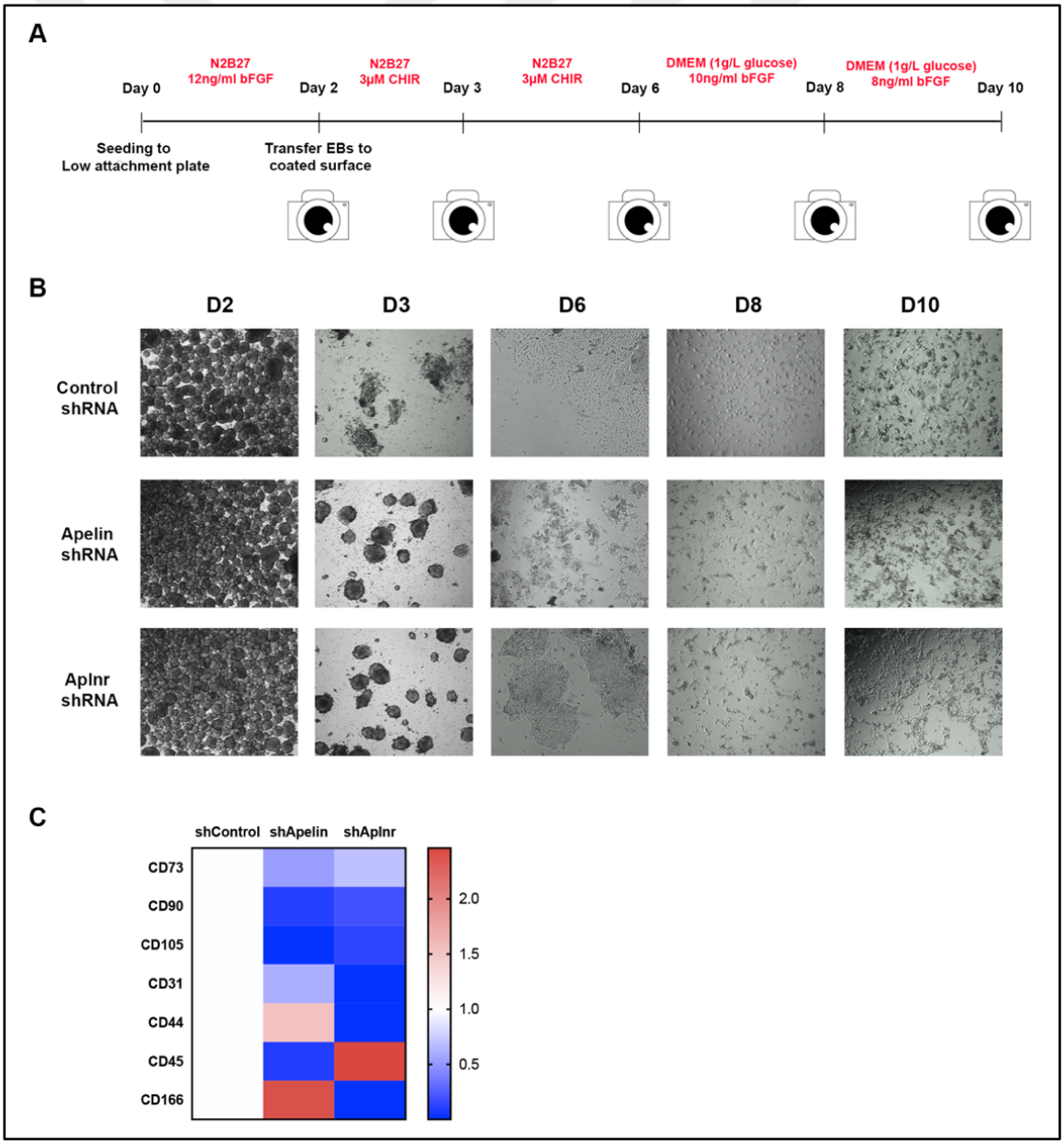


Figure 3.14. Effect of shRNA mediated silencing of Aplnr signaling components on MSC differentiation of R1 cells. A. MSC differentiation protocol for Control, shApelin and shAplnr cells. B. Morphological pictures of the cells taken at day 2, day 3, day 6, day 8 and day 10 during MSC differentiation. C. A heat map representation of relative gene expressions for the cells at day 10. Scale Bar: 200µm.

MSCs differentiated from siApelin and siAplnr treated R1 cells (Figure 3.15A) showed high cell death and low plastic adherence performance compared to siControl treated R1 cells. Also, MSC phenotype were not observed in siApelin and siAplnr treated R1 cells (Figure 3.15B). According to the mRNA expression analysis, while expression of all the markers were significantly downregulated in Aplnr siRNA treated group, only CD90, CDCD166 and CD44 gene expression levels were significantly upregulated in Apelin siRNA treated group compared to Control MSC group (Figure 3.15C).

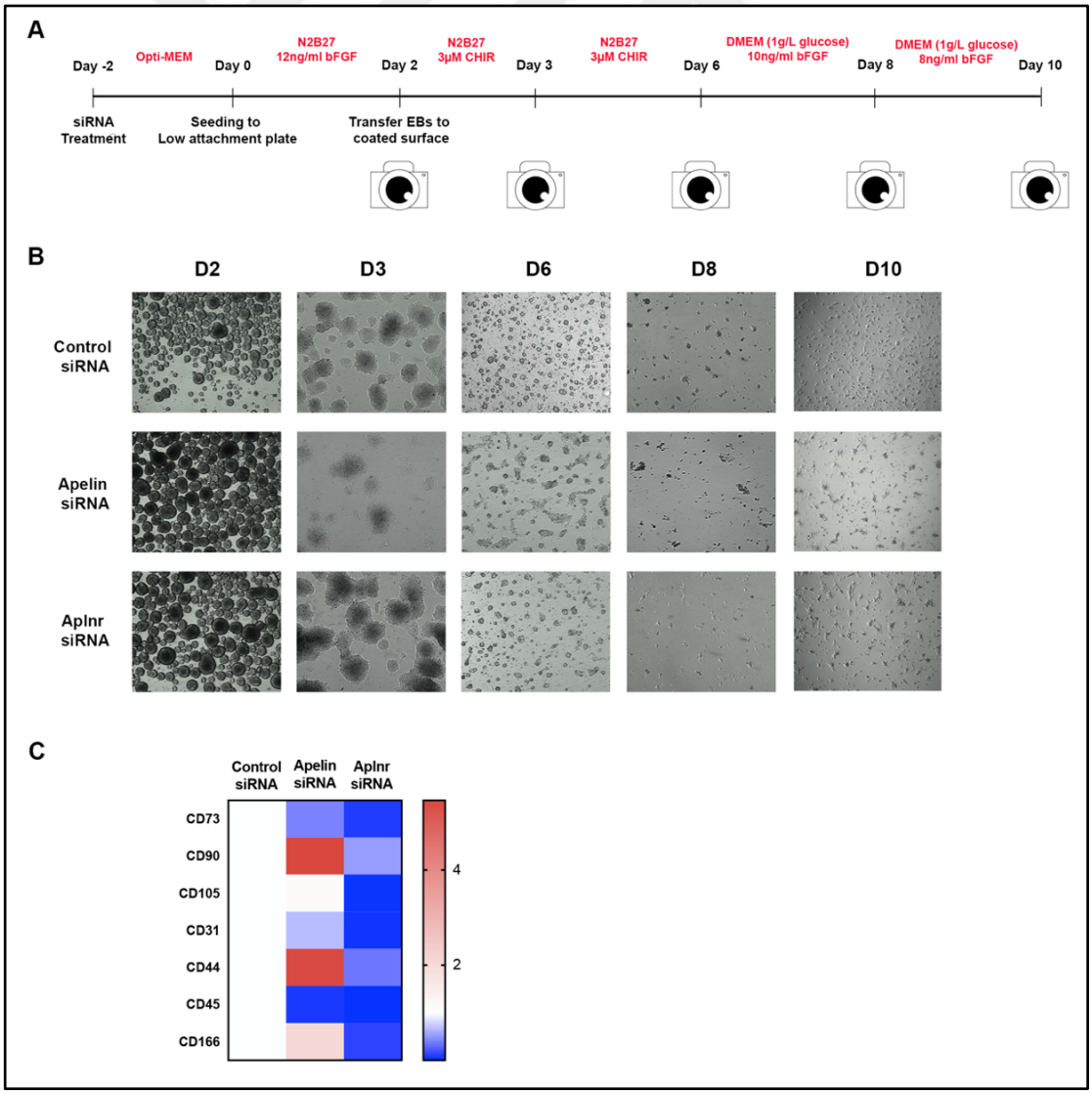


Figure 3.15. Effect of siRNA mediated silencing of Aplnr signaling components on MSC differentiation of R1 cells. A. MSC differentiation protocol for Control, siApelin and siAplnr cells. B. Morphological pictures of the cells taken at day 2, day 3, day 6, day 8 and day 10 during MSC differentiation. C. A heat map representation of relative gene expressions for the cells at day 10. Scale Bar: 200μm.

WT, Apelin KO, Aplnr KO and Elabela KO cells, which were generated from CRISPR-Cas9 mediated KO of Aplnr signaling component, were also differentiated according to the MSC differentiation protocol (Figure 3.16A). Cell death increased, MSC phenotype and plastic adherence were not achieved for Aplnr KO and Elabela KO MSCs at day 10. Nonetheless, Apelin KO MSCs possessed plastic adherence property and MSC morphology as WT MSC. Additionally, proliferation of Apelin KO MSCs noticeably increased compared to WT MSCs (Figure 3.16B). Furthermore, mRNA expression of CD73, CD90, CD105, CD31 and CD45 at day 10 were significantly downregulated in Apelin KO, Aplnr KO and Elabela KO cell compared to the expression levels in wild type cells. However, CD44 and CD166 expressions were significantly upregulated in Apelin KO and Aplnr KO cells but downregulated in Elabela KO cells (Figure 3.16C).

Overall, these data points positive effect of Aplnr signaling activity on MSC differentiation of EB-derived mesoderm cells as well as survival and proliferation of the MSCs.

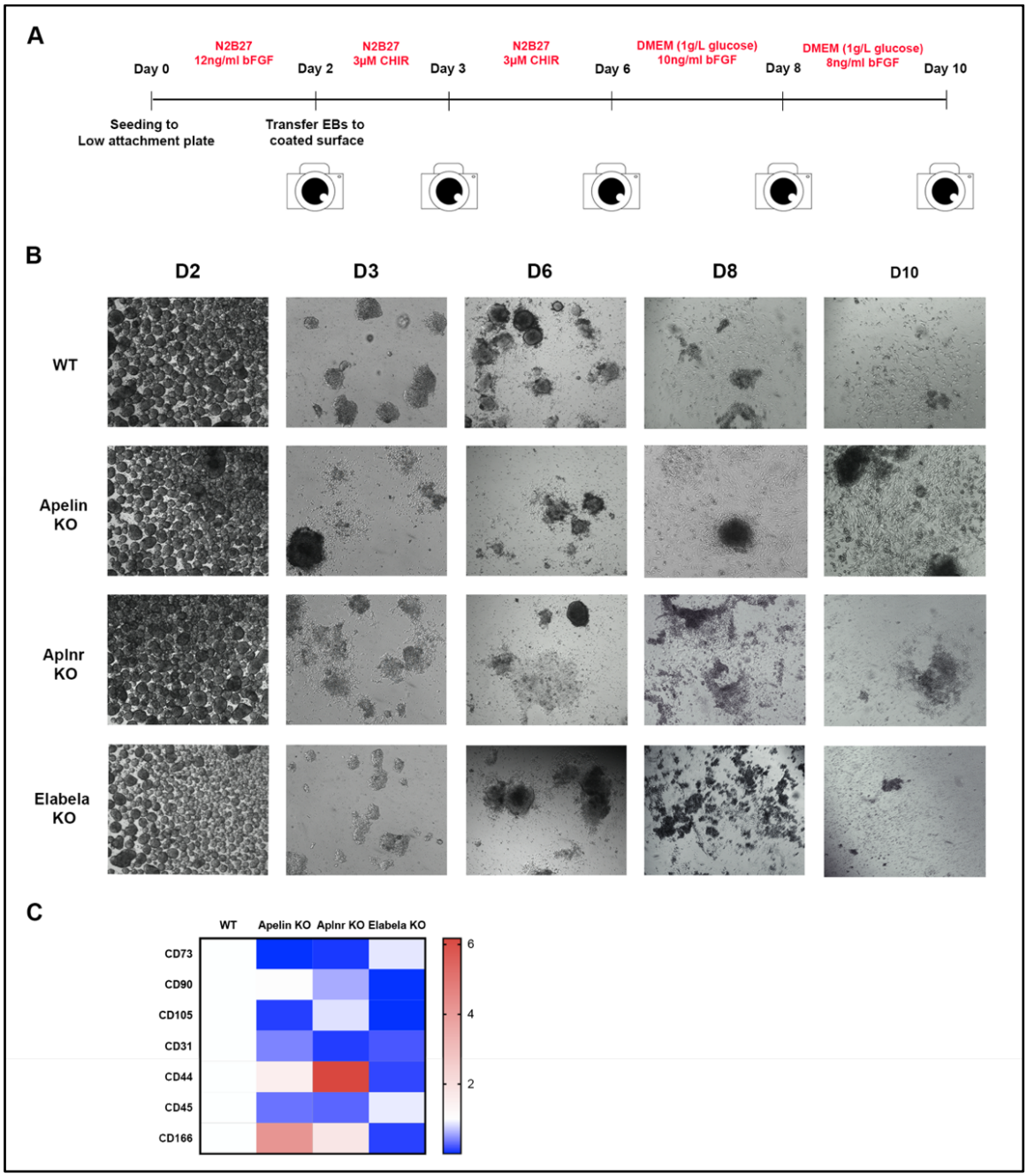


Figure 3.16. Effect of CRISPR-Cas9 mediated KO of Aplnr signaling components on MSC differentiation of R1 cells. A. MSC differentiation protocol for wild type, Apelin KO, Aplnr KO and Elabela KO cells. B. Morphological pictures of the cells taken at day 2, day 3, day 6, day 8 and day 10 during MSC differentiation. C. A heat map representation of relative gene expressions for the cells at day 10. Scale Bar: 200μm.

3.2. EFFECT OF APLNR SIGNALING ON MESODERM AND MSC DIFFERENTIATION OF HUMAN ESCS

3.2.1. Activation of Aplnr Signaling Enhances Cell Migration during Mesoderm Differentiation

To investigate the effect of Aplnr signaling pathway on migration of cells during mesoderm differentiation, Aplnr signaling was either activated by Apelin-13 and ML233 molecule or inhibited by shRNA, siRNA and CRISPR-Cas9 KO in H9 hESCs. EBs were generated in low attachment plate and transferred to Matrigel-gelatin coated surface at day 2 to attach and migrate during mesoderm differentiation. Apelin-13 peptide or ML233 was administered to the cells between day 2 and day 6 to observe its effect on the cell movement (Figure 3.17A, 3.17C, 3.18A and 3.18B). Total area of the EB increased 2 fold for Apelin-13 treated group compared to the total area of control EB at day 3 and day 6. Core area of Apelin group was 4 fold larger compared to core area of control group at day 3 and 0.5 fold larger at day 6. Migration area was also 2.5 fold bigger for Apelin-13 administered group at day 6 compared to migration area of control EBs. Although core intensity was similar for control, ML233 treated and Apelin-13 treated groups, migration intensity was found to be 3.5 fold higher at day 3 and 4.5 fold higher at day 6 in Apelin-13 administered EBs, while 1.5 fold higher for ML233 administered EBs at day 3 and day 6 compared to control EBs (Figure 3.17D, 3.17E, 3.17F, 3.18C and 3.18D).

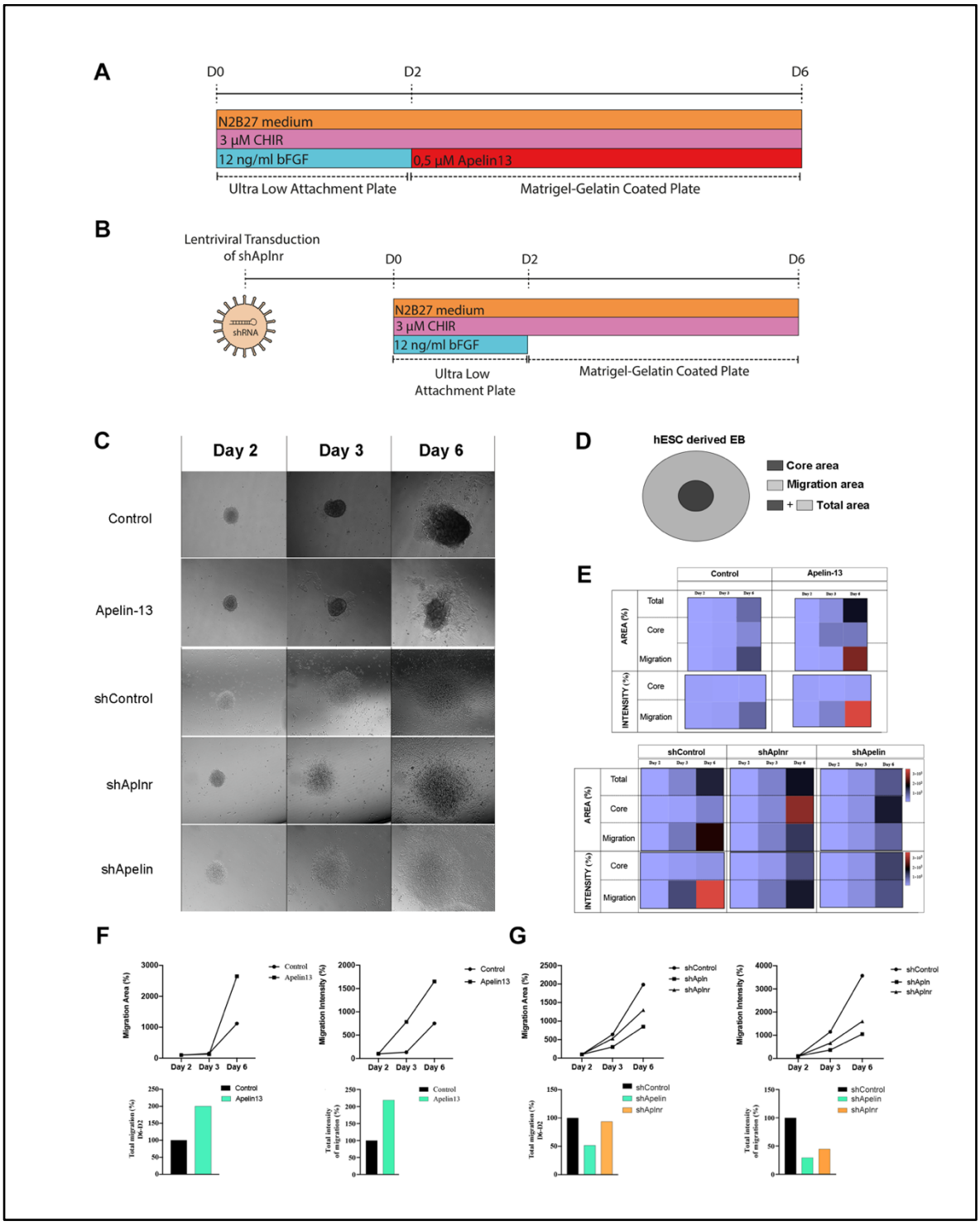


Figure 3.17. Effect of Aplnr signaling on migration of EBs during mesoderm differentiation of hESCs. A. EBs, formed from hESCs, were transferred to Matrigel-gelatin coated surface at day 2 and migration of the EBs were observed until day 6. B. H9 hESCs were transfected with Apelin and Aplnr shRNA viruses. Next day, media was changed with MTESR medium and the next day, the cells were used to make EBs in low attachment plates. At day 2, EBs were transferred to Matrigel-gelatin coated surface and the migration

was observed until day 6. C. Morphological pictures were taken at day 2, day 3 and day 6. D. Graphical illustration of total area, core area and migration area. E. Total area, core area and migration area (total area-core area) as well as core intensity and migration intensity were measured at day 2, day 3 and day 6 and visualized as heat maps for Control, Apelin-13, shControl, shApelin and shAplnr EBs. F. Line graph of migration area and migration intensity as well as bar graph of total migration area and total migration intensity for Apelin-13 administered EBs. G. Line graph of migration area and migration intensity as well as bar graph of total migration area and total migration intensity for shApelin and shAplnr EBs. Scale bar: 100μm.

To inhibit Aplnr signaling, Apelin shRNA and Aplnr shRNA viruses were given to H9 hESCs clusters in suspension. The cells were grown on Matrigel and were used to make EBs. At day 2, EBs were transferred to Matrigel-gelatin coated surface to migrate during mesoderm differentiation (Figure 3.17B and 3.17C). Although total area increased similarly for shAplnr EBs and shControl EBs, total area of shApelin EBs was almost half size of shControl EBs at day 6. Core area of shAplnr EBs was 3 fold larger at day 3 and 5.5 fold larger at day 6 compared to shControl EBs. Similarly, it was 2 fold bigger at day 3 and 3 fold bigger at day 6 for shApelin EBs compared to core area of shControl EBs. Migration area of shControl EBs were 2 fold larger compared to migration area of shApelin and shAplnr EBs at day 6. Intensity of core for shApelin and shAplnr were about 4 fold higher compared to core intensity of shControl. Migration intensity of shControl was 2 fold higher compared to shAplnr EBs and 4 fold higher compared to shApelin EBs at both day 3 and day 6 compared to migration intensity of shControl (Figure 3.17E and 3.17G). These results indicate that Aplnr signaling induces cell migration from EBs during mesoderm differentiation.

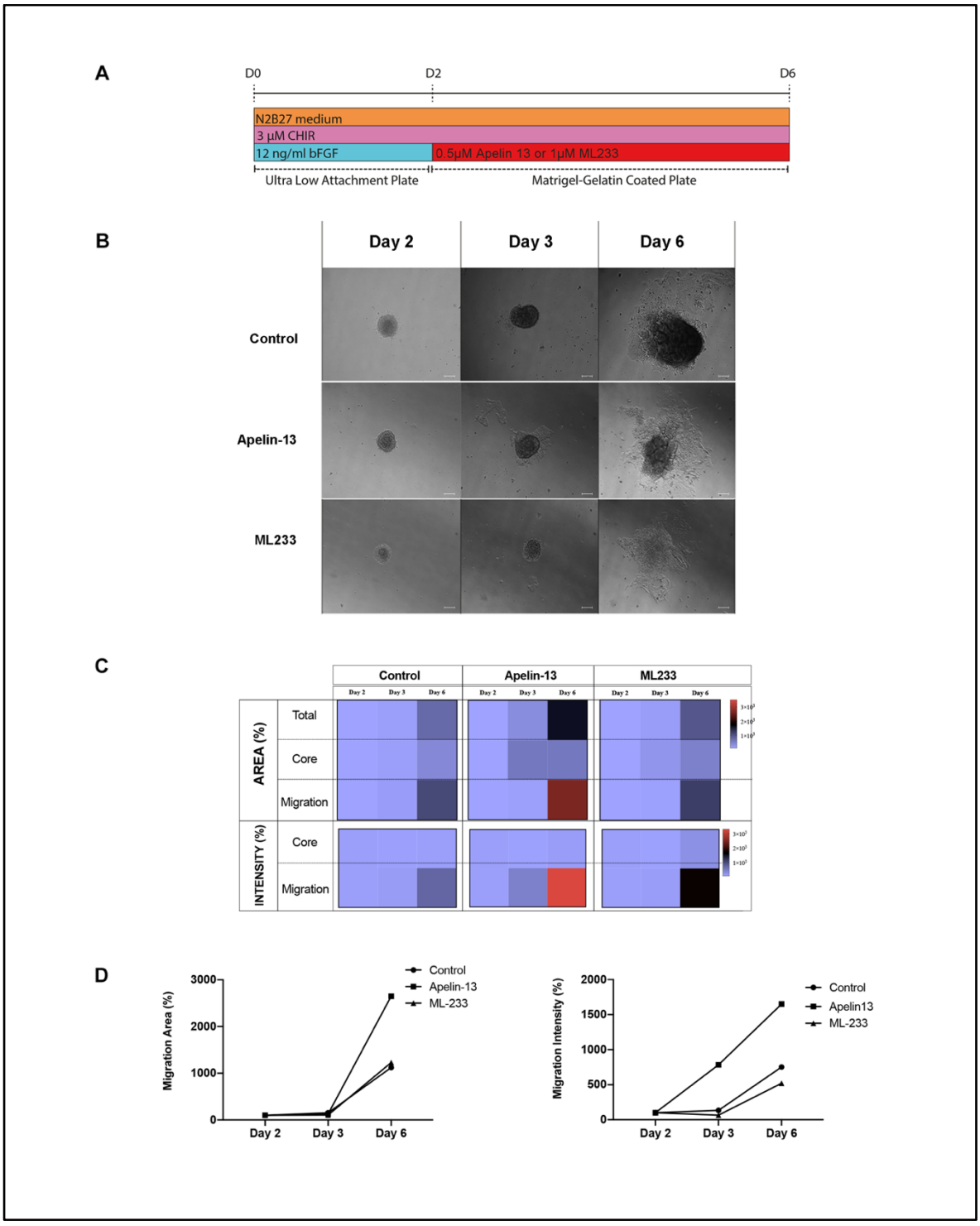


Figure 3.18. Effect of activation of Aplnr by Apelin-13 and ML233 on migration of EBs during mesoderm differentiation of hESCs. A. EBs, formed from hESCs, were transferred to Matrigel-gelatin coated surface at day 2 and migration of the EBs were observed with Apelin-13 or ML233 until day 6. B. Morphological pictures were taken at day 2, day 3 and day 6. C. Total area, core area and migration area (total area-core area) as well as core intensity and migration intensity were measured at day 2, day 3 and day 6 and visualized as

heat maps for Control, Apelin-13 and ML233 treated EBs. D. Line graph of migration area and migration intensity as well as bar graph of total migration area and total migration intensity for Apelin-13 and ML233 administered EBs. Scale bar: 100µm.

Aplnr signaling activity was also inhibited using CRISPR-Cas9 gene editing technology. gRNAs were designed to knock out Apelin, Aplnr and Elabela genes (Table 2.4, Figure 2.1 and 3.19A). The plasmids were engineered to transfect hESCs (Figure 3.19B and 3.19C) and effect of the CRISPR/Cas KO of the genes on hESC migration were observed during mesoderm differentiation (Figure 3.19D). EBs of Wild type, Apelin KO, Aplnr KO and Elabela KO cells (Figure 3.19E) cells at day 2 were transferred to Matrigel-gelatin coated surface and migration area and intensity of the EBs were observed until day 6 (Figure 3.19D and 3.19F). Although migration area of Apelin KO and Elabela KO EBs reduced compared to Wild Type, migration area of Aplnr increased significantly. Also, core intensity of Apelin KO and Aplnr KO EBs decreased compared to Wild Type EBs (Figure 3.19F, 3.19G and 3.19H).

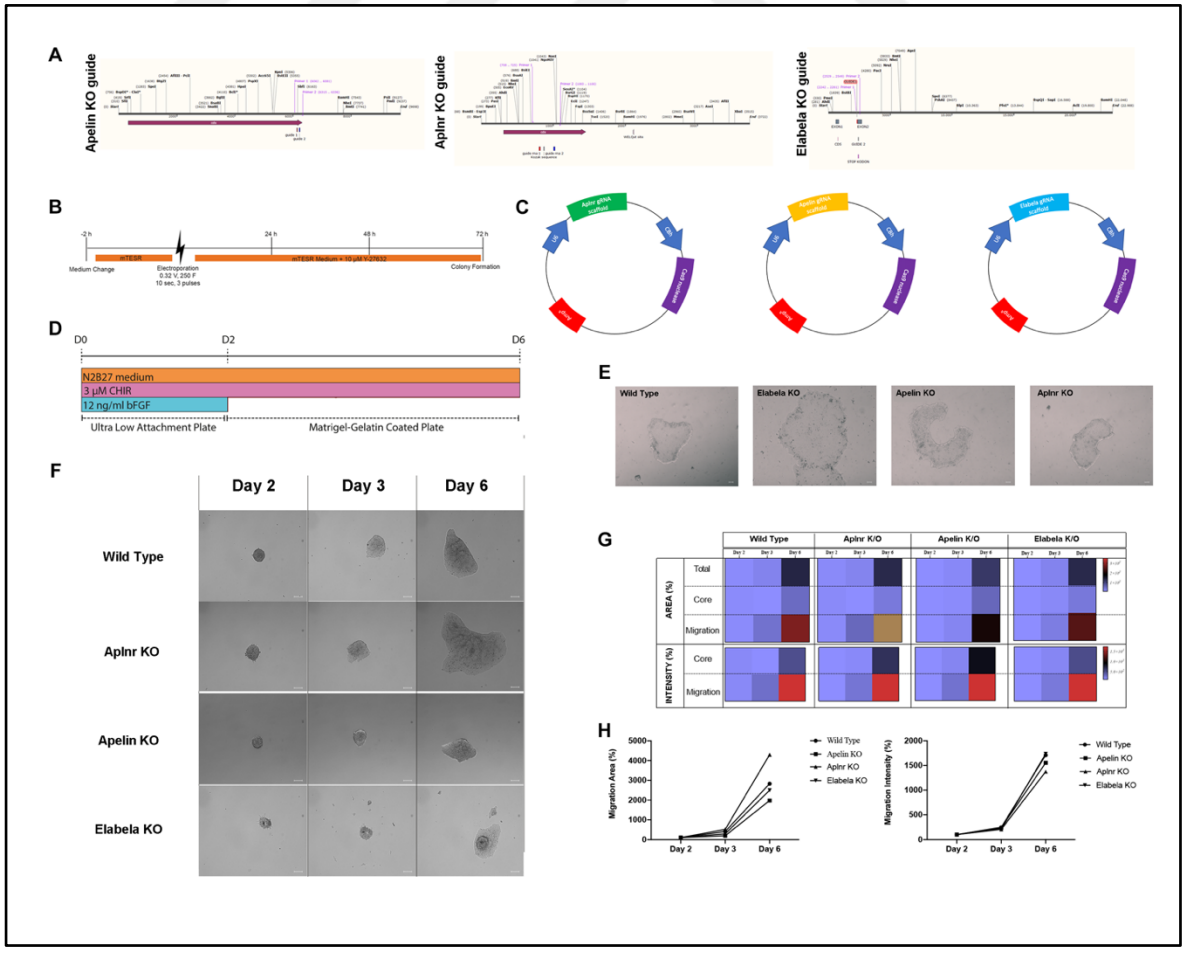


Figure 3.19. Effect of CRISPR-Cas9 mediated KO of Aplnr Signaling Components on migration of EBs during mesoderm differentiation of hESCs. A. Location of gRNAs on the target genes, Apelin, Aplnr and Elabela genes, for CRISPR/Cas9 gene editing technology. B. The protocol, which was used to transfect H9 cells with the CRISPR constructs, was schematically demonstrated. Two hours before electroporation of the CRISPR plasmids, media of hESCs were changed. Electroporation was applied to H9 cells at 0.32V, 250F for 3 minutes. The cells were plated in MTESR media, supplemented with 10uM Y-27632. C. Final CRISPR constructs for Apelin KO, Aplnr KO and Elabela KO were illustrated. D. The protocol, used to form EBS for mesoderm differentiation, were schematically drawn. EBs, formed from hESCs, were transferred to Matrigel-gelatin coated surface at day 2 and migration of the EBs were observed until day 6. E. Morphology of wild type, Apelin KO, Aplnr KO and Elabela KO colonies as monolayer at day 0. F. Morphological pictures were taken at day 2, day 3 and day 6. G. Total area, core area and migration area (total area-core area) as well as core intensity and migration intensity were measured at day 2, day 3 and day 6 and visualized as heat maps for the EBs. H. Line graph of migration area and migration intensity as well as bar graph of total migration area and total migration intensity of the EBs. Scale bar: 100μm.

Effect of Aplnr signaling suppression, by treatment with siRNA of Apelin and Aplnr, on migration of hESC-derived EBs during mesoderm differentiation was observed between day 2 and day 6 (Figure 3.20A and 3.20B). Aplnr siRNA treatment led to increased total area and core area compared to control siRNA treated EBs, while Apelin siRNA treatment didn’t show a significant change in terms of migration and intensity (Figure 3.20C and 3.20D).

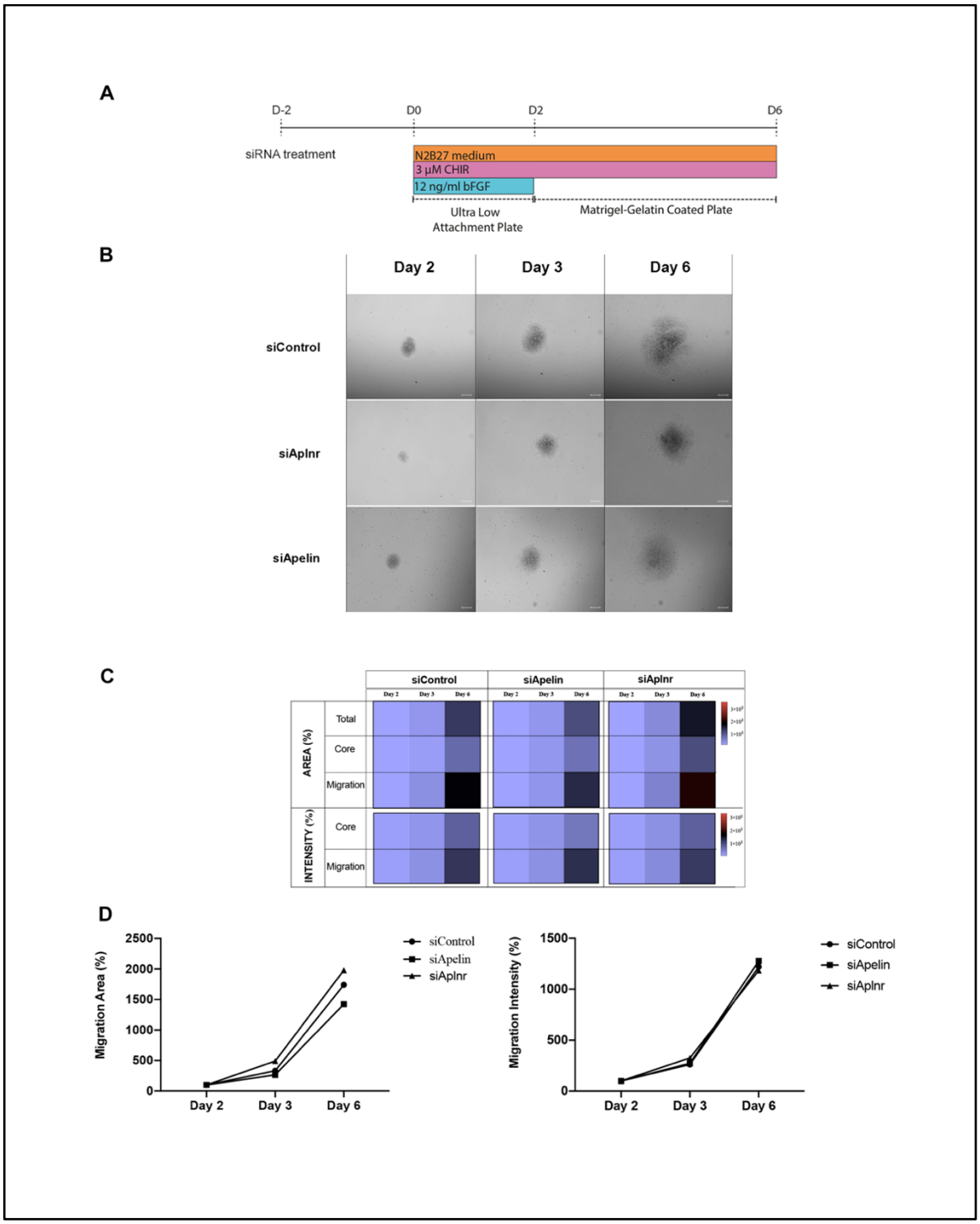


Figure 3.20. Effect of silencing Aplnr signaling by Apelin siRNA and Aplnr siRNA on migration of EBs during mesoderm differentiation of hESCs. A. H9 hESCs were transfected with Control siRNA, Apelin siRNA and Aplnr siRNA. After 2 days, the cells were used to make EBs in low attachment plates. At day 2, EBs were transferred to Matrigel-gelatin coated surface and the migration was observed until day 6. B. Morphological pictures were taken at day 2, day 3 and day 6. C. Total area, core area and

migration area (total area-core area) as well as core intensity and migration intensity were measured at day 2, day 3 and day 6 and visualized as heat maps for Control siRNA, Apelin siRNA and Aplnr siRNA treated EBs. D. Line graph of migration area and migration intensity as well as bar graph of total migration area and total migration intensity of the EBs. Scale bar: 100µm.

Moreover, to activate Aplnr signaling, Apelin, Aplnr and Elabela were also overexpressed and their effect on cell migration during mesoderm differentiation was observed between day 2 and day 6 (Figure 3.21A, 3.21B, 3.21C). Overexpression of Aplnr and Apelin increased migration area and migration intensity approximately 2 fold, whereas overexpression of Elabela enhanced them 1.5 fold compared to control cells (Figure 3.21D and 3.21E).

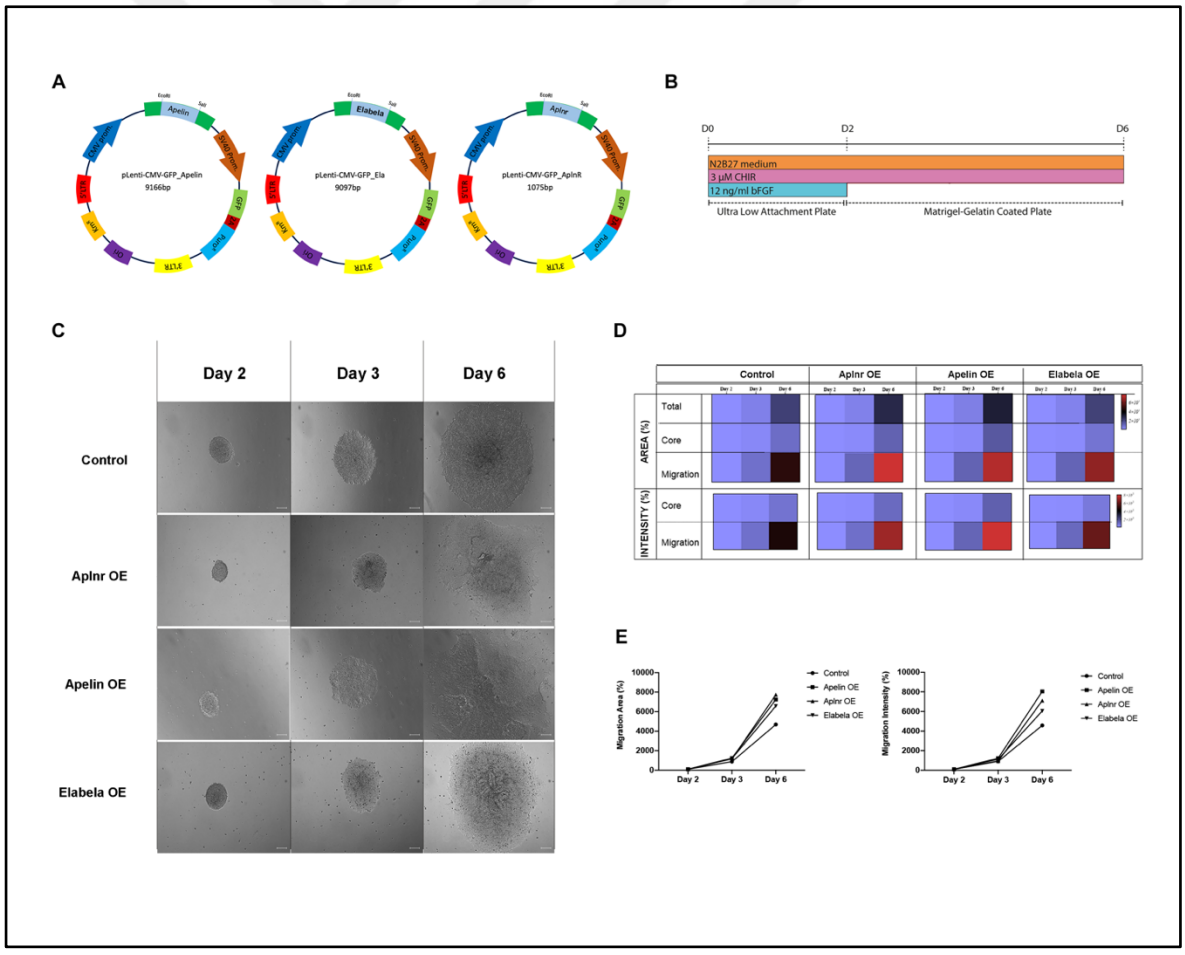


Figure 3.21. Effect of overexpressing Aplnr Signaling Components on migration of EBs during mesoderm differentiation of hESCs. A. Final constructs of lentiviral plasmids for Apelin, Aplnr and Elabela overexpression. B. The protocol, used to form EBS for mesoderm differentiation, were schematically drawn. EBs, formed from hESCs, were

transferred to Matrigel-gelatin coated surface at day 2 and migration of the EBs were observed until day 6. C. Morphological pictures were taken at day 2, day 3 and day 6. D. Total area, core area and migration area (total area-core area) as well as core intensity and migration intensity were measured at day 2, day 3 and day 6 and visualized as heat maps for the EBs. E. Line graph of migration area and migration intensity as well as bar graph of total migration area and total migration intensity of the EBs. Scale bar: 100μm.

All in all, migration area and migration intensity reduced when Aplnr signaling components were silenced or knocked out and increased when Aplnr signaling was activated or overexpressed. The data signifies the regulatory role of Aplnr signaling in cell movement during mesoderm differentiation of hESCs.

3.2.2. Activation of Aplnr Signaling Promotes Mesoderm Commitment of hESC-derived EBs

To investigate how Aplnr signaling activity affects mesoderm differentiation of hESC-derived EBs, Aplnr signaling activity was either induced by Apelin-13 and ML233 or reduced by shRNA, siRNA and CRISPR/Cas9 mediated gene KO. EBs were transferred to Matrigel-gelatin coated surface at day 2 and mesoderm differentiation was observed until day 6. Apelin was added to the medium from day 2 to day 6 (Figure 3.22A). Apelin and Aplnr gene expression levels were measured at day 3, next day of Apelin-13 administration to the media (Figure 3.22B). Antibody array was performed for control and Apelin-13 treated cells at day 6 and the membranes were shown in Figure 3.23A. Hierarchical cluster analysis and heat map analysis showed that the repeats of control and Apelin-13 are highly correlated, 0.94 and 0.99 correlation coefficient values, respectively, while control and Apelin groups were separated, the correlation coefficient values between 0.11 and 0.07 (Figure 3.22C, Figure 3.23B, 3.23C and 3.23D). The results indicated that PDGFRα expression, which is an early mesoderm marker [170,171], significantly increased in Apelin-13 treated cells compared to control cells. Also, Activin, which promotes mesoderm formation [172], Frizzled 7, a Wnt receptor, and Apelin were enhanced in Apelin-13 treated group compared to control group (Figure 3.22D and 3.23E). Wnt pathway was previously reported as a regulator of gastrulation movements, mesoderm induction as well as morphogenetic events and Aplnr is a target of Wnt pathway [127,172,173]. Expression of TGF-beta 1 and TGF-

beta 3, which induce mesoderm differentiation of hESCs [172,174,175], also increased with Apelin-13 treatment. Furthermore, Cryptic protein, which is required for Nodal signaling during mesendodermal specification [176], was expressed significantly higher in Apelin-13 treated cells. Moreover, expression of BMP proteins, which act through Brachyury (T/Bra) and play role in determination of mesodermal cell type [177,178], were enhanced with Apelin-13 administration (Figure 3.22D and 3.23E). However, although Brachyury mRNA expression level was upregulated at day 6 in Apelin-13 and ML233 treated groups compared to control group, expression of Apelin, Aplnr, Flk-1, PDGFRα and Tert were downregulated in the cells (Figure 3.22E and 3.24C). According to IF data at day 3, mesoderm marker, Flk1, and Aplnr expression increased 0.5 fold, while expression of ectoderm marker, Sox2, decreased 0.1 fold after Apelin-13 treatment compared to control cells. Akt, mTOR, MyoD, Mek1/2, Apelin, PDGFRα and Erk1/2 expressions were not significantly changed with Apelin-13 or ML233 administration, compared to control cells (Figure 3.22F, 3.22G, 3.24A and 3.24B). Additionally, differential expression analysis for mRNA seq and miRNA seq of hESC-derived mesoderm cells with and without Apelin-13 treatment at day 6 was assessed (Figure 3.25 and 3.26). As shown in principal component analysis (Figure 3.25A) and hierarchical cluster analysis with heat map (Figure 3.25B), the repeats of Apelin-13 treated cells were grouped together and separated from the control group. Figure 3.25C demonstrates significantly upregulated and down regulated mRNAs as volcano plot. According to enrichment analyses of top upregulated gene expressions in Apelin-13 treated group, molecular functions, including DNA binding, protein complex binding, enzyme binding, protein binding, increased. Also, cellular components, such as membrane bounded organelles, cytoplasm, plasma membrane, and biological processes, in terms of response to stimulus, regulation of biological and cellular processes, multicellular organismal process, cellular component organization and biogenesis and developmental process, were enhanced significantly in Apelin-13 treated group (Figure 3.25D, 3.26D, 3.26F and 3.26H). On the other hand, enrichment analyses of top downregulated gene expressions in Apelin-13 treated cells indicated that molecular functions, including small molecule binding, nucleic acid binding, RNA and protein binding, were reduced in Apelin-13 treated group. Cellular components, such as nucleus, intracellular and membrane bound organelles, and biological processes, consisting of cellular macromolecule metabolic process, regulation of cellular process, down regulated in Apelin-13 treated group (Figure 3.25E, Figure 3.26E, 3.26G and 3.26I). For miRNA seq, principal component analysis (Figure 3.25F) and hierarchical cluster

analysis with heat map (Figure 3.25G) shows the repeats of Apelin-13 treated cells were grouped together and separated from the control group. Figure 3.25H demonstrates significantly upregulated and down regulated miRNAs as volcano plot. Significantly upregulated miRNAs (Figure 3.27 and 3.28) and downregulated miRNAs (Figure 3.27E and 3.29) in Apelin-13 treated cells were listed with enrichment analysis and Kegg pathway analysis. Control and Apelin-13 treated mesoderm cells were subjected to a further analysis with LC/MS protein profiling (Figure 3.30, Table 3.4). Close correlation of Apelin-13 and control sample were observed with hierarchical cluster analysis and heat map, with 0.99 correlation coefficient value (Figure 3.30A and 3.30B). Distribution of protein quantification for significantly increased and decreased expressions with Apelin-13 treatment were demonstrated on the histogram (Figure 3.30C) and profile plot (Figure 3.30D). According to the gene ontology analysis, molecular functions, such as binding, transcription regulator activity and transporter activity increased while ATP-dependent activity, and translation regulator activity decreased in Apelin-13 treated group (Figure 3.30E). Biological processes, including biological regulation, developmental process and response to stimulus increased in Apelin-13 treated group (Figure 3.30F). Moreover, while EGFR signaling pathway and TGF-beta pathway activity increased in Apelin-13 treated group, Axon guidance and ubiquitin proteosome pathway activity decreased (Figure 3.30G). According to the protein-protein interaction network, generated using string, clustered network with clustering coefficient 0.2 contained 10 nodes and 1 edge with 0 expected edges for significantly upregulated proteins in Apelin-13 treated EBs. This indicates almost no interactions between the proteins. Clustered network with clustering coefficient 0.37 contained 25 nodes and 26 edges with 8 expected edges for significantly enhanced proteins in control EBs. These indicate much more interaction than the expected values (Figure 3.30H).

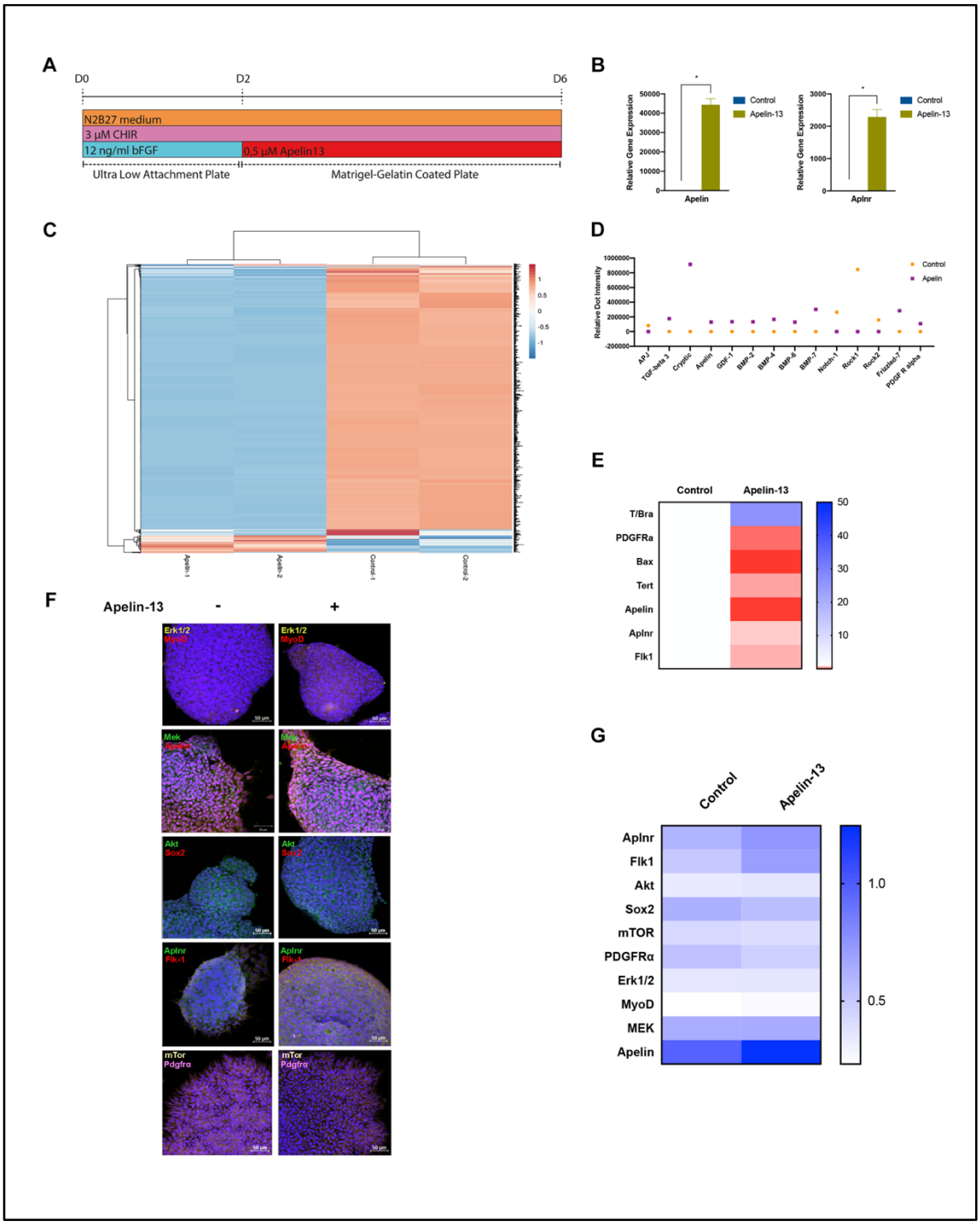


Figure 3.22. Effect of Aplnr Activity on Mesoderm Differentiation of hESCs. A. Protocol for mesoderm differentiation from hESC was shown. EBs, formed from hESCs, were transferred to Matrigel-gelatin coated surface at day 2 and incubated until day 6. B. Gene expression analysis for Aplnr and Apelin. C. Hierarchical cluster analysis and heat map representation of proteins from the antibody arrays of control group and Apelin-13 treated group at day 6 were shown. D. Relative dot intensities for selected proteins from the

antibody array were shown in the graph. E. Relative gene expression levels of the EBs at day 6 were shown as a heatmap. F. The EBs were fixed using 4% paraformaldehyde at the end of day 3 and they were analyzed for protein expression of the Apelin (red), Aplnr(green), MAPK pathway proteins, MEK1/2 (green) and ERK1/2(yellow), and mesoderm markers, Flk(red) and MyoD (magenta). DAPI (Blue) was used to stain nuclei of the cells. The merged images were shown. G. Intensities of the protein expressions were measured from the immunofluorescence images and represented as a heatmap. Scale Bar: 50µm. P<0.0001

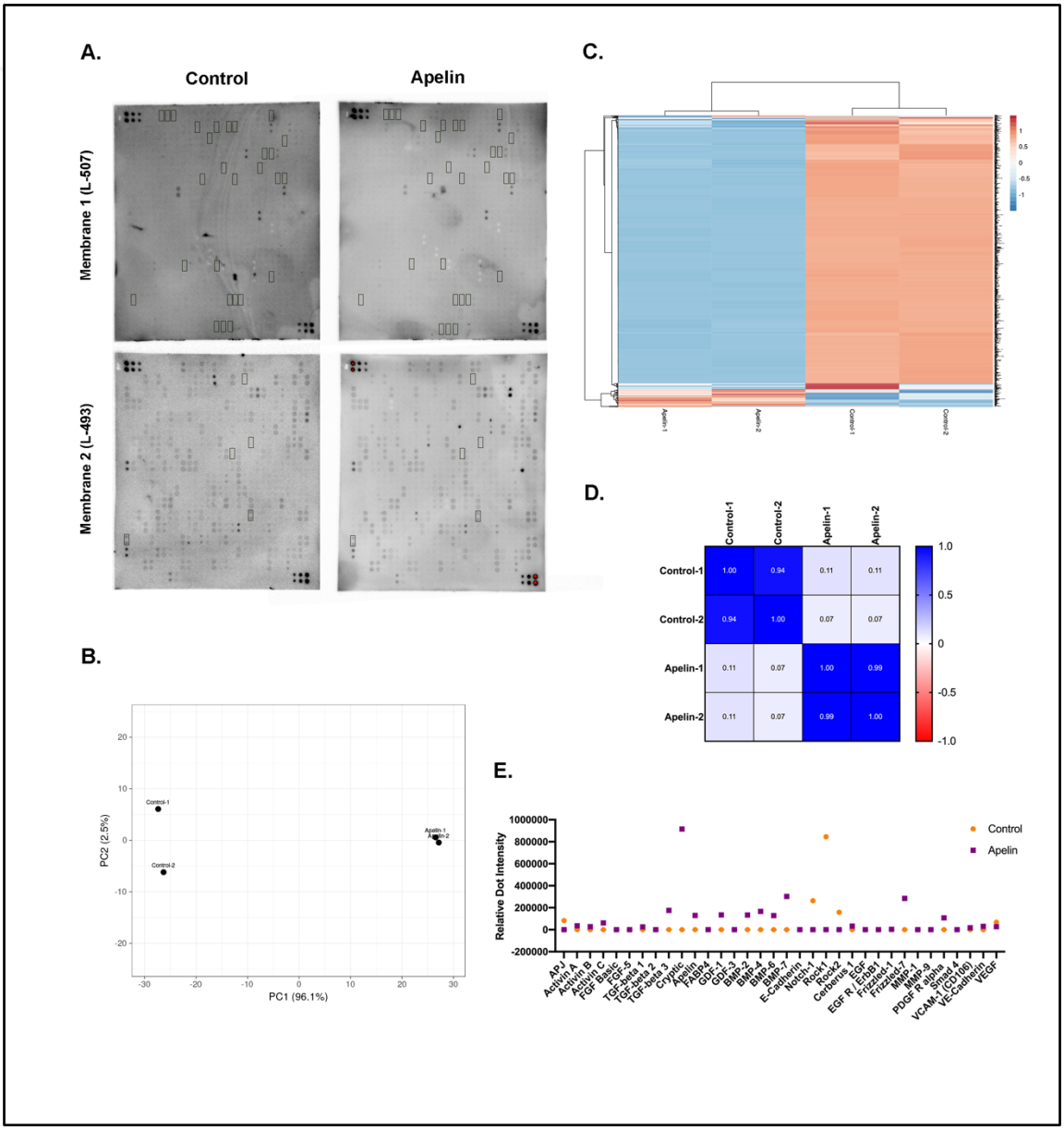


Figure 3.23. Antibody array analysis of hESC derived EBs treated with Apelin-13. A. Membranes of the antibody array for the day 6 mesoderm cells. Mesoderm related proteins

were selected with black boxes on the membranes. B. Principal component analysis (PCA) of the cells. C. Hierarchical cluster analysis and heat map representation of proteins from Control and Apelin-13 treated EBs at day 6. D. Correlation coefficient matrix of the proteins. E. A scattered graph indicating relative dot intensity for Control and Apelin-13 treated groups.

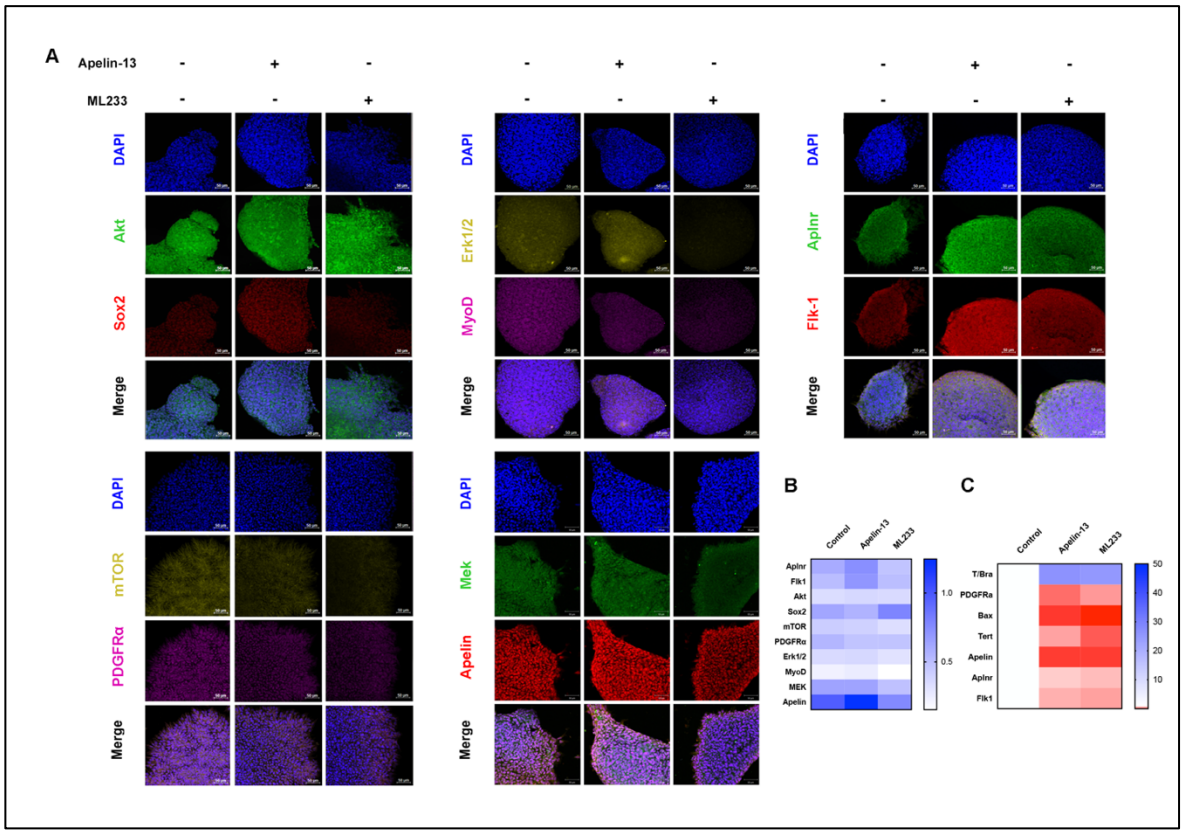


Figure 3.24. Effect of activation of Aplnr by Apelin-13 and ML233 on mesoderm differentiation of hESCs. A. The EBs were fixed using 4% paraformaldehyde at the end of day 3 and they were analyzed for protein expression of Apelin, Aplnr, MEK1/2, ERK1/2, Akt, Sox2, mTOR, PDGFRα, Flk1 and MyoD. DAPI was used to stain nuclei of the cells. B. Intensities of the protein expressions were measured from the immunofluorescence images and represented as a heatmap. C. Relative gene expression levels of the EBs at day 6 were shown as a heatmap. Scale Bar: 50µm.

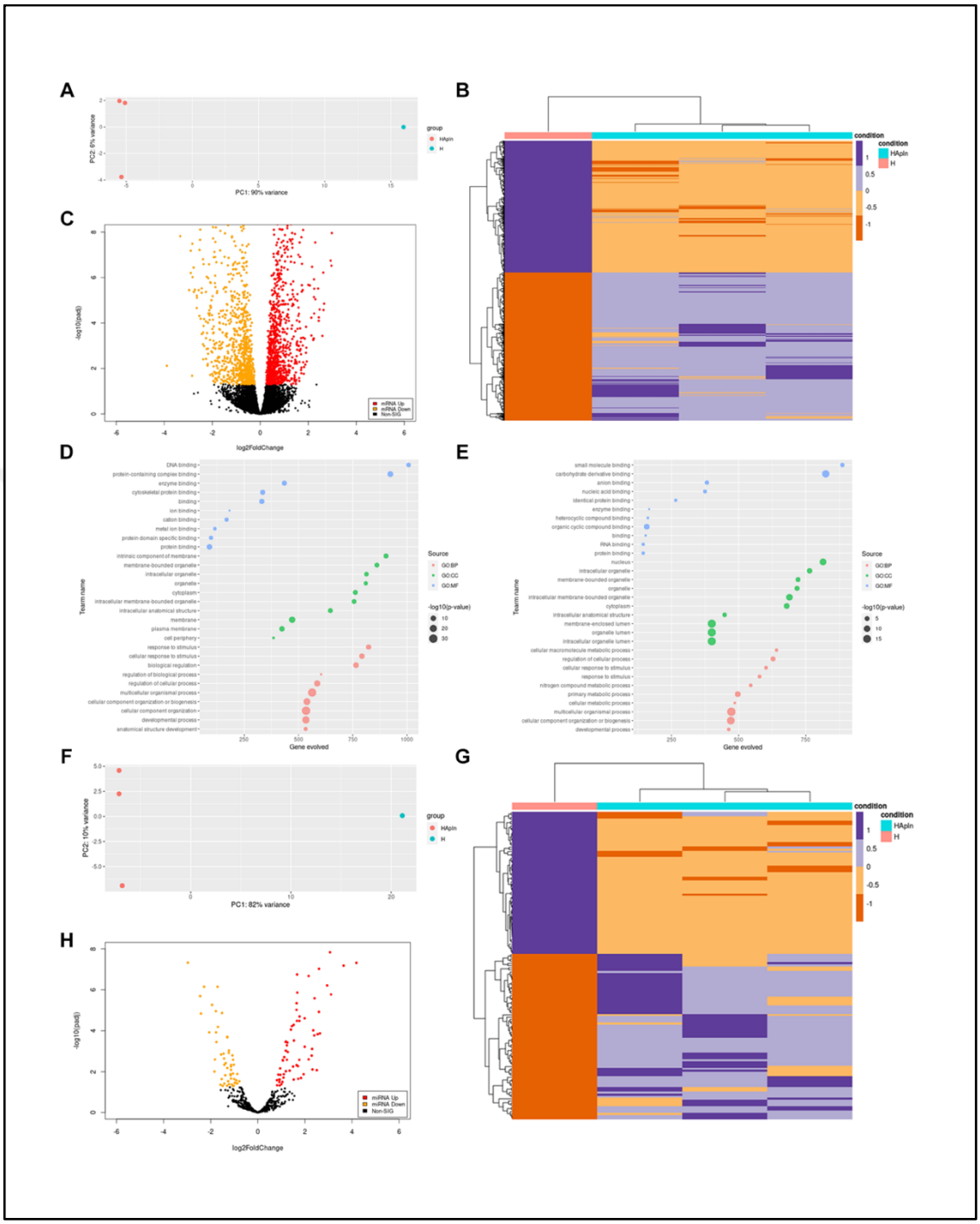


Figure 3.25. Differential expression analysis for mRNA seq and small RNA seq analyses of hESC derived mesodermal cells in the presence of Apelin-13 at day 6. A. Principal component analysis of hESC derived mesoderm cells at day 6 for control and Apelin-13 treated groups after mRNA seq analysis. B. Heat map representation analysis, C. Volcano plot analysis. D. Top 31 pathway enrichment analysis for upregulated genes. Biological process(BP), Cellular Component (CC) and Molecular Function (MF). E. Top 31 pathway enrichment analysis for downregulated genes. F. Principal component analysis of hESC

derived mesoderm cells at day 6 for control and Apelin-13 treated groups after miRNA seq analysis. G. Heat map representation analysis, H. Volcano plot analysis. H: control group, HApln: Apelin-13 treated group.

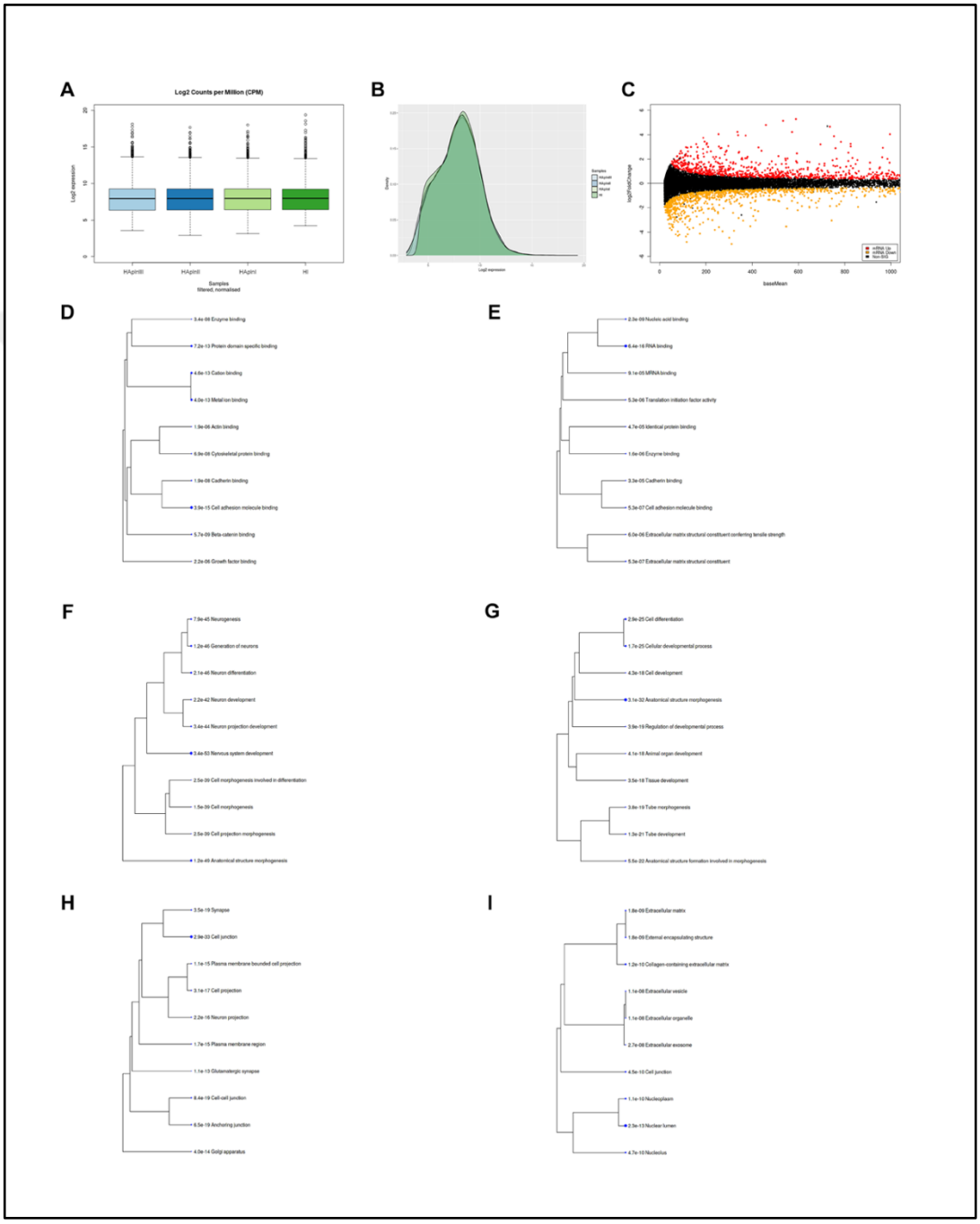
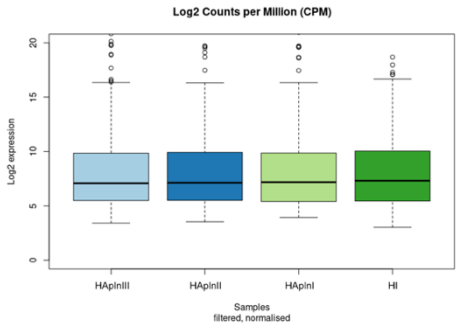


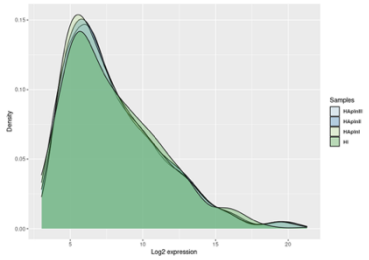
Figure 3.26. Differential expression analysis for mRNA seq analysis of hESC derived mesodermal cells in the presence of Apelin-13 at day 6. Data distribution of hESCs at day 6 (mesoderm) for control and Aplnr activation in differential expression analysis. A. Data distribution after normalization (Log 2 counts per million) B. Expression plots (Log 2

expression versus density) were shown. C. MA plot analysis. D. The samples were subjected to functional enrichment analysis. Molecular function tree for upregulated genes and E. downregulated genes. F. Biological process tree for upregulated genes and G. downregulated genes. H. Cellular component tree for upregulated genes and I. downregulated genes. H: control group, HApln: Apelin-13 treated group.

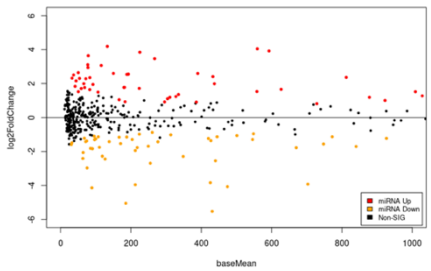
A



B



C



D

Up-regulated miRNAs	
hsa-miR-12136	hsa-miR-301a-3p
hsa-miR-3659	hsa-miR-21-5p
hsa-miR-30e-5p	hsa-miR-150-5p
hsa-miR-30e-3p	hsa-miR-153-3p
hsa-miR-30c-5p	hsa-miR-301b-3p
hsa-miR-101-3p	hsa-miR-33a-5p
hsa-miR-488-3p	hsa-let-7b-5p
hsa-miR-135b-5p	hsa-miR-15b-3p
hsa-miR-5100	hsa-miR-28-5p
hsa-miR-302e	hsa-miR-28-3p
hsa-miR-130a-5p	hsa-miR-576-5p
hsa-miR-130a-3p	hsa-miR-367-3p
hsa-miR-192-5p	hsa-miR-302d-3p
hsa-miR-139-5p	hsa-miR-302a-5p
hsa-miR-139-3p	hsa-miR-302a-3p
hsa-miR-708-5p	hsa-miR-302c-5p
hsa-miR-1251-5p	hsa-miR-302c-3p
hsa-miR-1251-3p	hsa-miR-302b-3p
hsa-miR-135a-5p	hsa-miR-874-5p
hsa-miR-135a-2-3p	hsa-miR-1294
hsa-miR-20a-3p	hsa-miR-146a-5p
hsa-miR-19b-3p	hsa-miR-30a-5p
hsa-miR-127-3p	hsa-miR-30a-3p
hsa-miR-379-5p	hsa-miR-148a-3p
hsa-miR-376c-3p	hsa-miR-590-3p
hsa-miR-1247-5p	hsa-miR-96-5p
hsa-miR-211-5p	hsa-miR-335-5p
hsa-miR-190a-5p	hsa-miR-29a-3p
hsa-miR-193b-3p	hsa-miR-204-5p
hsa-miR-365a-3p	hsa-miR-32-5p
hsa-miR-140-5p	hsa-miR-126-5p
hsa-miR-451a	hsa-miR-126-3p
hsa-miR-4732-3p	hsa-miR-221-5p
hsa-miR-193a-5p	hsa-miR-660-5p
hsa-miR-193a-3p	hsa-miR-374a-5p
hsa-miR-365b-5p	hsa-miR-361-5p
hsa-miR-365b-3p	hsa-miR-106a-5p
hsa-miR-454-5p	hsa-miR-106a-3p
hsa-miR-454-3p	

E

Down-regulated miRNAs	
hsa-miR-760	hsa-miR-6724-5p
hsa-miR-320b	hsa-miR-99a-5p
hsa-miR-205-5p	hsa-miR-1306-3p
hsa-miR-1307-5p	hsa-miR-1226-3p
hsa-miR-210-5p	hsa-miR-135a-3p
hsa-miR-483-5p	hsa-miR-551b-5p
hsa-miR-483-3p	hsa-miR-218-5p
hsa-miR-4687-3p	hsa-miR-218-1-3p
hsa-miR-4485-3p	hsa-miR-1269a
hsa-miR-1908-5p	hsa-miR-449a
hsa-miR-34c-3p	hsa-miR-449c-5p
hsa-let-7i-5p	hsa-miR-584-5p
hsa-miR-320d	hsa-miR-143-3p
hsa-miR-92a-1-5p	hsa-miR-145-5p
hsa-miR-4707-3p	hsa-miR-25-5p
hsa-miR-345-5p	hsa-miR-490-5p
hsa-miR-184	hsa-miR-598-3p
hsa-miR-940	hsa-miR-320a-3p
hsa-miR-497-5p	hsa-miR-4473
hsa-miR-324-3p	hsa-miR-219b-5p
hsa-miR-744-5p	hsa-miR-542-5p
hsa-miR-1269b	hsa-miR-503-5p
hsa-miR-1180-3p	hsa-miR-424-5p
hsa-miR-10a-5p	hsa-miR-424-3p
hsa-miR-3615	hsa-miR-504-5p
hsa-miR-636	hsa-miR-504-3p
hsa-miR-320c	hsa-miR-767-5p
hsa-miR-4741	
hsa-miR-3187-3p	
hsa-miR-6789-3p	
hsa-miR-181c-5p	
hsa-miR-181d-5p	
hsa-let-7e-5p	
hsa-miR-1301-3p	
hsa-miR-216a-5p	
hsa-miR-216b-5p	
hsa-miR-3679-5p	
hsa-miR-375-3p	
hsa-miR-4440	

Figure 3.27. miRNA seq analysis of hESC derived mesodermal cells in the presence of Apelin-13 at day 6. Data distribution of hESCs at day 6 (mesoderm) for control and Aplnr activation. A. Data distribution after normalization (Log 2 counts per million) B. Expression plots (Log 2 expression versus density) were shown. C. MA plot analysis. D. List of significantly upregulated miRNAs and E. downregulated miRNAs in Aplnr activated groups compared to control groups. H: control group, HApln: Apelin-13 treated group.

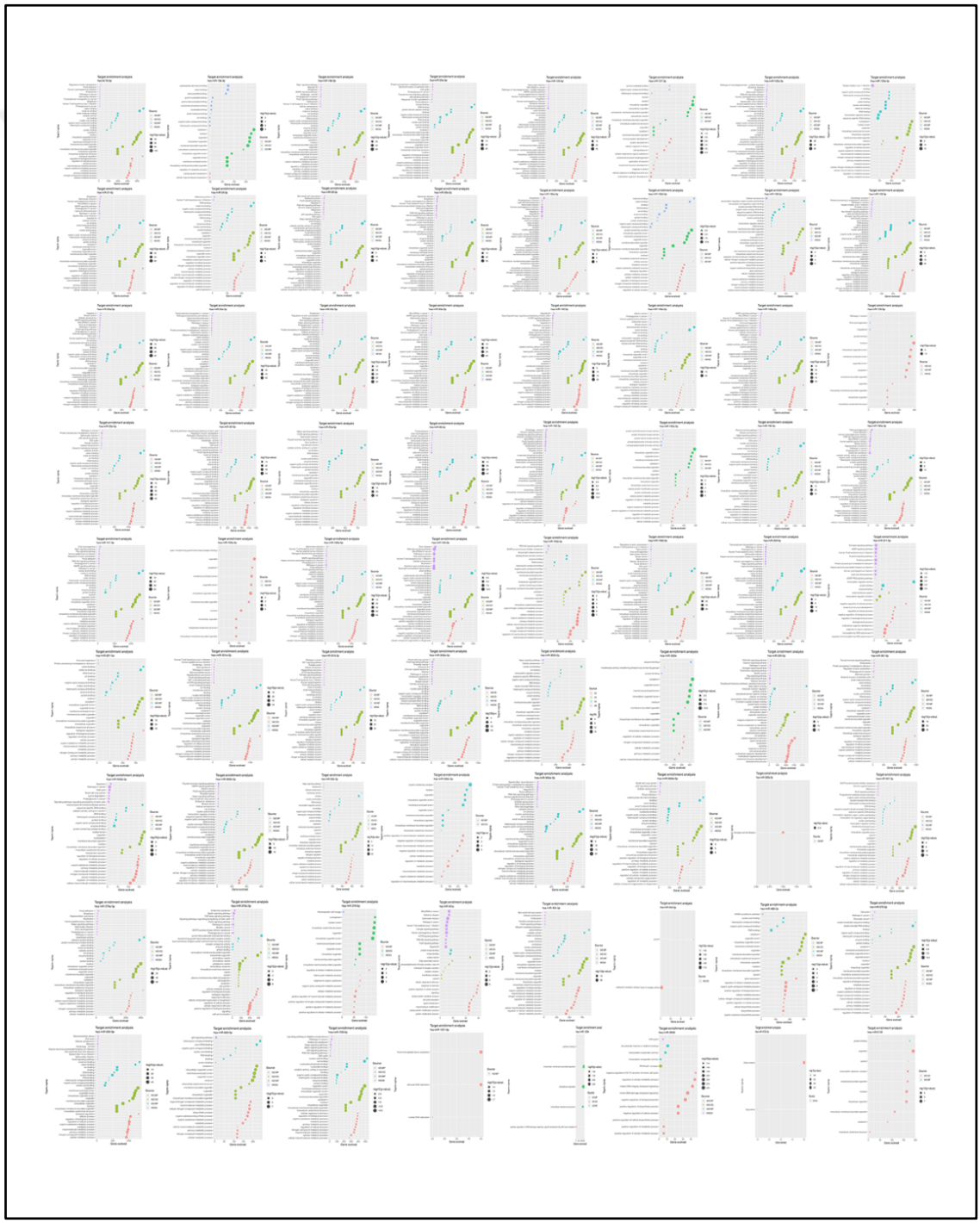


Figure 3.28. Functional Enrichment Analysis of Significantly Upregulated miRNAs in Apelin-13 treated mesoderm cells. BP:Biological Process, CC:Cellular Component, MF:Molecular Function



Figure 3.29. Functional Enrichment Analysis of Significantly Downregulated miRNAs in Apelin-13 treated mesoderm cells. BP:Biological Process, CC:Cellular Component, MF:Molecular Function

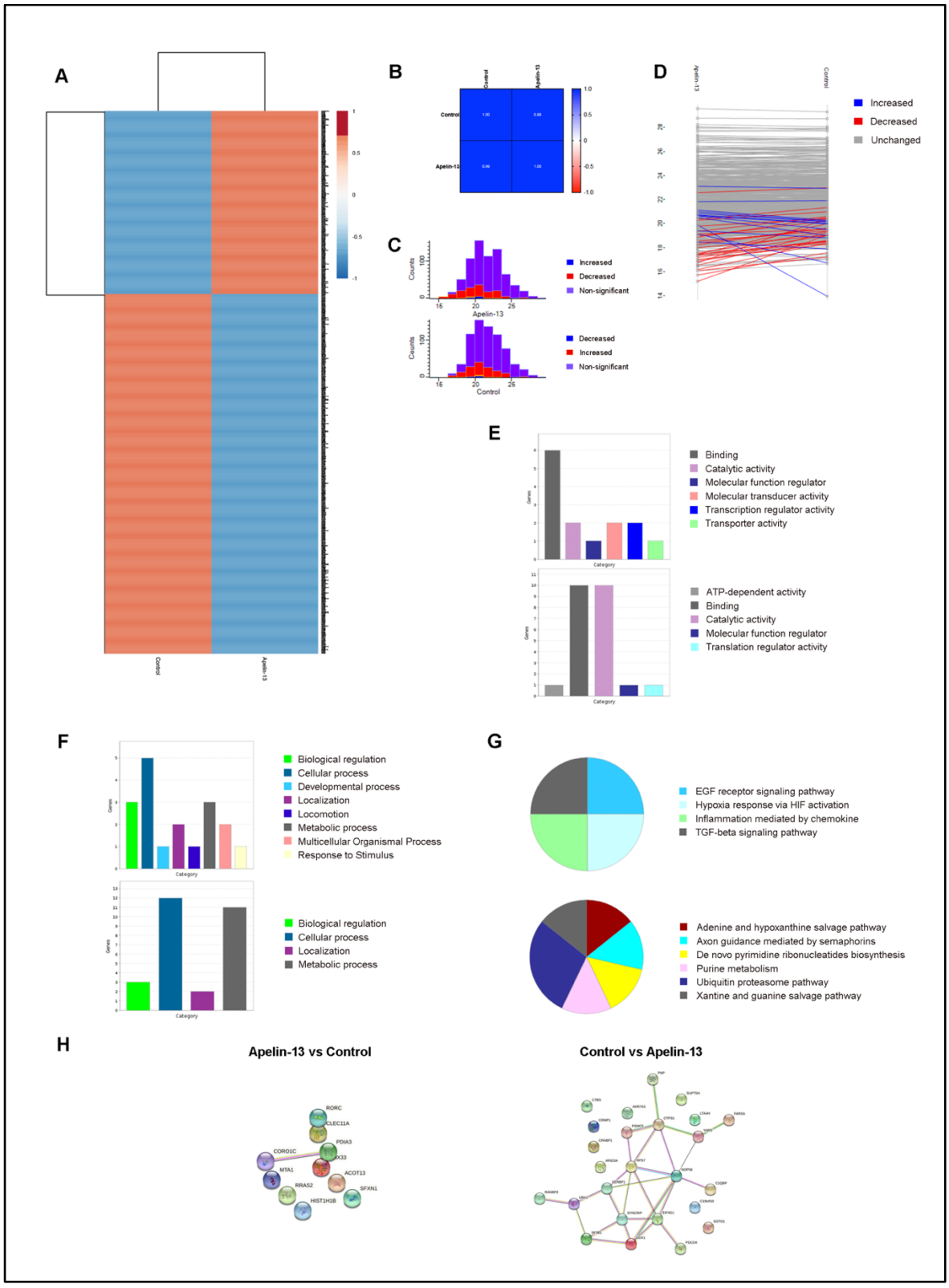


Figure 3.30. Protein profile of hESC derived EBs treated with Apelin-13. A. Hierarchical cluster analysis and heat map representation of proteins from control and Apelin-13 treated EBs at day 6. B. Correlation coefficient matrix of the proteins. C. Histogram indicating the

distribution of the protein quantification. D. Profile plot indicating the proteins, which were significantly upregulated (blue) and downregulated (red) after Apelin-13 treatment. The graphs demonstrating E. molecular functions, F. biological processes and G. related pathways of the upregulated (top) and downregulated (bottom) proteins in Apelin-13 treated EBs. H. Protein interaction network for the upregulated proteins in Apelin-13 treated EBs (left) and control group (right).

Table 3.4. Protein profiling data of control group and Apelin-13 treated group at day 6. Apelin-13 was added to the media between day 2 and day 6. Significantly increased (red) and decreased (black) proteins in Apelin-13 treated group compared to control group were listed on the table.

Accession	**Description**	**Abundance Ratio: Apelin-13/Control**
A0A5F9ZHF9	Phosphodiesterase	**61,724**
P51449	Nuclear receptor ROR-gamma	**5,245**
Q9H6R0	ATP-dependent RNA helicase	**2,768**
P62070	Ras-related protein R-Ras2	**1,922**
Q9Y240	C-type lectin domain family 11 member A	**1,714**
H0Y449	Y-box-binding protein 1	**1,701**
H7BZJ3	Protein disulfide-isomerase A3	**1,636**
P16401	Histone H1.5	**1,627**
Q9ULV4	Coronin-1C	**1,619**
A0A0U1RRI6	Centromere protein V-like protein 3	**1,616**
Q13330	Metastasis-associated protein MTA1	**1,612**
Q9H9B4	Sideroflexin-1	**1,514**
Q9NPJ3	Acyl-coenzyme A thioesterase 13	**1,505**
P09960	Leukotriene A-4 hydrolase	**0,498**

Q9Y285	Phenylalanine-tRNA ligase alpha subunit	**0,49**
O60506	Heterogeneous nuclear ribonucleoprotein Q	**0,485**
Q53EL6	Programmed cell death protein 4	**0,474**
P00491	Purine nucleoside phosphorylase	**0,473**
Q92499	ATP-dependent RNA helicase DDX1	**0,45**
P78417	Glutathione S-transferase omega-1	**0,444**
O75533	Splicing factor 3B subunit 1	**0,438**
Q9UBT2	SUMO-activating enzyme subunit 2	**0,414**
P49792	E3 SUMO-protein ligase RanBP2	**0,41**
Q99856	AT-rich interactive domain-containing protein 3A	**0,407**
O00267	Transcription elongation factor SPT5	**0,393**
Q04637	Eukaryotic translation initiation factor 4 gamma 1	**0,37**
Q14194	Dihydropyrimidinase-related protein 1	**0,346**
O00567	Nucleolar protein 56	**0,336**
P54577	Tyrosine-tRNA ligase, cytoplasmic	**0,324**
Q01459	Di-N-acetylchitobiase	**0,29**
P62195	26S proteasome regulatory subunit 8	**0,283**
P62081	40S ribosomal protein S7	**0,281**
Q8NC51	Plasminogen activator inhibitor 1 RNA-binding protein	**0,278**
P29762	Cellular retinoic acid-binding protein 1	**0,264**
P17812	CTP synthase 1	**0,214**
O95154	Aflatoxin B1 aldehyde reductase member 3	**0,171**
Q07021	Complement component 1 Q subcomponent-binding protein, mitochondrial	**0,077**
Q969H8	Myeloid-derived growth factor	**0,069**

For shApelin and shAplnr virus given hESC (Figure 3.31A), reduced expression of Apelin and Aplnr at day 0 were verified with pcr analysis (Figure 3.31B) before formation of EBs (Figure 3.31A). Gene expression data at day 6 also demonstrates low level of Apelin and Aplnr expression in shAplnr group compared to shControl group. On the other hand, Brachyury, PDGFRα and Tert gene expression significantly increased in both shApelin and shAplnr cells compared to shControl cells. While Foxf1 expression significantly reduced in both shApelin and shAplnr cells compared to shControl cells, Flk1 expression only reduced in shApelin cells and increased in shAplnr cells (Figure 3.31C and 3.32C). IF data analysis at day 3 revealed that Flk1 and Aplnr was expressed approximately 2 fold more in shControl cells, compared to shApelin and shAplnr cells. Interestingly, Sox2 expression level was also decreased about 1.2 fold in both shApelin and shAplnr cells compared to shControl cells. Expression levels of PDGFRα, Akt and mTOR were almost the same for all the groups. Erk1/2 and MyoD expression levels increased 2 fold in shAplnr cells, while Mek1/2 expression decreased 0.1 fold compared to control group. Also, Apelin expression level increased 0.2 fold in shApelin group compared to control group (Figure 3.31D, 3.31E, 3.32A and 3.32B).

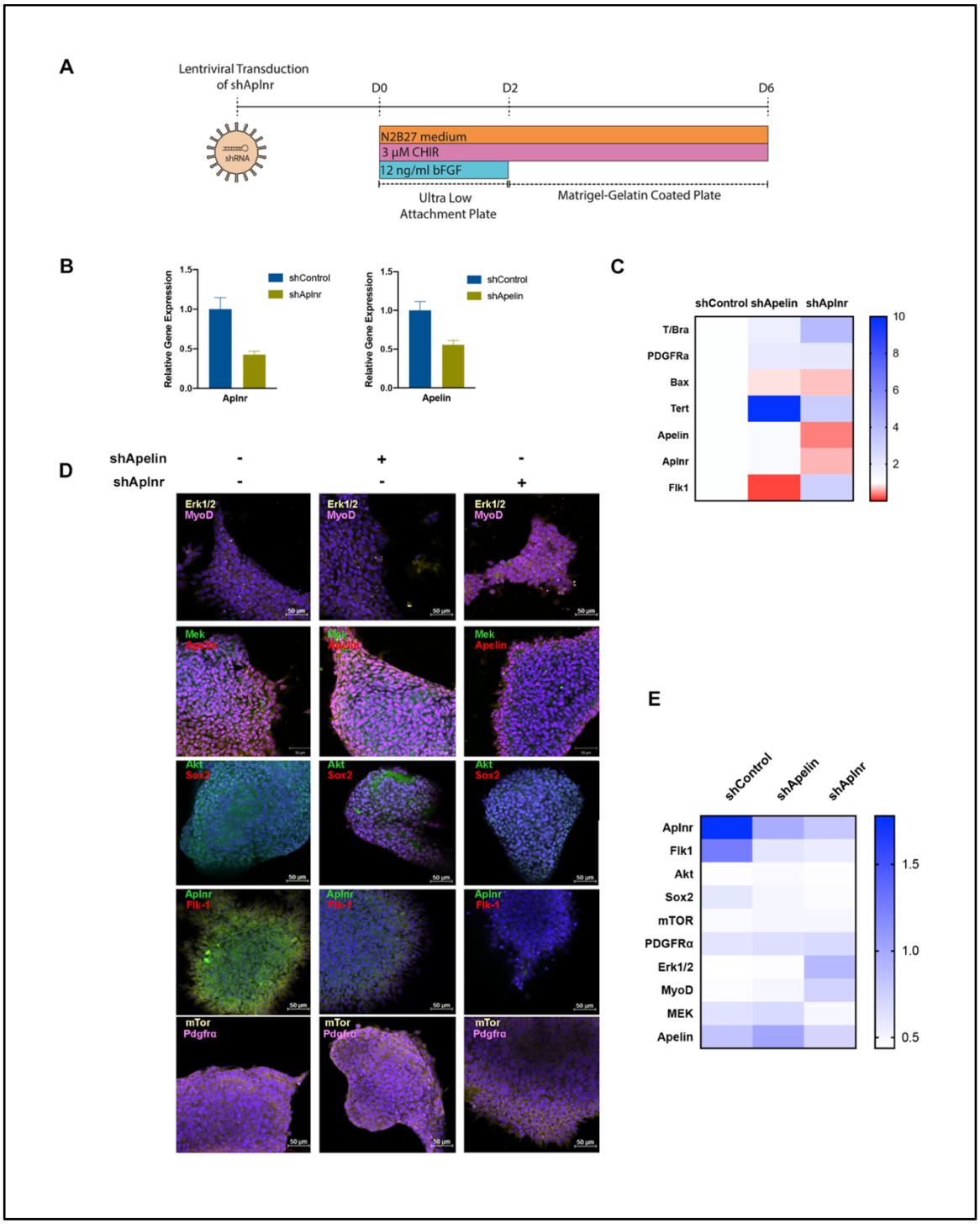


Figure 3.31. Effect of Downregulation of Aplnr Signaling Components on Mesoderm Differentiation of hESCs. A. Protocol for mesoderm differentiation of shRNA given hESC. shRNA lentiviruses were produced and given to hESCs via transduction. EBs, formed from the hESCs, were transferred to Matrigel-gelatin coated surface at day2 and incubated until day 6. B. Gene expression level of Apelin and Aplnr at day 0 to verify downregulation of the gene with the shRNA administration. C. Relative gene expression levels of the EBs at

day 6 were shown as a heatmap. D. The EBs were fixed using 4% paraformaldehyde at the end of day3 and they were analyzed for protein expression of the Apelin (red), Aplnr (green), MAPK pathway proteins, MEK1/2 (green) and ERK1/2(yellow), and mesoderm markers, Flk(red) and MyoD (magenta). DAPI (Blue) was used to stain nuclei of the cells. The merged images were shown. E. Intensities of the protein expressions were measured from the immunofluorescence images and represented as a heatmap. Scale Bar: 50µm.

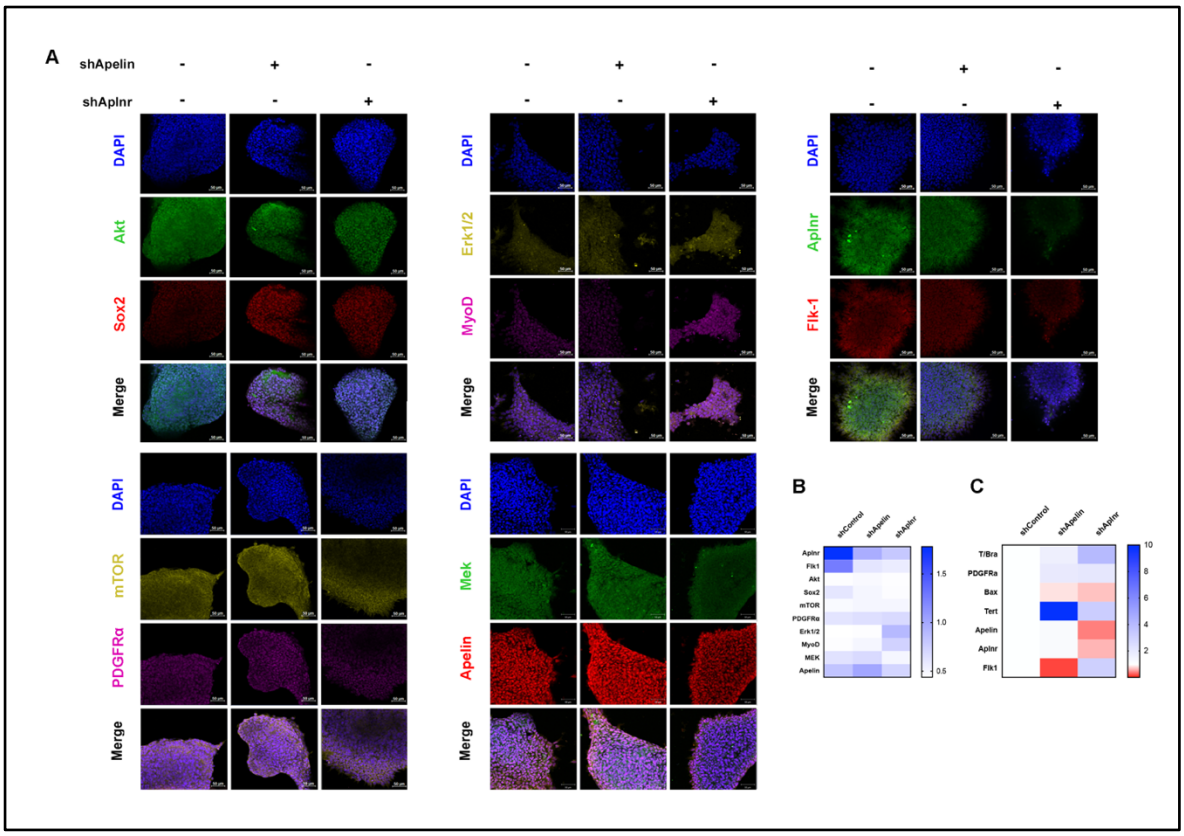


Figure 3.32. Effect of shRNA mediated Downregulation of Aplnr Signaling Components on Mesoderm Differentiation of hESCs. A. The EBs were fixed using 4% paraformaldehyde at the end of day 3 and they were analyzed for protein expression of Apelin, Aplnr, MEK1/2, ERK1/2, Akt, Sox2, mTOR, PDGFRα, Flk1 and MyoD. DAPI was used to stain nuclei of the cells. B. Intensities of the protein expressions were measured from the immunofluorescence images and represented as a heatmap. C. Relative gene expression levels of the EBs at day 6 were shown as a heatmap. Scale Bar: 50µm.

Effect of CRISPR/Cas9 mediated KO of Apelin, Aplnr and Elabela genes on mesoderm differentiation was assessed by gene and protein expression analysis (Figure 3.19D). According to the IF analysis of the EBs at day 3, Aplnr expression slightly reduced in all the

KO cell lines compared to control group. Although Flk1 expression was also slightly downregulated in Apelin KO and Elabela KO group, it was upregulated 0.1 fold in Aplnr KO cells compared to Control. Akt expression slightly increased in Aplnr KO cells, but its expression in the others was like the control. Expression of Sox2 increased 2.5 fold in Aplnr KO cells, 1.5 fold in Elabela KO cells compared to control group. Erk1/2 expression increased 0.5 fold in Aplnr KO cells compared to control. mTOR and MyoD expressions didn't show any significant change in the KO cells lines. On the other hand, PDGFRα expression reduced 0.5 fold in all KO cells compared to its expression in control. Also, Mek1/2 and Apelin expression levels reduced 0.5 fold in Apelin KO cells compared to control cells (Figure 3.33A and 3.33B). mRNA expression analysis at day 6 demonstrated significant increase at Tert gene expression in Apelin KO, Aplnr KO and Elabela KO cells compared to Wild Type. PDGFRα, Bax and Apelin was significantly upregulated in Aplnr KO cells while Brachyury expression was downregulated in Apelin KO cells. Moreover, Flk1 expression was not detected in Aplnr KO cells (Figure 3.33C).

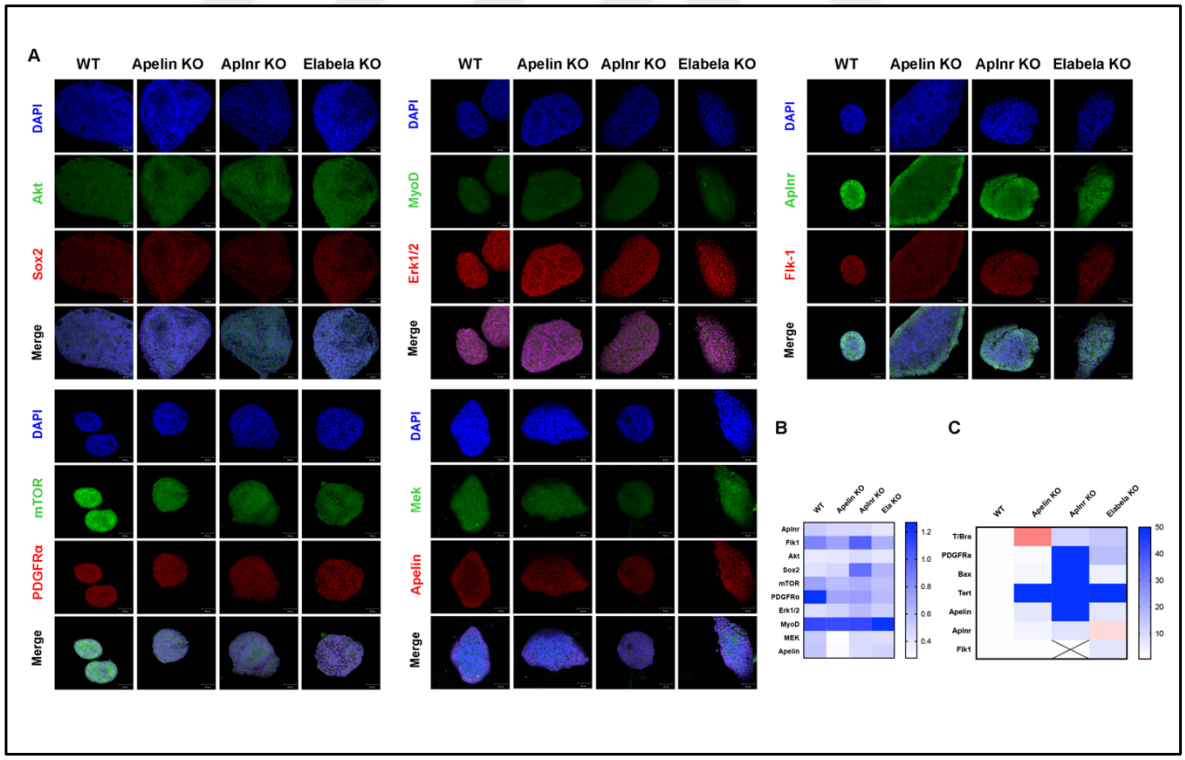


Figure 3.33. Effect of CRISPR-Cas9 mediated Knock Out of Aplnr Signaling Components on Mesoderm Differentiation of hESCs. A. The EBs were fixed using 4% paraformaldehyde at the end of day 3 and they were analyzed for protein expression of Apelin, Aplnr, MEK1/2, ERK1/2, Akt, Sox2, mTOR, PDGFRα, Flk1 and MyoD. DAPI

was used to stain nuclei of the cells. B. Intensities of the protein expressions were measured from the immunofluorescence images and represented as a heatmap. C. Relative gene expression levels of the EBs at day 6 were shown as a heatmap. Scale Bar: 50µm.

In order to further realize the effect of Aplnr signaling in mesoderm differentiation, Apelin and Aplnr siRNA treated hESC were made EB and differentiated with the mesoderm differentiation protocol (Figure 3.20A). IF data at day 3 demonstrates that Apelin siRNA didn't show a significant change on protein expression levels compared to control siRNA. However, Sox2 expression significantly increased while MyoD, Flk1 and Aplnr expression noticeably decreased in Aplnr siRNA treated cells (Figure 3.34A and 3.34B). According to mRNA expression analysis at day 6, Brachyury and PDGFRα significantly decreased and Apelin increased in both Apelin and Aplnr siRNA treated cells compared to control cells (Figure 3.34C).

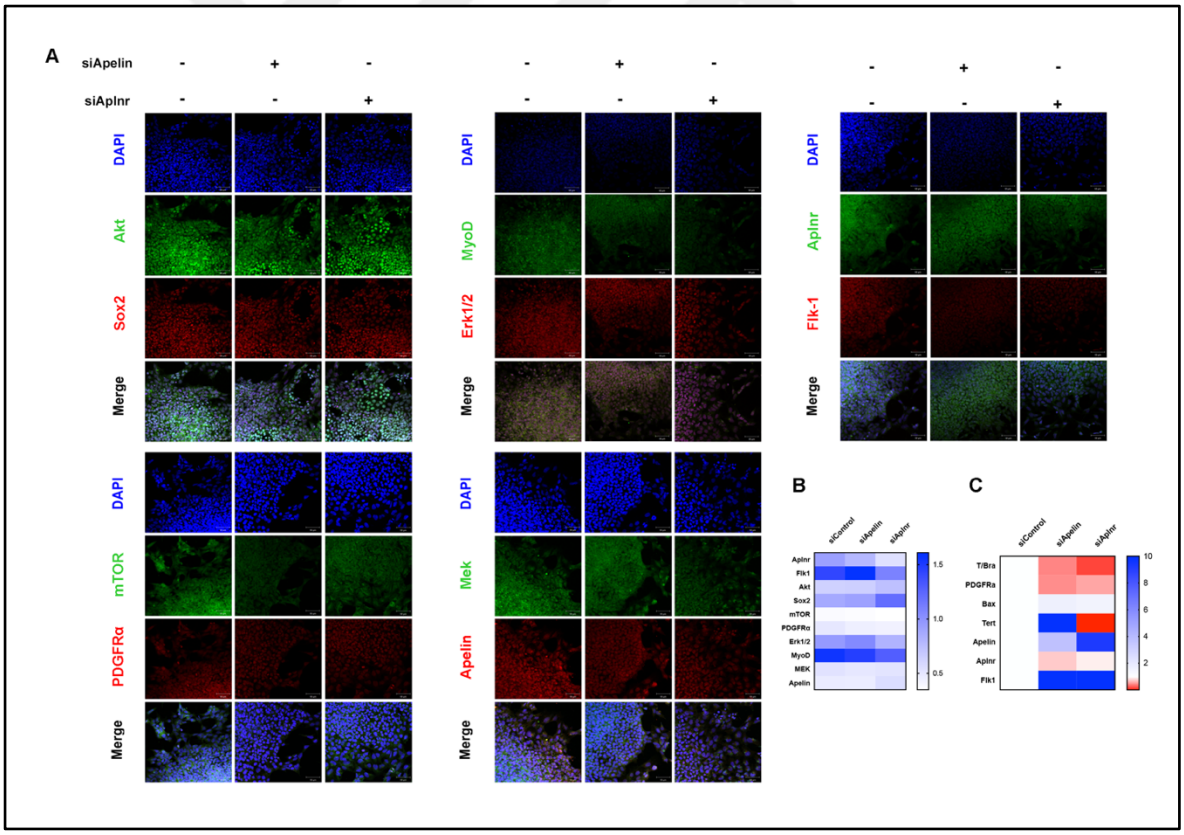


Figure 3.34. Effect of siRNA mediated Downregulation of Aplnr Signaling Components on Mesoderm Differentiation of hESCs. A. The EBs were fixed using 4% paraformaldehyde at the end of day 3 and they were analyzed for protein expression of Apelin, Aplnr, MEK1/2, ERK1/2, Akt, Sox2, mTOR, PDGFRα, Flk1 and MyoD. DAPI

was used to stain nuclei of the cells. B. Intensities of the protein expressions were measured from the immunofluorescence images and represented as a heatmap. C. Relative gene expression levels of the EBs at day 6 were shown as a heatmap. Scale Bar: 50µm.

Effect of Aplnr signaling on mesoderm differentiation was also investigated by transfecting Apelin, Aplnr and Elabela overexpressing plasmids to hESCs (Figure 3.21A). IF data at day 3 demonstrates that Aplnr expression increased 0.5 fold in Apelin overexpressing cells, and 2 fold for Aplnr and Elabela overexpressing cells compared to the control cells. Similarly, Flk1 expression was enhanced 6 fold for Apelin, 4 fold for Aplnr and 7 fold for Elabela overexpressing cells compared to control cells. Akt, Apelin and Erk1/2 expressions were not significantly changed, but Sox2 expression slightly decreased in the all-shRNA groups. On the other hand, mTOR and PDGFRα expressions increased slightly compared to control group. MyoD expression increased, 2fold, only in Aplnr oe group compared to control (Figure 3.35A and 3.35B). Moreover, mRNA expression data at day 6 showed significantly increased Brachyury, Bax, Apelin and Aplnr expressions in Aplnr overexpressed (oe) cells. On the other hand, Flk1 and Foxf1 expression levels significantly decreased in both Aplnr oe and Elabela oe cells compared to controls (Figure 3.35C).

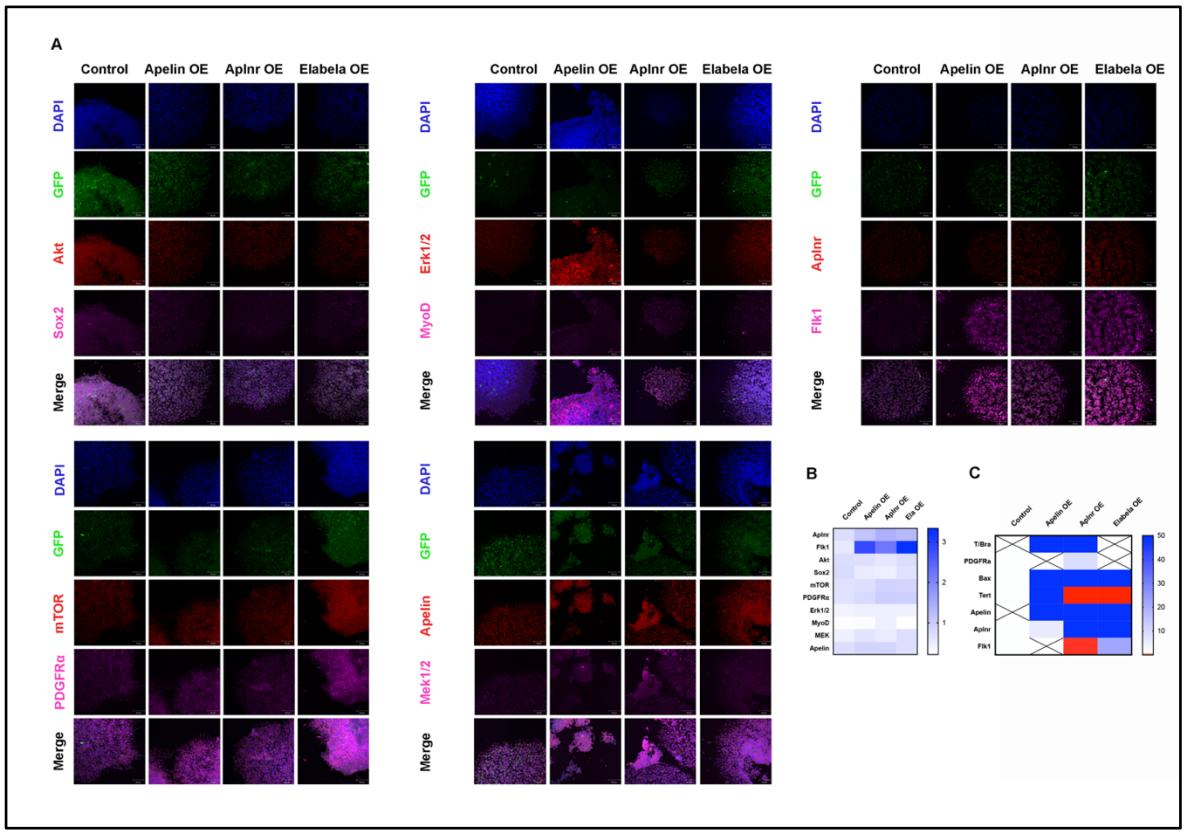


Figure 3.35. Effect of Overexpression of Aplnr Signaling Components on Mesoderm Differentiation of hESCs. A. The EBs were fixed using 4% paraformaldehyde at the end of day 3 and they were analyzed for protein expression of Apelin, Aplnr, MEK1/2, ERK1/2, Akt, Sox2, mTOR, PDGFRα, Flk1 and MyoD. DAPI was used to stain nuclei of the cells. B. Intensities of the protein expressions were measured from the immunofluorescence images and represented as a heatmap. C. Relative gene expression levels of the EBs at day 6 were shown as a heatmap. Scale Bar: 50µm.

Altogether, these data suggest the promoting effect of Aplnr signaling on mesoderm commitment of hESC-derived EBs. Also, protein, mRNA and miRNA analysis reveal that Aplnr signaling acts together with various signaling pathways, such as EGFR and TGF-beta signaling to induce mesoderm differentiation.

3.2.3. Aplnr Signaling Activity Enhances MSC Differentiation from hESC-derived mesoderm progenitors

To reveal the effect of Aplnr signaling on MSC Differentiation from hESCs, Apelin was administered to the media at the different points during MSC differentiation. After hESCs were made EBs, the EBs were transferred to Matrigel-gelatin coated surface at day 3. During the MSC differentiation, which takes 24 days, Apelin was added to the media between day 3 and day 5 (Option 2), day 5 and day 8 (Option 3), day 8 and day10 (Option 4), day 10 and day 24 (Option 5) and day 3 and day 24 (Option 6). Apelin was not added to the control group, Option 1 (Figure 3.36A and 3.37A). However, MSC cell phenotype with fibroblast cell morphology and plastic adherence were observed only in Option 1, Option 2 and Option 6 at day 10 and day24 (Figure 3.36D and 3.37B). Cell proliferation and viability were significantly higher after 24 hours, 48 hours and 72 hours for Option 2 group (Figure 3.36B and 3.36C) and cell doubling time of Option2 was almost half of control and Option 6 group (Figure 3.36E). On the other hand, Option 6 expressed MSC markers, CD73, CD90 and CD105, at least 2 fold more compared to DPSC, Option 1 and Option 2. Option 2 had a very similar mRNA expression level with DPSC (Figure 3.36F and 3.37C). Additionally, Control, Option 6 and DPSC didn't expressed CD45, a hematopoietic marker (Figure 3.36F). These selected groups were also analyzed for presence of MSC markers through flow cytometry. All of the options were positive for CD 44, CD90, CD105 and CD166 both at day 10 and

day 24. However, CD45 was negative only at day 24 for the options (Figure 3.36G and 3.38). Furthermore, according to IF results both control-derived MSCs and Option 6-derived MSCs were capable of osteogenic, adipogenic, chondrogenic, myogenic, endothelial, epithelial, odontogenic and neurogenic differentiation and expressed osteogenic marker, Col1, adipogenic marker AFABP, chondrogenic marker, Col2, myogenic markers, Desmin, MyH and MyoD, endothelial marker, VEGF, epithelial marker, Vimentin and EpCAM, odontogenic marker, DMP1, and neurogenic markers, TH and MAP2, significantly higher compared to the characterized MSCs. Moreover, while expression of Col1, Col2, AFABP, DMP1, Desmin and MyoD were enhanced 1,4-fold, 1.9-fold, 1.3-fold, 1.4-fold, 1.3-fold and 1.2-fold, respectively, in Option 6-derived MSCs, expression of Vimentin, EpCAM, TH and MAP2 reduced 1.1-fold, 1.4-fold, 1.7-fold and 1.3-fold, respectively, in Option 6-derived MSCs compared to control-derived MSCs. Additionally, Option 6-derived cells showed much better results for von Kossa, alizarin red, alcian blue and oil red O stainings compared to characterized MSCs and control-derived cells (Figure 3.36H, 3.36I, 3.39 and 3.40). To investigate deeper, differential expression analysis for mRNA seq of DPSC, Option 1-MSCs (HM) and Option 6-MSCs (HMApln) was assessed (Figure 3.41, 3.42 and 3.43). As shown in principal component analysis (Figure 3.41A) and hierarchical cluster analysis with heat map (Figure 3.41D, 3.42A and 3.43A), the repeats of each group were grouped together and each group separated clearly from the other groups. Figure 3.41E and 3.41F demonstrates significantly upregulated and down regulated mRNAs in the plots. Enrichment analysis in Figure 3.41 compare all hESC-derived groups (HM and HMApln) to DPSC. According to enrichment analyses of top upregulated gene expressions in hESC-derived MSCs, biological processes including cell cycle, transcription, cellular biosynthesis and RNA biosynthesis were enhanced (Figure 3.41G) but, regulation of cell migration, vesicle mediated transport, protein localization and transport were reduced compared to DPSCs (Figure 3.41H). Also, cellular components, such as nucleosome, DNA packaging complex, protein-DNA complex, chromosome telomeric region and cytoskeleton increased (Figure 3.41I) while endoplasmic reticulum and golgi compartments, lysosome, endosome, exosome and cellular junctions decreased (Figure 3.41J). Moreover, while enrichment analysis in Figure 3.42 compares only HM group to DPSC, enrichment analysis in Figure 3.43 compares HMApln group to DPSC. Molecular functions such as small molecule binding, ion binding, protein binding and catalytic activity were up regulated in HM group (Figure 3.42D and 3.42F) and HMApln group (Figure 3.43D and 3.43F) while nucleic acid and protein binding were down regulated

in HM group (Figure 3.42E and 3.42G) and HMApln group (Figure 3.43E and 3.43G). Proteins related to biological processes including cell communication, response to stimulus, localization were enhanced in HM group (Figure 3.42D and 3.42H) and HMApln group (Figure 3.43D and 3.43H) whereas metabolic process related proteins were reduced in HM group (Figure 3.42E and 3.42I) and HMApln group (Figure 3.43E and 3.43I). DPSC, control (Option 1) and Apelin-13 treated (Option 6) MSC were subjected to a further analysis with LC/MS protein profiling (Figure 3.44, Table 3.5). Close correlation of control and Apelin, with 0.86 correlation coefficient value, DPSC and Control, with 0.87 correlation coefficient value, DPSC and Apelin, with 0.75 correlation coefficient value, were observed with correlation coefficient matrix, PCA, hierarchical cluster analysis, and heat map, (Figure 3.44A, 3.44B and 3.44C). Distribution of protein quantification for significantly increased and decreased expressions in with Apelin-13 treatment were demonstrated on the histogram (Figure 3.44D). According to the gene ontology analysis, proteins related to molecular functions including cytoskeletal motor activity, transcription and translation regulator activity were enhanced in control MSC group compared to DPSC. Translation regulator activity, molecular transducer activity and ATP-dependent activity related proteins increased in Apelin-13 treated MSCs compared to control MSCs (Figure 3.44E). Proteins involved in biological processes, such as adhesion, regulation, developmental process, growth and signaling both increased and decreased in control MSCs compared to DPSCs. Also, adhesion, developmental process, growth, locomotion related protein expressions were upregulated in Apelin-13 treated MSCs compared to control MSCs (Figure 3.44F). Furthermore, while proteins related to pathways in terms of cadherin signaling pathway, glycolysis, EGFR signaling, FGF signaling, PDGF signaling, Ras signaling, PI3K signaling, TGF-beta signaling, p38 MAPK signaling and Wnt signaling pathways were enhanced, EGFR signaling, FGF signaling, PDGF signaling, Ras signaling, TGF-beta signaling, p38 MAPK signaling, FAS signaling, VEGF signaling, general transcription by RNA polymerase I and oxidative stress response were downregulated in control MSCs compared to DPSCs. ATP synthesis, Cadherin signaling, cell cycle, EGFR signaling, FAS signaling, FGF Signaling, general transcription by RNA polymerase I, hypoxia response via HIF activation, PDGF signaling, Ras signaling, PI3K signaling, TGF-beta signaling, VEGF signaling, Wnt signaling and p38 MAPK signaling pathways related proteins were expressed in Apelin MSC higher than in control MSC (Figure 3.44G). Furthermore, according to the protein-protein interaction network, generated using string, clustered network with

clustering coefficient 0.503 contained 185 nodes and 1964 edges with 695 expected edges for significantly upregulated proteins in control MSCs compared to DPSCs. Clustered network with clustering coefficient 0.454 contained 219 nodes and 2182 edges with 816 expected edges for significantly enhanced proteins in Apelin MSCs compared to control MSCs. These indicate much more interaction than the expected values (Figure 3.44H).

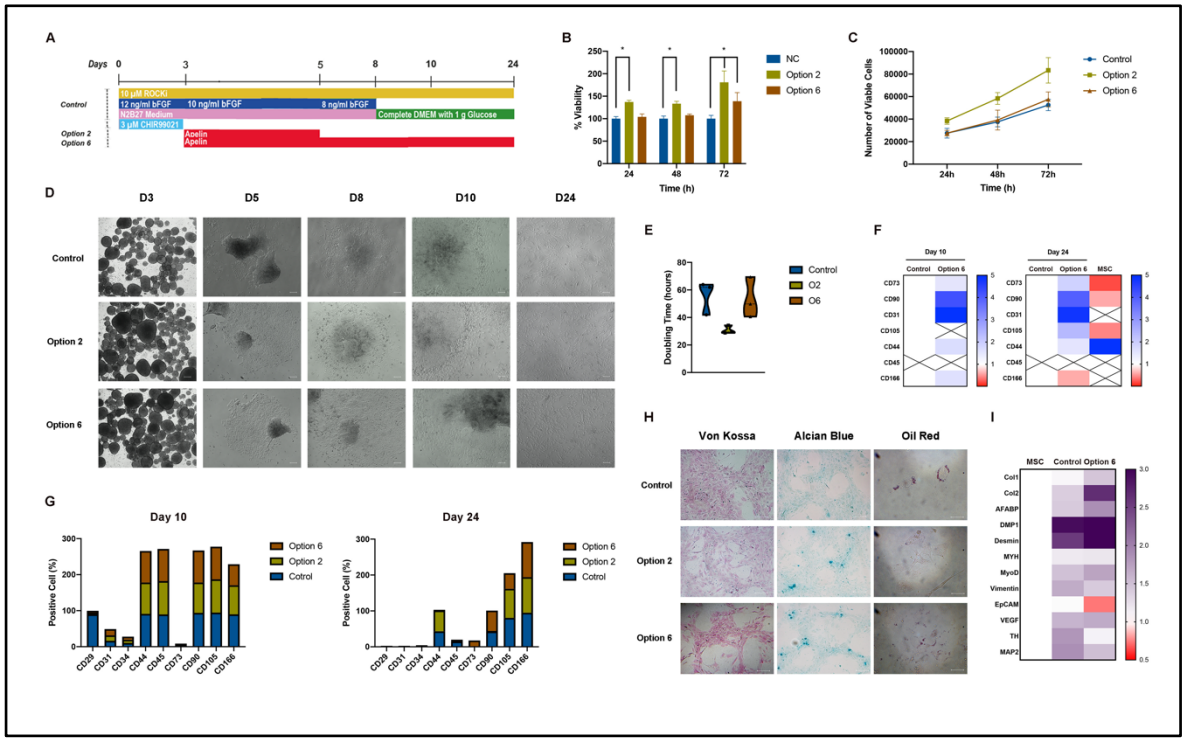


Figure 3.36. Aplnr activity supports MSC differentiation from hESCs. A. The 24 days protocol for MSC differentiation from hESC. B. Cell viability was measured for Option 1, Option 2 and Option 6 derived MSCs and was represented with a bar graph C. Viable cells were counted with Trypan Blue staining. D. Morphological pictures taken at day 3, day 5, day 8, day 10 and day24 during MSC differentiation from hESCs for Option 1, Option 2 and Option 6. E. Cell duplication time was calculated for Option 1, Option 2 and Option 6 derived MSCs. F. Heatmap visualization of mRNA expression levels for MSC markers. G. MSC markers were detected with flow cytometry analysis and a graphic was drown showing the positive cells for the markers. H. Morphological pictures after von Kossa, alcian blue and oil red O stainings were taken to demonstrate osteogenic, chondrogenic and adipogenic differentiation, respectively, for Option 1, Option 2 and Option 6 cells. I. Intensities of the protein expressions were measured from the immunofluorescence images and represented as a heatmap. Scale bar: 200µm. *P<0.0001

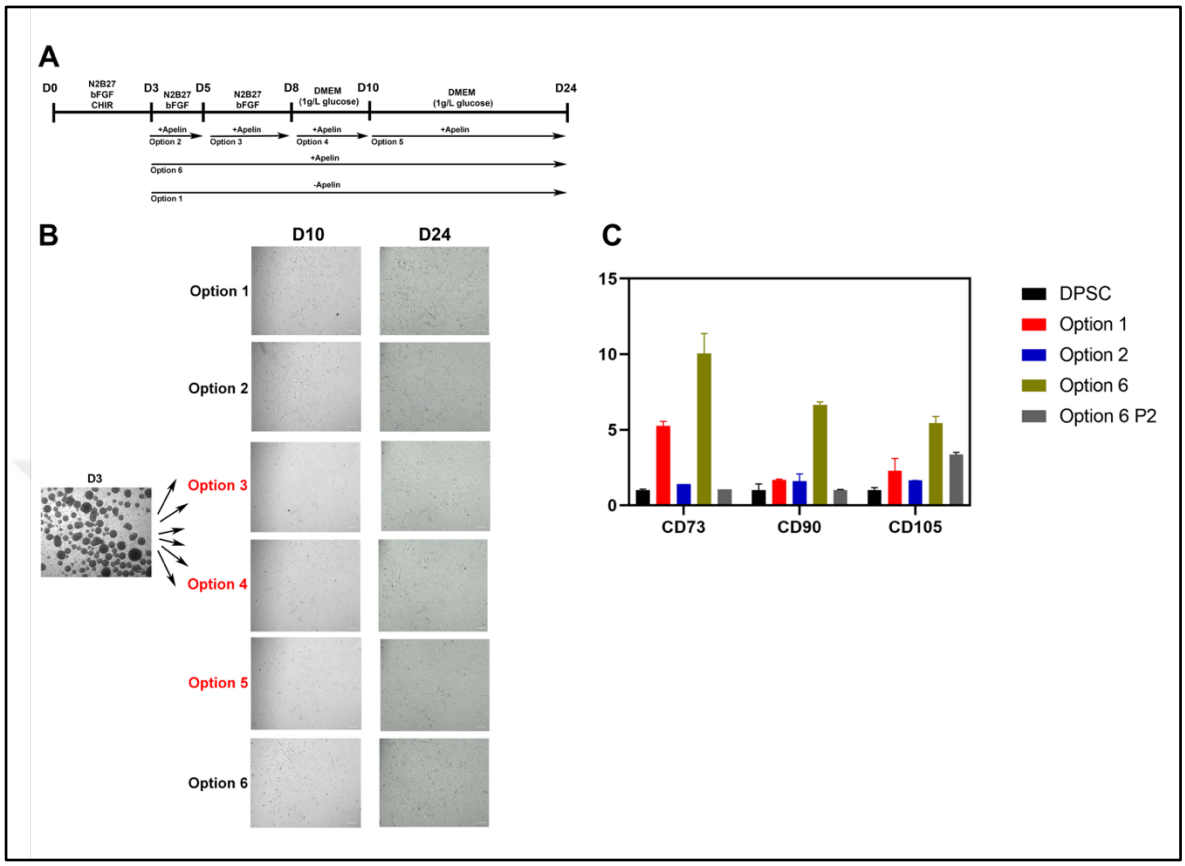


Figure 3.37. Optimization of Apelin-13 Administration during MSC Differentiation of hESCs. A. The 24 days protocol for MSC differentiation from hESC. B. Morphological pictures of hESCs taken at day 3, day 10 and day 24 during MSC differentiation. C. Heatmap visualization of mRNA expression levels for MSC markers at day 24. Scale bar: 200µm.

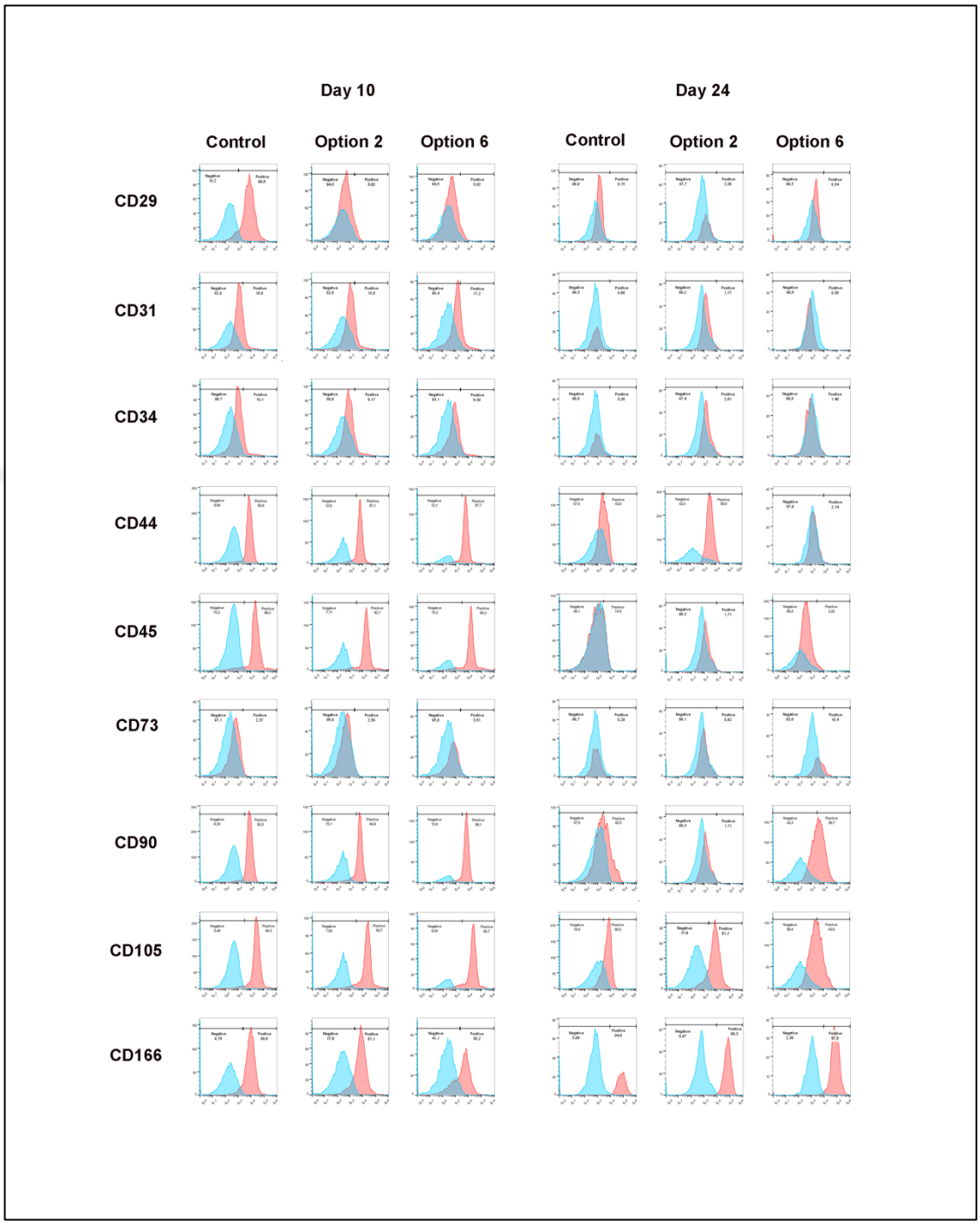


Figure 3.38. Characterization of hESC derived MSCs in the presence of Apelin-13. Flow cytometry analysis of mesenchymal stem cell marker expression and hematopoietic marker expression on hESC during MSC differentiation at day 10 and day 24. Control group and Apelin-13 treatment groups (Option 2 and Option 6) were compared.

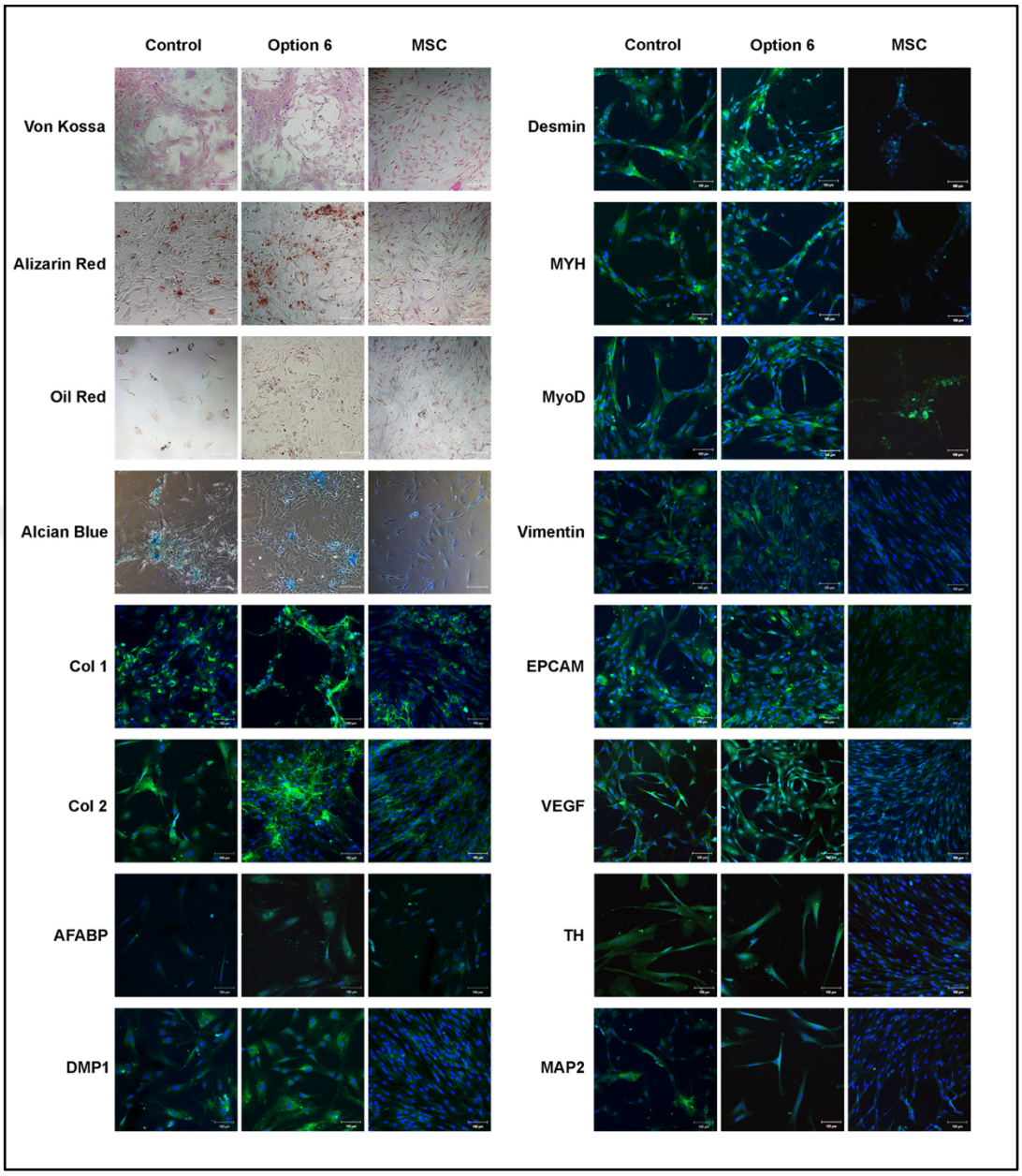


Figure 3.39. Differentiation of hESC derived MSCs and characterized MSCs into Multiple Cell Types in the presence of Apelin-13. Osteogenic differentiation was shown with von Kossa staining, alizarin red staining and Col1 immunostaining. Oil red O staining and AFABP immunostaining represented adipogenic differentiation. Chondrogenic differentiation was visualized with Alcian Blue staining and Col2 immunostaining. Desmin, MyoD and MYH immunostainings were performed after myogenic differentiation. Neurogenic differentiation was shown by TH and MAP2 immunostainings. Endothelial differentiation was visualized by VEGF immunostainings. Immunostainings for Vimentin and EpCAM was performed for epithelial differentiation. DMP1 immunostaining was shown to visualize odontogenic differentiation. Scale Bar: 100µm.

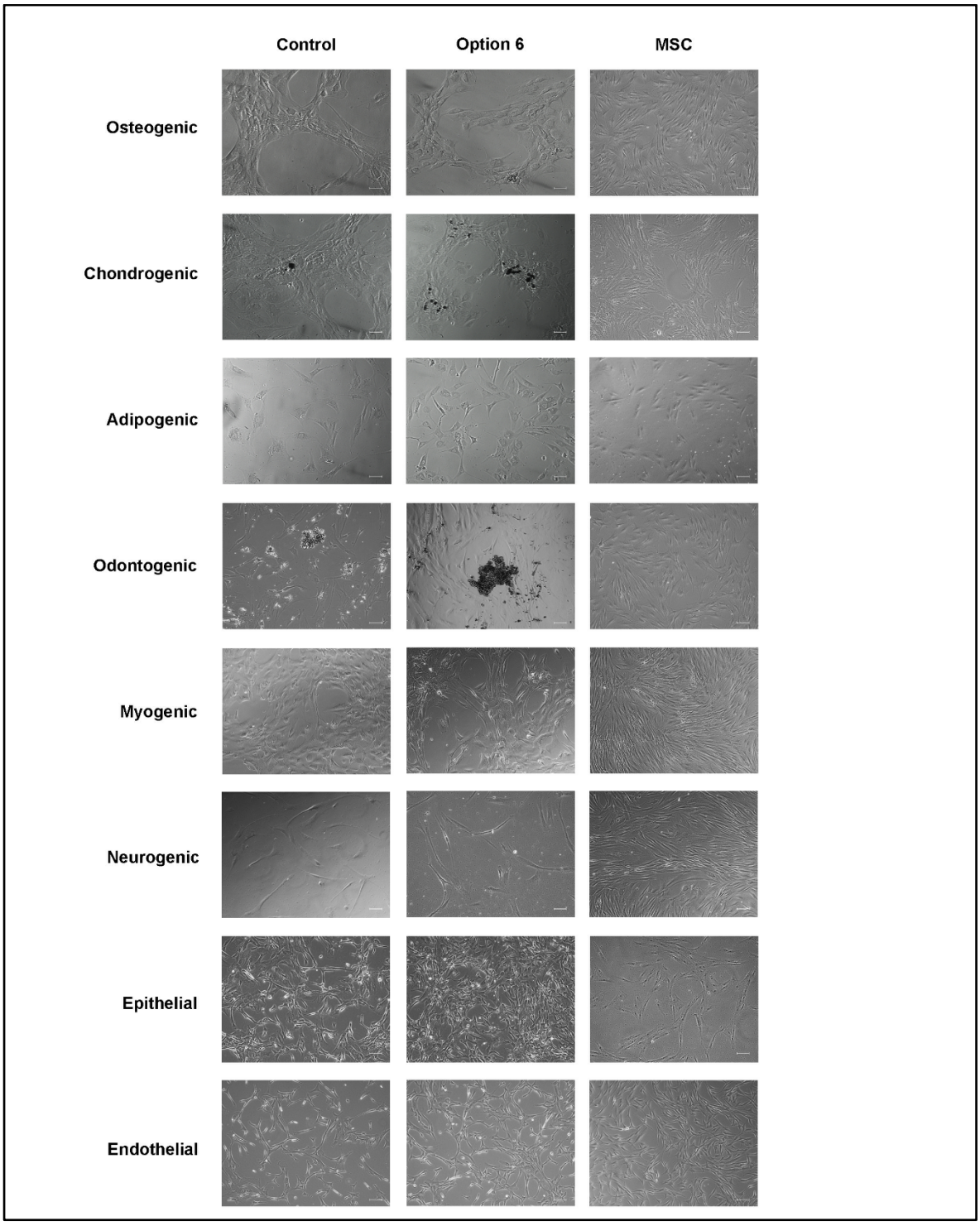


Figure 3.40. Morphology of Multiple Cell Type Differentiation from MSC and hESC derived MSCs. hESC derived MSC, which were differentiated with or without Apelin-13, were compared with original MSC in terms of multiple differentiation capacity. Cell morphology after osteogenic, chondrogenic, adipogenic, odontogenic, myogenic, neurogenic, epithelial and endothelial differentiations were demonstrated for MSC, Control-MSC and Option 6-MSC. Scale Bar: 100µm.

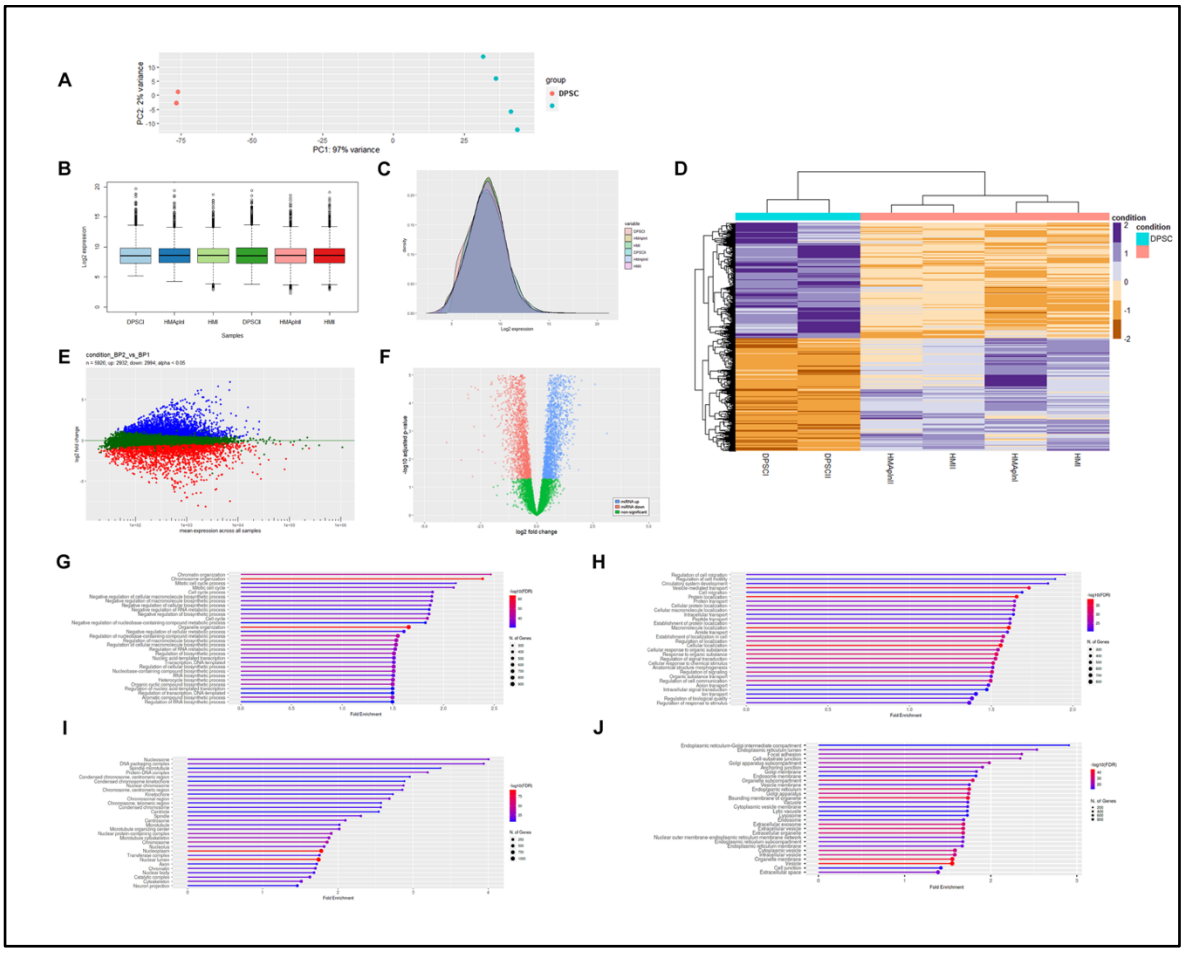


Figure 3.41. Differential expression analysis for mRNA seq of DPSC and hESC derived MSCs. A. Principal component analysis of DPSC and hESCs-derived MSCs, control (HM) and Apelin-13 groups (HMApln) after mRNA seq analysis. B. Data distribution after normalization (Log 2 counts per million) C. Expression plots (Log 2 expression versus density) were shown. D. Heat map representation analysis, E. MA plot analysis. F. Volcano plot analysis. G. The samples were subjected to functional enrichment analysis. All hESC-derived MSCs, control (HM) and Apelin-13 treated (HMApln), were compared to DPSC. Biological process tree for upregulated genes and H. downregulated genes. I. Cellular component tree for upregulated genes and J. downregulated genes.

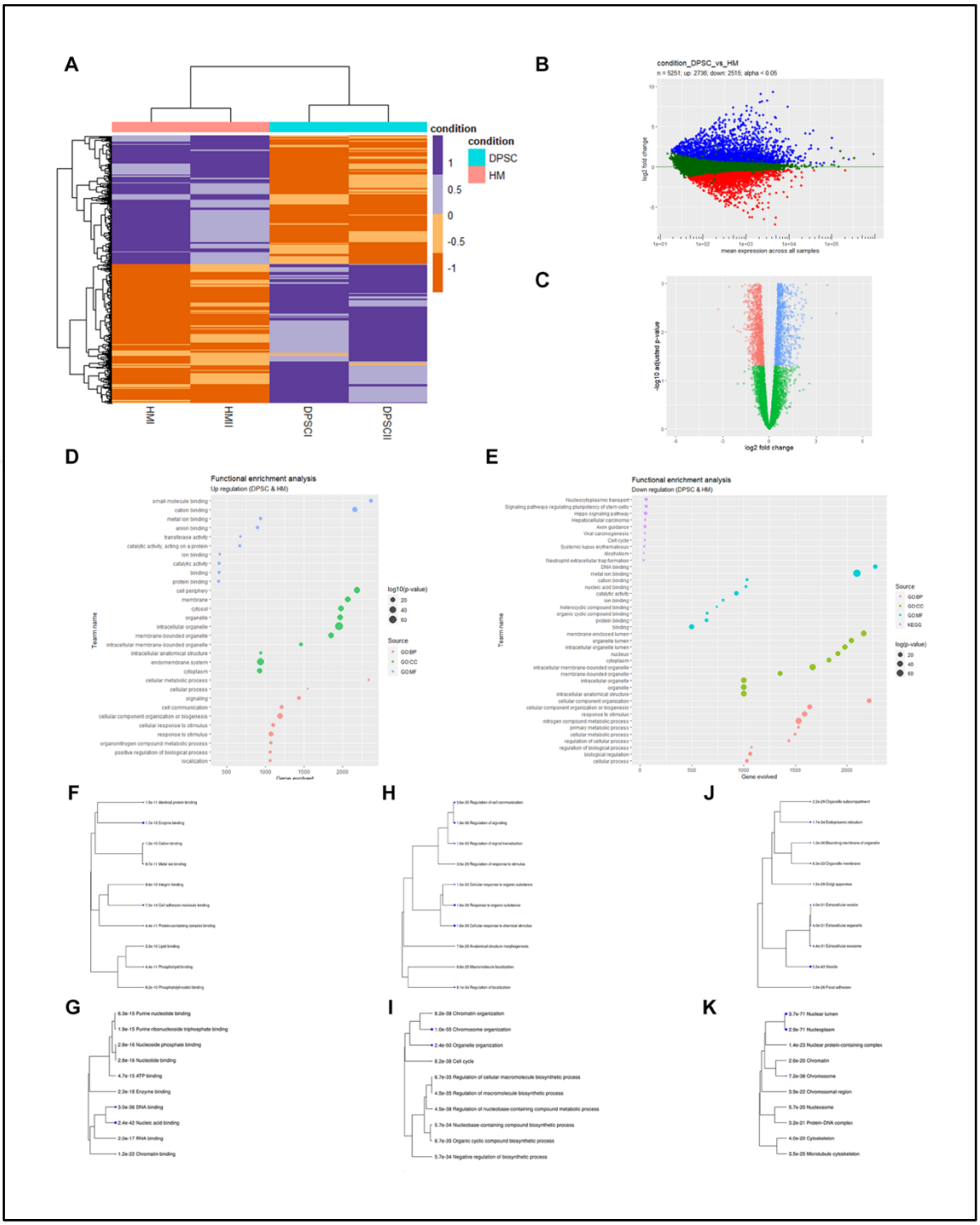


Figure 3.42. Differential expression analysis for mRNA seq of hESC-derived MSCs and DPSC. A. Heat map representation analysis of hESC derived MSCs (HM) and DPSCs. B. MA plot and C. Volcano plot analysis. D. Top 31 pathway enrichment analysis for upregulated genes in hESCs derived MSCs compared to DPSCs. Biological process(BP), Cellular Component (CC) and Molecular Function (MF). E. Top 31 pathway enrichment analysis for the downregulated genes. F. Molecular function tree for upregulated genes and

G. downregulated genes. H. Biological process tree for upregulated genes and I. downregulated genes. J. Cellular component tree for upregulated genes and K. downregulated genes.

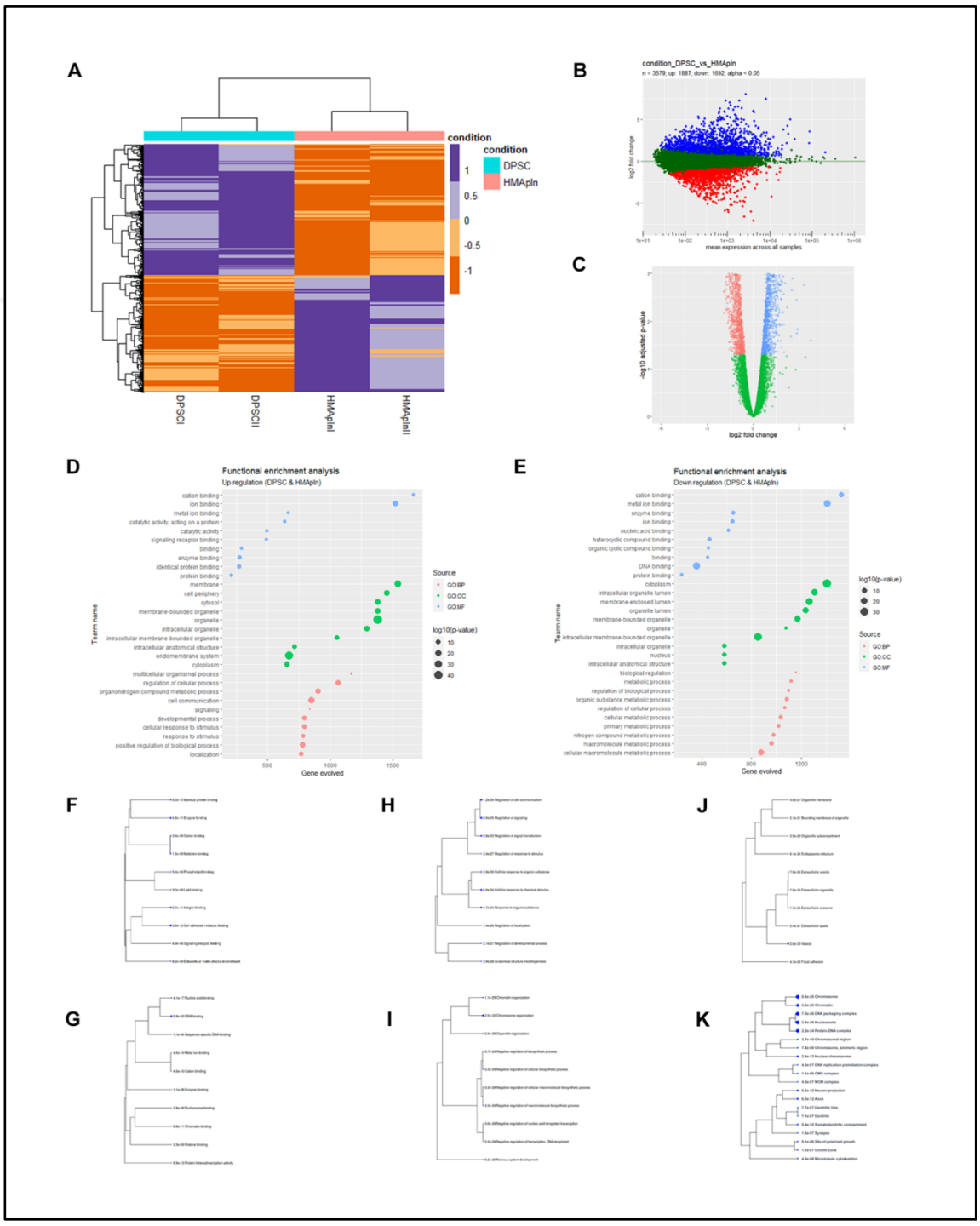


Figure 3.43. Differential expression analysis for mRNA seq of hESC-derived MSCs, in the presence of Apelin-13, and DPSCs. A. Heat map representation analysis of hESC derived MSCs for Apelin-13 treated group (HMApln) and DPSCs. B. MA plot and C. Volcano plot

analysis. D. Top 31 pathway enrichment analysis for upregulated genes in Aplnr activated hESCs derived MSCs compared to DPSCs. Biological process(BP), Cellular Component (CC) and Molecular Function (MF). E. Top 31 pathway enrichment analysis for the downregulated genes. F. Molecular function tree for upregulated genes and G. downregulated genes. H. Biological process tree for upregulated genes and I. downregulated genes. J. Cellular component tree for upregulated genes and K. downregulated genes.

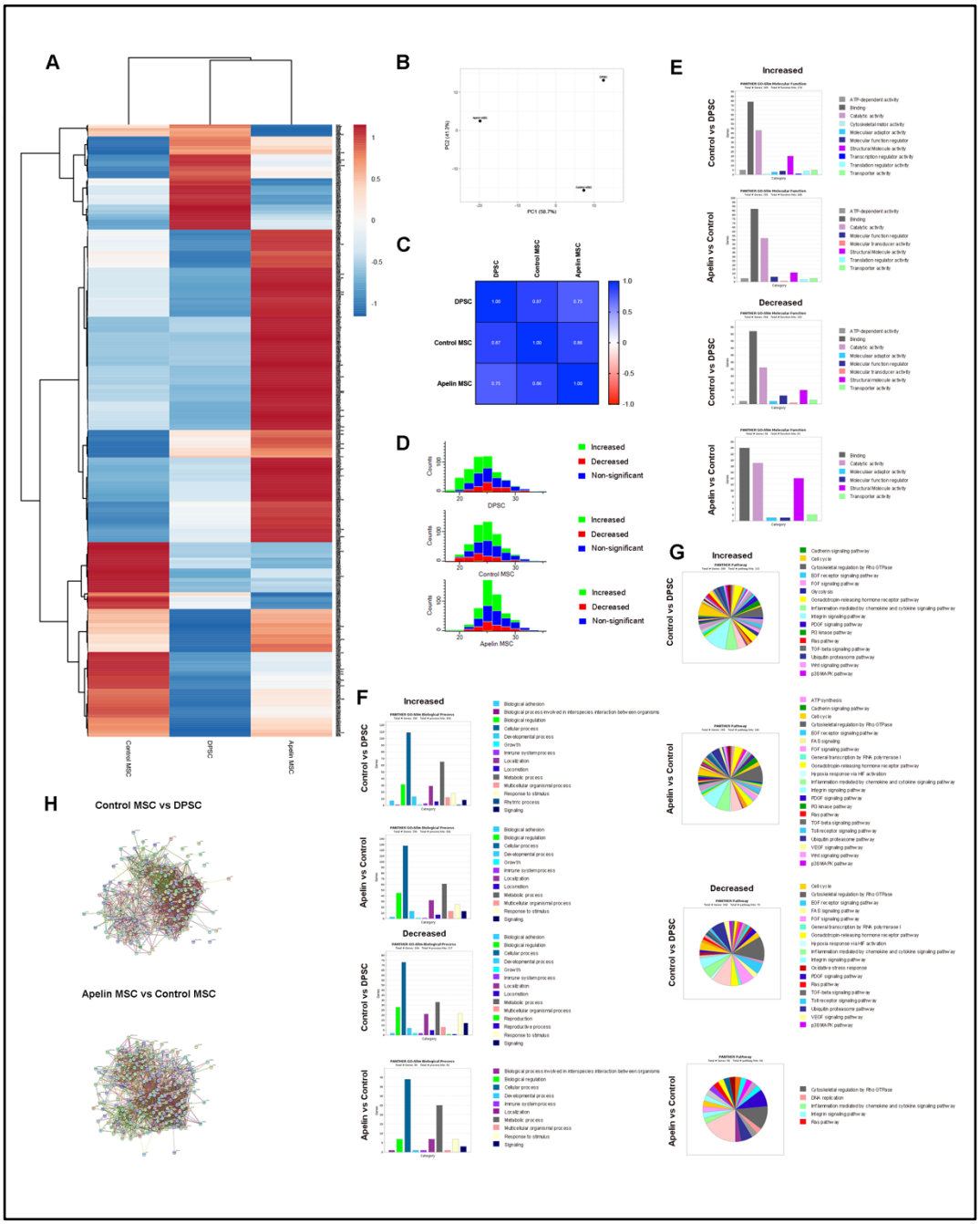


Figure 3.44. Protein profile of hESC derived MSCs treated with Apelin-13. A. Hierarchical cluster analysis and heat map representation of proteins from control and Apelin-13 treated MSCs and DPSCs. B. Principal component analysis and C. Correlation coefficient matrix of the proteins. D. Histogram indicating the distribution of the protein quantification. E. The graphs demonstrating molecular function, F. biological process and G. related pathways of the upregulated and downregulated proteins in control MSCs compared to DPSCs and Apelin-13 MSCs compared to control MSCs. H. Protein interaction network for the upregulated proteins in control MSCs compared to DPSCs and Apelin-13 MSCs compared to control MSCs.

Table 3.5. Protein profiling data of DPSC, Control MSC and Apelin-13 MSC groups at day 24. Significantly increased and decreased proteins in Control MSC compared to DPSC (increased: red, decreased: black) and Apelin MSC compared to Control MSC (increased: red, decreased: black) were listed on the table.

Accession	**Description**	**Abundance Ratio: Control MSC / DPSC**
P01023	Alpha-2-macroglobulin OS=Homo sapiens OX=9606 GN=A2M PE=1 SV=3	**211,6126849**
P30837	Aldehyde dehydrogenase X, mitochondrial OS=Homo sapiens OX=9606 GN=ALDH1B1 PE=1 SV=3	**128,0823078**
P54819	Adenylate kinase 2, mitochondrial OS=Homo sapiens OX=9606 GN=AK2 PE=1 SV=2	**112,9071987**
P22626	Heterogeneous nuclear ribonucleoproteins A2/B1 OS=Homo sapiens OX=9606 GN=HNRNPA2B1 PE=1 SV=2	**85,668181**
P47755	F-actin-capping protein subunit alpha-2 OS=Homo sapiens OX=9606 GN=CAPZA2 PE=1 SV=3	**65,07570187**
D6REX3	Protein transport protein Sec31A OS=Homo sapiens OX=9606 GN=SEC31A PE=1 SV=1	**52,59029483**
Q04917	14-3-3 protein eta OS=Homo sapiens OX=9606 GN=YWHAH PE=1 SV=4	**49,73848705**

P62917	60S ribosomal protein L8 OS=Homo sapiens OX=9606 GN=RPL8 PE=1 SV=2	**49,06324606**
P0DME0	Protein SETSIP OS=Homo sapiens OX=9606 GN=SETSIP PE=1 SV=1	**47,33651393**
Q7KZF4	Staphylococcal nuclease domain-containing protein 1 OS=Homo sapiens OX=9606 GN=SND1 PE=1 SV=1	**46,3179312**
P62829	60S ribosomal protein L23 OS=Homo sapiens OX=9606 GN=RPL23 PE=1 SV=1	**41,11835724**
P02786	Transferrin receptor protein 1 OS=Homo sapiens OX=9606 GN=TFRC PE=1 SV=2	**40,85345519**
P62266	40S ribosomal protein S23 OS=Homo sapiens OX=9606 GN=RPS23 PE=1 SV=3	**39,95443393**
P26006	Integrin alpha-3 OS=Homo sapiens OX=9606 GN=ITGA3 PE=1 SV=5	**39,13444533**
Q13838	Spliceosome RNA helicase DDX39B OS=Homo sapiens OX=9606 GN=DDX39B PE=1 SV=1	**38,12130196**
Q9UKX5	Integrin alpha-11 OS=Homo sapiens OX=9606 GN=ITGA11 PE=1 SV=2	**37,79113536**
Q04637	Eukaryotic translation initiation factor 4 gamma 1 OS=Homo sapiens OX=9606 GN=EIF4G1 PE=1 SV=4	**36,80935194**
E7EPK1	Septin OS=Homo sapiens OX=9606 GN=SEPTIN7 PE=1 SV=2	**34,398232**
P10412	Histone H1.4 OS=Homo sapiens OX=9606 GN=H1-4 PE=1 SV=2	**32,73806614**
P23381	Tryptophan--tRNA ligase, cytoplasmic OS=Homo sapiens OX=9606 GN=WARS1 PE=1 SV=2	**31,11198788**
P05141	ADP/ATP translocase 2 OS=Homo sapiens OX=9606 GN=SLC25A5 PE=1 SV=7	**30,95252501**
Q96AC1	Fermitin family homolog 2 OS=Homo sapiens OX=9606 GN=FERMT2 PE=1 SV=1	**26,25534596**

P02768	Albumin OS=Homo sapiens OX=9606 GN=ALB PE=1 SV=2	**22,58191873**
P05198	Eukaryotic translation initiation factor 2 subunit 1 OS=Homo sapiens OX=9606 GN=EIF2S1 PE=1 SV=3	**20,63509153**
P07996	Thrombospondin-1 OS=Homo sapiens OX=9606 GN=THBS1 PE=1 SV=2	**19,66736422**
Q16643	Drebrin OS=Homo sapiens OX=9606 GN=DBN1 PE=1 SV=4	**19,37644743**
Q00325	Phosphate carrier protein, mitochondrial OS=Homo sapiens OX=9606 GN=SLC25A3 PE=1 SV=2	**19,1147688**
P54578	Ubiquitin carboxyl-terminal hydrolase 14 OS=Homo sapiens OX=9606 GN=USP14 PE=1 SV=3	**18,79353465**
P02751	Fibronectin OS=Homo sapiens OX=9606 GN=FN1 PE=1 SV=5	**17,28447052**
P56537	Eukaryotic translation initiation factor 6 OS=Homo sapiens OX=9606 GN=EIF6 PE=1 SV=1	**16,99040123**
E9PR30	40S ribosomal protein S30 OS=Homo sapiens OX=9606 GN=FAU PE=1 SV=1	**16,81393259**
O14773	Tripeptidyl-peptidase 1 OS=Homo sapiens OX=9606 GN=TPP1 PE=1 SV=2	**15,72105101**
A0A494C039	Hypoxia up-regulated protein 1 OS=Homo sapiens OX=9606 GN=HYOU1 PE=1 SV=1	**14,77565457**
O75369	Filamin-B OS=Homo sapiens OX=9606 GN=FLNB PE=1 SV=2	**14,64194021**
B0YIW6	Coatomer subunit delta OS=Homo sapiens OX=9606 GN=ARCN1 PE=1 SV=1	**14,04040951**
Q8IV08	5'-3' exonuclease PLD3 OS=Homo sapiens OX=9606 GN=PLD3 PE=1 SV=1	**13,88432323**
Q9Y696	Chloride intracellular channel protein 4 OS=Homo sapiens OX=9606 GN=CLIC4 PE=1 SV=4	**13,70660295**

A0A087X020	Ribosome maturation protein SBDS OS=Homo sapiens OX=9606 GN=SBDS PE=1 SV=1	**13,64874536**
P04899	Guanine nucleotide-binding protein G(i) subunit alpha-2 OS=Homo sapiens OX=9606 GN=GNAI2 PE=1 SV=3	**12,46682487**
Q86V81	THO complex subunit 4 OS=Homo sapiens OX=9606 GN=ALYREF PE=1 SV=3	**12,10921613**
H0Y4R1	Inosine-5'-monophosphate dehydrogenase OS=Homo sapiens OX=9606 GN=IMPDH2 PE=1 SV=2	**11,98048119**
Q01650	Large neutral amino acids transporter small subunit 1 OS=Homo sapiens OX=9606 GN=SLC7A5 PE=1 SV=2	**11,85986662**
A8MUS3	60S ribosomal protein L23a OS=Homo sapiens OX=9606 GN=RPL23A PE=1 SV=1	**11,80625023**
A0A3B3ITT5	60S ribosomal protein L29 OS=Homo sapiens OX=9606 GN=RPL29 PE=1 SV=1	**11,45062575**
Q16881	Thioredoxin reductase 1, cytoplasmic OS=Homo sapiens OX=9606 GN=TXNRD1 PE=1 SV=3	**11,05900526**
Q9H1E3	Nuclear ubiquitous casein and cyclin-dependent kinase substrate 1 OS=Homo sapiens OX=9606 GN=NUCKS1 PE=1 SV=1	**10,96823591**
Q13263	Transcription intermediary factor 1-beta OS=Homo sapiens OX=9606 GN=TRIM28 PE=1 SV=5	**10,85756819**
Q12906	Interleukin enhancer-binding factor 3 OS=Homo sapiens OX=9606 GN=ILF3 PE=1 SV=3	**10,81164433**
P46777	60S ribosomal protein L5 OS=Homo sapiens OX=9606 GN=RPL5 PE=1 SV=3	**10,70975496**
P36957	Dihydrolipoyllysine-residue succinyltransferase component of 2-oxoglutarate dehydrogenase complex, mitochondrial OS=Homo sapiens OX=9606 GN=DLST PE=1 SV=4	**10,41577091**
Q6UVK1	Chondroitin sulfate proteoglycan 4 OS=Homo sapiens OX=9606 GN=CSPG4 PE=1 SV=2	**10,1407108**

Q9Y570	Protein phosphatase methylesterase 1 OS=Homo sapiens OX=9606 GN=PPME1 PE=1 SV=3	**9,919282293**
O00154	Cytosolic acyl coenzyme A thioester hydrolase OS=Homo sapiens OX=9606 GN=ACOT7 PE=1 SV=3	**9,773415215**
P60953	Cell division control protein 42 homolog OS=Homo sapiens OX=9606 GN=CDC42 PE=1 SV=2	**9,717202571**
Q12905	Interleukin enhancer-binding factor 2 OS=Homo sapiens OX=9606 GN=ILF2 PE=1 SV=2	**9,715201374**
P40429	60S ribosomal protein L13a OS=Homo sapiens OX=9606 GN=RPL13A PE=1 SV=2	**9,667737167**
O00151	PDZ and LIM domain protein 1 OS=Homo sapiens OX=9606 GN=PDLIM1 PE=1 SV=4	**9,138409972**
P48735	Isocitrate dehydrogenase [NADP], mitochondrial OS=Homo sapiens OX=9606 GN=IDH2 PE=1 SV=2	**9,089870402**
J3QQ67	60S ribosomal protein L18 (Fragment) OS=Homo sapiens OX=9606 GN=RPL18 PE=1 SV=1	**8,998060558**
P62140	Serine/threonine-protein phosphatase PP1-beta catalytic subunit OS=Homo sapiens OX=9606 GN=PPP1CB PE=1 SV=3	**8,94883472**
Q9ULV4	Coronin-1C OS=Homo sapiens OX=9606 GN=CORO1C PE=1 SV=1	**8,927574892**
Q562R1	Beta-actin-like protein 2 OS=Homo sapiens OX=9606 GN=ACTBL2 PE=1 SV=2	**8,911870339**
P61313	60S ribosomal protein L15 OS=Homo sapiens OX=9606 GN=RPL15 PE=1 SV=2	**8,874283453**
Q15758	Neutral amino acid transporter B(0) OS=Homo sapiens OX=9606 GN=SLC1A5 PE=1 SV=2	**8,82185491**
Q9Y617	Phosphoserine aminotransferase OS=Homo sapiens OX=9606 GN=PSAT1 PE=1 SV=2	**8,785341001**

P05787	Keratin, type II cytoskeletal 8 OS=Homo sapiens OX=9606 GN=KRT8 PE=1 SV=7	**8,686904175**
P08123	Collagen alpha-2(I) chain OS=Homo sapiens OX=9606 GN=COL1A2 PE=1 SV=7	**8,661429995**
A0A1C7CYX9	Dihydropyrimidinase-related protein 2 OS=Homo sapiens OX=9606 GN=DPYSL2 PE=1 SV=1	**8,285513486**
A0A2R8Y623	40S ribosomal protein S7 (Fragment) OS=Homo sapiens OX=9606 GN=RPS7 PE=1 SV=1	**8,219765043**
P05023	Sodium/potassium-transporting ATPase subunit alpha-1 OS=Homo sapiens OX=9606 GN=ATP1A1 PE=1 SV=1	**8,193367163**
P46783	40S ribosomal protein S10 OS=Homo sapiens OX=9606 GN=RPS10 PE=1 SV=1	**8,175343971**
P22234	Multifunctional protein ADE2 OS=Homo sapiens OX=9606 GN=PAICS PE=1 SV=3	**8,01917092**
P28072	Proteasome subunit beta type-6 OS=Homo sapiens OX=9606 GN=PSMB6 PE=1 SV=4	**7,842993122**
P51665	26S proteasome non-ATPase regulatory subunit 7 OS=Homo sapiens OX=9606 GN=PSMD7 PE=1 SV=2	**7,689323058**
P83731	60S ribosomal protein L24 OS=Homo sapiens OX=9606 GN=RPL24 PE=1 SV=1	**7,582637727**
P05783	Keratin, type I cytoskeletal 18 OS=Homo sapiens OX=9606 GN=KRT18 PE=1 SV=2	**7,499732383**
Q9BSJ8	Extended synaptotagmin-1 OS=Homo sapiens OX=9606 GN=ESYT1 PE=1 SV=1	**7,496696951**
O00764	Pyridoxal kinase OS=Homo sapiens OX=9606 GN=PDXK PE=1 SV=1	**7,473673227**
P62979	Ubiquitin-40S ribosomal protein S27a OS=Homo sapiens OX=9606 GN=RPS27A PE=1 SV=2	**7,456695915**
P02452	Collagen alpha-1(I) chain OS=Homo sapiens OX=9606 GN=COL1A1 PE=1 SV=5	**7,068149392**

P46776	60S ribosomal protein L27a OS=Homo sapiens OX=9606 GN=RPL27A PE=1 SV=2	**6,988978839**
A0A7I2YQC0	Nucleophosmin OS=Homo sapiens OX=9606 GN=NPM1 PE=1 SV=1	**6,975322971**
P53597	Succinate--CoA ligase [ADP/GDP-forming] subunit alpha, mitochondrial OS=Homo sapiens OX=9606 GN=SUCLG1 PE=1 SV=4	**6,74472001**
Q01813	ATP-dependent 6-phosphofructokinase, platelet type OS=Homo sapiens OX=9606 GN=PFKP PE=1 SV=2	**6,721412556**
P16989	Y-box-binding protein 3 OS=Homo sapiens OX=9606 GN=YBX3 PE=1 SV=4	**6,567300166**
P26639	Threonine--tRNA ligase 1, cytoplasmic OS=Homo sapiens OX=9606 GN=TARS1 PE=1 SV=3	**6,242145074**
O43776	Asparagine--tRNA ligase, cytoplasmic OS=Homo sapiens OX=9606 GN=NARS1 PE=1 SV=1	**6,219393366**
P43686	26S proteasome regulatory subunit 6B OS=Homo sapiens OX=9606 GN=PSMC4 PE=1 SV=2	**6,152195553**
P51991	Heterogeneous nuclear ribonucleoprotein A3 OS=Homo sapiens OX=9606 GN=HNRNPA3 PE=1 SV=2	**5,826067279**
P28070	Proteasome subunit beta type-4 OS=Homo sapiens OX=9606 GN=PSMB4 PE=1 SV=4	**5,728000952**
P41252	Isoleucine--tRNA ligase, cytoplasmic OS=Homo sapiens OX=9606 GN=IARS1 PE=1 SV=2	**5,682396468**
Q14195	Dihydropyrimidinase-related protein 3 OS=Homo sapiens OX=9606 GN=DPYSL3 PE=1 SV=1	**5,613152664**
P07814	Bifunctional glutamate/proline--tRNA ligase OS=Homo sapiens OX=9606 GN=EPRS1 PE=1 SV=5	**5,539785249**
P61604	10 kDa heat shock protein, mitochondrial OS=Homo sapiens OX=9606 GN=HSPE1 PE=1 SV=2	**5,4165673**

P35580	Myosin-10 OS=Homo sapiens OX=9606 GN=MYH10 PE=1 SV=3	**5,271583563**
Q6IAA8	Ragulator complex protein LAMTOR1 OS=Homo sapiens OX=9606 GN=LAMTOR1 PE=1 SV=2	**5,247456744**
P26038	Moesin OS=Homo sapiens OX=9606 GN=MSN PE=1 SV=3	**5,226618915**
P21281	V-type proton ATPase subunit B, brain isoform OS=Homo sapiens OX=9606 GN=ATP6V1B2 PE=1 SV=3	**5,06893369**
P62753	40S ribosomal protein S6 OS=Homo sapiens OX=9606 GN=RPS6 PE=1 SV=1	**4,943315737**
Q9UBQ7	Glyoxylate reductase/hydroxypyruvate reductase OS=Homo sapiens OX=9606 GN=GRHPR PE=1 SV=1	**4,856503428**
A0A6Q8PFE1	Apoptosis-inducing factor 1, mitochondrial OS=Homo sapiens OX=9606 GN=AIFM1 PE=1 SV=1	**4,801593166**
A0A2R8Y5A3	Catenin beta-1 OS=Homo sapiens OX=9606 GN=CTNNB1 PE=1 SV=1	**4,682343228**
B5MDF5	GTP-binding nuclear protein Ran OS=Homo sapiens OX=9606 GN=RAN PE=1 SV=1	**4,641421283**
P15880	40S ribosomal protein S2 OS=Homo sapiens OX=9606 GN=RPS2 PE=1 SV=2	**4,619903297**
P13674	Prolyl 4-hydroxylase subunit alpha-1 OS=Homo sapiens OX=9606 GN=P4HA1 PE=1 SV=2	**4,52442848**
Q15019	Septin-2 OS=Homo sapiens OX=9606 GN=SEPTIN2 PE=1 SV=1	**4,477993203**
Q9NR12	PDZ and LIM domain protein 7 OS=Homo sapiens OX=9606 GN=PDLIM7 PE=1 SV=1	**4,448234551**
O43175	D-3-phosphoglycerate dehydrogenase OS=Homo sapiens OX=9606 GN=PHGDH PE=1 SV=4	**4,39210996**
P11216	Glycogen phosphorylase, brain form OS=Homo sapiens OX=9606 GN=PYGB PE=1 SV=5	**4,336998953**

P39656	Dolichyl-diphosphooligosaccharide--protein glycosyltransferase 48 kDa subunit OS=Homo sapiens OX=9606 GN=DDOST PE=1 SV=4	**4,299303332**
P54727	UV excision repair protein RAD23 homolog B OS=Homo sapiens OX=9606 GN=RAD23B PE=1 SV=1	**4,223141561**
D6RER5	Septin OS=Homo sapiens OX=9606 GN=SEPTIN11 PE=1 SV=1	**4,204451406**
Q14240	Eukaryotic initiation factor 4A-II OS=Homo sapiens OX=9606 GN=EIF4A2 PE=1 SV=2	**4,194215492**
O60506	Heterogeneous nuclear ribonucleoprotein Q OS=Homo sapiens OX=9606 GN=SYNCRIP PE=1 SV=2	**4,19393549**
A0A7I2V3S3	Eukaryotic translation initiation factor 3 subunit E OS=Homo sapiens OX=9606 GN=EIF3E PE=1 SV=1	**4,152785196**
O43707	Alpha-actinin-4 OS=Homo sapiens OX=9606 GN=ACTN4 PE=1 SV=2	**4,117919948**
P07195	L-lactate dehydrogenase B chain OS=Homo sapiens OX=9606 GN=LDHB PE=1 SV=2	**3,992701094**
G3V5Z7	Proteasome subunit alpha type OS=Homo sapiens OX=9606 GN=PSMA6 PE=1 SV=1	**3,872829632**
H3BNC9	40S ribosomal protein S17 OS=Homo sapiens OX=9606 PE=3 SV=2	**3,830893884**
O95336	6-phosphogluconolactonase OS=Homo sapiens OX=9606 GN=PGLS PE=1 SV=2	**3,817574022**
P51659	Peroxisomal multifunctional enzyme type 2 OS=Homo sapiens OX=9606 GN=HSD17B4 PE=1 SV=3	**3,752071296**
P62263	40S ribosomal protein S14 OS=Homo sapiens OX=9606 GN=RPS14 PE=1 SV=3	**3,752007355**
P29692	Elongation factor 1-delta OS=Homo sapiens OX=9606 GN=EEF1D PE=1 SV=5	**3,686817364**

P61254	60S ribosomal protein L26 OS=Homo sapiens OX=9606 GN=RPL26 PE=1 SV=1	**3,638356625**
C9JIF9	Acyl-peptide hydrolase OS=Homo sapiens OX=9606 GN=APEH PE=1 SV=1	**3,598071313**
A0A0U1RRH7	Histone H2A OS=Homo sapiens OX=9606 PE=3 SV=1	**3,576779978**
P25789	Proteasome subunit alpha type-4 OS=Homo sapiens OX=9606 GN=PSMA4 PE=1 SV=1	**3,555756535**
Q92598	Heat shock protein 105 kDa OS=Homo sapiens OX=9606 GN=HSPH1 PE=1 SV=1	**3,504803235**
Q9H3N1	Thioredoxin-related transmembrane protein 1 OS=Homo sapiens OX=9606 GN=TMX1 PE=1 SV=1	**3,464639424**
P14866	Heterogeneous nuclear ribonucleoprotein L OS=Homo sapiens OX=9606 GN=HNRNPL PE=1 SV=2	**3,424868387**
Q07954	Prolow-density lipoprotein receptor-related protein 1 OS=Homo sapiens OX=9606 GN=LRP1 PE=1 SV=2	**3,412172292**
Q8NC51	Plasminogen activator inhibitor 1 RNA-binding protein OS=Homo sapiens OX=9606 GN=SERBP1 PE=1 SV=2	**3,402537405**
Q15907	Ras-related protein Rab-11B OS=Homo sapiens OX=9606 GN=RAB11B PE=1 SV=4	**3,373512967**
Q14697	Neutral alpha-glucosidase AB OS=Homo sapiens OX=9606 GN=GANAB PE=1 SV=3	**3,363309171**
P50281	Matrix metalloproteinase-14 OS=Homo sapiens OX=9606 GN=MMP14 PE=1 SV=3	**3,355915771**
Q96AY3	Peptidyl-prolyl cis-trans isomerase FKBP10 OS=Homo sapiens OX=9606 GN=FKBP10 PE=1 SV=1	**3,350032384**
Q02878	60S ribosomal protein L6 OS=Homo sapiens OX=9606 GN=RPL6 PE=1 SV=3	**3,348529368**
E9PAV3	Nascent polypeptide-associated complex subunit alpha, muscle-specific form OS=Homo sapiens OX=9606 GN=NACA PE=1 SV=1	**3,274394254**

Q00839	Heterogeneous nuclear ribonucleoprotein U OS=Homo sapiens OX=9606 GN=HNRNPU PE=1 SV=6	**3,199037253**
P36578	60S ribosomal protein L4 OS=Homo sapiens OX=9606 GN=RPL4 PE=1 SV=5	**3,176773428**
Q13885	Tubulin beta-2A chain OS=Homo sapiens OX=9606 GN=TUBB2A PE=1 SV=1	**3,144561053**
A8MXP9	Matrin-3 OS=Homo sapiens OX=9606 GN=MATR3 PE=1 SV=1	**3,073216348**
Q99584	Protein S100-A13 OS=Homo sapiens OX=9606 GN=S100A13 PE=1 SV=1	**3,028336021**
P10809	60 kDa heat shock protein, mitochondrial OS=Homo sapiens OX=9606 GN=HSPD1 PE=1 SV=2	**2,984272348**
P30050	60S ribosomal protein L12 OS=Homo sapiens OX=9606 GN=RPL12 PE=1 SV=1	**2,939859134**
P38646	Stress-70 protein, mitochondrial OS=Homo sapiens OX=9606 GN=HSPA9 PE=1 SV=2	**2,934380748**
Q8WX93	Palladin OS=Homo sapiens OX=9606 GN=PALLD PE=1 SV=3	**2,928526839**
P40123	Adenylyl cyclase-associated protein 2 OS=Homo sapiens OX=9606 GN=CAP2 PE=1 SV=1	**2,923143813**
D6RBZ0	Heterogeneous nuclear ribonucleoprotein A/B OS=Homo sapiens OX=9606 GN=HNRNPAB PE=1 SV=1	**2,916368411**
A0A024R4E5	High density lipoprotein binding protein (Vigilin), isoform CRA_a OS=Homo sapiens OX=9606 GN=HDLBP PE=1 SV=1	**2,915475891**
P23526	Adenosylhomocysteinase OS=Homo sapiens OX=9606 GN=AHCY PE=1 SV=4	**2,878958623**
O15460	Prolyl 4-hydroxylase subunit alpha-2 OS=Homo sapiens OX=9606 GN=P4HA2 PE=1 SV=1	**2,803705522**

A0A0A0MRJ6	Protein-L-isoaspartate O-methyltransferase OS=Homo sapiens OX=9606 GN=PCMT1 PE=1 SV=1	**2,803324844**
P08134	Rho-related GTP-binding protein RhoC OS=Homo sapiens OX=9606 GN=RHOC PE=1 SV=1	**2,800935594**
P29401	Transketolase OS=Homo sapiens OX=9606 GN=TKT PE=1 SV=3	**2,791547591**
A0A6Q8PGN5	Alanine--tRNA ligase OS=Homo sapiens OX=9606 GN=AARS1 PE=1 SV=1	**2,780529048**
Q99832	T-complex protein 1 subunit eta OS=Homo sapiens OX=9606 GN=CCT7 PE=1 SV=2	**2,779282918**
U3KQK0	Histone H2B OS=Homo sapiens OX=9606 GN=H2BC15 PE=1 SV=1	**2,742007859**
P50454	Serpin H1 OS=Homo sapiens OX=9606 GN=SERPINH1 PE=1 SV=2	**2,73433813**
P61160	Actin-related protein 2 OS=Homo sapiens OX=9606 GN=ACTR2 PE=1 SV=1	**2,724016514**
P35221	Catenin alpha-1 OS=Homo sapiens OX=9606 GN=CTNNA1 PE=1 SV=1	**2,674270886**
P49411	Elongation factor Tu, mitochondrial OS=Homo sapiens OX=9606 GN=TUFM PE=1 SV=2	**2,672194017**
P28066	Proteasome subunit alpha type-5 OS=Homo sapiens OX=9606 GN=PSMA5 PE=1 SV=3	**2,656490284**
P61026	Ras-related protein Rab-10 OS=Homo sapiens OX=9606 GN=RAB10 PE=1 SV=1	**2,64477835**
P30101	Protein disulfide-isomerase A3 OS=Homo sapiens OX=9606 GN=PDIA3 PE=1 SV=4	**2,641494797**
P13797	Plastin-3 OS=Homo sapiens OX=9606 GN=PLS3 PE=1 SV=4	**2,629914253**
M0R0C6	Far upstream element-binding protein 2 OS=Homo sapiens OX=9606 GN=KHSRP PE=1 SV=2	**2,619902474**

O43854	EGF-like repeat and discoidin I-like domain-containing protein 3 OS=Homo sapiens OX=9606 GN=EDIL3 PE=1 SV=1	**2,593685324**
P23246	Splicing factor, proline- and glutamine-rich OS=Homo sapiens OX=9606 GN=SFPQ PE=1 SV=2	**2,553288224**
P35268	60S ribosomal protein L22 OS=Homo sapiens OX=9606 GN=RPL22 PE=1 SV=2	**2,543728571**
O15143	Actin-related protein 2/3 complex subunit 1B OS=Homo sapiens OX=9606 GN=ARPC1B PE=1 SV=3	**2,543569298**
P62280	40S ribosomal protein S11 OS=Homo sapiens OX=9606 GN=RPS11 PE=1 SV=3	**2,529886368**
P35606	Coatomer subunit beta' OS=Homo sapiens OX=9606 GN=COPB2 PE=1 SV=2	**2,515461041**
P35527	Keratin, type I cytoskeletal 9 OS=Homo sapiens OX=9606 GN=KRT9 PE=1 SV=3	**2,490509907**
O75396	Vesicle-trafficking protein SEC22b OS=Homo sapiens OX=9606 GN=SEC22B PE=1 SV=5	**2,483474996**
P00505	Aspartate aminotransferase, mitochondrial OS=Homo sapiens OX=9606 GN=GOT2 PE=1 SV=3	**2,441328272**
P09429	High mobility group protein B1 OS=Homo sapiens OX=9606 GN=HMGB1 PE=1 SV=3	**2,441044626**
Q9NZL9	Methionine adenosyltransferase 2 subunit beta OS=Homo sapiens OX=9606 GN=MAT2B PE=1 SV=1	**2,365643481**
P62424	60S ribosomal protein L7a OS=Homo sapiens OX=9606 GN=RPL7A PE=1 SV=2	**2,302618985**
P33176	Kinesin-1 heavy chain OS=Homo sapiens OX=9606 GN=KIF5B PE=1 SV=1	**2,30163182**
A6NCE7	Microtubule-associated proteins 1A/1B light chain 3 beta 2 OS=Homo sapiens OX=9606 GN=MAP1LC3B2 PE=2 SV=1	**2,264890087**

P17987	T-complex protein 1 subunit alpha OS=Homo sapiens OX=9606 GN=TCP1 PE=1 SV=1	**2,260621243**
P40926	Malate dehydrogenase, mitochondrial OS=Homo sapiens OX=9606 GN=MDH2 PE=1 SV=3	**2,257966445**
P49368	T-complex protein 1 subunit gamma OS=Homo sapiens OX=9606 GN=CCT3 PE=1 SV=4	**2,242935138**
B7Z4C8	60S ribosomal protein L31 OS=Homo sapiens OX=9606 GN=RPL31 PE=1 SV=1	**2,242584633**
Q02543	60S ribosomal protein L18a OS=Homo sapiens OX=9606 GN=RPL18A PE=1 SV=2	**2,213907042**
P60174	Triosephosphate isomerase OS=Homo sapiens OX=9606 GN=TPI1 PE=1 SV=4	**2,194700486**
P21333	Filamin-A OS=Homo sapiens OX=9606 GN=FLNA PE=1 SV=4	**2,194189957**
A0A7P0Z4P5	4F2 cell-surface antigen heavy chain OS=Homo sapiens OX=9606 GN=SLC3A2 PE=1 SV=1	**2,189792188**
B7Z6Z4	Myosin light polypeptide 6 OS=Homo sapiens OX=9606 GN=MYL6 PE=1 SV=1	**2,18251185**
A0A0U1RRM4	Polypyrimidine tract-binding protein 1 OS=Homo sapiens OX=9606 GN=PTBP1 PE=1 SV=1	**2,172794516**
P40227	T-complex protein 1 subunit zeta OS=Homo sapiens OX=9606 GN=CCT6A PE=1 SV=3	**2,168829242**
P26641	Elongation factor 1-gamma OS=Homo sapiens OX=9606 GN=EEF1G PE=1 SV=3	**2,165761931**
P55072	Transitional endoplasmic reticulum ATPase OS=Homo sapiens OX=9606 GN=VCP PE=1 SV=4	**2,149823121**
P62701	40S ribosomal protein S4, X isoform OS=Homo sapiens OX=9606 GN=RPS4X PE=1 SV=2	**2,136071751**
Q9Y490	Talin-1 OS=Homo sapiens OX=9606 GN=TLN1 PE=1 SV=3	**2,074750933**

H7BZJ3	Protein disulfide-isomerase A3 (Fragment) OS=Homo sapiens OX=9606 GN=PDIA3 PE=1 SV=1	**2,073030017**
P50395	Rab GDP dissociation inhibitor beta OS=Homo sapiens OX=9606 GN=GDI2 PE=1 SV=2	**2,064675213**
H7BY16	Nucleolin OS=Homo sapiens OX=9606 GN=NCL PE=1 SV=9	**2,06190405**
P27348	14-3-3 protein theta OS=Homo sapiens OX=9606 GN=YWHAQ PE=1 SV=1	**2,05930997**
P27635	60S ribosomal protein L10 OS=Homo sapiens OX=9606 GN=RPL10 PE=1 SV=4	**2,043873174**
A0A6Q8PH84	Ras-related protein Rab-7a OS=Homo sapiens OX=9606 GN=RAB7A PE=1 SV=1	**2,02580611**
P49773	Adenosine 5'-monophosphoramidase HINT1 OS=Homo sapiens OX=9606 GN=HINT1 PE=1 SV=2	**2,024057112**
Q13162	Peroxiredoxin-4 OS=Homo sapiens OX=9606 GN=PRDX4 PE=1 SV=1	**2,01979587**
P18669	Phosphoglycerate mutase 1 OS=Homo sapiens OX=9606 GN=PGAM1 PE=1 SV=2	**2,008123463**
O00231	26S proteasome non-ATPase regulatory subunit 11 OS=Homo sapiens OX=9606 GN=PSMD11 PE=1 SV=3	**0,499556757**
Q15369	Elongin-C OS=Homo sapiens OX=9606 GN=ELOC PE=1 SV=1	**0,497790777**
P52565	Rho GDP-dissociation inhibitor 1 OS=Homo sapiens OX=9606 GN=ARHGDIA PE=1 SV=3	**0,496982671**
Q13409	Cytoplasmic dynein 1 intermediate chain 2 OS=Homo sapiens OX=9606 GN=DYNC1I2 PE=1 SV=3	**0,496939294**
Q07960	Rho GTPase-activating protein 1 OS=Homo sapiens OX=9606 GN=ARHGAP1 PE=1 SV=1	**0,491049387**
P08238	Heat shock protein HSP 90-beta OS=Homo sapiens OX=9606 GN=HSP90AB1 PE=1 SV=4	**0,489026269**

E9PIE3	Caveolae-associated protein 3 OS=Homo sapiens OX=9606 GN=CAVIN3 PE=1 SV=1	**0,48878784**
P30086	Phosphatidylethanolamine-binding protein 1 OS=Homo sapiens OX=9606 GN=PEBP1 PE=1 SV=3	**0,48767699**
P07737	Profilin-1 OS=Homo sapiens OX=9606 GN=PFN1 PE=1 SV=2	**0,485719642**
P31946	14-3-3 protein beta/alpha OS=Homo sapiens OX=9606 GN=YWHAB PE=1 SV=3	**0,480424927**
P35998	26S proteasome regulatory subunit 7 OS=Homo sapiens OX=9606 GN=PSMC2 PE=1 SV=3	**0,474888985**
O15144	Actin-related protein 2/3 complex subunit 2 OS=Homo sapiens OX=9606 GN=ARPC2 PE=1 SV=1	**0,473576567**
A0A1W2PRS1	Lysosome membrane protein 2 (Fragment) OS=Homo sapiens OX=9606 GN=SCARB2 PE=1 SV=1	**0,472833151**
O75083	WD repeat-containing protein 1 OS=Homo sapiens OX=9606 GN=WDR1 PE=1 SV=4	**0,469429369**
Q9UNZ2	NSFL1 cofactor p47 OS=Homo sapiens OX=9606 GN=NSFL1C PE=1 SV=2	**0,467593799**
P62249	40S ribosomal protein S16 OS=Homo sapiens OX=9606 GN=RPS16 PE=1 SV=2	**0,467397471**
A0A7P0T9C4	Cytoplasmic dynein 1 heavy chain 1 OS=Homo sapiens OX=9606 GN=DYNC1H1 PE=1 SV=1	**0,460993668**
P62913	60S ribosomal protein L11 OS=Homo sapiens OX=9606 GN=RPL11 PE=1 SV=2	**0,458691948**
P62942	Peptidyl-prolyl cis-trans isomerase FKBP1A OS=Homo sapiens OX=9606 GN=FKBP1A PE=1 SV=2	**0,452932446**
A0A7P0TAE9	Calnexin OS=Homo sapiens OX=9606 GN=CANX PE=1 SV=1	**0,451577997**
P07954	Fumarate hydratase, mitochondrial OS=Homo sapiens OX=9606 GN=FH PE=1 SV=3	**0,447961732**

Q15366	Poly(rC)-binding protein 2 OS=Homo sapiens OX=9606 GN=PCBP2 PE=1 SV=1	**0,447455279**
A0A087WVQ6	Clathrin heavy chain OS=Homo sapiens OX=9606 GN=CLTC PE=1 SV=1	**0,447382704**
Q9BUF5	Tubulin beta-6 chain OS=Homo sapiens OX=9606 GN=TUBB6 PE=1 SV=1	**0,446473445**
P68371	Tubulin beta-4B chain OS=Homo sapiens OX=9606 GN=TUBB4B PE=1 SV=1	**0,446204874**
P26640	Valine--tRNA ligase OS=Homo sapiens OX=9606 GN=VARS1 PE=1 SV=4	**0,446065497**
Q15293	Reticulocalbin-1 OS=Homo sapiens OX=9606 GN=RCN1 PE=1 SV=1	**0,442556599**
P42766	60S ribosomal protein L35 OS=Homo sapiens OX=9606 GN=RPL35 PE=1 SV=2	**0,439315062**
O15212	Prefoldin subunit 6 OS=Homo sapiens OX=9606 GN=PFDN6 PE=1 SV=1	**0,429989981**
P08758	Annexin A5 OS=Homo sapiens OX=9606 GN=ANXA5 PE=1 SV=2	**0,429647627**
P08670	Vimentin OS=Homo sapiens OX=9606 GN=VIM PE=1 SV=4	**0,420644248**
Q9H0U4	Ras-related protein Rab-1B OS=Homo sapiens OX=9606 GN=RAB1B PE=1 SV=1	**0,41541514**
P62820	Ras-related protein Rab-1A OS=Homo sapiens OX=9606 GN=RAB1A PE=1 SV=3	**0,414078653**
F8WCF6	Actin-related protein 2/3 complex subunit 4 OS=Homo sapiens OX=9606 GN=ARPC4-TTLL3 PE=3 SV=1	**0,413034603**
A0A804HKI2	Leucine-rich PPR motif-containing protein, mitochondrial OS=Homo sapiens OX=9606 GN=LRPPRC PE=4 SV=1	**0,406526076**
P05091	Aldehyde dehydrogenase, mitochondrial OS=Homo sapiens OX=9606 GN=ALDH2 PE=1 SV=2	**0,403455938**

G8JLB6	Heterogeneous nuclear ribonucleoprotein H OS=Homo sapiens OX=9606 GN=HNRNPH1 PE=1 SV=1	**0,402890872**
P62136	Serine/threonine-protein phosphatase PP1-alpha catalytic subunit OS=Homo sapiens OX=9606 GN=PPP1CA PE=1 SV=1	**0,399882379**
Q14247	Src substrate cortactin OS=Homo sapiens OX=9606 GN=CTTN PE=1 SV=2	**0,394505677**
P09110	3-ketoacyl-CoA thiolase, peroxisomal OS=Homo sapiens OX=9606 GN=ACAA1 PE=1 SV=2	**0,394440631**
Q9UII2	ATPase inhibitor, mitochondrial OS=Homo sapiens OX=9606 GN=ATP5IF1 PE=1 SV=1	**0,391301519**
O43852	Calumenin OS=Homo sapiens OX=9606 GN=CALU PE=1 SV=2	**0,386958169**
Q9UHD8	Septin-9 OS=Homo sapiens OX=9606 GN=SEPTIN9 PE=1 SV=2	**0,386027616**
O75915	PRA1 family protein 3 OS=Homo sapiens OX=9606 GN=ARL6IP5 PE=1 SV=1	**0,385346051**
Q14847	LIM and SH3 domain protein 1 OS=Homo sapiens OX=9606 GN=LASP1 PE=1 SV=2	**0,383704739**
P30044	Peroxiredoxin-5, mitochondrial OS=Homo sapiens OX=9606 GN=PRDX5 PE=1 SV=4	**0,381049216**
P61158	Actin-related protein 3 OS=Homo sapiens OX=9606 GN=ACTR3 PE=1 SV=3	**0,380023095**
O94925	Glutaminase kidney isoform, mitochondrial OS=Homo sapiens OX=9606 GN=GLS PE=1 SV=1	**0,378869904**
A0A7P0TA71	Protein disulfide-isomerase OS=Homo sapiens OX=9606 GN=P4HB PE=1 SV=1	**0,375700146**
P11142	Heat shock cognate 71 kDa protein OS=Homo sapiens OX=9606 GN=HSPA8 PE=1 SV=1	**0,369039683**

P00387	NADH-cytochrome b5 reductase 3 OS=Homo sapiens OX=9606 GN=CYB5R3 PE=1 SV=3	**0,363417441**
P63000	Ras-related C3 botulinum toxin substrate 1 OS=Homo sapiens OX=9606 GN=RAC1 PE=1 SV=1	**0,362120182**
P23396	40S ribosomal protein S3 OS=Homo sapiens OX=9606 GN=RPS3 PE=1 SV=2	**0,360802119**
Q13200	26S proteasome non-ATPase regulatory subunit 2 OS=Homo sapiens OX=9606 GN=PSMD2 PE=1 SV=3	**0,358132589**
E9PL57	NEDD8-MDP1 readthrough (Fragment) OS=Homo sapiens OX=9606 GN=NEDD8-MDP1 PE=4 SV=1	**0,341424144**
P32119	Peroxiredoxin-2 OS=Homo sapiens OX=9606 GN=PRDX2 PE=1 SV=5	**0,33922593**
Q9BVC6	Transmembrane protein 109 OS=Homo sapiens OX=9606 GN=TMEM109 PE=1 SV=1	**0,338990873**
P08133	Annexin A6 OS=Homo sapiens OX=9606 GN=ANXA6 PE=1 SV=3	**0,332236469**
O15511	Actin-related protein 2/3 complex subunit 5 OS=Homo sapiens OX=9606 GN=ARPC5 PE=1 SV=3	**0,322417293**
Q9Y3B3	Transmembrane emp24 domain-containing protein 7 OS=Homo sapiens OX=9606 GN=TMED7 PE=1 SV=2	**0,321669098**
A0A6Q8PH20	Calpain inhibitor OS=Homo sapiens OX=9606 GN=CAST PE=1 SV=1	**0,318255491**
O14907	Tax1-binding protein 3 OS=Homo sapiens OX=9606 GN=TAX1BP3 PE=1 SV=2	**0,307605851**
P30153	Serine/threonine-protein phosphatase 2A 65 kDa regulatory subunit A alpha isoform OS=Homo sapiens OX=9606 GN=PPP2R1A PE=1 SV=4	**0,295724222**
Q14315	Filamin-C OS=Homo sapiens OX=9606 GN=FLNC PE=1 SV=3	**0,295195437**

Q09666	Neuroblast differentiation-associated protein AHNAK OS=Homo sapiens OX=9606 GN=AHNAK PE=1 SV=2	**0,292041608**
Q96KP4	Cytosolic non-specific dipeptidase OS=Homo sapiens OX=9606 GN=CNDP2 PE=1 SV=2	**0,288070428**
P40121	Macrophage-capping protein OS=Homo sapiens OX=9606 GN=CAPG PE=1 SV=2	**0,278113541**
P05387	60S acidic ribosomal protein P2 OS=Homo sapiens OX=9606 GN=RPLP2 PE=1 SV=1	**0,277690672**
H7BYY1	Tropomyosin 1 (Alpha), isoform CRA_m OS=Homo sapiens OX=9606 GN=TPM1 PE=1 SV=1	**0,244911606**
P04083	Annexin A1 OS=Homo sapiens OX=9606 GN=ANXA1 PE=1 SV=2	**0,238475531**
P18085	ADP-ribosylation factor 4 OS=Homo sapiens OX=9606 GN=ARF4 PE=1 SV=3	**0,234854931**
P11166	Solute carrier family 2, facilitated glucose transporter member 1 OS=Homo sapiens OX=9606 GN=SLC2A1 PE=1 SV=2	**0,233351578**
A0A087WWU8	Tropomyosin alpha-3 chain OS=Homo sapiens OX=9606 GN=TPM3 PE=1 SV=1	**0,229470888**
P50502	Hsc70-interacting protein OS=Homo sapiens OX=9606 GN=ST13 PE=1 SV=2	**0,228516076**
P37837	Transaldolase OS=Homo sapiens OX=9606 GN=TALDO1 PE=1 SV=2	**0,228201675**
P46821	Microtubule-associated protein 1B OS=Homo sapiens OX=9606 GN=MAP1B PE=1 SV=2	**0,226981474**
P05455	Lupus La protein OS=Homo sapiens OX=9606 GN=SSB PE=1 SV=2	**0,222357474**
P60866	40S ribosomal protein S20 OS=Homo sapiens OX=9606 GN=RPS20 PE=1 SV=1	**0,221809459**

P67936	Tropomyosin alpha-4 chain OS=Homo sapiens OX=9606 GN=TPM4 PE=1 SV=3	**0,216319918**
P63244	Receptor of activated protein C kinase 1 OS=Homo sapiens OX=9606 GN=RACK1 PE=1 SV=3	**0,211388536**
B0QZ18	Copine-1 OS=Homo sapiens OX=9606 GN=CPNE1 PE=1 SV=1	**0,200480549**
P62906	60S ribosomal protein L10a OS=Homo sapiens OX=9606 GN=RPL10A PE=1 SV=2	**0,195837721**
P12111	Collagen alpha-3(VI) chain OS=Homo sapiens OX=9606 GN=COL6A3 PE=1 SV=5	**0,195408782**
P09382	Galectin-1 OS=Homo sapiens OX=9606 GN=LGALS1 PE=1 SV=2	**0,181130351**
Q13561	Dynactin subunit 2 OS=Homo sapiens OX=9606 GN=DCTN2 PE=1 SV=4	**0,179261481**
Q6NZI2	Caveolae-associated protein 1 OS=Homo sapiens OX=9606 GN=CAVIN1 PE=1 SV=1	**0,175734732**
Q96HC4	PDZ and LIM domain protein 5 OS=Homo sapiens OX=9606 GN=PDLIM5 PE=1 SV=5	**0,164462543**
E9PGC8	Microtubule-associated protein 1A OS=Homo sapiens OX=9606 GN=MAP1A PE=1 SV=1	**0,155326356**
Q15436	Protein transport protein Sec23A OS=Homo sapiens OX=9606 GN=SEC23A PE=1 SV=2	**0,147827611**
Q15084	Protein disulfide-isomerase A6 OS=Homo sapiens OX=9606 GN=PDIA6 PE=1 SV=1	**0,144309988**
Q86VP6	Cullin-associated NEDD8-dissociated protein 1 OS=Homo sapiens OX=9606 GN=CAND1 PE=1 SV=2	**0,138777803**
P61088	Ubiquitin-conjugating enzyme E2 N OS=Homo sapiens OX=9606 GN=UBE2N PE=1 SV=1	**0,134758486**
Q01995	Transgelin OS=Homo sapiens OX=9606 GN=TAGLN PE=1 SV=4	**0,131005564**

P27797	Calreticulin OS=Homo sapiens OX=9606 GN=CALR PE=1 SV=1	**0,130905176**
C9J813	Caldesmon (Fragment) OS=Homo sapiens OX=9606 GN=CALD1 PE=1 SV=1	**0,130497874**
P30040	Endoplasmic reticulum resident protein 29 OS=Homo sapiens OX=9606 GN=ERP29 PE=1 SV=4	**0,128528193**
O00299	Chloride intracellular channel protein 1 OS=Homo sapiens OX=9606 GN=CLIC1 PE=1 SV=4	**0,118484784**
P06396	Gelsolin OS=Homo sapiens OX=9606 GN=GSN PE=1 SV=1	**0,117587762**
Q15046	Lysine--tRNA ligase OS=Homo sapiens OX=9606 GN=KARS1 PE=1 SV=3	**0,105353527**
Q9Y281	Cofilin-2 OS=Homo sapiens OX=9606 GN=CFL2 PE=1 SV=1	**0,100330722**
P00338	L-lactate dehydrogenase A chain OS=Homo sapiens OX=9606 GN=LDHA PE=1 SV=2	**0,099537915**
P55209	Nucleosome assembly protein 1-like 1 OS=Homo sapiens OX=9606 GN=NAP1L1 PE=1 SV=1	**0,098560976**
O00560	Syntenin-1 OS=Homo sapiens OX=9606 GN=SDCBP PE=1 SV=1	**0,098391582**
O60664	Perilipin-3 OS=Homo sapiens OX=9606 GN=PLIN3 PE=1 SV=3	**0,095634484**
O00487	26S proteasome non-ATPase regulatory subunit 14 OS=Homo sapiens OX=9606 GN=PSMD14 PE=1 SV=1	**0,092224302**
A0A0B4J2C3	Translationally-controlled tumor protein OS=Homo sapiens OX=9606 GN=TPT1 PE=1 SV=1	**0,087710507**
Q969H8	Myeloid-derived growth factor OS=Homo sapiens OX=9606 GN=MYDGF PE=1 SV=1	**0,082409541**
Q13509	Tubulin beta-3 chain OS=Homo sapiens OX=9606 GN=TUBB3 PE=1 SV=2	**0,080130629**

Q9Y3F4	Serine-threonine kinase receptor-associated protein OS=Homo sapiens OX=9606 GN=STRAP PE=1 SV=1	**0,077067143**
P07686	Beta-hexosaminidase subunit beta OS=Homo sapiens OX=9606 GN=HEXB PE=1 SV=3	**0,067819251**
P36776	Lon protease homolog, mitochondrial OS=Homo sapiens OX=9606 GN=LONP1 PE=1 SV=2	**0,063969069**
P60903	Protein S100-A10 OS=Homo sapiens OX=9606 GN=S100A10 PE=1 SV=2	**0,050693934**
Q15075	Early endosome antigen 1 OS=Homo sapiens OX=9606 GN=EEA1 PE=1 SV=2	**0,050444685**
Q07065	Cytoskeleton-associated protein 4 OS=Homo sapiens OX=9606 GN=CKAP4 PE=1 SV=2	**0,049415286**
P62258	14-3-3 protein epsilon OS=Homo sapiens OX=9606 GN=YWHAE PE=1 SV=1	**0,048773281**
Q14764	Major vault protein OS=Homo sapiens OX=9606 GN=MVP PE=1 SV=4	**0,042453487**
Q9NYL9	Tropomodulin-3 OS=Homo sapiens OX=9606 GN=TMOD3 PE=1 SV=1	**0,042145704**
P80723	Brain acid soluble protein 1 OS=Homo sapiens OX=9606 GN=BASP1 PE=1 SV=2	**0,04068743**
Q9NQC3	Reticulon-4 OS=Homo sapiens OX=9606 GN=RTN4 PE=1 SV=2	**0,035542327**
A0A0C4DGQ5	Calcium-activated neutral proteinase small subunit OS=Homo sapiens OX=9606 GN=CAPNS1 PE=1 SV=1	**0,031010763**
P10599	Thioredoxin OS=Homo sapiens OX=9606 GN=TXN PE=1 SV=3	**0,022209854**
P16070	CD44 antigen OS=Homo sapiens OX=9606 GN=CD44 PE=1 SV=3	**0,008775473**

Accession	Description	Abundance Ratio: Apelin MSC / Control MSC
P60903	Protein S100-A10 OS=Homo sapiens OX=9606 GN=S100A10 PE=1 SV=2	**526,8183461**
P16070	CD44 antigen OS=Homo sapiens OX=9606 GN=CD44 PE=1 SV=3	**233,5027021**
P31949	Protein S100-A11 OS=Homo sapiens OX=9606 GN=S100A11 PE=1 SV=2	**163,7425117**
A0A0B4J2C3	Translationally-controlled tumor protein OS=Homo sapiens OX=9606 GN=TPT1 PE=1 SV=1	**72,62546787**
F8W6I7	Helix-destabilizing protein OS=Homo sapiens OX=9606 GN=HNRNPA1 PE=1 SV=2	**54,14574109**
Q15436	Protein transport protein Sec23A OS=Homo sapiens OX=9606 GN=SEC23A PE=1 SV=2	**53,02801916**
P46821	Microtubule-associated protein 1B OS=Homo sapiens OX=9606 GN=MAP1B PE=1 SV=2	**49,82649326**
P09382	Galectin-1 OS=Homo sapiens OX=9606 GN=LGALS1 PE=1 SV=2	**40,94627736**
P05091	Aldehyde dehydrogenase, mitochondrial OS=Homo sapiens OX=9606 GN=ALDH2 PE=1 SV=2	**40,63049121**
P80723	Brain acid soluble protein 1 OS=Homo sapiens OX=9606 GN=BASP1 PE=1 SV=2	**39,11149214**
O15144	Actin-related protein 2/3 complex subunit 2 OS=Homo sapiens OX=9606 GN=ARPC2 PE=1 SV=1	**38,87586074**
Q96HC4	PDZ and LIM domain protein 5 OS=Homo sapiens OX=9606 GN=PDLIM5 PE=1 SV=5	**36,7022534**
P05387	60S acidic ribosomal protein P2 OS=Homo sapiens OX=9606 GN=RPLP2 PE=1 SV=1	**33,60918754**

P31948	Stress-induced-phosphoprotein 1 OS=Homo sapiens OX=9606 GN=STIP1 PE=1 SV=1	**31,72307448**
C9J813	Caldesmon (Fragment) OS=Homo sapiens OX=9606 GN=CALD1 PE=1 SV=1	**26,20736706**
P29966	Myristoylated alanine-rich C-kinase substrate OS=Homo sapiens OX=9606 GN=MARCKS PE=1 SV=4	**24,23635145**
P12111	Collagen alpha-3(VI) chain OS=Homo sapiens OX=9606 GN=COL6A3 PE=1 SV=5	**22,5888622**
J3QRS3	Myosin regulatory light chain 12A OS=Homo sapiens OX=9606 GN=MYL12A PE=1 SV=1	**22,44543095**
P18085	ADP-ribosylation factor 4 OS=Homo sapiens OX=9606 GN=ARF4 PE=1 SV=3	**21,10514757**
P61088	Ubiquitin-conjugating enzyme E2 N OS=Homo sapiens OX=9606 GN=UBE2N PE=1 SV=1	**20,63987132**
P68032	Actin, alpha cardiac muscle 1 OS=Homo sapiens OX=9606 GN=ACTC1 PE=1 SV=1	**19,77804167**
P63244	Receptor of activated protein C kinase 1 OS=Homo sapiens OX=9606 GN=RACK1 PE=1 SV=3	**19,26714804**
O43242	26S proteasome non-ATPase regulatory subunit 3 OS=Homo sapiens OX=9606 GN=PSMD3 PE=1 SV=2	**18,42080466**
P30040	Endoplasmic reticulum resident protein 29 OS=Homo sapiens OX=9606 GN=ERP29 PE=1 SV=4	**17,42126448**
Q8IVF2	Protein AHNAK2 OS=Homo sapiens OX=9606 GN=AHNAK2 PE=1 SV=2	**15,68991022**
P61247	40S ribosomal protein S3a OS=Homo sapiens OX=9606 GN=RPS3A PE=1 SV=2	**15,58402457**
P27797	Calreticulin OS=Homo sapiens OX=9606 GN=CALR PE=1 SV=1	**15,44061216**

Q86VP6	Cullin-associated NEDD8-dissociated protein 1 OS=Homo sapiens OX=9606 GN=CAND1 PE=1 SV=2	**15,08215897**
P55209	Nucleosome assembly protein 1-like 1 OS=Homo sapiens OX=9606 GN=NAP1L1 PE=1 SV=1	**14,88069661**
Q9NQC3	Reticulon-4 OS=Homo sapiens OX=9606 GN=RTN4 PE=1 SV=2	**14,83588796**
P62258	14-3-3 protein epsilon OS=Homo sapiens OX=9606 GN=YWHAE PE=1 SV=1	**14,66595067**
A0A0C4DGQ5	Calcium-activated neutral proteinase small subunit OS=Homo sapiens OX=9606 GN=CAPNS1 PE=1 SV=1	**14,38073765**
Q15181	Inorganic pyrophosphatase OS=Homo sapiens OX=9606 GN=PPA1 PE=1 SV=2	**14,30118811**
P46778	60S ribosomal protein L21 OS=Homo sapiens OX=9606 GN=RPL21 PE=1 SV=2	**13,69246725**
Q15075	Early endosome antigen 1 OS=Homo sapiens OX=9606 GN=EEA1 PE=1 SV=2	**13,59588379**
P10599	Thioredoxin OS=Homo sapiens OX=9606 GN=TXN PE=1 SV=3	**13,43251716**
B7Z4C8	60S ribosomal protein L31 OS=Homo sapiens OX=9606 GN=RPL31 PE=1 SV=1	**13,36600547**
P01023	Alpha-2-macroglobulin OS=Homo sapiens OX=9606 GN=A2M PE=1 SV=3	**13,09920107**
Q9NYL9	Tropomodulin-3 OS=Homo sapiens OX=9606 GN=TMOD3 PE=1 SV=1	**12,69259671**
P35580	Myosin-10 OS=Homo sapiens OX=9606 GN=MYH10 PE=1 SV=3	**12,63696245**
P61158	Actin-related protein 3 OS=Homo sapiens OX=9606 GN=ACTR3 PE=1 SV=3	**12,2730774**

Q9Y3B3	Transmembrane emp24 domain-containing protein 7 OS=Homo sapiens OX=9606 GN=TMED7 PE=1 SV=2	**11,938237**
O15511	Actin-related protein 2/3 complex subunit 5 OS=Homo sapiens OX=9606 GN=ARPC5 PE=1 SV=3	**11,8465896**
P05455	Lupus La protein OS=Homo sapiens OX=9606 GN=SSB PE=1 SV=2	**11,44615168**
Q15084	Protein disulfide-isomerase A6 OS=Homo sapiens OX=9606 GN=PDIA6 PE=1 SV=1	**11,0175743**
Q01995	Transgelin OS=Homo sapiens OX=9606 GN=TAGLN PE=1 SV=4	**10,70057828**
P28074	Proteasome subunit beta type-5 OS=Homo sapiens OX=9606 GN=PSMB5 PE=1 SV=3	**10,46755449**
P62857	40S ribosomal protein S28 OS=Homo sapiens OX=9606 GN=RPS28 PE=1 SV=1	**10,35054535**
Q9Y3F4	Serine-threonine kinase receptor-associated protein OS=Homo sapiens OX=9606 GN=STRAP PE=1 SV=1	**10,15234541**
P50502	Hsc70-interacting protein OS=Homo sapiens OX=9606 GN=ST13 PE=1 SV=2	**9,831256484**
A0A804HKI2	Leucine-rich PPR motif-containing protein, mitochondrial OS=Homo sapiens OX=9606 GN=LRPPRC PE=4 SV=1	**9,740058599**
P36776	Lon protease homolog, mitochondrial OS=Homo sapiens OX=9606 GN=LONP1 PE=1 SV=2	**9,474962164**
Q9Y281	Cofilin-2 OS=Homo sapiens OX=9606 GN=CFL2 PE=1 SV=1	**9,189151219**
Q8NBS9	Thioredoxin domain-containing protein 5 OS=Homo sapiens OX=9606 GN=TXNDC5 PE=1 SV=2	**9,106894087**
E9PAV3	Nascent polypeptide-associated complex subunit alpha, muscle-specific form OS=Homo sapiens OX=9606 GN=NACA PE=1 SV=1	**9,005389601**

P07942	Laminin subunit beta-1 OS=Homo sapiens OX=9606 GN=LAMB1 PE=1 SV=2	**8,594873663**
P07686	Beta-hexosaminidase subunit beta OS=Homo sapiens OX=9606 GN=HEXB PE=1 SV=3	**8,581703103**
P20908	Collagen alpha-1(V) chain OS=Homo sapiens OX=9606 GN=COL5A1 PE=1 SV=3	**8,519573066**
Q07960	Rho GTPase-activating protein 1 OS=Homo sapiens OX=9606 GN=ARHGAP1 PE=1 SV=1	**8,293263319**
Q09666	Neuroblast differentiation-associated protein AHNAK OS=Homo sapiens OX=9606 GN=AHNAK PE=1 SV=2	**8,269380089**
Q13200	26S proteasome non-ATPase regulatory subunit 2 OS=Homo sapiens OX=9606 GN=PSMD2 PE=1 SV=3	**8,260818473**
A0A6Q8PFE1	Apoptosis-inducing factor 1, mitochondrial OS=Homo sapiens OX=9606 GN=AIFM1 PE=1 SV=1	**8,245324065**
P49755	Transmembrane emp24 domain-containing protein 10 OS=Homo sapiens OX=9606 GN=TMED10 PE=1 SV=2	**8,161493152**
Q15758	Neutral amino acid transporter B(0) OS=Homo sapiens OX=9606 GN=SLC1A5 PE=1 SV=2	**7,954420542**
P62820	Ras-related protein Rab-1A OS=Homo sapiens OX=9606 GN=RAB1A PE=1 SV=3	**7,937934635**
A0A7P0Z4P5	4F2 cell-surface antigen heavy chain OS=Homo sapiens OX=9606 GN=SLC3A2 PE=1 SV=1	**7,839926477**
P00338	L-lactate dehydrogenase A chain OS=Homo sapiens OX=9606 GN=LDHA PE=1 SV=2	**7,575212464**
P46940	Ras GTPase-activating-like protein IQGAP1 OS=Homo sapiens OX=9606 GN=IQGAP1 PE=1 SV=1	**7,55848351**

Q14315	Filamin-C OS=Homo sapiens OX=9606 GN=FLNC PE=1 SV=3	**7,529201276**
P13667	Protein disulfide-isomerase A4 OS=Homo sapiens OX=9606 GN=PDIA4 PE=1 SV=2	**7,471843495**
P35579	Myosin-9 OS=Homo sapiens OX=9606 GN=MYH9 PE=1 SV=4	**7,429037508**
P35606	Coatomer subunit beta' OS=Homo sapiens OX=9606 GN=COPB2 PE=1 SV=2	**7,356646476**
Q9Y2Q3	Glutathione S-transferase kappa 1 OS=Homo sapiens OX=9606 GN=GSTK1 PE=1 SV=3	**7,347331997**
A0A804HII9	Alpha-actinin-1 OS=Homo sapiens OX=9606 GN=ACTN1 PE=4 SV=1	**7,321891107**
P60866	40S ribosomal protein S20 OS=Homo sapiens OX=9606 GN=RPS20 PE=1 SV=1	**7,28232912**
P39019	40S ribosomal protein S19 OS=Homo sapiens OX=9606 GN=RPS19 PE=1 SV=2	**7,194737606**
Q13561	Dynactin subunit 2 OS=Homo sapiens OX=9606 GN=DCTN2 PE=1 SV=4	**7,109917278**
P16989	Y-box-binding protein 3 OS=Homo sapiens OX=9606 GN=YBX3 PE=1 SV=4	**7,052525706**
P43487	Ran-specific GTPase-activating protein OS=Homo sapiens OX=9606 GN=RANBP1 PE=1 SV=1	**7,011840136**
P17931	Galectin-3 OS=Homo sapiens OX=9606 GN=LGALS3 PE=1 SV=5	**7,010425644**
E7EUI6	Integrin beta OS=Homo sapiens OX=9606 GN=ITGB1 PE=1 SV=2	**6,868228275**
O94925	Glutaminase kidney isoform, mitochondrial OS=Homo sapiens OX=9606 GN=GLS PE=1 SV=1	**6,801900409**
O60664	Perilipin-3 OS=Homo sapiens OX=9606 GN=PLIN3 PE=1 SV=3	**6,780906841**

P06396	Gelsolin OS=Homo sapiens OX=9606 GN=GSN PE=1 SV=1	**6,540843197**
P78371	T-complex protein 1 subunit beta OS=Homo sapiens OX=9606 GN=CCT2 PE=1 SV=4	**6,532704663**
P07954	Fumarate hydratase, mitochondrial OS=Homo sapiens OX=9606 GN=FH PE=1 SV=3	**6,51479009**
P41252	Isoleucine--tRNA ligase, cytoplasmic OS=Homo sapiens OX=9606 GN=IARS1 PE=1 SV=2	**6,45411001**
P99999	Cytochrome c OS=Homo sapiens OX=9606 GN=CYCS PE=1 SV=2	**6,314072244**
P61224	Ras-related protein Rap-1b OS=Homo sapiens OX=9606 GN=RAP1B PE=1 SV=1	**6,288870904**
P42766	60S ribosomal protein L35 OS=Homo sapiens OX=9606 GN=RPL35 PE=1 SV=2	**6,234644161**
P23284	Peptidyl-prolyl cis-trans isomerase B OS=Homo sapiens OX=9606 GN=PPIB PE=1 SV=2	**6,220218136**
Q9P2E9	Ribosome-binding protein 1 OS=Homo sapiens OX=9606 GN=RRBP1 PE=1 SV=5	**6,159308116**
P12956	X-ray repair cross-complementing protein 6 OS=Homo sapiens OX=9606 GN=XRCC6 PE=1 SV=2	**6,109222471**
F8WCF6	Actin-related protein 2/3 complex subunit 4 OS=Homo sapiens OX=9606 GN=ARPC4-TTLL3 PE=3 SV=1	**6,061652894**
O75390	Citrate synthase, mitochondrial OS=Homo sapiens OX=9606 GN=CS PE=1 SV=2	**6,000188001**
P62979	Ubiquitin-40S ribosomal protein S27a OS=Homo sapiens OX=9606 GN=RPS27A PE=1 SV=2	**5,978284167**
P30153	Serine/threonine-protein phosphatase 2A 65 kDa regulatory subunit A alpha isoform OS=Homo sapiens OX=9606 GN=PPP2R1A PE=1 SV=4	**5,857781557**

P46781	40S ribosomal protein S9 OS=Homo sapiens OX=9606 GN=RPS9 PE=1 SV=3	**5,675782683**
P37802	Transgelin-2 OS=Homo sapiens OX=9606 GN=TAGLN2 PE=1 SV=3	**5,623816389**
Q9UNZ2	NSFL1 cofactor p47 OS=Homo sapiens OX=9606 GN=NSFL1C PE=1 SV=2	**5,617689054**
P30086	Phosphatidylethanolamine-binding protein 1 OS=Homo sapiens OX=9606 GN=PEBP1 PE=1 SV=3	**5,562001346**
Q6UVK1	Chondroitin sulfate proteoglycan 4 OS=Homo sapiens OX=9606 GN=CSPG4 PE=1 SV=2	**5,487991431**
O60701	UDP-glucose 6-dehydrogenase OS=Homo sapiens OX=9606 GN=UGDH PE=1 SV=1	**5,460245221**
P23396	40S ribosomal protein S3 OS=Homo sapiens OX=9606 GN=RPS3 PE=1 SV=2	**5,371592474**
A0A7P0TAE9	Calnexin OS=Homo sapiens OX=9606 GN=CANX PE=1 SV=1	**5,359652992**
D6RER5	Septin OS=Homo sapiens OX=9606 GN=SEPTIN11 PE=1 SV=1	**5,347554813**
P14868	Aspartate--tRNA ligase, cytoplasmic OS=Homo sapiens OX=9606 GN=DARS1 PE=1 SV=2	**5,314738633**
P50914	60S ribosomal protein L14 OS=Homo sapiens OX=9606 GN=RPL14 PE=1 SV=4	**5,288137992**
K7ELC2	40S ribosomal protein S15 OS=Homo sapiens OX=9606 GN=RPS15 PE=1 SV=1	**5,241181476**
F6S8M0	N-acetylglucosamine-6-sulfatase OS=Homo sapiens OX=9606 GN=GNS PE=1 SV=1	**5,21169654**
P62942	Peptidyl-prolyl cis-trans isomerase FKBP1A OS=Homo sapiens OX=9606 GN=FKBP1A PE=1 SV=2	**5,165070067**

O00487	26S proteasome non-ATPase regulatory subunit 14 OS=Homo sapiens OX=9606 GN=PSMD14 PE=1 SV=1	**5,110585003**
A0A6Q8PGN5	Alanine--tRNA ligase OS=Homo sapiens OX=9606 GN=AARS1 PE=1 SV=1	**5,041951856**
P05023	Sodium/potassium-transporting ATPase subunit alpha-1 OS=Homo sapiens OX=9606 GN=ATP1A1 PE=1 SV=1	**5,032930585**
J3QQ67	60S ribosomal protein L18 (Fragment) OS=Homo sapiens OX=9606 GN=RPL18 PE=1 SV=1	**4,916798799**
O00560	Syntenin-1 OS=Homo sapiens OX=9606 GN=SDCBP PE=1 SV=1	**4,81858985**
O00299	Chloride intracellular channel protein 1 OS=Homo sapiens OX=9606 GN=CLIC1 PE=1 SV=4	**4,805358413**
Q13162	Peroxiredoxin-4 OS=Homo sapiens OX=9606 GN=PRDX4 PE=1 SV=1	**4,799715531**
P30044	Peroxiredoxin-5, mitochondrial OS=Homo sapiens OX=9606 GN=PRDX5 PE=1 SV=4	**4,699484053**
R4GNH3	26S proteasome regulatory subunit 6A OS=Homo sapiens OX=9606 GN=PSMC3 PE=1 SV=1	**4,624167504**
P61978	Heterogeneous nuclear ribonucleoprotein K OS=Homo sapiens OX=9606 GN=HNRNPK PE=1 SV=1	**4,609714479**
Q14764	Major vault protein OS=Homo sapiens OX=9606 GN=MVP PE=1 SV=4	**4,595738935**
A0A1W2PRS1	Lysosome membrane protein 2 (Fragment) OS=Homo sapiens OX=9606 GN=SCARB2 PE=1 SV=1	**4,561468529**
A0A6Q8PH20	Calpain inhibitor OS=Homo sapiens OX=9606 GN=CAST PE=1 SV=1	**4,548952151**
P14866	Heterogeneous nuclear ribonucleoprotein L OS=Homo sapiens OX=9606 GN=HNRNPL PE=1 SV=2	**4,520588047**

P27695	DNA-(apurinic or apyrimidinic site) endonuclease OS=Homo sapiens OX=9606 GN=APEX1 PE=1 SV=2	**4,509195591**
Q15293	Reticulocalbin-1 OS=Homo sapiens OX=9606 GN=RCN1 PE=1 SV=1	**4,495397964**
P30084	Enoyl-CoA hydratase, mitochondrial OS=Homo sapiens OX=9606 GN=ECHS1 PE=1 SV=4	**4,471998742**
P02751	Fibronectin OS=Homo sapiens OX=9606 GN=FN1 PE=1 SV=5	**4,445724392**
P62249	40S ribosomal protein S16 OS=Homo sapiens OX=9606 GN=RPS16 PE=1 SV=2	**4,438830105**
E9PHZ5	Cathepsin B OS=Homo sapiens OX=9606 GN=CTSB PE=1 SV=9	**4,406458013**
P28070	Proteasome subunit beta type-4 OS=Homo sapiens OX=9606 GN=PSMB4 PE=1 SV=4	**4,33702429**
Q02952	A-kinase anchor protein 12 OS=Homo sapiens OX=9606 GN=AKAP12 PE=1 SV=4	**4,19785046**
Q13509	Tubulin beta-3 chain OS=Homo sapiens OX=9606 GN=TUBB3 PE=1 SV=2	**4,191226686**
G3V5Z7	Proteasome subunit alpha type OS=Homo sapiens OX=9606 GN=PSMA6 PE=1 SV=1	**4,084267734**
Q13838	Spliceosome RNA helicase DDX39B OS=Homo sapiens OX=9606 GN=DDX39B PE=1 SV=1	**3,958147049**
P62906	60S ribosomal protein L10a OS=Homo sapiens OX=9606 GN=RPL10A PE=1 SV=2	**3,925451781**
A8MXP9	Matrin-3 OS=Homo sapiens OX=9606 GN=MATR3 PE=1 SV=1	**3,892188767**
P13797	Plastin-3 OS=Homo sapiens OX=9606 GN=PLS3 PE=1 SV=4	**3,795134959**
O14907	Tax1-binding protein 3 OS=Homo sapiens OX=9606 GN=TAX1BP3 PE=1 SV=2	**3,782871126**

P08238	Heat shock protein HSP 90-beta OS=Homo sapiens OX=9606 GN=HSP90AB1 PE=1 SV=4	**3,758169562**
P54577	Tyrosine--tRNA ligase, cytoplasmic OS=Homo sapiens OX=9606 GN=YARS1 PE=1 SV=4	**3,712588515**
P0DME0	Protein SETSIP OS=Homo sapiens OX=9606 GN=SETSIP PE=1 SV=1	**3,708109675**
P62136	Serine/threonine-protein phosphatase PP1-alpha catalytic subunit OS=Homo sapiens OX=9606 GN=PPP1CA PE=1 SV=1	**3,707229507**
P50281	Matrix metalloproteinase-14 OS=Homo sapiens OX=9606 GN=MMP14 PE=1 SV=3	**3,696755146**
E9PFW3	AP-2 complex subunit mu OS=Homo sapiens OX=9606 GN=AP2M1 PE=1 SV=1	**3,695506538**
P34932	Heat shock 70 kDa protein 4 OS=Homo sapiens OX=9606 GN=HSPA4 PE=1 SV=4	**3,678239465**
Q562R1	Beta-actin-like protein 2 OS=Homo sapiens OX=9606 GN=ACTBL2 PE=1 SV=2	**3,62078221**
Q02818	Nucleobindin-1 OS=Homo sapiens OX=9606 GN=NUCB1 PE=1 SV=4	**3,590858952**
H0Y4R1	Inosine-5'-monophosphate dehydrogenase OS=Homo sapiens OX=9606 GN=IMPDH2 PE=1 SV=2	**3,582975989**
Q16643	Drebrin OS=Homo sapiens OX=9606 GN=DBN1 PE=1 SV=4	**3,572533135**
P35998	26S proteasome regulatory subunit 7 OS=Homo sapiens OX=9606 GN=PSMC2 PE=1 SV=3	**3,551510437**
Q9NR45	Sialic acid synthase OS=Homo sapiens OX=9606 GN=NANS PE=1 SV=2	**3,548368244**
H0YMV8	40S ribosomal protein S27 OS=Homo sapiens OX=9606 GN=RPS27L PE=1 SV=1	**3,535003222**

Q9Y5M8	Signal recognition particle receptor subunit beta OS=Homo sapiens OX=9606 GN=SRPRB PE=1 SV=3	**3,499115171**
O43852	Calumenin OS=Homo sapiens OX=9606 GN=CALU PE=1 SV=2	**3,496260783**
Q15907	Ras-related protein Rab-11B OS=Homo sapiens OX=9606 GN=RAB11B PE=1 SV=4	**3,481393836**
A0A7I2V3S3	Eukaryotic translation initiation factor 3 subunit E OS=Homo sapiens OX=9606 GN=EIF3E PE=1 SV=1	**3,438327814**
Q6NZI2	Caveolae-associated protein 1 OS=Homo sapiens OX=9606 GN=CAVIN1 PE=1 SV=1	**3,435199996**
A0A0U1RRH7	Histone H2A OS=Homo sapiens OX=9606 PE=3 SV=1	**3,418051857**
P07737	Profilin-1 OS=Homo sapiens OX=9606 GN=PFN1 PE=1 SV=2	**3,408448106**
P26640	Valine--tRNA ligase OS=Homo sapiens OX=9606 GN=VARS1 PE=1 SV=4	**3,393024783**
P37837	Transaldolase OS=Homo sapiens OX=9606 GN=TALDO1 PE=1 SV=2	**3,371691694**
P00387	NADH-cytochrome b5 reductase 3 OS=Homo sapiens OX=9606 GN=CYB5R3 PE=1 SV=3	**3,364453175**
O15212	Prefoldin subunit 6 OS=Homo sapiens OX=9606 GN=PFDN6 PE=1 SV=1	**3,361684024**
O60493	Sorting nexin-3 OS=Homo sapiens OX=9606 GN=SNX3 PE=1 SV=3	**3,325886486**
P05141	ADP/ATP translocase 2 OS=Homo sapiens OX=9606 GN=SLC25A5 PE=1 SV=7	**3,312284416**
P04181	Ornithine aminotransferase, mitochondrial OS=Homo sapiens OX=9606 GN=OAT PE=1 SV=1	**3,285262879**
Q969H8	Myeloid-derived growth factor OS=Homo sapiens OX=9606 GN=MYDGF PE=1 SV=1	**3,282663266**

B0YIW6	Coatomer subunit delta OS=Homo sapiens OX=9606 GN=ARCN1 PE=1 SV=1	**3,279735779**
P60842	Eukaryotic initiation factor 4A-I OS=Homo sapiens OX=9606 GN=EIF4A1 PE=1 SV=1	**3,266091035**
G8JLB6	Heterogeneous nuclear ribonucleoprotein H OS=Homo sapiens OX=9606 GN=HNRNPH1 PE=1 SV=1	**3,255565649**
Q14103	Heterogeneous nuclear ribonucleoprotein D0 OS=Homo sapiens OX=9606 GN=HNRNPD PE=1 SV=1	**3,225382705**
A0A6Q8PH84	Ras-related protein Rab-7a OS=Homo sapiens OX=9606 GN=RAB7A PE=1 SV=1	**3,154866727**
P09429	High mobility group protein B1 OS=Homo sapiens OX=9606 GN=HMGB1 PE=1 SV=3	**3,099066041**
O00231	26S proteasome non-ATPase regulatory subunit 11 OS=Homo sapiens OX=9606 GN=PSMD11 PE=1 SV=3	**3,071841885**
P26641	Elongation factor 1-gamma OS=Homo sapiens OX=9606 GN=EEF1G PE=1 SV=3	**3,070208276**
O95336	6-phosphogluconolactonase OS=Homo sapiens OX=9606 GN=PGLS PE=1 SV=2	**3,040239148**
O15143	Actin-related protein 2/3 complex subunit 1B OS=Homo sapiens OX=9606 GN=ARPC1B PE=1 SV=3	**3,039181598**
P11216	Glycogen phosphorylase, brain form OS=Homo sapiens OX=9606 GN=PYGB PE=1 SV=5	**3,030138597**
H7BY16	Nucleolin OS=Homo sapiens OX=9606 GN=NCL PE=1 SV=9	**3,024947134**
P36957	Dihydrolipoyllysine-residue succinyltransferase component of 2-oxoglutarate dehydrogenase complex, mitochondrial OS=Homo sapiens OX=9606 GN=DLST PE=1 SV=4	**2,987782278**

P00505	Aspartate aminotransferase, mitochondrial OS=Homo sapiens OX=9606 GN=GOT2 PE=1 SV=3	**2,986429629**
G5E9Q6	Profilin OS=Homo sapiens OX=9606 GN=PFN2 PE=1 SV=1	**2,98584516**
P25788	Proteasome subunit alpha type-3 OS=Homo sapiens OX=9606 GN=PSMA3 PE=1 SV=2	**2,942195956**
O75874	Isocitrate dehydrogenase [NADP] cytoplasmic OS=Homo sapiens OX=9606 GN=IDH1 PE=1 SV=2	**2,923900055**
Q07065	Cytoskeleton-associated protein 4 OS=Homo sapiens OX=9606 GN=CKAP4 PE=1 SV=2	**2,914406499**
P08133	Annexin A6 OS=Homo sapiens OX=9606 GN=ANXA6 PE=1 SV=3	**2,904890355**
Q13492	Phosphatidylinositol-binding clathrin assembly protein OS=Homo sapiens OX=9606 GN=PICALM PE=1 SV=2	**2,903795116**
P49368	T-complex protein 1 subunit gamma OS=Homo sapiens OX=9606 GN=CCT3 PE=1 SV=4	**2,874585223**
P55084	Trifunctional enzyme subunit beta, mitochondrial OS=Homo sapiens OX=9606 GN=HADHB PE=1 SV=3	**2,850735476**
A0A1B0GW77	Aldehyde dehydrogenase (NAD(+)) OS=Homo sapiens OX=9606 GN=ALDH7A1 PE=1 SV=1	**2,827666742**
A0A024R4E5	High density lipoprotein binding protein (Vigilin), isoform CRA_a OS=Homo sapiens OX=9606 GN=HDLBP PE=1 SV=1	**2,822925058**
O75083	WD repeat-containing protein 1 OS=Homo sapiens OX=9606 GN=WDR1 PE=1 SV=4	**2,814489201**
P09211	Glutathione S-transferase P OS=Homo sapiens OX=9606 GN=GSTP1 PE=1 SV=2	**2,778181944**
P68104	Elongation factor 1-alpha 1 OS=Homo sapiens OX=9606 GN=EEF1A1 PE=1 SV=1	**2,777493836**

M0QXB4	Coatomer subunit epsilon OS=Homo sapiens OX=9606 GN=COPE PE=1 SV=1	**2,772837484**
P53597	Succinate--CoA ligase [ADP/GDP-forming] subunit alpha, mitochondrial OS=Homo sapiens OX=9606 GN=SUCLG1 PE=1 SV=4	**2,766144108**
A0A7P0TA71	Protein disulfide-isomerase OS=Homo sapiens OX=9606 GN=P4HB PE=1 SV=1	**2,758093297**
P52306	Rap1 GTPase-GDP dissociation stimulator 1 OS=Homo sapiens OX=9606 GN=RAP1GDS1 PE=1 SV=3	**2,757442269**
A0A7P0T9C4	Cytoplasmic dynein 1 heavy chain 1 OS=Homo sapiens OX=9606 GN=DYNC1H1 PE=1 SV=1	**2,720398409**
P61160	Actin-related protein 2 OS=Homo sapiens OX=9606 GN=ACTR2 PE=1 SV=1	**2,713707907**
O00425	Insulin-like growth factor 2 mRNA-binding protein 3 OS=Homo sapiens OX=9606 GN=IGF2BP3 PE=1 SV=2	**2,525248529**
U3KQK0	Histone H2B OS=Homo sapiens OX=9606 GN=H2BC15 PE=1 SV=1	**2,515678376**
P51148	Ras-related protein Rab-5C OS=Homo sapiens OX=9606 GN=RAB5C PE=1 SV=2	**2,49717743**
Q02790	Peptidyl-prolyl cis-trans isomerase FKBP4 OS=Homo sapiens OX=9606 GN=FKBP4 PE=1 SV=3	**2,481224111**
P63000	Ras-related C3 botulinum toxin substrate 1 OS=Homo sapiens OX=9606 GN=RAC1 PE=1 SV=1	**2,476070736**
P22392	Nucleoside diphosphate kinase B OS=Homo sapiens OX=9606 GN=NME2 PE=1 SV=1	**2,428655142**
C9JH19	Cathepsin D OS=Homo sapiens OX=9606 GN=CTSD PE=1 SV=2	**2,406855812**
P52907	F-actin-capping protein subunit alpha-1 OS=Homo sapiens OX=9606 GN=CAPZA1 PE=1 SV=3	**2,400534376**

Q92598	Heat shock protein 105 kDa OS=Homo sapiens OX=9606 GN=HSPH1 PE=1 SV=1	**2,400442247**
H0YMW4	Annexin OS=Homo sapiens OX=9606 GN=ANXA2 PE=1 SV=2	**2,392792487**
Q14240	Eukaryotic initiation factor 4A-II OS=Homo sapiens OX=9606 GN=EIF4A2 PE=1 SV=2	**2,388903818**
P67936	Tropomyosin alpha-4 chain OS=Homo sapiens OX=9606 GN=TPM4 PE=1 SV=3	**2,387421589**
P35221	Catenin alpha-1 OS=Homo sapiens OX=9606 GN=CTNNA1 PE=1 SV=1	**2,384127015**
P11142	Heat shock cognate 71 kDa protein OS=Homo sapiens OX=9606 GN=HSPA8 PE=1 SV=1	**2,376739839**
A0A494C039	Hypoxia up-regulated protein 1 OS=Homo sapiens OX=9606 GN=HYOU1 PE=1 SV=1	**2,360862088**
Q9HDC9	Adipocyte plasma membrane-associated protein OS=Homo sapiens OX=9606 GN=APMAP PE=1 SV=2	**2,333617913**
A0A0S2Z4G6	Tropomyosin 1 (Alpha), isoform CRA_o (Fragment) OS=Homo sapiens OX=9606 GN=TPM1 PE=1 SV=1	**2,310669031**
Q99832	T-complex protein 1 subunit eta OS=Homo sapiens OX=9606 GN=CCT7 PE=1 SV=2	**2,305197996**
P52565	Rho GDP-dissociation inhibitor 1 OS=Homo sapiens OX=9606 GN=ARHGDIA PE=1 SV=3	**2,293938653**
P07900	Heat shock protein HSP 90-alpha OS=Homo sapiens OX=9606 GN=HSP90AA1 PE=1 SV=5	**2,266838755**
Q9Y617	Phosphoserine aminotransferase OS=Homo sapiens OX=9606 GN=PSAT1 PE=1 SV=2	**2,251181617**
Q9UKX5	Integrin alpha-11 OS=Homo sapiens OX=9606 GN=ITGA11 PE=1 SV=2	**2,243128179**

P26639	Threonine--tRNA ligase 1, cytoplasmic OS=Homo sapiens OX=9606 GN=TARS1 PE=1 SV=3	**2,231283922**
P04899	Guanine nucleotide-binding protein G(i) subunit alpha-2 OS=Homo sapiens OX=9606 GN=GNAI2 PE=1 SV=3	**2,214177568**
Q02543	60S ribosomal protein L18a OS=Homo sapiens OX=9606 GN=RPL18A PE=1 SV=2	**2,199757435**
A0A087WWU8	Tropomyosin alpha-3 chain OS=Homo sapiens OX=9606 GN=TPM3 PE=1 SV=1	**2,194542913**
O15460	Prolyl 4-hydroxylase subunit alpha-2 OS=Homo sapiens OX=9606 GN=P4HA2 PE=1 SV=1	**2,188269474**
P40227	T-complex protein 1 subunit zeta OS=Homo sapiens OX=9606 GN=CCT6A PE=1 SV=3	**2,125731557**
P54886	Delta-1-pyrroline-5-carboxylate synthase OS=Homo sapiens OX=9606 GN=ALDH18A1 PE=1 SV=2	**2,104008852**
O75915	PRA1 family protein 3 OS=Homo sapiens OX=9606 GN=ARL6IP5 PE=1 SV=1	**2,103757595**
P10768	S-formylglutathione hydrolase OS=Homo sapiens OX=9606 GN=ESD PE=1 SV=2	**2,097326477**
A0A087WVQ6	Clathrin heavy chain OS=Homo sapiens OX=9606 GN=CLTC PE=1 SV=1	**2,097025325**
Q15366	Poly(rC)-binding protein 2 OS=Homo sapiens OX=9606 GN=PCBP2 PE=1 SV=1	**2,082673114**
P61604	10 kDa heat shock protein, mitochondrial OS=Homo sapiens OX=9606 GN=HSPE1 PE=1 SV=2	**2,059715652**
P26038	Moesin OS=Homo sapiens OX=9606 GN=MSN PE=1 SV=3	**2,059468995**
P38117	Electron transfer flavoprotein subunit beta OS=Homo sapiens OX=9606 GN=ETFB PE=1 SV=3	**2,051571264**

P07996	Thrombospondin-1 OS=Homo sapiens OX=9606 GN=THBS1 PE=1 SV=2	**2,022635926**
Q01813	ATP-dependent 6-phosphofructokinase, platelet type OS=Homo sapiens OX=9606 GN=PFKP PE=1 SV=2	**2,022603259**
P25789	Proteasome subunit alpha type-4 OS=Homo sapiens OX=9606 GN=PSMA4 PE=1 SV=1	**2,020988604**
P24752	Acetyl-CoA acetyltransferase, mitochondrial OS=Homo sapiens OX=9606 GN=ACAT1 PE=1 SV=1	**0,500876342**
P14618	Pyruvate kinase PKM OS=Homo sapiens OX=9606 GN=PKM PE=1 SV=4	**0,498117541**
P62753	40S ribosomal protein S6 OS=Homo sapiens OX=9606 GN=RPS6 PE=1 SV=1	**0,482570655**
Q96P70	Importin-9 OS=Homo sapiens OX=9606 GN=IPO9 PE=1 SV=3	**0,475487175**
P04843	Dolichyl-diphosphooligosaccharide--protein glycosyltransferase subunit 1 OS=Homo sapiens OX=9606 GN=RPN1 PE=1 SV=1	**0,47437655**
P05783	Keratin, type I cytoskeletal 18 OS=Homo sapiens OX=9606 GN=KRT18 PE=1 SV=2	**0,472419797**
P11766	Alcohol dehydrogenase class-3 OS=Homo sapiens OX=9606 GN=ADH5 PE=1 SV=4	**0,471905591**
P07437	Tubulin beta chain OS=Homo sapiens OX=9606 GN=TUBB PE=1 SV=2	**0,460699108**
Q99536	Synaptic vesicle membrane protein VAT-1 homolog OS=Homo sapiens OX=9606 GN=VAT1 PE=1 SV=2	**0,460214708**
Q14247	Src substrate cortactin OS=Homo sapiens OX=9606 GN=CTTN PE=1 SV=2	**0,459031277**
A0A087X020	Ribosome maturation protein SBDS OS=Homo sapiens OX=9606 GN=SBDS PE=1 SV=1	**0,458015477**

A0A3B3ITT5	60S ribosomal protein L29 OS=Homo sapiens OX=9606 GN=RPL29 PE=1 SV=1	**0,446761271**
Q9H299	SH3 domain-binding glutamic acid-rich-like protein 3 OS=Homo sapiens OX=9606 GN=SH3BGRL3 PE=1 SV=1	**0,44420592**
O43854	EGF-like repeat and discoidin I-like domain-containing protein 3 OS=Homo sapiens OX=9606 GN=EDIL3 PE=1 SV=1	**0,443641175**
P00367	Glutamate dehydrogenase 1, mitochondrial OS=Homo sapiens OX=9606 GN=GLUD1 PE=1 SV=2	**0,436232636**
A0A7I2YQC0	Nucleophosmin OS=Homo sapiens OX=9606 GN=NPM1 PE=1 SV=1	**0,427754317**
O43175	D-3-phosphoglycerate dehydrogenase OS=Homo sapiens OX=9606 GN=PHGDH PE=1 SV=4	**0,422311733**
H3BNC9	40S ribosomal protein S17 OS=Homo sapiens OX=9606 PE=3 SV=2	**0,414356598**
P18669	Phosphoglycerate mutase 1 OS=Homo sapiens OX=9606 GN=PGAM1 PE=1 SV=2	**0,412970625**
O00764	Pyridoxal kinase OS=Homo sapiens OX=9606 GN=PDXK PE=1 SV=1	**0,388267823**
A0A2R8Y5A3	Catenin beta-1 OS=Homo sapiens OX=9606 GN=CTNNB1 PE=1 SV=1	**0,379649212**
P35268	60S ribosomal protein L22 OS=Homo sapiens OX=9606 GN=RPL22 PE=1 SV=2	**0,37581357**
E9PL57	NEDD8-MDP1 readthrough (Fragment) OS=Homo sapiens OX=9606 GN=NEDD8-MDP1 PE=4 SV=1	**0,35862085**
Q00325	Phosphate carrier protein, mitochondrial OS=Homo sapiens OX=9606 GN=SLC25A3 PE=1 SV=2	**0,349692718**
M0R0C6	Far upstream element-binding protein 2 OS=Homo sapiens OX=9606 GN=KHSRP PE=1 SV=2	**0,325766382**

P61254	60S ribosomal protein L26 OS=Homo sapiens OX=9606 GN=RPL26 PE=1 SV=1	**0,32302358**
Q7KZF4	Staphylococcal nuclease domain-containing protein 1 OS=Homo sapiens OX=9606 GN=SND1 PE=1 SV=1	**0,322748872**
Q9NZL9	Methionine adenosyltransferase 2 subunit beta OS=Homo sapiens OX=9606 GN=MAT2B PE=1 SV=1	**0,316934778**
P62280	40S ribosomal protein S11 OS=Homo sapiens OX=9606 GN=RPS11 PE=1 SV=3	**0,303588936**
Q9H0D6	5'-3' exoribonuclease 2 OS=Homo sapiens OX=9606 GN=XRN2 PE=1 SV=1	**0,302940574**
Q8WWM7	Ataxin-2-like protein OS=Homo sapiens OX=9606 GN=ATXN2L PE=1 SV=2	**0,297305678**
P68371	Tubulin beta-4B chain OS=Homo sapiens OX=9606 GN=TUBB4B PE=1 SV=1	**0,28838821**
P28066	Proteasome subunit alpha type-5 OS=Homo sapiens OX=9606 GN=PSMA5 PE=1 SV=3	**0,28759648**
P36578	60S ribosomal protein L4 OS=Homo sapiens OX=9606 GN=RPL4 PE=1 SV=5	**0,282586255**
Q07812	Apoptosis regulator BAX OS=Homo sapiens OX=9606 GN=BAX PE=1 SV=1	**0,282477162**
Q99961	Endophilin-A2 OS=Homo sapiens OX=9606 GN=SH3GL1 PE=1 SV=1	**0,277130769**
A8MUS3	60S ribosomal protein L23a OS=Homo sapiens OX=9606 GN=RPL23A PE=1 SV=1	**0,242493248**
C9JIF9	Acyl-peptide hydrolase OS=Homo sapiens OX=9606 GN=APEH PE=1 SV=1	**0,233774777**
O75396	Vesicle-trafficking protein SEC22b OS=Homo sapiens OX=9606 GN=SEC22B PE=1 SV=5	**0,229601968**

Q15942	Zyxin OS=Homo sapiens OX=9606 GN=ZYX PE=1 SV=1	**0,227892661**
P62263	40S ribosomal protein S14 OS=Homo sapiens OX=9606 GN=RPS14 PE=1 SV=3	**0,226163456**
Q02878	60S ribosomal protein L6 OS=Homo sapiens OX=9606 GN=RPL6 PE=1 SV=3	**0,223660411**
Q14195	Dihydropyrimidinase-related protein 3 OS=Homo sapiens OX=9606 GN=DPYSL3 PE=1 SV=1	**0,217560981**
P39656	Dolichyl-diphosphooligosaccharide--protein glycosyltransferase 48 kDa subunit OS=Homo sapiens OX=9606 GN=DDOST PE=1 SV=4	**0,211695144**
P62829	60S ribosomal protein L23 OS=Homo sapiens OX=9606 GN=RPL23 PE=1 SV=1	**0,209821795**
Q13409	Cytoplasmic dynein 1 intermediate chain 2 OS=Homo sapiens OX=9606 GN=DYNC1I2 PE=1 SV=3	**0,208754578**
O14773	Tripeptidyl-peptidase 1 OS=Homo sapiens OX=9606 GN=TPP1 PE=1 SV=2	**0,19101428**
O00151	PDZ and LIM domain protein 1 OS=Homo sapiens OX=9606 GN=PDLIM1 PE=1 SV=4	**0,190574298**
Q96C90	Protein phosphatase 1 regulatory subunit 14B OS=Homo sapiens OX=9606 GN=PPP1R14B PE=1 SV=3	**0,187944781**
P61313	60S ribosomal protein L15 OS=Homo sapiens OX=9606 GN=RPL15 PE=1 SV=2	**0,174407408**
O00469	Procollagen-lysine,2-oxoglutarate 5-dioxygenase 2 OS=Homo sapiens OX=9606 GN=PLOD2 PE=1 SV=2	**0,173198472**
P54578	Ubiquitin carboxyl-terminal hydrolase 14 OS=Homo sapiens OX=9606 GN=USP14 PE=1 SV=3	**0,168648115**
E9PR30	40S ribosomal protein S30 OS=Homo sapiens OX=9606 GN=FAU PE=1 SV=1	**0,166753719**

P08670	Vimentin OS=Homo sapiens OX=9606 GN=VIM PE=1 SV=4	**0,163922033**
Q9UBQ7	Glyoxylate reductase/hydroxypyruvate reductase OS=Homo sapiens OX=9606 GN=GRHPR PE=1 SV=1	**0,161730381**
P02768	Albumin OS=Homo sapiens OX=9606 GN=ALB PE=1 SV=2	**0,133977971**
P62266	40S ribosomal protein S23 OS=Homo sapiens OX=9606 GN=RPS23 PE=1 SV=3	**0,133312701**
Q9BUF5	Tubulin beta-6 chain OS=Homo sapiens OX=9606 GN=TUBB6 PE=1 SV=1	**0,106123223**
Q9H2U2	Inorganic pyrophosphatase 2, mitochondrial OS=Homo sapiens OX=9606 GN=PPA2 PE=1 SV=2	**0,105219519**
Q9Y570	Protein phosphatase methylesterase 1 OS=Homo sapiens OX=9606 GN=PPME1 PE=1 SV=3	**0,090764981**
E9PIE3	Caveolae-associated protein 3 OS=Homo sapiens OX=9606 GN=CAVIN3 PE=1 SV=1	**0,089261133**
O00154	Cytosolic acyl coenzyme A thioester hydrolase OS=Homo sapiens OX=9606 GN=ACOT7 PE=1 SV=3	**0,086359611**
A0A2R8Y623	40S ribosomal protein S7 (Fragment) OS=Homo sapiens OX=9606 GN=RPS7 PE=1 SV=1	**0,070383847**
P62917	60S ribosomal protein L8 OS=Homo sapiens OX=9606 GN=RPL8 PE=1 SV=2	**0,059408271**
P08134	Rho-related GTP-binding protein RhoC OS=Homo sapiens OX=9606 GN=RHOC PE=1 SV=1	**0,041420994**
Q9H1E3	Nuclear ubiquitous casein and cyclin-dependent kinase substrate 1 OS=Homo sapiens OX=9606 GN=NUCKS1 PE=1 SV=1	**0,03925446**
Q16881	Thioredoxin reductase 1, cytoplasmic OS=Homo sapiens OX=9606 GN=TXNRD1 PE=1 SV=3	**0,036261452**

P35527	Keratin, type I cytoskeletal 9 OS=Homo sapiens OX=9606 GN=KRT9 PE=1 SV=3	**0,034641028**

CRISPR-Cas9 KO hESCs, Apelin KO, Aplnr KO and Elabela KO cells, were also differentiated with the MSC differentiation protocol to further investigate role of Aplnr signaling during MSC differentiation (Figure 3.45A) and morphological pictures were taken at day 3, day 5, day 8, day 10 and day 24 (Figure 3.45B). MSC surface markers, CD44, CD90, CD105 and CD166, were expressed more Wild Type derived cells compared to the KO derived cells and hematapoietic markers, CD31, CD34 and CD45, were not expressed in wild type and the other KO derived cells after day 24 (Figure 3.45C and 3.46). mRNA expression levels at day 24 also verified that Wild Type cells didn't express CD45 and slightly expressed CD31, quite less than the KO groups. CD44, CD105 and CD166 mRNA expression levels also higher the KO groups (Figure 3.45D). Cell viability and proliferation were significantly higher in Wild type derived MSCs, while Elabela KO derived cells showed quite low viability and proliferation compared to other groups (Figure 3.45E, 3.45F and 3.45G). Moreover, Wild Type derived MSCs were capable of osteogenic, adipogenic, chondrogenic, myogenic, endothelial, epithelial, odontogenic and neurogenic differentiation. Nonetheless, Apelin KO, Aplnr KO and Elabela KO derived cells had low level expression of MAP2, Col1, Col2, and AFABP, and were not able to express odontogenic, epithelial, endothelial and myogenic markers. Additionally, von Kossa, alizarin red, oil red O and alcian blue results indicated better osteogenic, adipogenic and chondrogenic differentiation potential of Wild type derived MSCs compared to the others (Figure 3.47, 3.48 and 3.49).

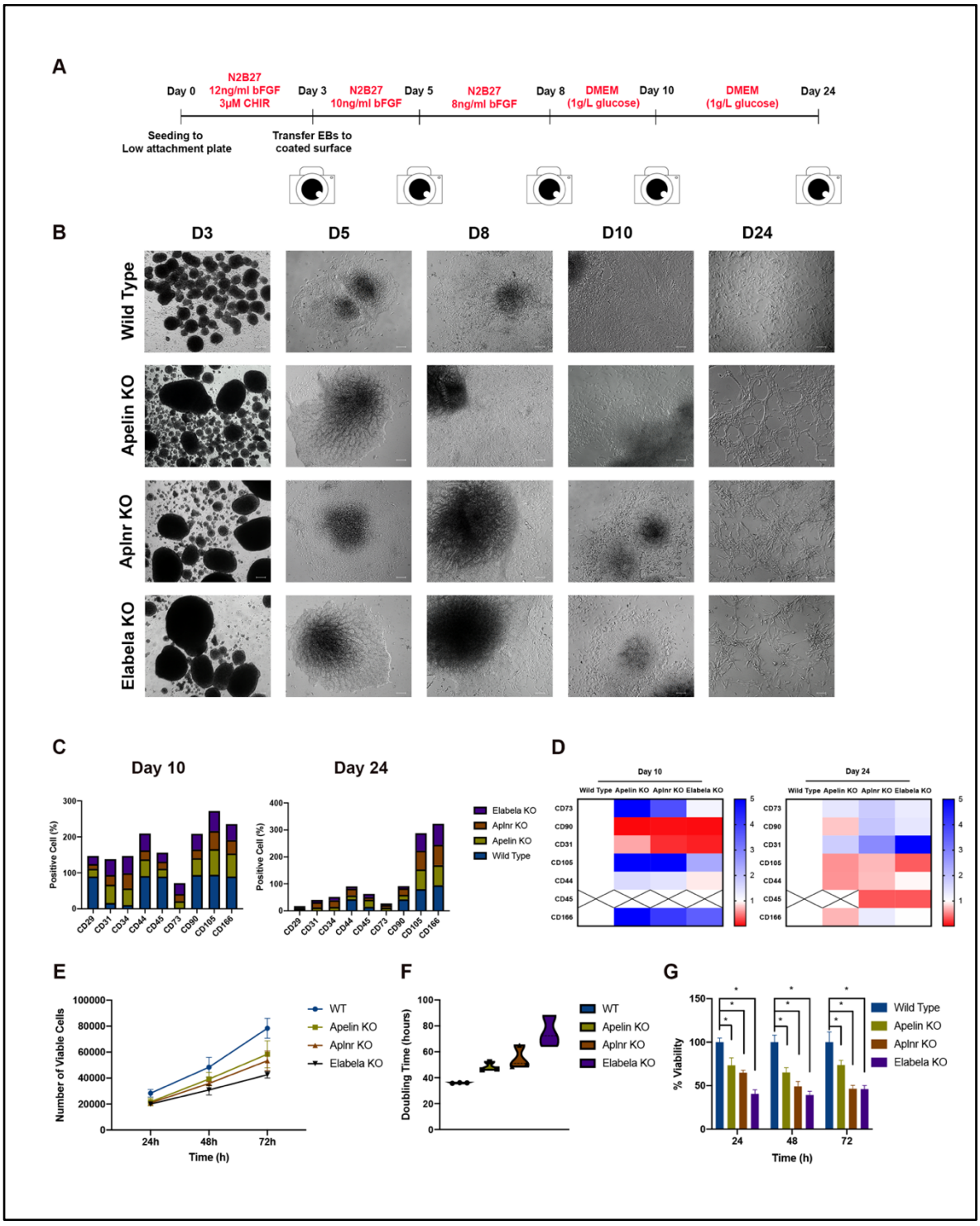


Figure 3.45. Knock Out of Aplnr Signaling Components Hinders MSC Differentiation from hESCs. A. The 24 days protocol for MSC differentiation from hESC. B. Morphological pictures taken at day 3, day 5, day 8, day 10 and day24 during MSC differentiation from Wild Type, Apelin KO, Aplnr KO and Elabela KO cells. C. MSC markers were detected with flow cytometry analysis and a graphic was drown showing the positive cells for the markers. D. Heatmap visualization of mRNA expression levels for

MSC markers at day 10 and day 24. E. Viable cells were counted with Trypan Blue staining and F. Cell duplication time was calculated for the differentiated cells. G. Cell viability was measured and represented with a bar graph for the differentiated cells. Scale bar: 200µm. *P<0.0001

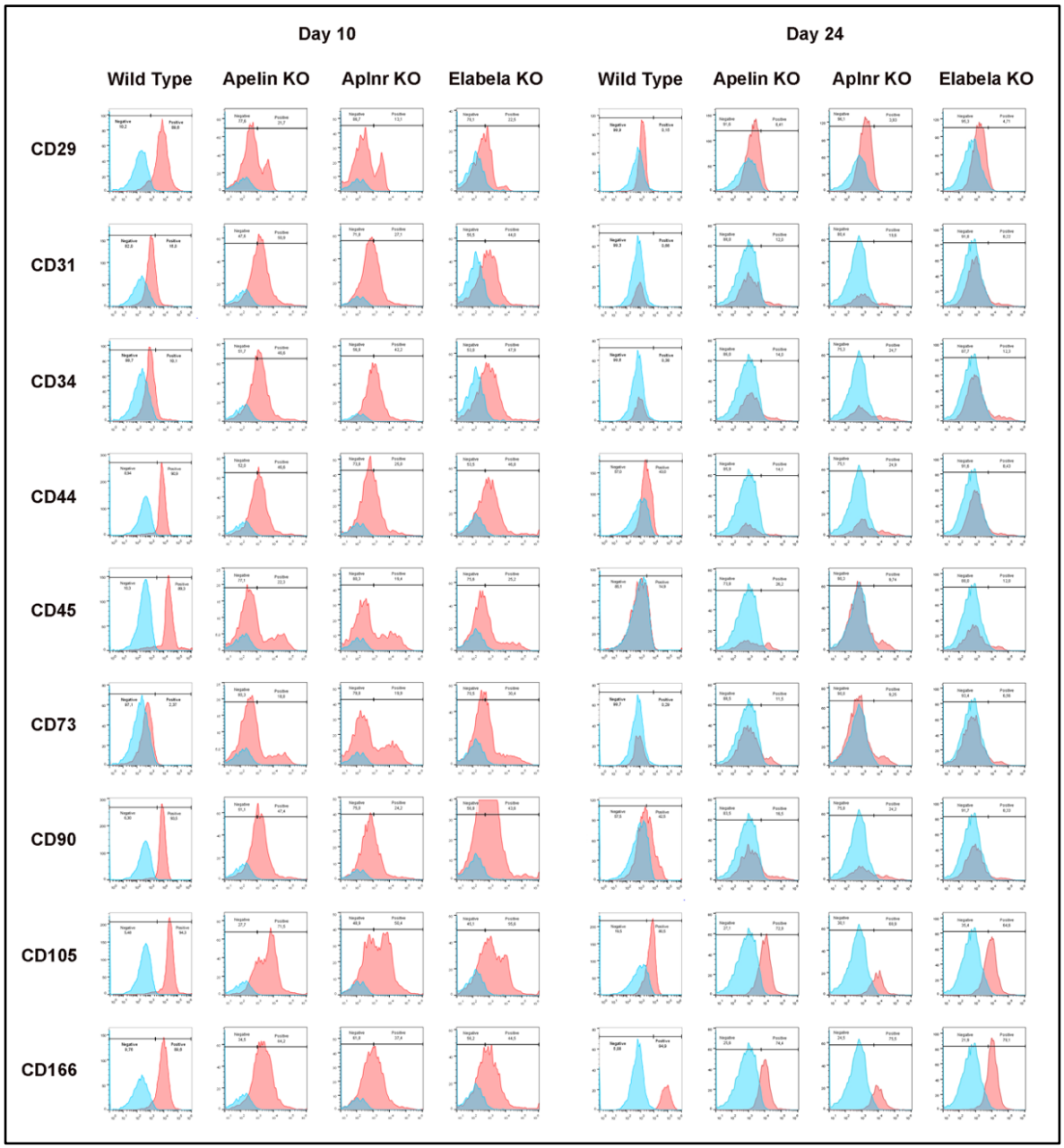


Figure 3.46. Characterization of hESC derived MSCs when Aplnr Signaling Pathway Components were Knocked Out. Flow cytometry analysis of mesenchymal stem cell marker expression and hematopoietic marker expression on hESC during MSC differentiation at day 10 and day 24. Wild Type, Apelin KO, Aplnr KO and Elabela KO cell groups were compared.

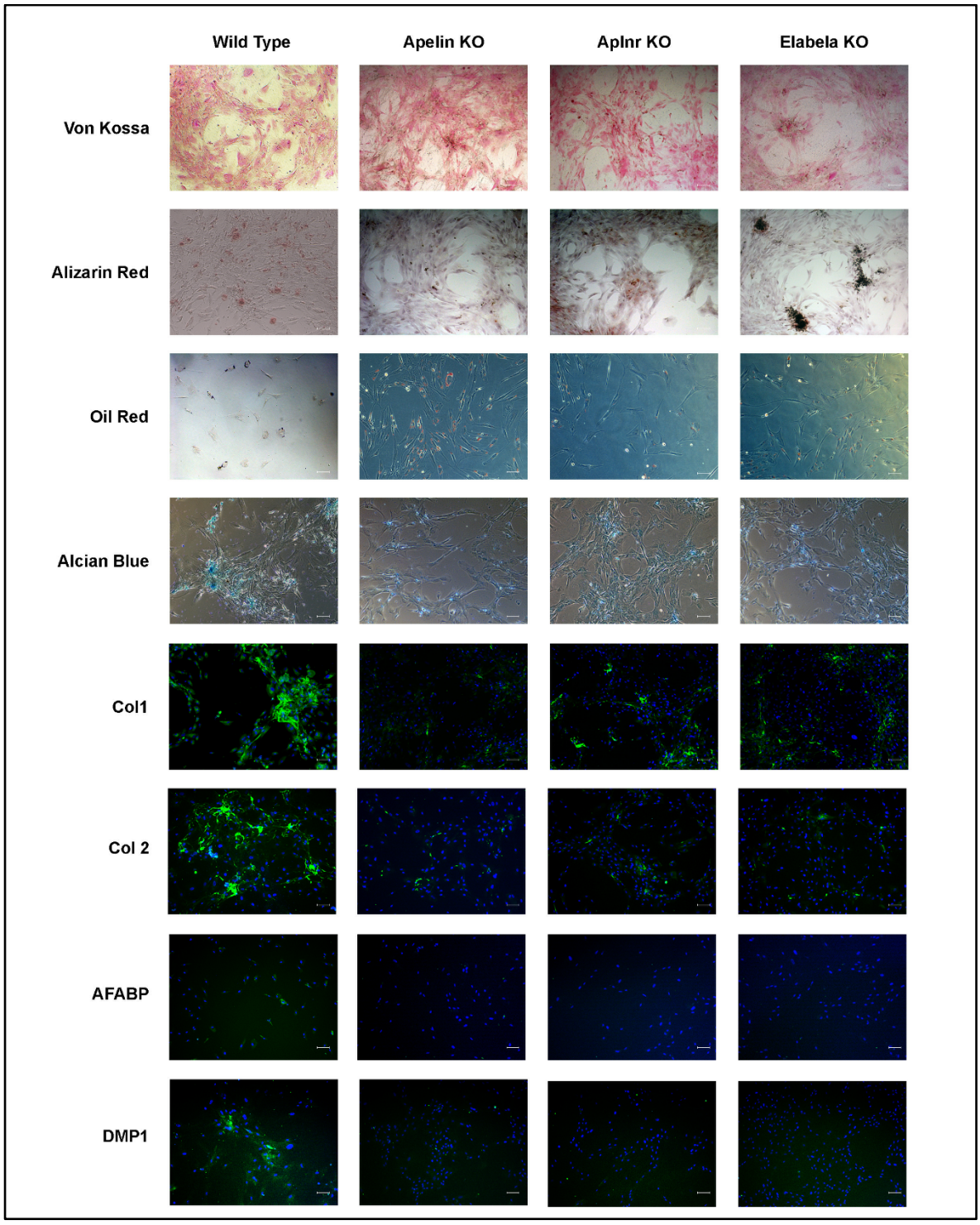


Figure 3.47. Differentiation of hESC derived MSCs into Ostegenic, Adipogenic, Chondrogenic and Odontogenic Cell Types when Aplnr Signaling Pathway Components were Knocked Out. Osteogenic differentiation was shown with von Kossa staining, alizarin red staining and Col1 immunostaining. Oil red O staining and AFABP immunostaining represented adipogenic differentiation. Chondrogenic differentiation was visualized with alcian blue staining and Col2 immunostaining. DMP1 immunostaining was shown to

visualize odontogenic differentiation. Scale Bar: 100µm.

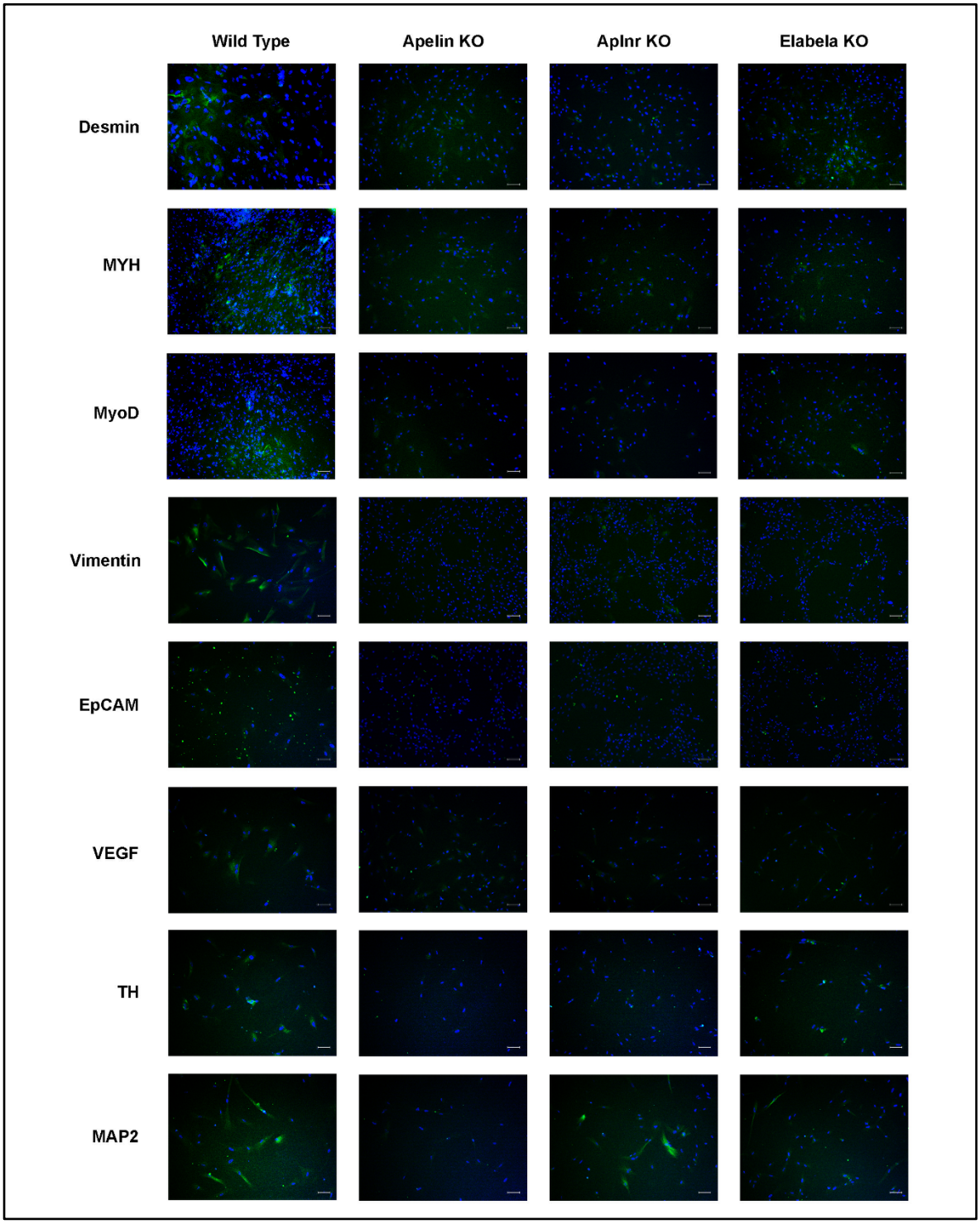


Figure 3.48. Differentiation of hESC derived MSCs into Epithelial, Endothelial, Myogenic and Neurogenic Cell Types when Aplnr Signaling Pathway Components were Knocked Out. Desmin, MyoD and MYH immunostainings were performed after myogenic differentiation. Neurogenic differentiation was shown by TH and MAP2 immunostainings.

Endothelial differentiation was visualized by VEGF immunostainings. Immunostainings for Vimentin and EpCAM was performed for epithelial differentiation. Scale Bar: 100µm.

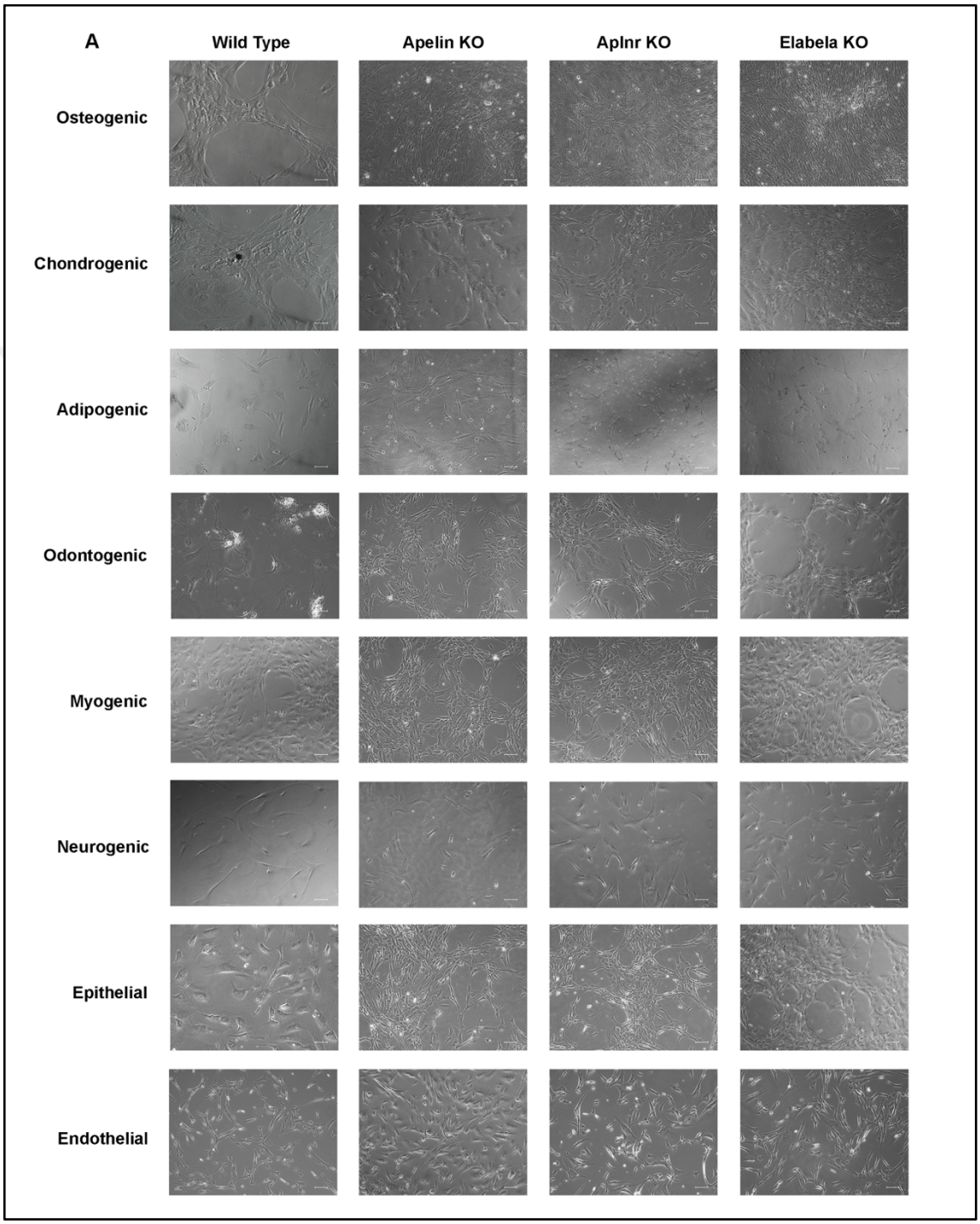


Figure 3.49. Morphology of Multiple Cell Type Differentiation from hESC derived MSCs when Aplnr Signaling Pathway Components were knocked out. MSCs, which were derived from Wild Type, Apelin KO, Aplnr KO and Elabela KO cells, were compared with each other in terms of multiple differentiation capacity. Cell morphology after osteogenic,

chondrogenic, adipogenic, odontogenic, myogenic, neurogenic, epithelial and endothelial differentiations were demonstrated. Scale Bar: 100µm.

hESCs after lentiviral infection of Apelin shRNA, Aplnr shRNA and control shRNA were differentiated according to MSC differentiation protocol to get a better understanding of the effect of Aplnr signaling during MSC differentiation (Figure 3.50A) and morphological pictures were taken at day 3, day 5, day 8, day 10 and day 24 (Figure 3.50B). Flow cytometry results didn't indicate any obvious difference at the surface markers of the groups, as MSCs markers and hematapoietic markers were expressed about the same percentage of the populations at day 10 and day 24 (Figure 3.50C and 3.51). According to gene expression level data at day 24, interestingly CD90 was expressed by shApelin and shAplnr groups higher than shControl and CD45 was not expressed in any group. Additionally, CD73 was expressed only in shControl (Figure 3.50D). However, cell viability and proliferation of the cells derived from shAplnr infected hESCs were significantly lower compared to control group (Figure 3.50E, 3.50F and 3.50G). Moreover, adipogenic, chondrogenic, myogenic, epithelial, odontogenic and neurogenic differentiation capacity of shApelin and shAplnr derived cells were very low compared to shControl derived cells (Figure 3.52 and 3.53). According to PCR results, shRNA transfected groups expressed E-cadherin less than MSC and Hacat after epithelial differentiation. V-cadherin expression level was also lower in shRNA groups compared to MSC and Huvec. Osteocalcin expression was downregulated at osteogenic differentiated shApelin and shAplnr groups compared to shControl and MSC groups. Aggrecan expression was lower in shAplnr cells compared shControl and MSCs after chondrogenic differentiation. Interestingly, Adiponectin expression level after adipogenic differentiation and B-tubulin expression level after neurogenic differentiation were higher in shApelin and shAplnr groups compared to shControl and MSCs after adipogenic differentiation. DSPP expression after odontogenic differentiation were enhanced in all shRNA treated cells whereas α-sma expression after myogenic differentiation was quite low in all shRNA treated cells compared to MSC (Figure 3.54). shControl MSC, shApelin MSC and shAplnr MSC were subjected to a further analysis with LC/MS protein profiling (Figure 3.55, Table 3.6). Close correlation between shControl and shApelin, with 0.91 correlation coefficient value, shControl and shAplnr, with 0.99 correlation coefficient value, were observed with correlation coefficient matrix, PCA, hierarchical cluster analysis, and heat map, (Figure 3.55A, Figure 3.55B and Figure 3.55C).

Distribution of protein quantification for significantly increased and decreased expressions with shRNA treatment were demonstrated on the histogram (Figure 3.55D). According to the gene ontology analysis, molecular functions, such as cytoskeletal motor activity, molecular transducer activity and translation regulator activity, increased in shApelin compared to shControl and cytoskeletal motor activity and molecular transducer activity increased in Aplnr MSCs compared to shControl MSCs (Figure 3.55E). Proteins related to biological processes, including growth, locomotion and reproduction were enhanced in shApelin MSC compared to shControl MSCs, while adhesion increased in shAplnr MSCs compared to shControl MSCs (Figure 3.55F). Furthermore, while proteins related to pathways in terms of hypoxia response via HIF activation, EGFR signaling, FAS signaling, FGF signaling, PDGFR signaling, TGF-beta signaling, VEGF signaling, Toll receptor signaling and Wnt signaling were enhanced in shApelin MSC compared to shControl MSC, DNA replication and p38 MAPK pathway related proteins decreased. Also, DNA replication, FAS signaling, Ras pathway and Toll receptor pathway related proteins were enhanced in shAplnr MSC compared to shControl MSCs (Figure 3.55G).

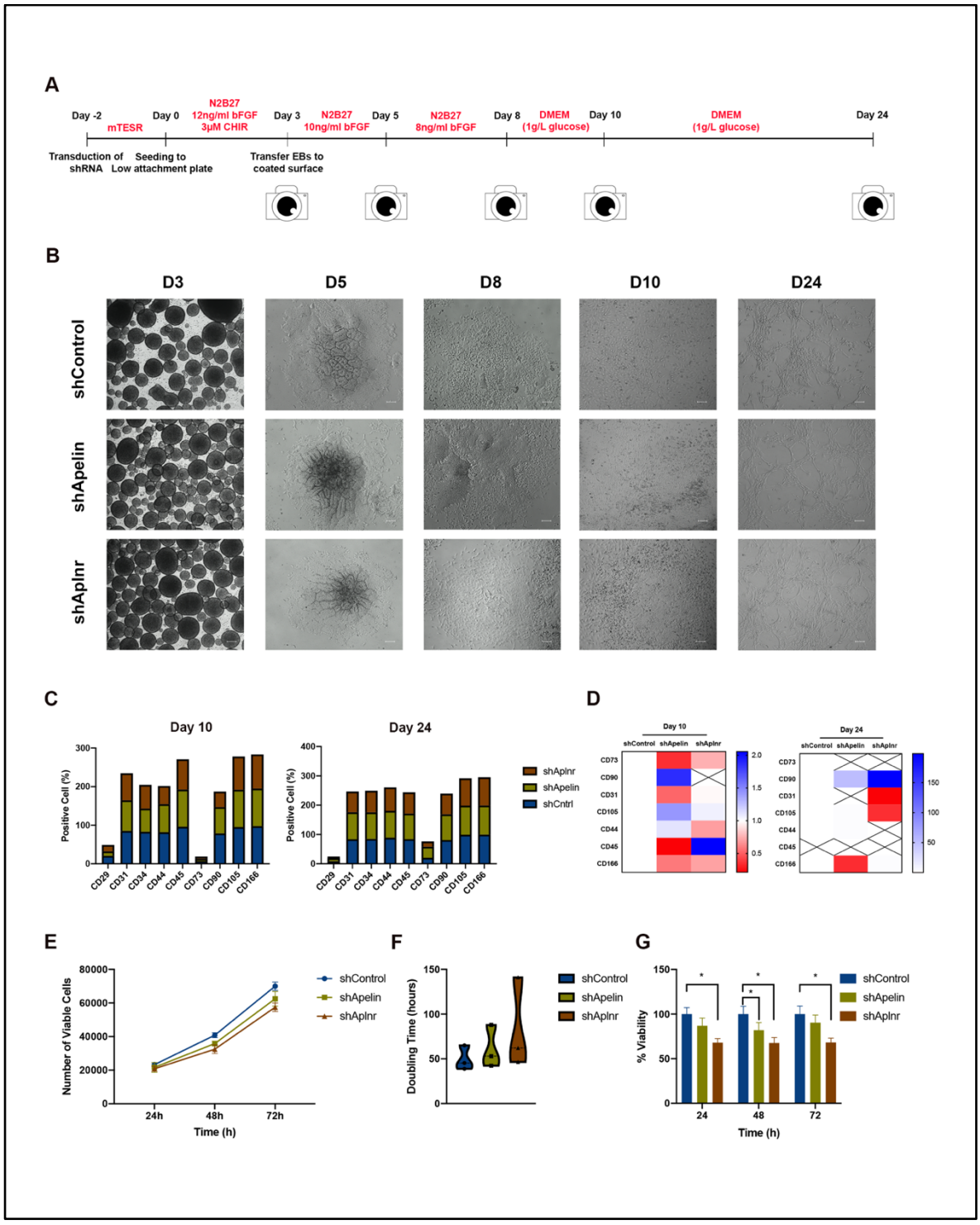


Figure 3.50. Knock Down of Aplnr Signaling Components by shRNA Hinders MSC Differentiation from hESCs. A. The 24 days protocol for MSC differentiation from hESC. B. Morphological pictures taken at day 3, day 5, day 8, day 10 and day 24 during MSC differentiation from Control shRNA, Apelin shRNA and Aplnr shRNA treated cells. C. MSC markers were detected with flow cytometry analysis and a graphic was drown showing the positive cells for the markers. D. Heatmap visualization of mRNA expression

levels for MSC markers at day 10 and day 24. E. Viable cells were counted with Trypan Blue staining and F. Cell duplication time was calculated for the differentiated cells. G. Cell viability was measured and represented with a bar graph for the differentiated cells. Scale bar: 200µm. *P<0.0001

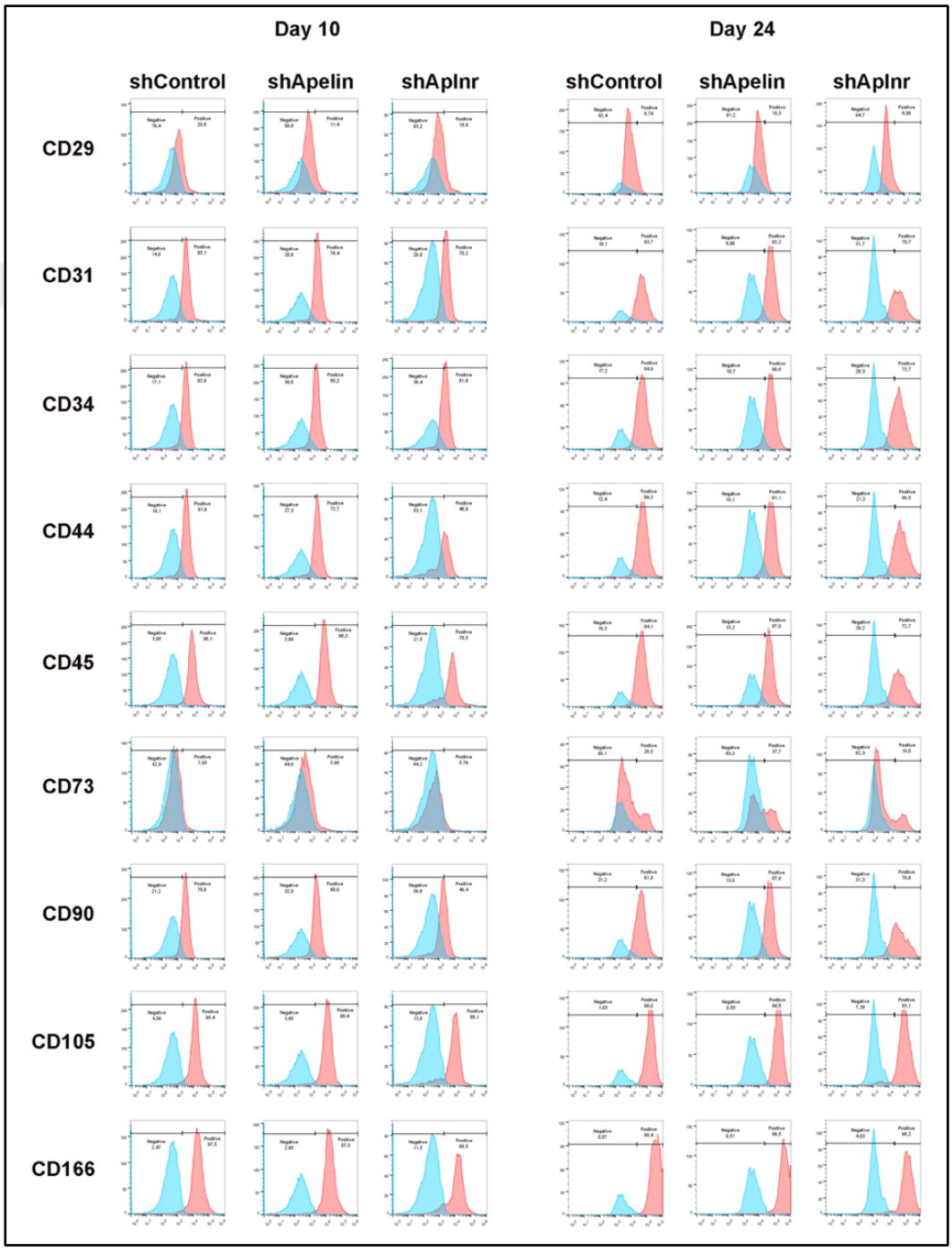


Figure 3.51. Characterization of hESC derived MSCs when Aplnr Signaling Pathway Components were Knocked Down via shRNA. Flow cytometry analysis of mesenchymal stem cell marker expression and hematopoietic marker expression on hESC during MSC

differentiation at day 10 and day 24. Differentiated hESCs, which were silenced with Control shRNA, Apelin shRNA and Aplnr shRNA, were compared.

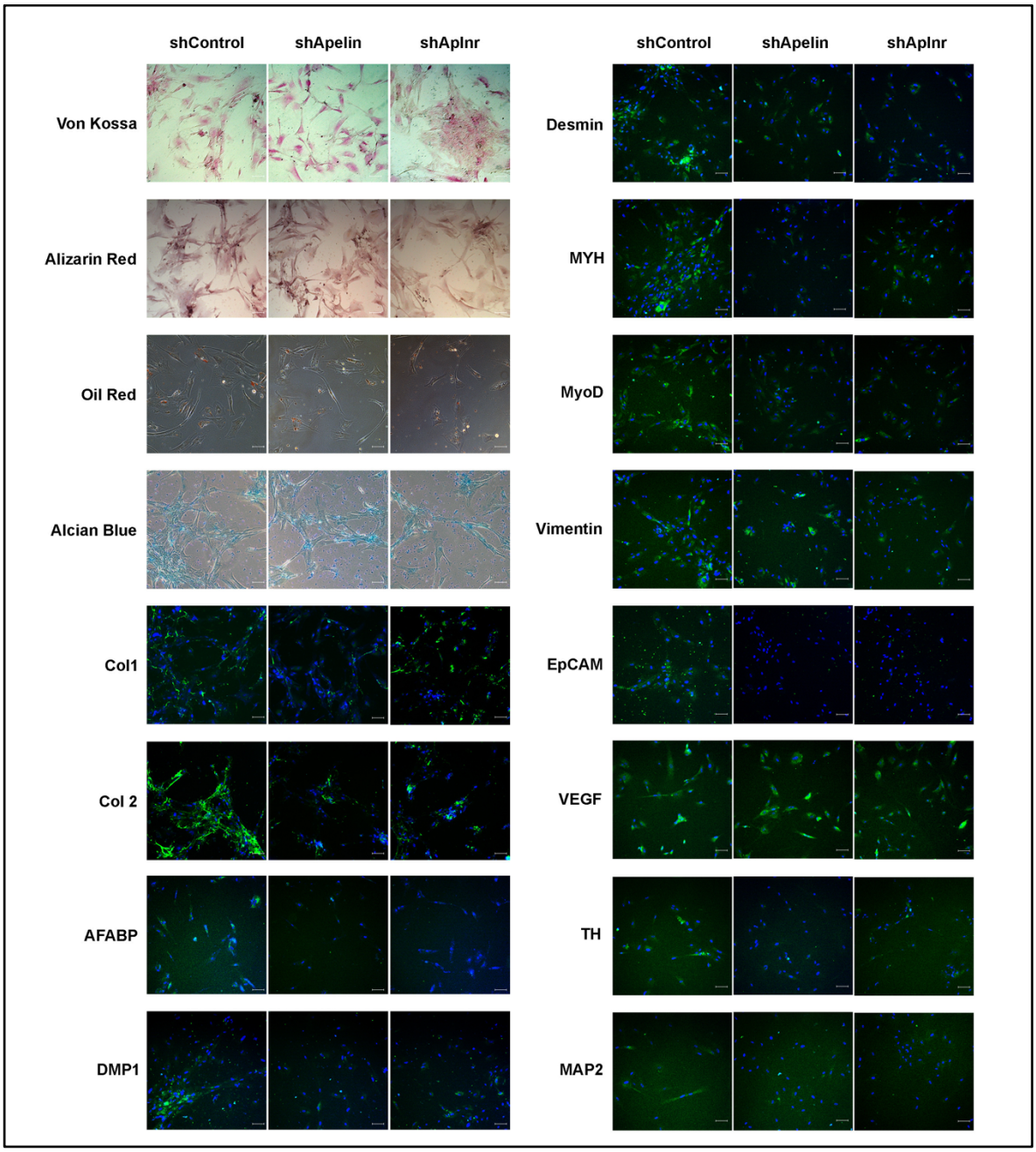


Figure 3.52. Differentiation of hESC derived MSCs into multiple cell types when Aplnr signaling pathway components were knocked down via shRNA. Osteogenic differentiation was shown with von Kossa staining, alizarin red staining and Col1 immunostaining. Oil red O staining and AFABP immunostaining represented adipogenic differentiation. Chondrogenic differentiation was visualized with alcian blue staining and Col2 immunostaining. DMP1 immunostaining was shown to visualize odontogenic

differentiation. Desmin, MyoD and MYH immunostainings were performed after myogenic differentiation. Neurogenic differentiation was shown by TH and MAP2 immunostainings. Endothelial differentiation was visualized by VEGF immunostainings. Immunostainings for Vimentin and EpCAM was performed for epithelial differentiation. Scale Bar: 100µm.

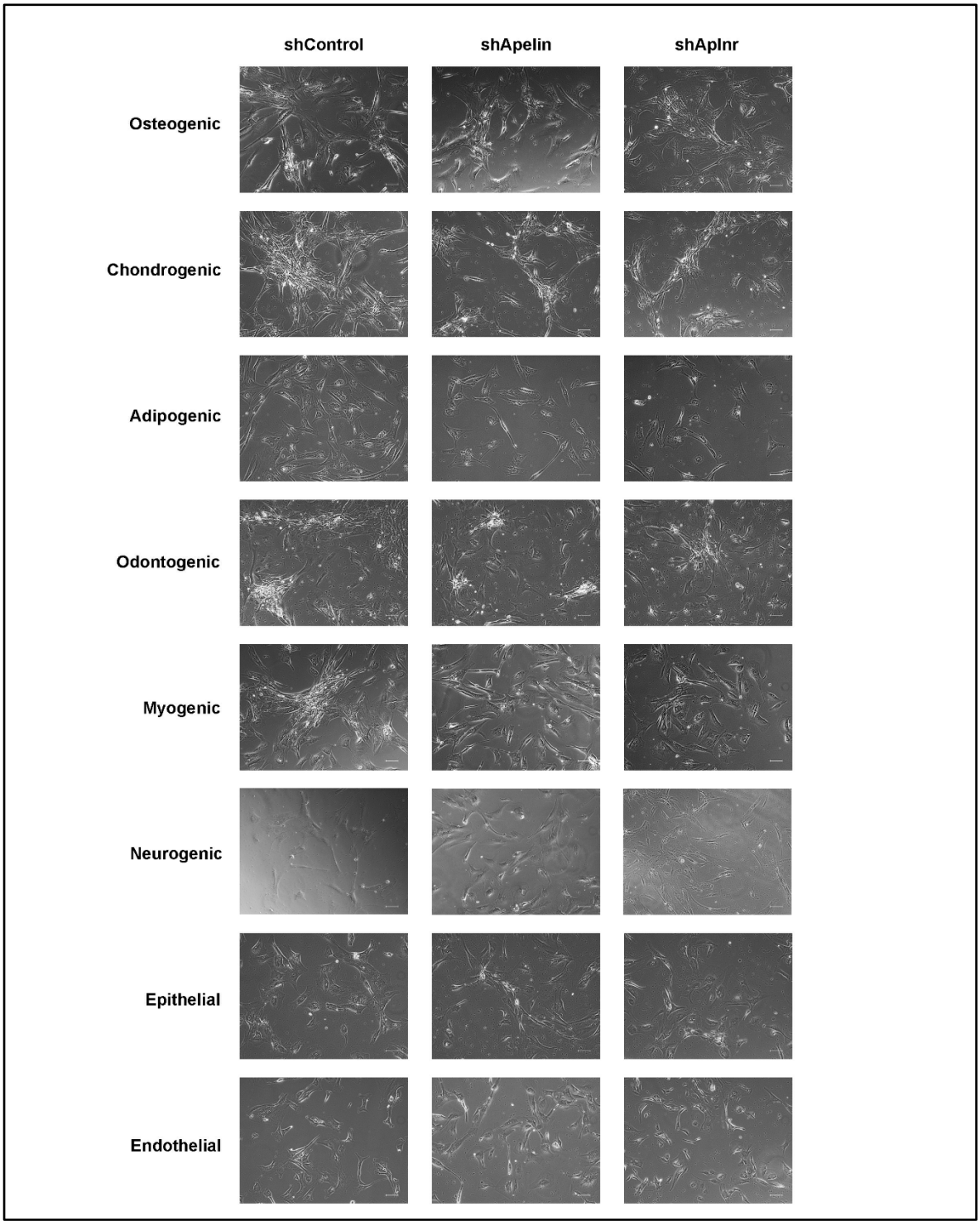


Figure 3.53. Morphology of Multiple Cell Type Differentiation from hESC derived MSCs when Aplnr Signaling Pathway Components were knocked down via shRNA. MSCs, which were derived from Control, Apelin and Aplnr shRNA transfected hESC, were compared with each other in terms of multiple differentiation capacity. Cell morphology after osteogenic, chondrogenic, adipogenic, odontogenic, myogenic, neurogenic, epithelial and endothelial differentiations were demonstrated. Scale Bar: 100µm.

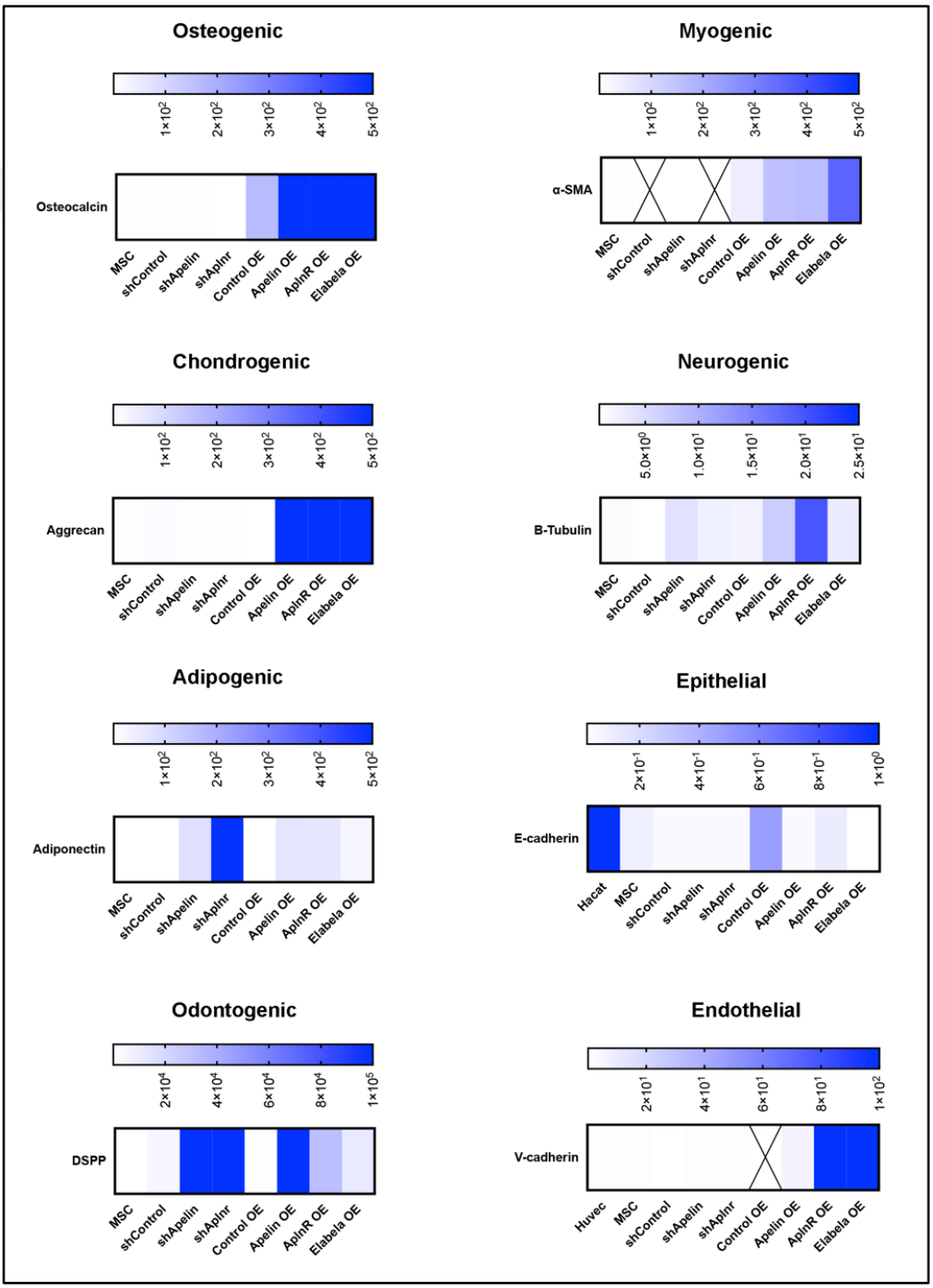


Figure 3.54. Gene expression Verification of Multiple Differentiation from hESC-derived MSCs when Aplnr signaling components were overexpressed or silenced via shRNA. Heatmap visualization of mRNA expression levels of Adipogenic, Chondrogenic, Osteogenic, Odontogenic, Neurogenic, Myogenic, Endothelial and Epithelial markers.

Furthermore, according to the protein-protein interaction network, generated using string, clustered network with clustering coefficient 0.411 contained 49 nodes and 56 edges with 16 expected edges for significantly decreased proteins in shApelin MSCs compared to shControl MSCs. Clustered network with clustering coefficient 0.407 contained 50 nodes and 54 edges with 22 expected edges for significantly downregulated proteins in shAplnr MSCs compared to shControl MSCs. These indicate much more interaction than the expected values (Figure 3.55H).

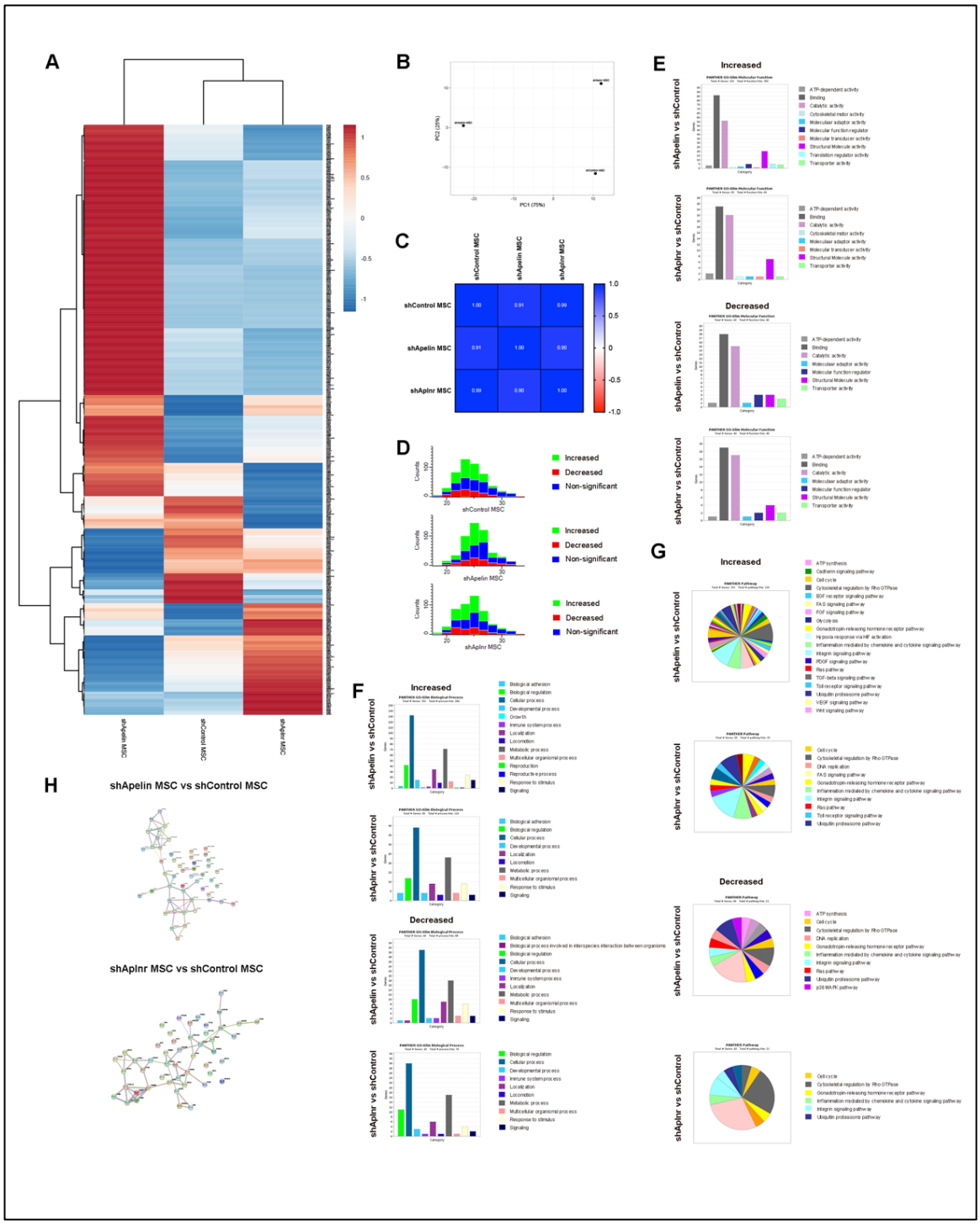


Figure 3.55. Protein profile of hESC derived MSCs when Aplnr components were silenced by shRNA. A. Hierarchical cluster analysis and heat map representation of proteins from shControl-, shApelin- and shAplnr-derived MSCs. B. Principal component analysis and C. Correlation coefficient matrix of the proteins. D. Histogram indicating the distribution of the protein quantification. E. The graphs demonstrating molecular function, F. biological process and G. related pathways of the upregulated and downregulated proteins in

shApelin and shAplnr MSCs compared to shControl MSCS. H. Protein interaction network for the downregulated proteins in shApelin and shAplnr MSCs compared to shControl MSCS.

Apelin, Aplnr and control siRNA treated hESC were also differentiated according to the MSC differentiation protocol for better comprehension of the function of Aplnr signaling during MSC differentiation (Figure 3.56A) and morphological pictures were taken at day 3, day 5, day 8, day 10 and day 24 (Figure 3.56B). Control siRNA treated cells had more negative cell population for hematapoietic markers, CD31, CD34 and CD45, at both day 10 and day 24 compared to Apelin and Aplnr siRNA treated cells and all the groups had CD73, CD 105 and CD 166 positive cell populations (Figure 3.56C and 3.57). Furthermore, CD31 almost was not expressed in siControl cells at day 24, while siApelin and siAplnr groups expressed significantly higher compared to siControl group. Also, CD44 and CD105 expression levels were significantly higher than shAplnr group. Interestingly, CD90, CD44 and CD166 markers were upregulated in siApelin compared to siControl group (Figure 3.56D). However, cell viability and proliferation of the cells derived from the siRNA treated hESCs didn't have a noticeable difference in terms of cell viability and proliferation (Figure 3.56E, 3.56F and 3.56G). Moreover, adipogenic, chondrogenic, osteogenic, myogenic, endothelial and odontogenic differentiation capacity of siApelin and siAplnr derived cells were lower compared to siControl derived cells. Expression of Col1, Col2, AFABP and DMP1 reduced 3.3-fold, 1.7-fold, 1.7-fold and 3.3-fold, respectively, in siApelin group and decreased 3.3-fold, 3.3-fold, 2-fold and 1.4-fold, respectively, in siAplnr group compared to siControl group. Also, siApelin expressed Desmin, MYH, MyoD and VEGF 1.4-fold, 1.7-fold, 2.5-fold and 1.1-fold, respectively, lower compared to the expression levels in siControl group. However, Vimentin, EpCAM and TH expression levels increased 1.3-fold, 1.4-fold and 2.5-fold, respectively, in siApelin group compared to siControl group. Additionally, MAP2, TH, Vimentin and EpCAM expression in siAplnr group were 2-fold, 3.1-fold, 3.8-fold and 2.4-fold, respectively, higher in siControl group (Figure 3.56H, 3.58 and 3.59).

Table 3.6. Protein profiling data of shControl MSC, shApelin MSC and shAplnr MSC groups at day 24. Significantly increased and decreased proteins in shApelin MSC compared to shControl MSC (increased: red, decreased: blue) and shAplnr MSC compared to shControl MSC (increased: pink, decreased: purple) were listed on the table.

Accession	Description	Abundance Ratio: shAplnr MSC / shControl MSC	Abundance Ratio: shApelin MSC / shControl MSC
P13489	Ribonuclease inhibitor OS=Homo sapiens OX=9606 GN=RNH1 PE=1 SV=2	8,422227625	16,65757768
sP27695	DNA-(apurinic or apyrimidinic site) endonuclease OS=Homo sapiens OX=9606 GN=APEX1 PE=1 SV=2	7,168965274	9,732826047
P07996	Thrombospondin-1 OS=Homo sapiens OX=9606 GN=THBS1 PE=1 SV=2	6,753395493	2,132023086
G3V5Z7	Proteasome subunit alpha type OS=Homo sapiens OX=9606 GN=PSMA6 PE=1 SV=1	6,690733111	52,51503501
P52306	Rap1 GTPase-GDP dissociation stimulator 1 OS=Homo sapiens OX=9606 GN=RAP1GDS1 PE=1 SV=3	5,78925426	5,186333336
P62249	40S ribosomal protein S16 OS=Homo sapiens OX=9606 GN=RPS16 PE=1 SV=2	5,715480761	16,47237669
E9PFW3	AP-2 complex subunit mu OS=Homo sapiens OX=9606 GN=AP2M1 PE=1 SV=1	5,333739784	2,505936401
O00487	26S proteasome non-ATPase regulatory subunit 14 OS=Homo sapiens OX=9606 GN=PSMD14 PE=1 SV=1	5,214254829	5,640553577
P63244	Receptor of activated protein C kinase 1 OS=Homo sapiens OX=9606 GN=RACK1 PE=1 SV=3	5,213350367	8,388124224
Q969H8	Myeloid-derived growth factor OS=Homo sapiens OX=9606 GN=MYDGF PE=1 SV=1	5,009857373	12,74791338
Q9H1E3	Nuclear ubiquitous casein and cyclin-dependent kinase substrate 1 OS=Homo	4,335708551	1,124001374

	sapiens OX=9606 GN=NUCKS1 PE=1 SV=1		
Q9Y3B3	Transmembrane emp24 domain-containing protein 7 OS=Homo sapiens OX=9606 GN=TMED7 PE=1 SV=2	**4,189334564**	**9,541594193**
O75915	PRA1 family protein 3 OS=Homo sapiens OX=9606 GN=ARL6IP5 PE=1 SV=1	**3,88021007**	**0,421364856**
Q9UKX5	Integrin alpha-11 OS=Homo sapiens OX=9606 GN=ITGA11 PE=1 SV=2	**3,848121409**	**2,295068467**
P01023	Alpha-2-macroglobulin OS=Homo sapiens OX=9606 GN=A2M PE=1 SV=3	**3,67217005**	**16,06137221**
P62266	40S ribosomal protein S23 OS=Homo sapiens OX=9606 GN=RPS23 PE=1 SV=3	**3,497850138**	**3,029408891**
Q96AC1	Fermitin family homolog 2 OS=Homo sapiens OX=9606 GN=FERMT2 PE=1 SV=1	**3,432933192**	**13,99400559**
P41252	Isoleucine--tRNA ligase, cytoplasmic OS=Homo sapiens OX=9606 GN=IARS1 PE=1 SV=2	**3,348929586**	**10,24830002**
Q15758	Neutral amino acid transporter B(0) OS=Homo sapiens OX=9606 GN=SLC1A5 PE=1 SV=2	**3,321488087**	**8,956233042**
O00154	Cytosolic acyl coenzyme A thioester hydrolase OS=Homo sapiens OX=9606 GN=ACOT7 PE=1 SV=3	**3,303416184**	**6,516977404**
Q9H0D6	5'-3' exoribonuclease 2 OS=Homo sapiens OX=9606 GN=XRN2 PE=1 SV=1	**3,098540652**	**0,498455076**
P61247	40S ribosomal protein S3a OS=Homo sapiens OX=9606 GN=RPS3A PE=1 SV=2	**2,908423286**	**12,6390802**
Q15075	Early endosome antigen 1 OS=Homo sapiens OX=9606 GN=EEA1 PE=1 SV=2	**2,806333979**	**2,554379009**
P43686	26S proteasome regulatory subunit 6B OS=Homo sapiens OX=9606 GN=PSMC4 PE=1 SV=2	**2,795820935**	**3,101405831**
P16070	CD44 antigen OS=Homo sapiens OX=9606 GN=CD44 PE=1 SV=3	**2,786579174**	**11,39193703**

H3BNC9	40S ribosomal protein S17 OS=Homo sapiens OX=9606 PE=3 SV=2	**2,737471194**	**3,47738407**
O15212	Prefoldin subunit 6 OS=Homo sapiens OX=9606 GN=PFDN6 PE=1 SV=1	**2,677909265**	**10,51664916**
P34897	Serine hydroxymethyltransferase, mitochondrial OS=Homo sapiens OX=9606 GN=SHMT2 PE=1 SV=3	**2,638740877**	**2,149334532**
P10412	Histone H1.4 OS=Homo sapiens OX=9606 GN=H1-4 PE=1 SV=2	**2,572489163**	**1,153442566**
E7EPK1	Septin OS=Homo sapiens OX=9606 GN=SEPTIN7 PE=1 SV=2	**2,570760802**	**3,069194037**
Q9UHD8	Septin-9 OS=Homo sapiens OX=9606 GN=SEPTIN9 PE=1 SV=2	**2,532926993**	**2,122577916**
A0A1B0GW77	Aldehyde dehydrogenase (NAD(+)) OS=Homo sapiens OX=9606 GN=ALDH7A1 PE=1 SV=1	**2,499949764**	**3,555660474**
P14868	Aspartate--tRNA ligase, cytoplasmic OS=Homo sapiens OX=9606 GN=DARS1 PE=1 SV=2	**2,486194198**	**17,83525114**
P62269	40S ribosomal protein S18 OS=Homo sapiens OX=9606 GN=RPS18 PE=1 SV=3	**2,456924449**	**7,608136389**
Q96P70	Importin-9 OS=Homo sapiens OX=9606 GN=IPO9 PE=1 SV=3	**2,428300972**	**1,603571044**
Q8WX93	Palladin OS=Homo sapiens OX=9606 GN=PALLD PE=1 SV=3	**2,417856153**	**1,562592843**
P08123	Collagen alpha-2(I) chain OS=Homo sapiens OX=9606 GN=COL1A2 PE=1 SV=7	**2,406050458**	**1,650763723**
Q9UNZ2	NSFL1 cofactor p47 OS=Homo sapiens OX=9606 GN=NSFL1C PE=1 SV=2	**2,404315459**	**2,884334447**
P54578	Ubiquitin carboxyl-terminal hydrolase 14 OS=Homo sapiens OX=9606 GN=USP14 PE=1 SV=3	**2,35848096**	**11,27681251**
P46776	60S ribosomal protein L27a OS=Homo sapiens OX=9606 GN=RPL27A PE=1 SV=2	**2,348457063**	**2,049316374**

A0A0C4DGQ5	Calcium-activated neutral proteinase small subunit OS=Homo sapiens OX=9606 GN=CAPNS1 PE=1 SV=1	2,343988656	14,87794782
Q9NR45	Sialic acid synthase OS=Homo sapiens OX=9606 GN=NANS PE=1 SV=2	2,333150115	9,793394242
Q15084	Protein disulfide-isomerase A6 OS=Homo sapiens OX=9606 GN=PDIA6 PE=1 SV=1	2,316795808	4,751399577
P40121	Macrophage-capping protein OS=Homo sapiens OX=9606 GN=CAPG PE=1 SV=2	2,282578329	2,696413848
P00387	NADH-cytochrome b5 reductase 3 OS=Homo sapiens OX=9606 GN=CYB5R3 PE=1 SV=3	2,277443675	1,324281906
P60866	40S ribosomal protein S20 OS=Homo sapiens OX=9606 GN=RPS20 PE=1 SV=1	2,264193838	11,30539316
P33176	Kinesin-1 heavy chain OS=Homo sapiens OX=9606 GN=KIF5B PE=1 SV=1	2,228254487	4,777349719
P83731	60S ribosomal protein L24 OS=Homo sapiens OX=9606 GN=RPL24 PE=1 SV=1	2,226453022	1,706111596
O15144	Actin-related protein 2/3 complex subunit 2 OS=Homo sapiens OX=9606 GN=ARPC2 PE=1 SV=1	2,184068384	28,90528697
P54819	Adenylate kinase 2, mitochondrial OS=Homo sapiens OX=9606 GN=AK2 PE=1 SV=2	2,176054707	0,285855866
P50281	Matrix metalloproteinase-14 OS=Homo sapiens OX=9606 GN=MMP14 PE=1 SV=3	2,161263701	4,518773656
P02452	Collagen alpha-1(I) chain OS=Homo sapiens OX=9606 GN=COL1A1 PE=1 SV=5	2,14985184	1,301206544
A0A0U1RRH7	Histone H2A OS=Homo sapiens OX=9606 PE=3 SV=1	2,133820454	3,072314957
A8MXP9	Matrin-3 OS=Homo sapiens OX=9606 GN=MATR3 PE=1 SV=1	2,123614158	0,93253176

P48735	Isocitrate dehydrogenase [NADP], mitochondrial OS=Homo sapiens OX=9606 GN=IDH2 PE=1 SV=2	**2,113796377**	**1,45038406**
Q15046	Lysine--tRNA ligase OS=Homo sapiens OX=9606 GN=KARS1 PE=1 SV=3	**2,092237926**	**4,202414988**
P61088	Ubiquitin-conjugating enzyme E2 N OS=Homo sapiens OX=9606 GN=UBE2N PE=1 SV=1	**2,084653261**	**6,584885107**
P00505	Aspartate aminotransferase, mitochondrial OS=Homo sapiens OX=9606 GN=GOT2 PE=1 SV=3	**2,075321752**	**12,16907066**
P08134	Rho-related GTP-binding protein RhoC OS=Homo sapiens OX=9606 GN=RHOC PE=1 SV=1	**2,074536722**	**0,576281898**
O75390	Citrate synthase, mitochondrial OS=Homo sapiens OX=9606 GN=CS PE=1 SV=2	**2,074425782**	**3,677639124**
P07954	Fumarate hydratase, mitochondrial OS=Homo sapiens OX=9606 GN=FH PE=1 SV=3	**2,060620687**	**3,108059639**
P23396	40S ribosomal protein S3 OS=Homo sapiens OX=9606 GN=RPS3 PE=1 SV=2	**2,05145396**	**3,667026594**
Q9UL25	Ras-related protein Rab-21 OS=Homo sapiens OX=9606 GN=RAB21 PE=1 SV=3	**2,027243623**	**1,031021546**
A2A274	Aconitate hydratase, mitochondrial OS=Homo sapiens OX=9606 GN=ACO2 PE=1 SV=1	**2,011752674**	**0,932473992**
P54687	Branched-chain-amino-acid aminotransferase, cytosolic OS=Homo sapiens OX=9606 GN=BCAT1 PE=1 SV=3	**1,97208217**	**6,1927923**
P17931	Galectin-3 OS=Homo sapiens OX=9606 GN=LGALS3 PE=1 SV=5	**1,95770007**	**35,75771994**
Q86V81	THO complex subunit 4 OS=Homo sapiens OX=9606 GN=ALYREF PE=1 SV=3	**1,932836495**	**3,543504976**

P04181	Ornithine aminotransferase, mitochondrial OS=Homo sapiens OX=9606 GN=OAT PE=1 SV=1	**1,921084282**	8,53612425
P28070	Proteasome subunit beta type-4 OS=Homo sapiens OX=9606 GN=PSMB4 PE=1 SV=4	**1,898572827**	18,69661184
P62701	40S ribosomal protein S4, X isoform OS=Homo sapiens OX=9606 GN=RPS4X PE=1 SV=2	**1,881577079**	2,698792511
Q13162	Peroxiredoxin-4 OS=Homo sapiens OX=9606 GN=PRDX4 PE=1 SV=1	**1,879644394**	2,8208783
E9PIE3	Caveolae-associated protein 3 OS=Homo sapiens OX=9606 GN=CAVIN3 PE=1 SV=1	**1,82855255**	**0,214582092**
Q15366	Poly(rC)-binding protein 2 OS=Homo sapiens OX=9606 GN=PCBP2 PE=1 SV=1	**1,799869328**	4,448420372
O94925	Glutaminase kidney isoform, mitochondrial OS=Homo sapiens OX=9606 GN=GLS PE=1 SV=1	**1,797148222**	6,917479778
H7BYY1	Tropomyosin 1 (Alpha), isoform CRA_m OS=Homo sapiens OX=9606 GN=TPM1 PE=1 SV=1	**1,795441024**	**0,242385645**
P36957	Dihydrolipoyllysine-residue succinyltransferase component of 2-oxoglutarate dehydrogenase complex, mitochondrial OS=Homo sapiens OX=9606 GN=DLST PE=1 SV=4	**1,775759542**	5,294764262
Q7KZF4	Staphylococcal nuclease domain-containing protein 1 OS=Homo sapiens OX=9606 GN=SND1 PE=1 SV=1	**1,769663482**	2,062122743
O14974	Protein phosphatase 1 regulatory subunit 12A OS=Homo sapiens OX=9606 GN=PPP1R12A PE=1 SV=1	**1,765152575**	**0,420554503**
P12956	X-ray repair cross-complementing protein 6 OS=Homo sapiens OX=9606 GN=XRCC6 PE=1 SV=2	**1,739433759**	3,637728307

R4GNH3	26S proteasome regulatory subunit 6A OS=Homo sapiens OX=9606 GN=PSMC3 PE=1 SV=1	**1,738009929**	4,906730411
A0A5K1VW95	Malate dehydrogenase OS=Homo sapiens OX=9606 GN=MDH1 PE=1 SV=1	**1,736429637**	3,088084652
F6S8M0	N-acetylglucosamine-6-sulfatase OS=Homo sapiens OX=9606 GN=GNS PE=1 SV=1	**1,723187929**	16,5550696
Q14195	Dihydropyrimidinase-related protein 3 OS=Homo sapiens OX=9606 GN=DPYSL3 PE=1 SV=1	**1,721492793**	3,529517834
P61981	14-3-3 protein gamma OS=Homo sapiens OX=9606 GN=YWHAG PE=1 SV=2	**1,720286818**	3,326554858
P15880	40S ribosomal protein S2 OS=Homo sapiens OX=9606 GN=RPS2 PE=1 SV=2	**1,714803065**	29,44704646
H0YMW4	Annexin OS=Homo sapiens OX=9606 GN=ANXA2 PE=1 SV=2	**1,708252219**	2,382745024
P40429	60S ribosomal protein L13a OS=Homo sapiens OX=9606 GN=RPL13A PE=1 SV=2	**1,700648963**	3,390517558
Q86VP6	Cullin-associated NEDD8-dissociated protein 1 OS=Homo sapiens OX=9606 GN=CAND1 PE=1 SV=2	**1,698558409**	7,870002363
A0A0U1RRM4	Polypyrimidine tract-binding protein 1 OS=Homo sapiens OX=9606 GN=PTBP1 PE=1 SV=1	**1,6878189**	6,486952938
P28072	Proteasome subunit beta type-6 OS=Homo sapiens OX=9606 GN=PSMB6 PE=1 SV=4	**1,686032219**	4,177658206
P02786	Transferrin receptor protein 1 OS=Homo sapiens OX=9606 GN=TFRC PE=1 SV=2	**1,679810562**	**0,370808425**
P00338	L-lactate dehydrogenase A chain OS=Homo sapiens OX=9606 GN=LDHA PE=1 SV=2	**1,67618048**	6,098249222
Q8WWM7	Ataxin-2-like protein OS=Homo sapiens OX=9606 GN=ATXN2L PE=1 SV=2	**1,675643207**	**0,197098891**

Q96C90	Protein phosphatase 1 regulatory subunit 14B OS=Homo sapiens OX=9606 GN=PPP1R14B PE=1 SV=3	**1,659160558**	**0,273448864**
P20908	Collagen alpha-1(V) chain OS=Homo sapiens OX=9606 GN=COL5A1 PE=1 SV=3	**1,627015366**	**2,166987257**
P62913	60S ribosomal protein L11 OS=Homo sapiens OX=9606 GN=RPL11 PE=1 SV=2	**1,621703875**	**2,120662247**
P09382	Galectin-1 OS=Homo sapiens OX=9606 GN=LGALS1 PE=1 SV=2	**1,619291558**	**208,0219813**
P23284	Peptidyl-prolyl cis-trans isomerase B OS=Homo sapiens OX=9606 GN=PPIB PE=1 SV=2	**1,616588467**	**13,24584192**
P53597	Succinate--CoA ligase [ADP/GDP-forming] subunit alpha, mitochondrial OS=Homo sapiens OX=9606 GN=SUCLG1 PE=1 SV=4	**1,616156443**	**5,604904211**
A0A0B4J2C3	Translationally-controlled tumor protein OS=Homo sapiens OX=9606 GN=TPT1 PE=1 SV=1	**1,615510321**	**35,33187715**
P07942	Laminin subunit beta-1 OS=Homo sapiens OX=9606 GN=LAMB1 PE=1 SV=2	**1,573039758**	**2,073765229**
A0A2R8Y623	40S ribosomal protein S7 (Fragment) OS=Homo sapiens OX=9606 GN=RPS7 PE=1 SV=1	**1,547557165**	**0,393936706**
P51991	Heterogeneous nuclear ribonucleoprotein A3 OS=Homo sapiens OX=9606 GN=HNRNPA3 PE=1 SV=2	**1,542959035**	**0,308800238**
P60903	Protein S100-A10 OS=Homo sapiens OX=9606 GN=S100A10 PE=1 SV=2	**1,528809486**	**7,279855804**
O00560	Syntenin-1 OS=Homo sapiens OX=9606 GN=SDCBP PE=1 SV=1	**1,526396543**	**0,040758265**
P62829	60S ribosomal protein L23 OS=Homo sapiens OX=9606 GN=RPL23 PE=1 SV=1	**1,500493036**	**15,74528704**

P60842	Eukaryotic initiation factor 4A-I OS=Homo sapiens OX=9606 GN=EIF4A1 PE=1 SV=1	**1,483358891**	2,998442024
A0A0C4DGV4	Late endosomal/lysosomal adaptor and MAPK and MTOR activator 5 OS=Homo sapiens OX=9606 GN=LAMTOR5 PE=1 SV=1	**1,458511635**	**0,387062035**
P50991	T-complex protein 1 subunit delta OS=Homo sapiens OX=9606 GN=CCT4 PE=1 SV=4	**1,45091767**	2,659375396
Q99961	Endophilin-A2 OS=Homo sapiens OX=9606 GN=SH3GL1 PE=1 SV=1	**1,445277346**	**0,314265396**
P35998	26S proteasome regulatory subunit 7 OS=Homo sapiens OX=9606 GN=PSMC2 PE=1 SV=3	**1,425306019**	2,325838557
Q15369	Elongin-C OS=Homo sapiens OX=9606 GN=ELOC PE=1 SV=1	**1,421529493**	3,958231914
A6NCE7	Microtubule-associated proteins 1A/1B light chain 3 beta 2 OS=Homo sapiens OX=9606 GN=MAP1LC3B2 PE=2 SV=1	**1,399443522**	**0,30128941**
A0A024R4E5	High density lipoprotein binding protein (Vigilin), isoform CRA_a OS=Homo sapiens OX=9606 GN=HDLBP PE=1 SV=1	**1,395160702**	4,178457252
B1AK88	F-actin-capping protein subunit beta OS=Homo sapiens OX=9606 GN=CAPZB PE=1 SV=1	**1,389022831**	3,490433722
P06396	Gelsolin OS=Homo sapiens OX=9606 GN=GSN PE=1 SV=1	**1,375678193**	41,09395034
P08133	Annexin A6 OS=Homo sapiens OX=9606 GN=ANXA6 PE=1 SV=3	**1,374074399**	2,011912156
O43242	26S proteasome non-ATPase regulatory subunit 3 OS=Homo sapiens OX=9606 GN=PSMD3 PE=1 SV=2	**1,363969069**	3,879765511
P62906	60S ribosomal protein L10a OS=Homo sapiens OX=9606 GN=RPL10A PE=1 SV=2	**1,3531117**	5,63660389
P18124	60S ribosomal protein L7 OS=Homo sapiens OX=9606 GN=RPL7 PE=1 SV=1	**1,349643395**	2,104046215

B5MDF5	GTP-binding nuclear protein Ran OS=Homo sapiens OX=9606 GN=RAN PE=1 SV=1	**1,333336957**	3,062074652
P61586	Transforming protein RhoA OS=Homo sapiens OX=9606 GN=RHOA PE=1 SV=1	**1,329157781**	3,564868368
Q00325	Phosphate carrier protein, mitochondrial OS=Homo sapiens OX=9606 GN=SLC25A3 PE=1 SV=2	**1,323651376**	6,27515084
Q562R1	Beta-actin-like protein 2 OS=Homo sapiens OX=9606 GN=ACTBL2 PE=1 SV=2	**1,309141516**	44,22847574
G5E9Q6	Profilin OS=Homo sapiens OX=9606 GN=PFN2 PE=1 SV=1	**1,305559488**	4,040832793
P18085	ADP-ribosylation factor 4 OS=Homo sapiens OX=9606 GN=ARF4 PE=1 SV=3	**1,304360188**	167,8620547
D6RER5	Septin OS=Homo sapiens OX=9606 GN=SEPTIN11 PE=1 SV=1	**1,302340706**	10,70958546
H0Y4R1	Inosine-5'-monophosphate dehydrogenase OS=Homo sapiens OX=9606 GN=IMPDH2 PE=1 SV=2	**1,301778189**	4,156317727
P61604	10 kDa heat shock protein, mitochondrial OS=Homo sapiens OX=9606 GN=HSPE1 PE=1 SV=2	**1,300045952**	3,068568794
P25789	Proteasome subunit alpha type-4 OS=Homo sapiens OX=9606 GN=PSMA4 PE=1 SV=1	**1,297896062**	6,83493252
P07737	Profilin-1 OS=Homo sapiens OX=9606 GN=PFN1 PE=1 SV=2	**1,288282745**	5,058845591
P60953	Cell division control protein 42 homolog OS=Homo sapiens OX=9606 GN=CDC42 PE=1 SV=2	**1,287683423**	**0,2818261**
P53621	Coatomer subunit alpha OS=Homo sapiens OX=9606 GN=COPA PE=1 SV=2	**1,261699733**	2,607412707
P08238	Heat shock protein HSP 90-beta OS=Homo sapiens OX=9606 GN=HSP90AB1 PE=1 SV=4	**1,239448435**	2,191054788

P09525	Annexin A4 OS=Homo sapiens OX=9606 GN=ANXA4 PE=1 SV=4	**1,238904799**	**0,345413801**
P78371	T-complex protein 1 subunit beta OS=Homo sapiens OX=9606 GN=CCT2 PE=1 SV=4	**1,234287418**	**4,740627512**
Q9H2U2	Inorganic pyrophosphatase 2, mitochondrial OS=Homo sapiens OX=9606 GN=PPA2 PE=1 SV=2	**1,2311272**	**0,205792042**
O14907	Tax1-binding protein 3 OS=Homo sapiens OX=9606 GN=TAX1BP3 PE=1 SV=2	**1,22602781**	**4,194056489**
O95336	6-phosphogluconolactonase OS=Homo sapiens OX=9606 GN=PGLS PE=1 SV=2	**1,208603506**	**2,106166367**
A0A804HII9	Alpha-actinin-1 OS=Homo sapiens OX=9606 GN=ACTN1 PE=4 SV=1	**1,207711268**	**6,450913611**
A0A2R8Y5A3	Catenin beta-1 OS=Homo sapiens OX=9606 GN=CTNNB1 PE=1 SV=1	**1,203142003**	**0,292219205**
P26038	Moesin OS=Homo sapiens OX=9606 GN=MSN PE=1 SV=3	**1,199014161**	**4,639655811**
P46778	60S ribosomal protein L21 OS=Homo sapiens OX=9606 GN=RPL21 PE=1 SV=2	**1,192942816**	**33,42182608**
P25788	Proteasome subunit alpha type-3 OS=Homo sapiens OX=9606 GN=PSMA3 PE=1 SV=2	**1,192418195**	**2,931672568**
P62424	60S ribosomal protein L7a OS=Homo sapiens OX=9606 GN=RPL7A PE=1 SV=2	**1,187554201**	**2,966429231**
P60174	Triosephosphate isomerase OS=Homo sapiens OX=9606 GN=TPI1 PE=1 SV=4	**1,183290812**	**2,279447443**
A0A669KB53	Signal transducer and activator of transcription OS=Homo sapiens OX=9606 GN=STAT1 PE=1 SV=1	**1,178281168**	**4,551947364**
Q9Y2D5	A-kinase anchor protein 2 OS=Homo sapiens OX=9606 GN=AKAP2 PE=1 SV=3	**1,168743605**	**0,094173182**
D6REX3	Protein transport protein Sec31A OS=Homo sapiens OX=9606 GN=SEC31A PE=1 SV=1	**1,16800571**	**2,59941548**

P05141	ADP/ATP translocase 2 OS=Homo sapiens OX=9606 GN=SLC25A5 PE=1 SV=7	**1,167302963**	2,762718384
M0R0C6	Far upstream element-binding protein 2 OS=Homo sapiens OX=9606 GN=KHSRP PE=1 SV=2	**1,161643136**	**0,352261363**
P51665	26S proteasome non-ATPase regulatory subunit 7 OS=Homo sapiens OX=9606 GN=PSMD7 PE=1 SV=2	**1,159458264**	**0,302779925**
Q9P2E9	Ribosome-binding protein 1 OS=Homo sapiens OX=9606 GN=RRBP1 PE=1 SV=5	**1,154336217**	2,079916482
O15460	Prolyl 4-hydroxylase subunit alpha-2 OS=Homo sapiens OX=9606 GN=P4HA2 PE=1 SV=1	**1,147565935**	3,455749455
P23526	Adenosylhomocysteinase OS=Homo sapiens OX=9606 GN=AHCY PE=1 SV=4	**1,141378633**	4,280107465
A0A3B3ITT5	60S ribosomal protein L29 OS=Homo sapiens OX=9606 GN=RPL29 PE=1 SV=1	**1,139882548**	2,115544452
P80723	Brain acid soluble protein 1 OS=Homo sapiens OX=9606 GN=BASP1 PE=1 SV=2	**1,138766838**	7,617824856
Q9H299	SH3 domain-binding glutamic acid-rich-like protein 3 OS=Homo sapiens OX=9606 GN=SH3BGRL3 PE=1 SV=1	**1,138740083**	**0,329067437**
Q9NQC3	Reticulon-4 OS=Homo sapiens OX=9606 GN=RTN4 PE=1 SV=2	**1,135451474**	3,487239983
D6RBZ0	Heterogeneous nuclear ribonucleoprotein A/B OS=Homo sapiens OX=9606 GN=HNRNPAB PE=1 SV=1	**1,131139988**	19,79563291
P62857	40S ribosomal protein S28 OS=Homo sapiens OX=9606 GN=RPS28 PE=1 SV=1	**1,130329935**	3,386440528
P09429	High mobility group protein B1 OS=Homo sapiens OX=9606 GN=HMGB1 PE=1 SV=3	**1,127179524**	3,482695795

P02751	Fibronectin OS=Homo sapiens OX=9606 GN=FN1 PE=1 SV=5	**1,126121633**	2,637643107
Q96KP4	Cytosolic non-specific dipeptidase OS=Homo sapiens OX=9606 GN=CNDP2 PE=1 SV=2	**1,123465824**	2,028516153
E9PAV3	Nascent polypeptide-associated complex subunit alpha, muscle-specific form OS=Homo sapiens OX=9606 GN=NACA PE=1 SV=1	**1,123458597**	7,831291817
P62937	Peptidyl-prolyl cis-trans isomerase A OS=Homo sapiens OX=9606 GN=PPIA PE=1 SV=2	**1,122230645**	2,253768006
Q15907	Ras-related protein Rab-11B OS=Homo sapiens OX=9606 GN=RAB11B PE=1 SV=4	**1,121648819**	4,582950449
P62241	40S ribosomal protein S8 OS=Homo sapiens OX=9606 GN=RPS8 PE=1 SV=2	**1,114337964**	2,097604111
P62258	14-3-3 protein epsilon OS=Homo sapiens OX=9606 GN=YWHAE PE=1 SV=1	**1,096532428**	5,370023614
P23381	Tryptophan--tRNA ligase, cytoplasmic OS=Homo sapiens OX=9606 GN=WARS1 PE=1 SV=2	**1,09478408**	3,226501164
Q02952	A-kinase anchor protein 12 OS=Homo sapiens OX=9606 GN=AKAP12 PE=1 SV=4	**1,093824987**	2,189208537
O60701	UDP-glucose 6-dehydrogenase OS=Homo sapiens OX=9606 GN=UGDH PE=1 SV=1	**1,091377298**	2,576265513
Q07960	Rho GTPase-activating protein 1 OS=Homo sapiens OX=9606 GN=ARHGAP1 PE=1 SV=1	**1,087015766**	6,366883411
Q01518	Adenylyl cyclase-associated protein 1 OS=Homo sapiens OX=9606 GN=CAP1 PE=1 SV=5	**1,085397381**	2,860105013
P99999	Cytochrome c OS=Homo sapiens OX=9606 GN=CYCS PE=1 SV=2	**1,06297525**	6,389270112
P24534	Elongation factor 1-beta OS=Homo sapiens OX=9606 GN=EEF1B2 PE=1 SV=3	**1,060138857**	**0,19781994**

P04083	Annexin A1 OS=Homo sapiens OX=9606 GN=ANXA1 PE=1 SV=2	**1,059735742**	2,690966707
P34932	Heat shock 70 kDa protein 4 OS=Homo sapiens OX=9606 GN=HSPA4 PE=1 SV=4	**1,054874188**	4,917955632
P22392	Nucleoside diphosphate kinase B OS=Homo sapiens OX=9606 GN=NME2 PE=1 SV=1	**1,050450847**	3,609650367
O15143	Actin-related protein 2/3 complex subunit 1B OS=Homo sapiens OX=9606 GN=ARPC1B PE=1 SV=3	**1,050274514**	6,735245048
P30086	Phosphatidylethanolamine-binding protein 1 OS=Homo sapiens OX=9606 GN=PEBP1 PE=1 SV=3	**1,048870297**	3,870184954
Q15436	Protein transport protein Sec23A OS=Homo sapiens OX=9606 GN=SEC23A PE=1 SV=2	**1,046106113**	5,061183507
P25705	ATP synthase subunit alpha, mitochondrial OS=Homo sapiens OX=9606 GN=ATP5F1A PE=1 SV=1	**1,046053293**	**0,481337541**
P10809	60 kDa heat shock protein, mitochondrial OS=Homo sapiens OX=9606 GN=HSPD1 PE=1 SV=2	**1,044775262**	**0,469647164**
A0A6Q8PGN5	Alanine--tRNA ligase OS=Homo sapiens OX=9606 GN=AARS1 PE=1 SV=1	**1,034919882**	7,189943
A0A0A0MTJ9	Neutral cholesterol ester hydrolase 1 OS=Homo sapiens OX=9606 GN=NCEH1 PE=1 SV=1	**1,022684158**	**0,072584856**
P29966	Myristoylated alanine-rich C-kinase substrate OS=Homo sapiens OX=9606 GN=MARCKS PE=1 SV=4	**1,02166124**	6,127460302
Q16658	Fascin OS=Homo sapiens OX=9606 GN=FSCN1 PE=1 SV=3	**0,998014162**	2,175821432
P68104	Elongation factor 1-alpha 1 OS=Homo sapiens OX=9606 GN=EEF1A1 PE=1 SV=1	**0,993906355**	2,699093651
Q14315	Filamin-C OS=Homo sapiens OX=9606 GN=FLNC PE=1 SV=3	**0,982249461**	6,437894778

P08670	Vimentin OS=Homo sapiens OX=9606 GN=VIM PE=1 SV=4	**0,980693311**	**0,376816255**
K7ELC2	40S ribosomal protein S15 OS=Homo sapiens OX=9606 GN=RPS15 PE=1 SV=1	**0,977506098**	2,180362987
O00299	Chloride intracellular channel protein 1 OS=Homo sapiens OX=9606 GN=CLIC1 PE=1 SV=4	**0,973078027**	2,213631618
P27797	Calreticulin OS=Homo sapiens OX=9606 GN=CALR PE=1 SV=1	**0,969362329**	13,17951741
P13674	Prolyl 4-hydroxylase subunit alpha-1 OS=Homo sapiens OX=9606 GN=P4HA1 PE=1 SV=2	**0,964146403**	**0,366232559**
A0A087WWU8	Tropomyosin alpha-3 chain OS=Homo sapiens OX=9606 GN=TPM3 PE=1 SV=1	**0,953939325**	2,083151387
P61353	60S ribosomal protein L27 OS=Homo sapiens OX=9606 GN=RPL27 PE=1 SV=2	**0,953021374**	8,586503798
E9PR30	40S ribosomal protein S30 OS=Homo sapiens OX=9606 GN=FAU PE=1 SV=1	**0,950091749**	**0,500613814**
H7BY16	Nucleolin OS=Homo sapiens OX=9606 GN=NCL PE=1 SV=9	**0,949724241**	4,955031248
Q14103	Heterogeneous nuclear ribonucleoprotein D0 OS=Homo sapiens OX=9606 GN=HNRNPD PE=1 SV=1	**0,943317249**	3,296680339
Q99584	Protein S100-A13 OS=Homo sapiens OX=9606 GN=S100A13 PE=1 SV=1	**0,930731067**	2,566410288
P10599	Thioredoxin OS=Homo sapiens OX=9606 GN=TXN PE=1 SV=3	**0,926360936**	2,729269463
P37802	Transgelin-2 OS=Homo sapiens OX=9606 GN=TAGLN2 PE=1 SV=3	**0,925768353**	3,933973431
P23246	Splicing factor, proline- and glutamine-rich OS=Homo sapiens OX=9606 GN=SFPQ PE=1 SV=2	**0,920095167**	**0,193975654**
P35606	Coatomer subunit beta' OS=Homo sapiens OX=9606 GN=COPB2 PE=1 SV=2	**0,916648293**	39,43233531
P08758	Annexin A5 OS=Homo sapiens OX=9606 GN=ANXA5 PE=1 SV=2	**0,91398003**	4,189223234

Q13200	26S proteasome non-ATPase regulatory subunit 2 OS=Homo sapiens OX=9606 GN=PSMD2 PE=1 SV=3	**0,910283292**	**0,446488204**
A0A7P0TAE9	Calnexin OS=Homo sapiens OX=9606 GN=CANX PE=1 SV=1	**0,901794477**	**2,114883768**
P30041	Peroxiredoxin-6 OS=Homo sapiens OX=9606 GN=PRDX6 PE=1 SV=3	**0,892552543**	**0,172864503**
P61160	Actin-related protein 2 OS=Homo sapiens OX=9606 GN=ACTR2 PE=1 SV=1	**0,884556215**	**6,1892089**
Q9BVC6	Transmembrane protein 109 OS=Homo sapiens OX=9606 GN=TMEM109 PE=1 SV=1	**0,883557768**	**2,079626423**
P54577	Tyrosine--tRNA ligase, cytoplasmic OS=Homo sapiens OX=9606 GN=YARS1 PE=1 SV=4	**0,883287608**	**2,279051265**
P09211	Glutathione S-transferase P OS=Homo sapiens OX=9606 GN=GSTP1 PE=1 SV=2	**0,883205331**	**4,966543577**
P46783	40S ribosomal protein S10 OS=Homo sapiens OX=9606 GN=RPS10 PE=1 SV=1	**0,877379056**	**0,314993661**
P46781	40S ribosomal protein S9 OS=Homo sapiens OX=9606 GN=RPS9 PE=1 SV=3	**0,877253564**	**35,92844848**
P18206	Vinculin OS=Homo sapiens OX=9606 GN=VCL PE=1 SV=4	**0,859057455**	**2,712906083**
Q14240	Eukaryotic initiation factor 4A-II OS=Homo sapiens OX=9606 GN=EIF4A2 PE=1 SV=2	**0,855351487**	**2,342699538**
P40227	T-complex protein 1 subunit zeta OS=Homo sapiens OX=9606 GN=CCT6A PE=1 SV=3	**0,85223973**	**2,20365234**
C9JH19	Cathepsin D OS=Homo sapiens OX=9606 GN=CTSD PE=1 SV=2	**0,851352395**	**3,094069719**
Q96HC4	PDZ and LIM domain protein 5 OS=Homo sapiens OX=9606 GN=PDLIM5 PE=1 SV=5	**0,837796549**	**4,538822903**
A0A804HKI2	Leucine-rich PPR motif-containing protein, mitochondrial OS=Homo sapiens OX=9606 GN=LRPPRC PE=4 SV=1	**0,831209105**	**3,046193608**

P09110	3-ketoacyl-CoA thiolase, peroxisomal OS=Homo sapiens OX=9606 GN=ACAA1 PE=1 SV=2	**0,811694387**	**0,410231708**
Q05682	Caldesmon OS=Homo sapiens OX=9606 GN=CALD1 PE=1 SV=3	**0,811339411**	**0,332301866**
Q15942	Zyxin OS=Homo sapiens OX=9606 GN=ZYX PE=1 SV=1	**0,809937697**	**0,261715512**
P30084	Enoyl-CoA hydratase, mitochondrial OS=Homo sapiens OX=9606 GN=ECHS1 PE=1 SV=4	**0,804176853**	**2,333919954**
Q14247	Src substrate cortactin OS=Homo sapiens OX=9606 GN=CTTN PE=1 SV=2	**0,803836055**	**0,240017171**
P51148	Ras-related protein Rab-5C OS=Homo sapiens OX=9606 GN=RAB5C PE=1 SV=2	**0,792206238**	**2,995459378**
E9PL57	NEDD8-MDP1 readthrough (Fragment) OS=Homo sapiens OX=9606 GN=NEDD8-MDP1 PE=4 SV=1	**0,78951478**	**0,433818663**
P52565	Rho GDP-dissociation inhibitor 1 OS=Homo sapiens OX=9606 GN=ARHGDIA PE=1 SV=3	**0,78595463**	**4,022018822**
P11766	Alcohol dehydrogenase class-3 OS=Homo sapiens OX=9606 GN=ADH5 PE=1 SV=4	**0,778191445**	**0,409287596**
P35580	Myosin-10 OS=Homo sapiens OX=9606 GN=MYH10 PE=1 SV=3	**0,777872005**	**4,505664017**
O75874	Isocitrate dehydrogenase [NADP] cytoplasmic OS=Homo sapiens OX=9606 GN=IDH1 PE=1 SV=2	**0,772477609**	**3,384516208**
P50914	60S ribosomal protein L14 OS=Homo sapiens OX=9606 GN=RPL14 PE=1 SV=4	**0,767294218**	**2,734650273**
B7Z6Z4	Myosin light polypeptide 6 OS=Homo sapiens OX=9606 GN=MYL6 PE=1 SV=1	**0,765628691**	**0,364634922**
F8WCF6	Actin-related protein 2/3 complex subunit 4 OS=Homo sapiens OX=9606 GN=ARPC4-TTLL3 PE=3 SV=1	**0,764027054**	**18,69213244**

P27635	60S ribosomal protein L10 OS=Homo sapiens OX=9606 GN=RPL10 PE=1 SV=4	**0,762027671**	6,92322804
P00558	Phosphoglycerate kinase 1 OS=Homo sapiens OX=9606 GN=PGK1 PE=1 SV=3	**0,748793477**	2,744619807
P30040	Endoplasmic reticulum resident protein 29 OS=Homo sapiens OX=9606 GN=ERP29 PE=1 SV=4	**0,748558209**	20,02689134
C9J813	Caldesmon (Fragment) OS=Homo sapiens OX=9606 GN=CALD1 PE=1 SV=1	**0,741645028**	14,54539724
Q96QK1	Vacuolar protein sorting-associated protein 35 OS=Homo sapiens OX=9606 GN=VPS35 PE=1 SV=2	**0,741219388**	3,10410394
A0A7P0Z4P5	4F2 cell-surface antigen heavy chain OS=Homo sapiens OX=9606 GN=SLC3A2 PE=1 SV=1	**0,735118015**	2,57729233
Q07065	Cytoskeleton-associated protein 4 OS=Homo sapiens OX=9606 GN=CKAP4 PE=1 SV=2	**0,734754293**	4,803760714
O75083	WD repeat-containing protein 1 OS=Homo sapiens OX=9606 GN=WDR1 PE=1 SV=4	**0,727240812**	2,841205801
P55884	Eukaryotic translation initiation factor 3 subunit B OS=Homo sapiens OX=9606 GN=EIF3B PE=1 SV=3	**0,717959553**	4,492011586
Q8NBS9	Thioredoxin domain-containing protein 5 OS=Homo sapiens OX=9606 GN=TXNDC5 PE=1 SV=2	**0,715602881**	3,044775745
P78417	Glutathione S-transferase omega-1 OS=Homo sapiens OX=9606 GN=GSTO1 PE=1 SV=2	**0,707934635**	7,591475677
P62820	Ras-related protein Rab-1A OS=Homo sapiens OX=9606 GN=RAB1A PE=1 SV=3	**0,705053217**	2,511340965
A0A7I2YQC0	Nucleophosmin OS=Homo sapiens OX=9606 GN=NPM1 PE=1 SV=1	**0,696326933**	**0,281265458**

H0YMV8	40S ribosomal protein S27 OS=Homo sapiens OX=9606 GN=RPS27L PE=1 SV=1	**0,693656882**	20,91622043
P47755	F-actin-capping protein subunit alpha-2 OS=Homo sapiens OX=9606 GN=CAPZA2 PE=1 SV=3	**0,683892422**	3,72471192
Q99536	Synaptic vesicle membrane protein VAT-1 homolog OS=Homo sapiens OX=9606 GN=VAT1 PE=1 SV=2	**0,676498239**	**0,463004739**
O00151	PDZ and LIM domain protein 1 OS=Homo sapiens OX=9606 GN=PDLIM1 PE=1 SV=4	**0,668904267**	**0,20813764**
P0DME0	Protein SETSIP OS=Homo sapiens OX=9606 GN=SETSIP PE=1 SV=1	**0,653868127**	10,27619952
Q96JJ7	Protein disulfide-isomerase TMX3 OS=Homo sapiens OX=9606 GN=TMX3 PE=1 SV=2	**0,653749694**	**0,392434897**
Q9H3N1	Thioredoxin-related transmembrane protein 1 OS=Homo sapiens OX=9606 GN=TMX1 PE=1 SV=1	**0,639341807**	**0,133161794**
I3L504	Eukaryotic translation initiation factor 5A-1 OS=Homo sapiens OX=9606 GN=EIF5A PE=1 SV=1	**0,635538194**	5,44715124
G8JLB6	Heterogeneous nuclear ribonucleoprotein H OS=Homo sapiens OX=9606 GN=HNRNPH1 PE=1 SV=1	**0,634934624**	13,27462308
Q01813	ATP-dependent 6-phosphofructokinase, platelet type OS=Homo sapiens OX=9606 GN=PFKP PE=1 SV=2	**0,631164837**	3,741055725
Q9Y617	Phosphoserine aminotransferase OS=Homo sapiens OX=9606 GN=PSAT1 PE=1 SV=2	**0,629299783**	3,96887366
E7EUC7	UTP--glucose-1-phosphate uridylyltransferase OS=Homo sapiens OX=9606 GN=UGP2 PE=1 SV=1	**0,628692908**	11,69417637
P49411	Elongation factor Tu, mitochondrial OS=Homo sapiens OX=9606 GN=TUFM PE=1 SV=2	**0,627224314**	5,824515573

P68032	Actin, alpha cardiac muscle 1 OS=Homo sapiens OX=9606 GN=ACTC1 PE=1 SV=1	**0,616300057**	2,752131452
A0A6Q8PFE1	Apoptosis-inducing factor 1, mitochondrial OS=Homo sapiens OX=9606 GN=AIFM1 PE=1 SV=1	**0,589531286**	6,8088283
P05787	Keratin, type II cytoskeletal 8 OS=Homo sapiens OX=9606 GN=KRT8 PE=1 SV=7	**0,587401247**	2,676665352
O75396	Vesicle-trafficking protein SEC22b OS=Homo sapiens OX=9606 GN=SEC22B PE=1 SV=5	**0,582953257**	**0,121143584**
Q9Y281	Cofilin-2 OS=Homo sapiens OX=9606 GN=CFL2 PE=1 SV=1	**0,576299302**	14,14205982
P62942	Peptidyl-prolyl cis-trans isomerase FKBP1A OS=Homo sapiens OX=9606 GN=FKBP1A PE=1 SV=2	**0,571439224**	3,926699989
O00425	Insulin-like growth factor 2 mRNA-binding protein 3 OS=Homo sapiens OX=9606 GN=IGF2BP3 PE=1 SV=2	**0,539346974**	2,230860798
P35579	Myosin-9 OS=Homo sapiens OX=9606 GN=MYH9 PE=1 SV=4	**0,53415138**	5,954426479
Q01995	Transgelin OS=Homo sapiens OX=9606 GN=TAGLN PE=1 SV=4	**0,523422583**	6,193948374
P35527	Keratin, type I cytoskeletal 9 OS=Homo sapiens OX=9606 GN=KRT9 PE=1 SV=3	**0,521348359**	**0,335207597**
P46821	Microtubule-associated protein 1B OS=Homo sapiens OX=9606 GN=MAP1B PE=1 SV=2	**0,518678487**	3,311240321
E9PHZ5	Cathepsin B OS=Homo sapiens OX=9606 GN=CTSB PE=1 SV=9	**0,5186117**	2,537455738
Q9Y5M8	Signal recognition particle receptor subunit beta OS=Homo sapiens OX=9606 GN=SRPRB PE=1 SV=3	**0,517099702**	**0,271545952**
P06744	Glucose-6-phosphate isomerase OS=Homo sapiens OX=9606 GN=GPI PE=1 SV=4	**0,511632592**	5,194485981

O43707	Alpha-actinin-4 OS=Homo sapiens OX=9606 GN=ACTN4 PE=1 SV=2	0,497510999	2,387900615
F5H5D3	Tubulin alpha chain OS=Homo sapiens OX=9606 GN=TUBA1C PE=1 SV=1	0,497400477	0,888397805
Q13409	Cytoplasmic dynein 1 intermediate chain 2 OS=Homo sapiens OX=9606 GN=DYNC1I2 PE=1 SV=3	0,485625175	0,194577644
Q9H0U4	Ras-related protein Rab-1B OS=Homo sapiens OX=9606 GN=RAB1B PE=1 SV=1	0,484344769	9,060039783
P16989	Y-box-binding protein 3 OS=Homo sapiens OX=9606 GN=YBX3 PE=1 SV=4	0,484093251	1,556817491
A0A087X020	Ribosome maturation protein SBDS OS=Homo sapiens OX=9606 GN=SBDS PE=1 SV=1	0,468808633	1,360425588
P30837	Aldehyde dehydrogenase X, mitochondrial OS=Homo sapiens OX=9606 GN=ALDH1B1 PE=1 SV=3	0,467630256	0,590470708
P31949	Protein S100-A11 OS=Homo sapiens OX=9606 GN=S100A11 PE=1 SV=2	0,461441656	23,38553021
J3QQ67	60S ribosomal protein L18 (Fragment) OS=Homo sapiens OX=9606 GN=RPL18 PE=1 SV=1	0,456531789	9,221095688
A0A7P0T9C4	Cytoplasmic dynein 1 heavy chain 1 OS=Homo sapiens OX=9606 GN=DYNC1H1 PE=1 SV=1	0,453623194	1,543942838
O14773	Tripeptidyl-peptidase 1 OS=Homo sapiens OX=9606 GN=TPP1 PE=1 SV=2	0,435859662	0,684516304
P36543	V-type proton ATPase subunit E 1 OS=Homo sapiens OX=9606 GN=ATP6V1E1 PE=1 SV=1	0,434354914	0,157416616
Q15293	Reticulocalbin-1 OS=Homo sapiens OX=9606 GN=RCN1 PE=1 SV=1	0,433241549	0,788847396
Q9Y570	Protein phosphatase methylesterase 1 OS=Homo sapiens OX=9606 GN=PPME1 PE=1 SV=3	0,432153648	0,413158375
P05455	Lupus La protein OS=Homo sapiens OX=9606 GN=SSB PE=1 SV=2	0,431909626	6,179009707

F8W6I7	Helix-destabilizing protein OS=Homo sapiens OX=9606 GN=HNRNPA1 PE=1 SV=2	0,425305275	12,88496538
O60664	Perilipin-3 OS=Homo sapiens OX=9606 GN=PLIN3 PE=1 SV=3	0,410032832	4,424696679
P32119	Peroxiredoxin-2 OS=Homo sapiens OX=9606 GN=PRDX2 PE=1 SV=5	0,409295924	2,647655419
B0YIW6	Coatomer subunit delta OS=Homo sapiens OX=9606 GN=ARCN1 PE=1 SV=1	0,402768599	2,184546597
Q9UBQ7	Glyoxylate reductase/hydroxypyruvate reductase OS=Homo sapiens OX=9606 GN=GRHPR PE=1 SV=1	0,401638337	3,084695375
P30044	Peroxiredoxin-5, mitochondrial OS=Homo sapiens OX=9606 GN=PRDX5 PE=1 SV=4	0,39827001	0,648527837
P40123	Adenylyl cyclase-associated protein 2 OS=Homo sapiens OX=9606 GN=CAP2 PE=1 SV=1	0,387956229	1,599766452
Q6IAA8	Ragulator complex protein LAMTOR1 OS=Homo sapiens OX=9606 GN=LAMTOR1 PE=1 SV=2	0,378027278	0,533751601
P68371	Tubulin beta-4B chain OS=Homo sapiens OX=9606 GN=TUBB4B PE=1 SV=1	0,376295561	0,66086742
P54727	UV excision repair protein RAD23 homolog B OS=Homo sapiens OX=9606 GN=RAD23B PE=1 SV=1	0,37098755	1,911373899
P61158	Actin-related protein 3 OS=Homo sapiens OX=9606 GN=ACTR3 PE=1 SV=3	0,357915451	6,580190333
P52907	F-actin-capping protein subunit alpha-1 OS=Homo sapiens OX=9606 GN=CAPZA1 PE=1 SV=3	0,35212396	1,369282846
Q9C0H2	Protein tweety homolog 3 OS=Homo sapiens OX=9606 GN=TTYH3 PE=1 SV=3	0,348086826	0,94013751
Q14764	Major vault protein OS=Homo sapiens OX=9606 GN=MVP PE=1 SV=4	0,323852806	0,896901195

O00231	26S proteasome non-ATPase regulatory subunit 11 OS=Homo sapiens OX=9606 GN=PSMD11 PE=1 SV=3	0,321633098	2,687837614
P11216	Glycogen phosphorylase, brain form OS=Homo sapiens OX=9606 GN=PYGB PE=1 SV=5	0,316018245	5,359457154
O00764	Pyridoxal kinase OS=Homo sapiens OX=9606 GN=PDXK PE=1 SV=1	0,310606496	1,294818391
P04843	Dolichyl-diphosphooligosaccharide--protein glycosyltransferase subunit 1 OS=Homo sapiens OX=9606 GN=RPN1 PE=1 SV=1	0,307454312	0,224799989
Q8IVF2	Protein AHNAK2 OS=Homo sapiens OX=9606 GN=AHNAK2 PE=1 SV=2	0,30421262	0,785681986
J3QRS3	Myosin regulatory light chain 12A OS=Homo sapiens OX=9606 GN=MYL12A PE=1 SV=1	0,303261122	2,512616893
E9PGC8	Microtubule-associated protein 1A OS=Homo sapiens OX=9606 GN=MAP1A PE=1 SV=1	0,277679205	0,100170811
P10768	S-formylglutathione hydrolase OS=Homo sapiens OX=9606 GN=ESD PE=1 SV=2	0,253331128	2,180310976
P28074	Proteasome subunit beta type-5 OS=Homo sapiens OX=9606 GN=PSMB5 PE=1 SV=3	0,226047775	11,35991011
A0A1W2PRS1	Lysosome membrane protein 2 (Fragment) OS=Homo sapiens OX=9606 GN=SCARB2 PE=1 SV=1	0,208456654	0,676346604
Q9BUF5	Tubulin beta-6 chain OS=Homo sapiens OX=9606 GN=TUBB6 PE=1 SV=1	0,202715603	0,462070991
P46940	Ras GTPase-activating-like protein IQGAP1 OS=Homo sapiens OX=9606 GN=IQGAP1 PE=1 SV=1	0,196500614	6,428451773
P05387	60S acidic ribosomal protein P2 OS=Homo sapiens OX=9606 GN=RPLP2 PE=1 SV=1	0,196321933	18,05812773
P39656	Dolichyl-diphosphooligosaccharide--protein glycosyltransferase 48 kDa	0,193809358	1,243966954

	subunit OS=Homo sapiens OX=9606 GN=DDOST PE=1 SV=4		
Q9NYL9	Tropomodulin-3 OS=Homo sapiens OX=9606 GN=TMOD3 PE=1 SV=1	0,192788538	0,687802232
Q13885	Tubulin beta-2A chain OS=Homo sapiens OX=9606 GN=TUBB2A PE=1 SV=1	0,190535457	0,903243904
O15511	Actin-related protein 2/3 complex subunit 5 OS=Homo sapiens OX=9606 GN=ARPC5 PE=1 SV=3	0,187475913	5,240872165
P50502	Hsc70-interacting protein OS=Homo sapiens OX=9606 GN=ST13 PE=1 SV=2	0,167253845	3,372123314
Q16881	Thioredoxin reductase 1, cytoplasmic OS=Homo sapiens OX=9606 GN=TXNRD1 PE=1 SV=3	0,157450487	0,832144006
P07686	Beta-hexosaminidase subunit beta OS=Homo sapiens OX=9606 GN=HEXB PE=1 SV=3	0,120956848	0,169223267
Q13509	Tubulin beta-3 chain OS=Homo sapiens OX=9606 GN=TUBB3 PE=1 SV=2	0,117039813	3,666227539
Q15181	Inorganic pyrophosphatase OS=Homo sapiens OX=9606 GN=PPA1 PE=1 SV=2	0,109264748	2,887946341
Q13492	Phosphatidylinositol-binding clathrin assembly protein OS=Homo sapiens OX=9606 GN=PICALM PE=1 SV=2	0,104774637	1,286607531
M0QXB4	Coatomer subunit epsilon OS=Homo sapiens OX=9606 GN=COPE PE=1 SV=1	0,072672383	1,711712012

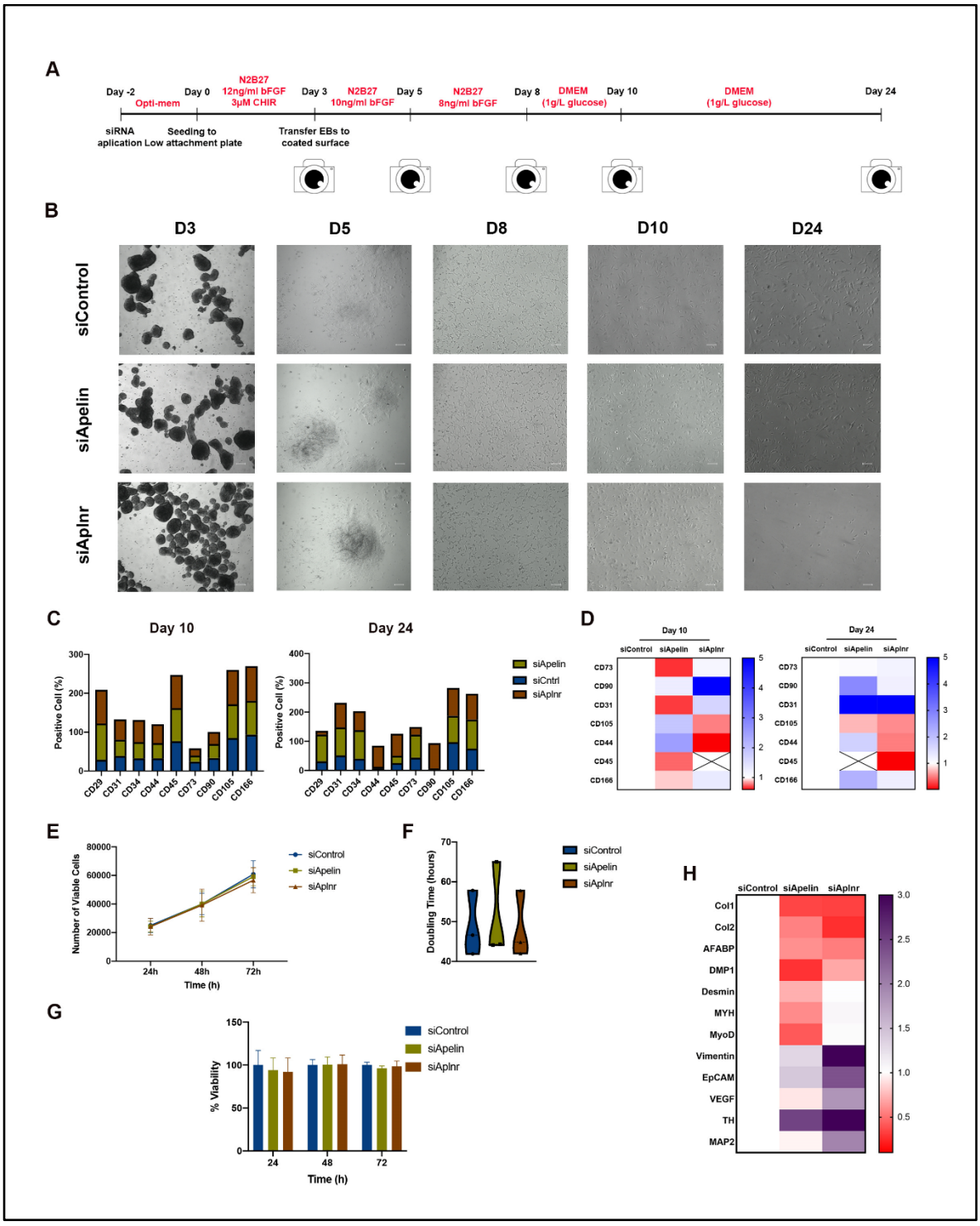


Figure 3.56. Silencing Aplnr Signaling Components by siRNA Treatment Hinders MSC Differentiation from hESCs. A. The 24 days protocol for MSC differentiation from hESC. B. Morphological pictures taken at day 3, day 5, day 8, day 10 and day24 during MSC differentiation from Control siRNA, Apelin siRNA and Aplnr siRNA treated cells. C. MSC markers were detected with flow cytometry analysis and a graphic was drown showing the positive cells for the markers. D. Heatmap visualization of mRNA expression

levels for MSC markers at day 10 and day 24. E. Viable cells were counted with Trypan Blue staining and F. Cell duplication time was calculated for the differentiated cells. G. Cell viability was measured and represented with a bar graph for the differentiated cells. H. Intensities of the protein expressions were measured from the immunofluorescence images and represented as a heatmap. Scale bar: 200µm. *P<0.0001

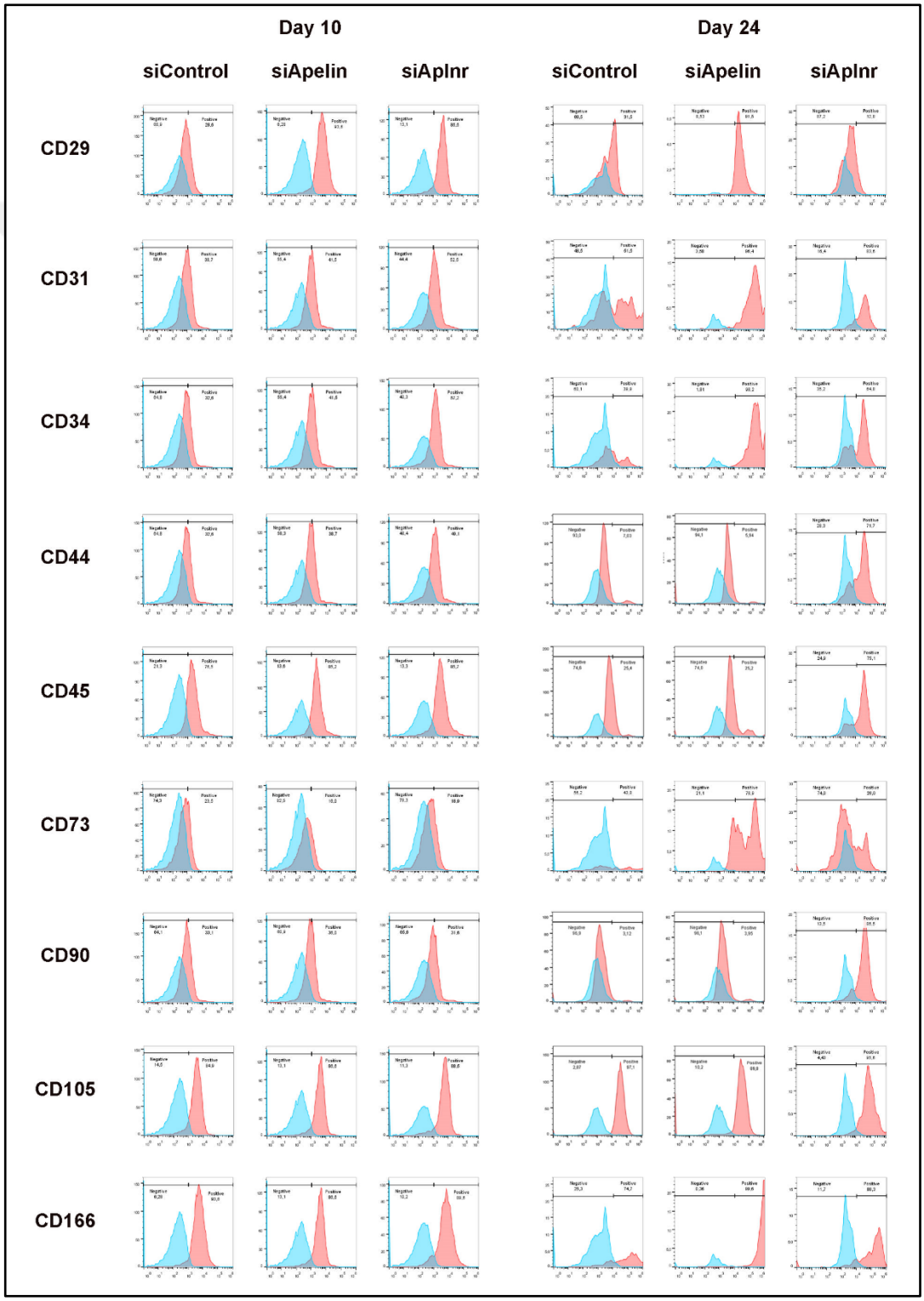


Figure 3.57. Characterization of hESC derived MSCs when Aplnr Signaling Pathway Components were Silenced via siRNA. Flow cytometry analysis of mesenchymal stem cell marker expression and hematopoietic marker expression on hESCs during MSC differentiation at day 10 and day 24. Differentiated hESCs, which were silenced with Control siRNA, Apelin siRNA and Aplnr siRNA, were compared.

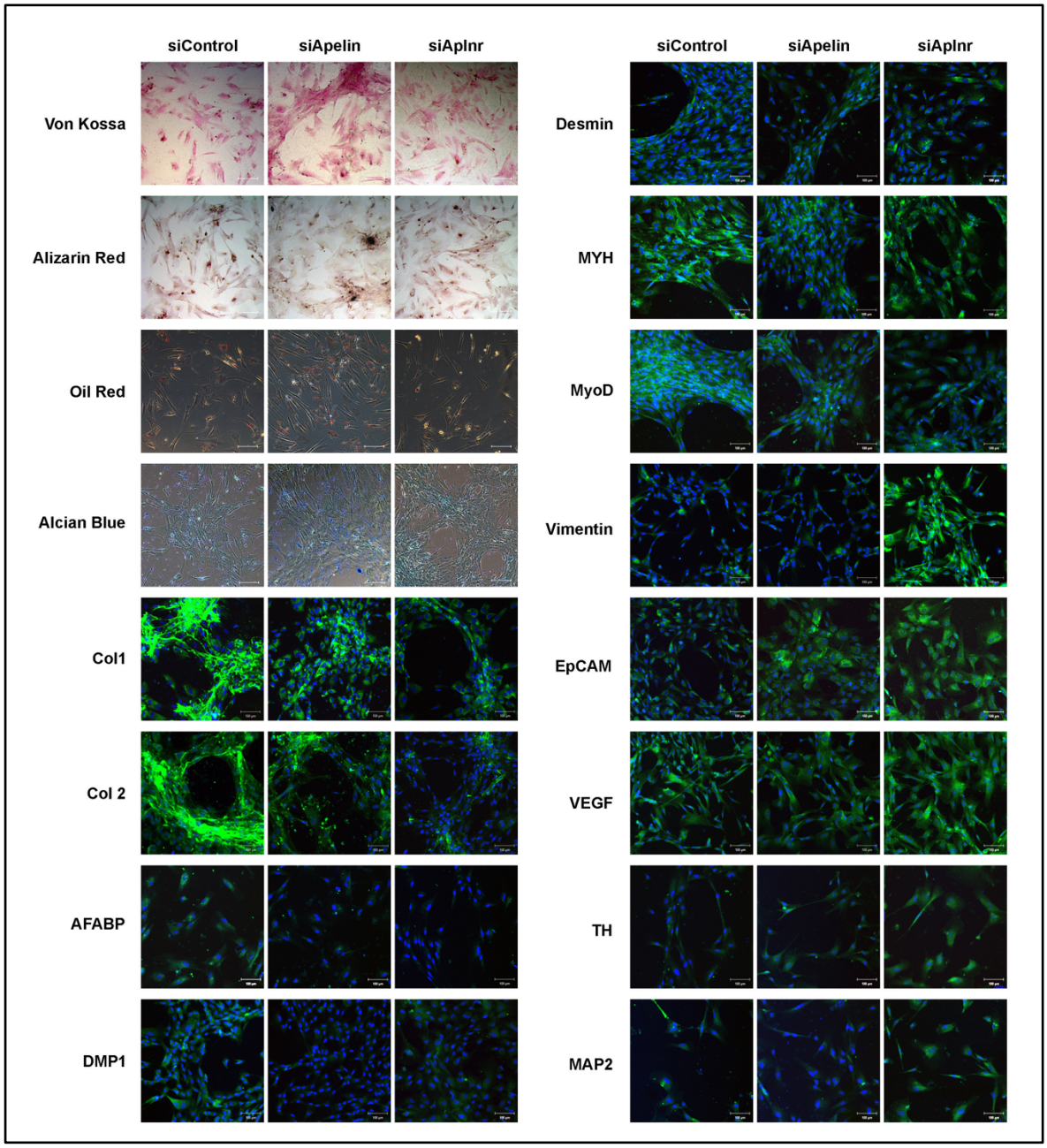


Figure 3.58. Differentiation of hESC derived MSCs into multiple cell types when Aplnr signaling pathway components were silenced via siRNA. Osteogenic differentiation was shown with von Kossa staining, alizarin red staining and Col1 immunostaining. Oil red O

staining and AFABP immunostaining represented adipogenic differentiation. Chondrogenic differentiation was visualized with alcian blue staining and Col2 immunostaining. DMP1 immunostaining was shown to visualize odontogenic differentiation. Desmin, MyoD and MYH immunostainings were performed after myogenic differentiation. Neurogenic differentiation was shown by TH and MAP2 immunostainings. Endothelial differentiation was visualized by VEGF immunostainings. Immunostainings for Vimentin and EpCAM was performed for epithelial differentiation. Scale Bar: 100µm.

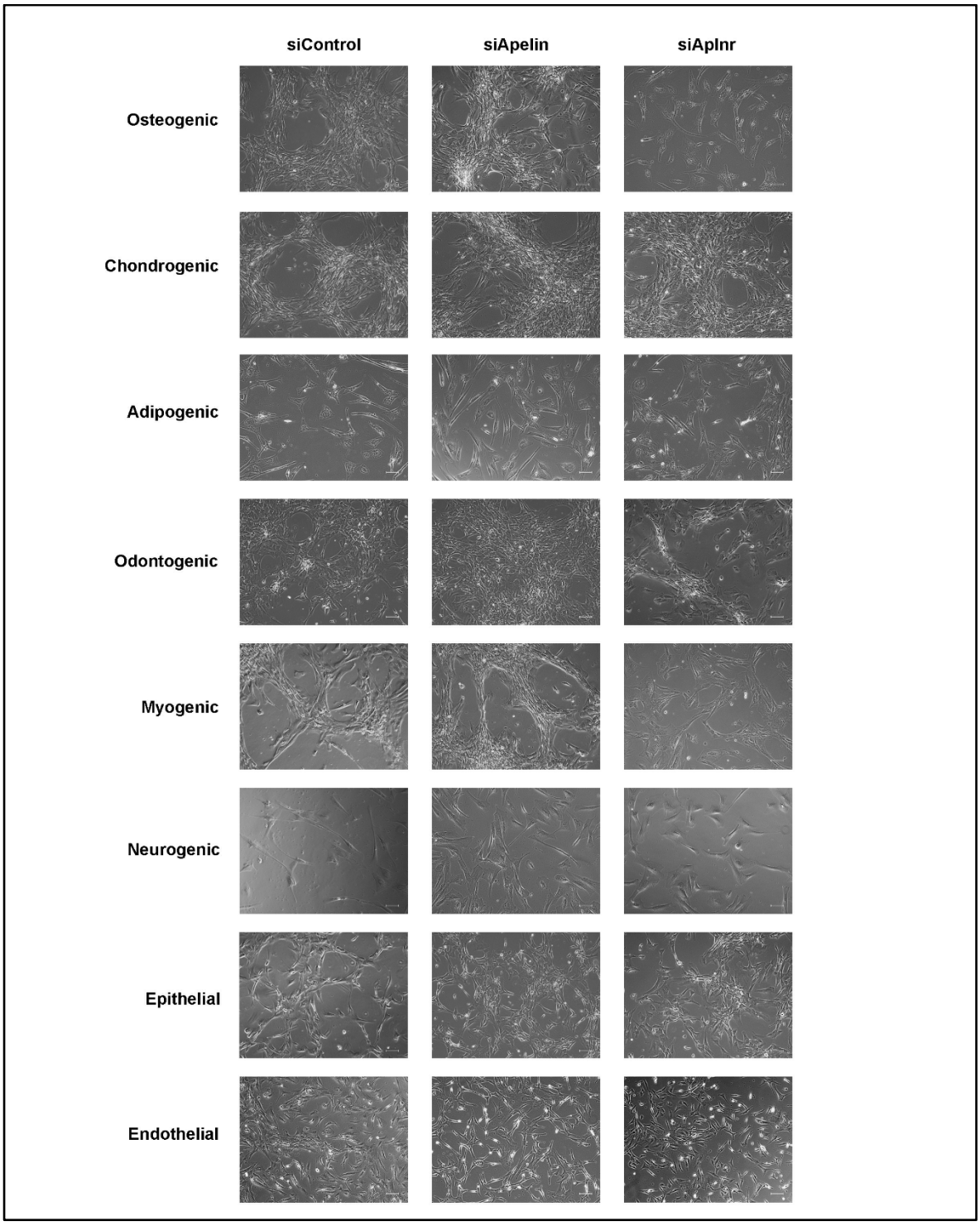


Figure 3.59. Morphology of Multiple Cell Type Differentiation from hESC derived MSCs when Aplnr Signaling Pathway Components were silenced via siRNA. MSCs, which were derived from Control, Apelin and Aplnr siRNA treated hESC, were compared with each other in terms of multiple differentiation capacity. Cell morphology after osteogenic, chondrogenic, adipogenic, odontogenic, myogenic, neurogenic, epithelial and endothelial differentiations were demonstrated. Scale Bar: 100µm.

Lastly, Apelin, Aplnr and Elabela overexpressing cells differentiated according to MSC differentiation protocol to analyze deeper the effect of Aplnr signaling on MSC differentiation (Figure 3.60A) and morphological pictures were taken at day 3, day 5, day 8, day 10 and day 24 (Figure 3.60B). Interestingly, all the groups were only positive for CD73, CD105 and CD166 (Figure 3.60C and 3.61). According to mRNA expression data at day 24, CD73 and CD90 expressions were upregulated and CD31 and CD45 expression levels were downregulated in Apelin oe and Aplnr oe groups compared to control group. Interestingly, Elabela expressed all markers less than control group (Figure 3.60D). Although control and Apelin oe cells were similar in terms of viability and proliferation, Aplnr oe and Elabela oe cells had significantly higher viability and proliferation rate compared to the others (Figure 3.60E, 3.60F and 3.60G). Furthermore, Apelin oe , Aplnr oe and Elabela oe cells were more capable of adipogenic, chondrogenic, osteogenic, myogenic, endothelial and odontogenic differentiation compared to control cells. Apelin oe group expressed Col1, Col2, AFABP, Desmin and MYH proteins 1.4-fold, 3.5-fold, 1.2-fold, 1.3-fold and 1.1-fold, respectively, higher than Control group, but expression of Vimentin, EpCAM, VEGF, TH and MAP2 in Apelin oe group were expressed 1.1-fold, 1.4-fold, 1.3-fold, 1.1-fold and 1.3-fold, respectively, lower in the control group. Protein expression of Col1, Col2, AFABP, DMP1, Desmin, MYH, MyoD and VEGF were enhanced 3.8-fold, 2.8-fold, 1.2-fold, 1.2-fold, 2.5-fold, 2-fold, 1.2-fold and 1.9-fold, respectively and expression of MAP2 reduced 1.1-fold in Aplnr oe group compared to the expression levels in control group. For Elabela oe group, while expression of Col1, Col2, AFABP, Desmin, MyoD and VEGF increased 6.9-fold, 4.1-fold, 1.2-fold, 1.5-fold, 1.2-fold and 2-fold, respectively, expression of EpCAM, TH and MAP2 reduced approximately 1.4-fold compared to the expression levels in control group (Figure 3.60H, 3.62, 3.63 and 3.64). According to PCR results, control oe and Aplnr oe group expressed E-cadherin higher than MSCs but less than Hacat after epithelial differentiation. After endothelial differentiation, V-cadherin expression level was significantly upregulated in Apelin oe, Aplnr oe and Elabela oe groups compared to Control, MSC and Huvec. All overexpression groups expressed osteocalcin after osteogenic differentiation, Aggrecan after chondrogenic differentiation, Adiponectin after adipogenic differentiation, DSPP after odontogenic differentiation, α-sma after myogenic differentiation and B-tubulin after neurogenic differentiation significantly higher than control and MSC groups (Figure 3.54).

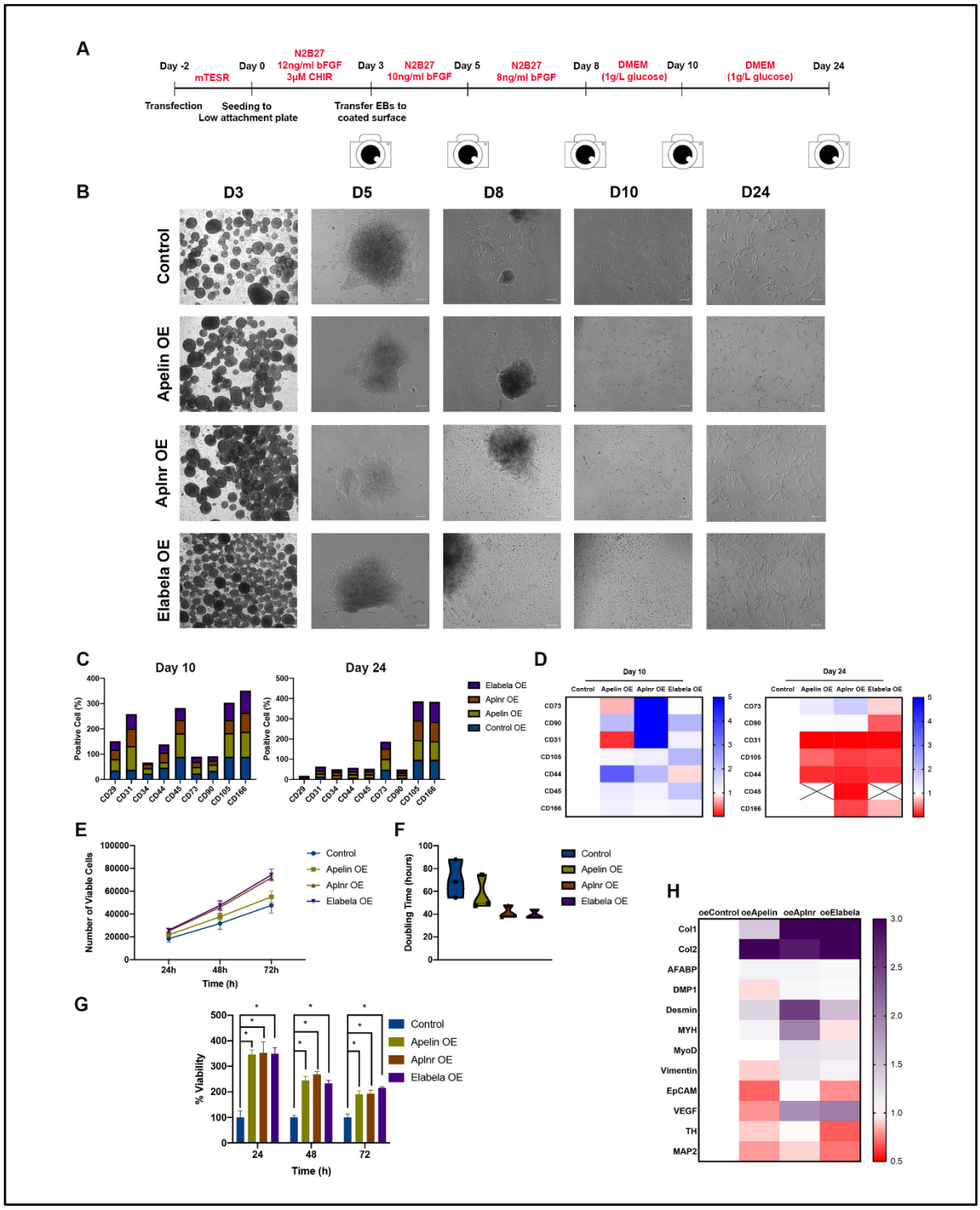


Figure 3.60. Overexpression of Aplnr Signaling Components Enhances MSC Differentiation from hESCs. A. The 24 days protocol for MSC differentiation from hESC. B. Morphological pictures taken at day 3, day 5, day 8, day 10 and day 24 during MSC differentiation from Control, Apelin overexpressing, Aplnr overexpressing and Elabela overexpressing cells. C. MSC markers were detected with flow cytometry analysis and a graphic was drown showing the positive cells for the markers. D. Heatmap visualization of

mRNA expression levels for MSC markers at day 10 and day 24. E. Viable cells were counted with Trypan Blue staining and F. Cell duplication time was calculated for the differentiated cells. G. Cell viability was measured and represented with a bar graph for the differentiated cells. H. Intensities of the protein expressions were measured from the immunofluorescence images and represented as a heatmap. Scale bar: 200µm. *P<0.0001

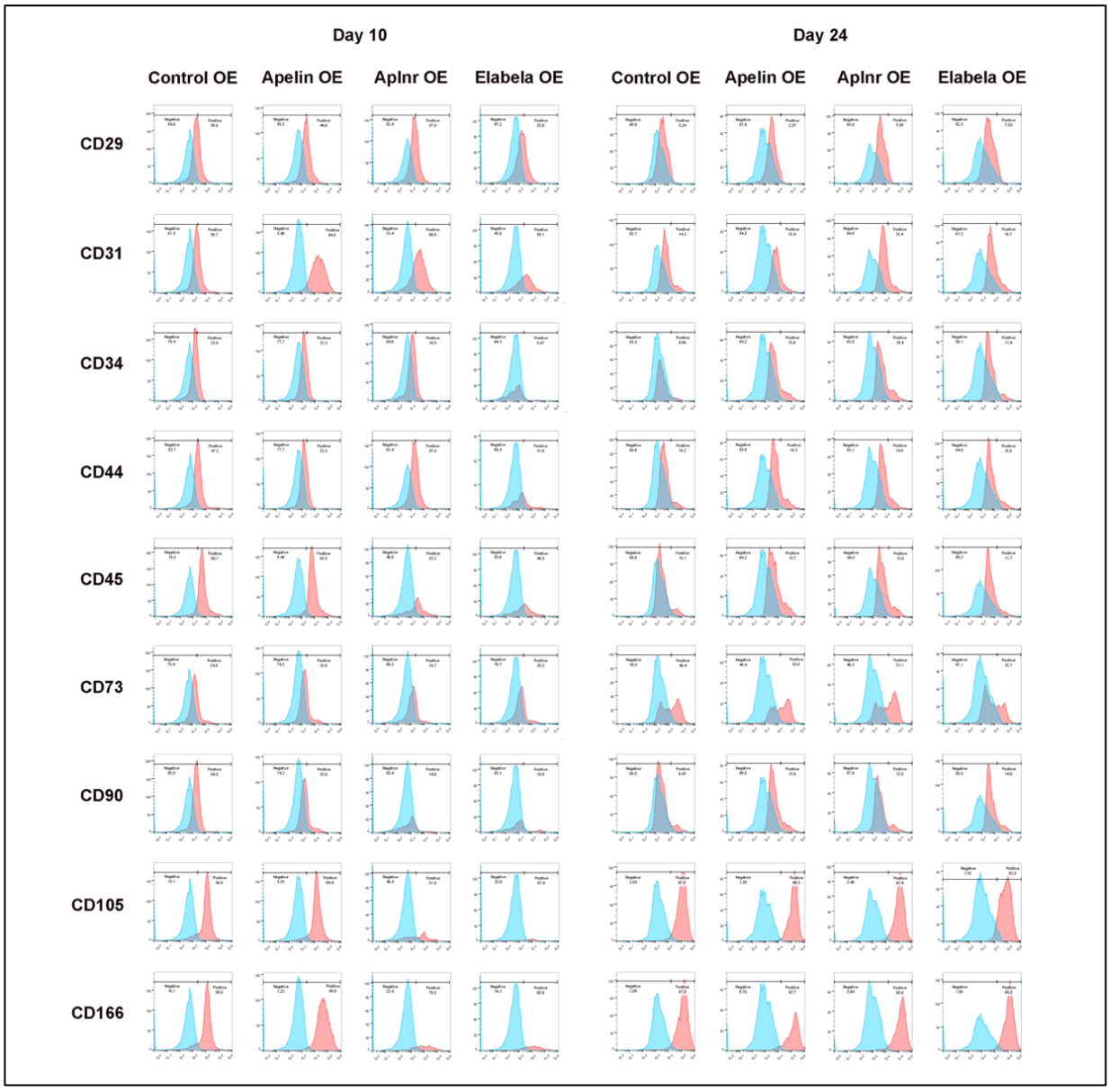


Figure 3.61. Characterization of hESC derived MSCs when Aplnr Signaling Pathway Components were overexpressed. Flow cytometry analysis of mesenchymal stem cell marker expression and hematopoietic marker expression on hESC during MSC differentiation at day 10 and day 24. Differentiated hESCs, which were transfected with Apelin, Aplnr and Elabela expressing lentiviral plasmids, were compared.

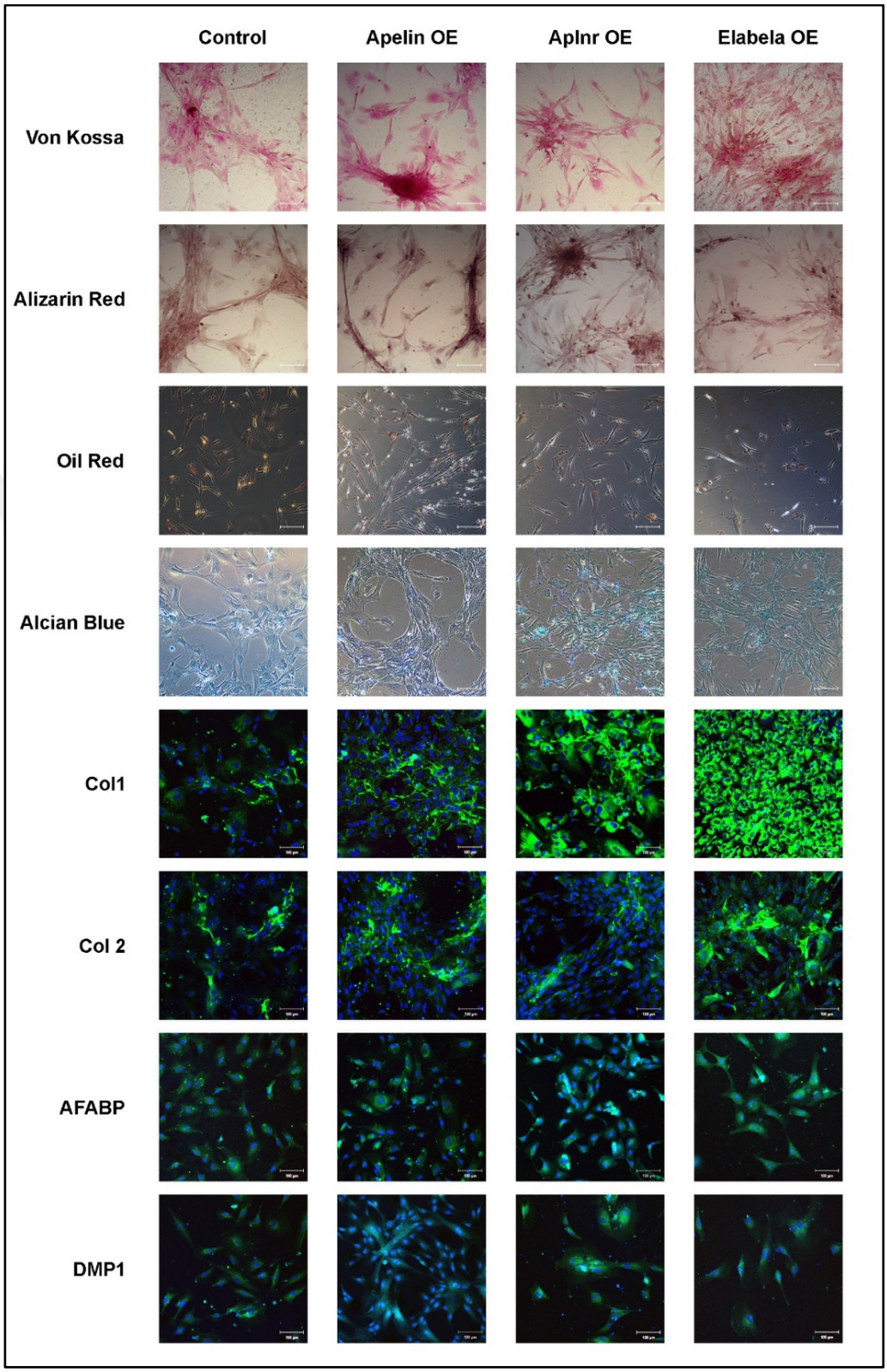


Figure 3.62. Differentiation of hESC derived MSCs into Ostegenic, Adipogenic, Chondrogenic and Odontogenic Cell Types when Aplnr Signaling Pathway Components were Overexpressed. Osteogenic differentiation was shown with von Kossa staining,

alizarin red staining and Col1 immunostaining. Oil red O staining and AFABP immunostaining represented adipogenic differentiation. Chondrogenic differentiation was visualized with alcian blue staining and Col2 immunostaining. DMP1 immunostaining was shown to visualize odontogenic differentiation. Scale Bar: 100μm.

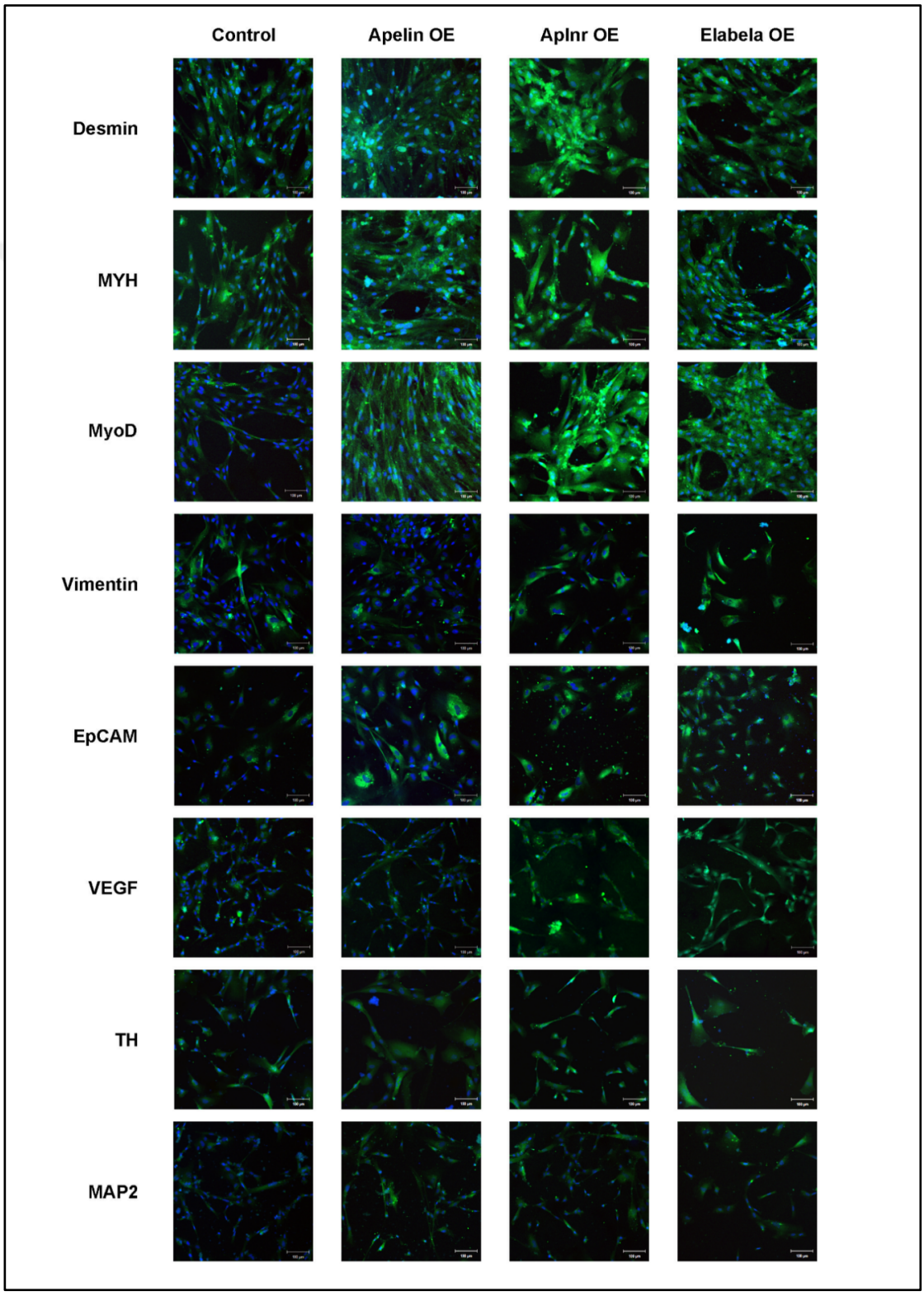


Figure 3.63. Differentiation of hESC derived MSCs into Epithelial, Endothelial, Myogenic and Neurogenic Cell Types when Aplnr Signaling Pathway Components were Overexpressed. Desmin, MyoD and MYH immunostainings were performed after myogenic differentiation. Neurogenic differentiation was shown by TH and MAP2 immunostainings. Endothelial differentiation was visualized by VEGF immunostainings. Immunostainings for Vimentin and EpCAM was performed for epithelial differentiation. Scale Bar: 100µm.

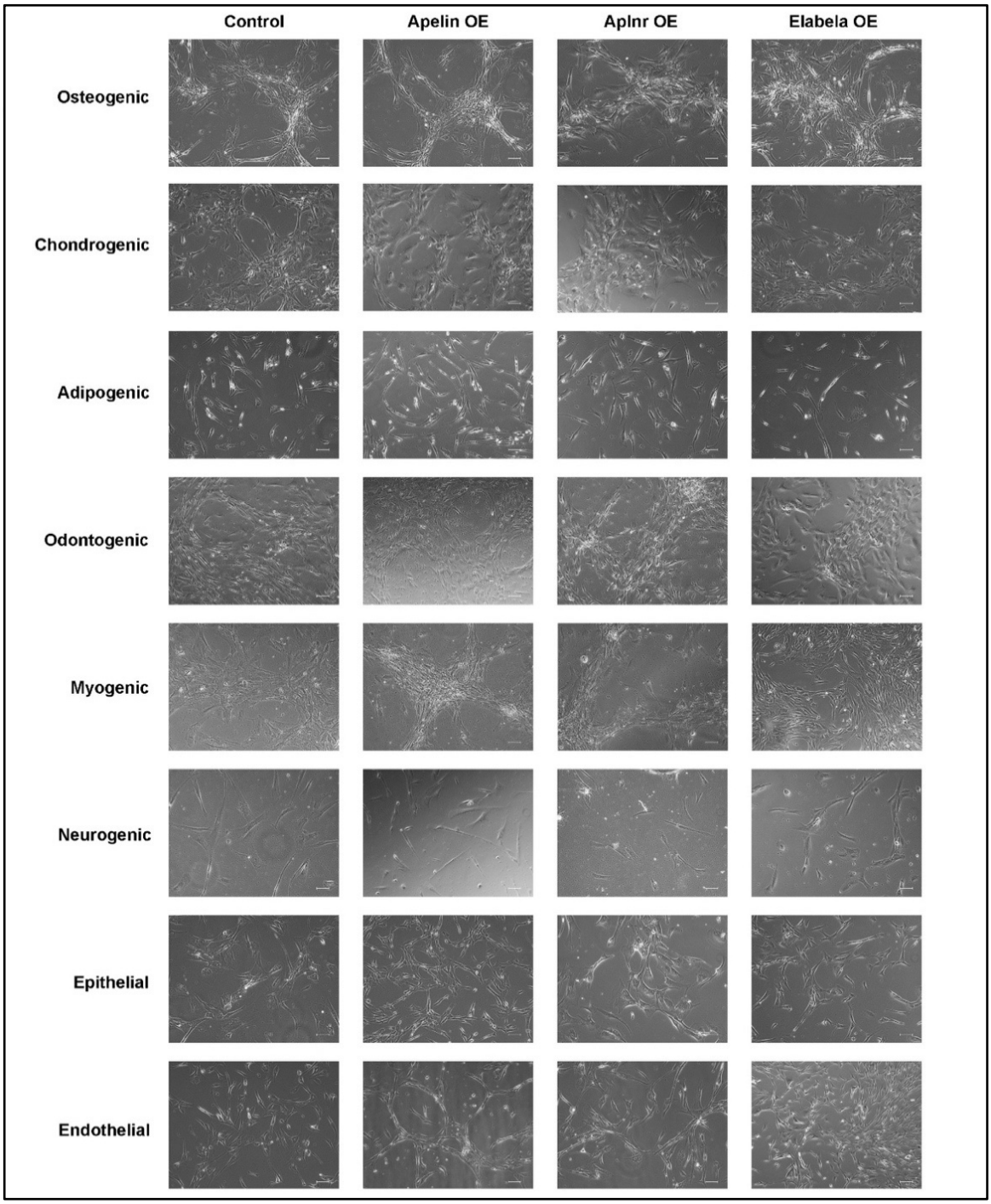


Figure 3.64. Morphology of Multiple Cell Type Differentiation from hESC derived MSCs when Aplnr Signaling Pathway Components were Overexpressed. MSCs, which were derived from Control, Apelin, Aplnr and Elabela overexpressing hESC, were compared with each other in terms of multiple differentiation capacity. Cell morphology after osteogenic, chondrogenic, adipogenic, odontogenic, myogenic, neurogenic, epithelial and endothelial differentiations were demonstrated. Scale Bar: 100µm.

To sum up, activity of Aplnr signaling not only improves MSC differentiation from hESC, but also enhance viability, proliferation and differentiation capacity of the MSCs. Furthermore, protein profiling and mRNA analysis reveal that Aplnr signaling show its effects via numerous signaling pathways, such as EGFR, TGF-beta, Wnt, PDGF and FGF signaling pathways to act on MSC differentiation.

3.2.4. Aplnr Signaling is Require for Modulation of Migration Rate During Mesoderm Differentiation and Cell Survival During MSC Differentiation of hESC-derived EBs.

To investigate direct effect of Aplnr on mesoderm cell migration and MSC differentiation, various media compositions (Figure 3.65A) were used to select the most and the least Aplnr positive populations and their differentiation to MSCs were observed. Morphological images of the EBs were taken at day 2, day 3 and day 6 during migration and mesoderm differentiation of EBs (Figure 3.65B). Migration area and migration intensity of Option I EBs and Option III EBs were significantly higher compared to others, while Option VI EBs possessed the smallest migration area and the lowest migration intensity (Figure 3.65C and 3.65D). However, Option III and IV generated the least Aplnr positive population whereas the highest amount of Aplnr positive cells were obtained from Option V and VI at day 2. At day 3, Option III had the lowest Aplnr positive population, while Option VI had the highest amount of Aplnr positive cells. Interestingly, low Aplnr positive population became high Aplnr positive population while high Aplnr positive populations reduced the Aplnr positive cell number at day 6 (Figure 3.65E and 3.65F). So, by considering these results, protocols for Option a and Option b were formulated to obtain MSCs from low Aplnr positive population and high Aplnr positive population, respectively (Figure 3.66A). However, while Option b, high Aplnr population, successfully differentiated into MSCs, Option a couldn’t

proliferate and lost cell viability. Option a cells were all dead after day 10 and morphological photos couldn't be taken (Figure 3.66B). So, Aplnr rich cell populations migrate slower than Aplnr poor populations. Furthermore, Aplnr expression is essential for survival, proliferation and differentiation of hESC-derived MSCs.

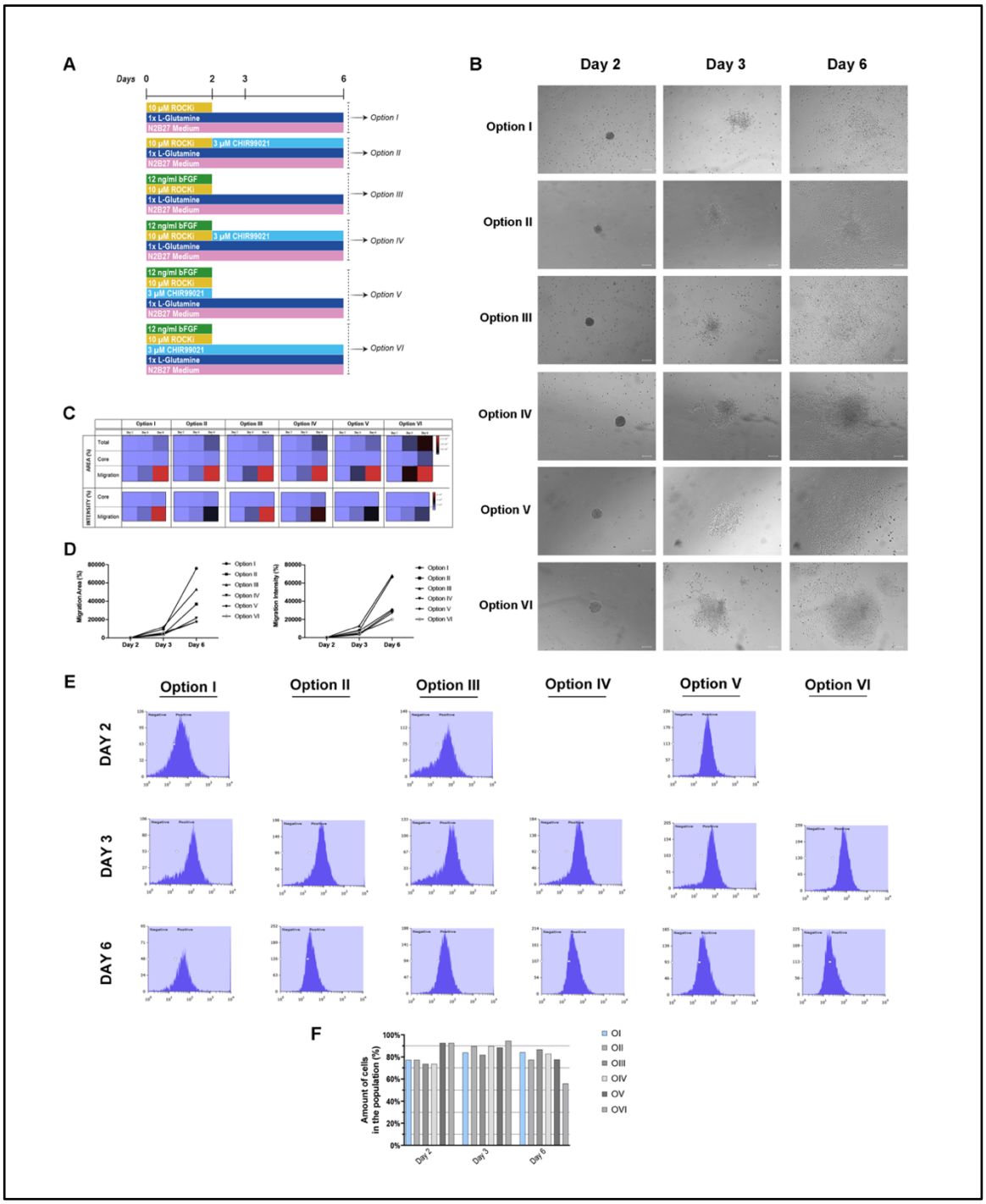


Figure 3.65. Selection of high and low Aplnr positive populations and their effect on migration of hESCs-derived EBs during mesoderm differentiation. A. Medium

supplements for each media options and timeline for mesoderm differentiation of H9 cells were shown. H9 cell-derived EBs were transferred to Matrigel-gelatin coated surface at day 2 and their migration were observed until day 6. B. Morphological pictures of the EBs were taken at day 2, day 3 and day 6. C. Total area, core area and migration area (total area-core area) as well as core intensity and migration intensity were measured at day 2, day 3 and day 6 and visualized as a heat map. D. Scattered line graphs of migration area and migration intensity at day 2, day 3 and day6 as well as bar graphs of total migration area and total migration intensity between day 6 and day 2 were drawn. E. The cells were fixed with 4% PFA at day 2, day 3 and day 6. Aplnr antibody was used, and the cells were examined with flow cytometry. F. Percentage of Aplnr positive cells in the populations were shown in the graph. Scale bar: 100µm.

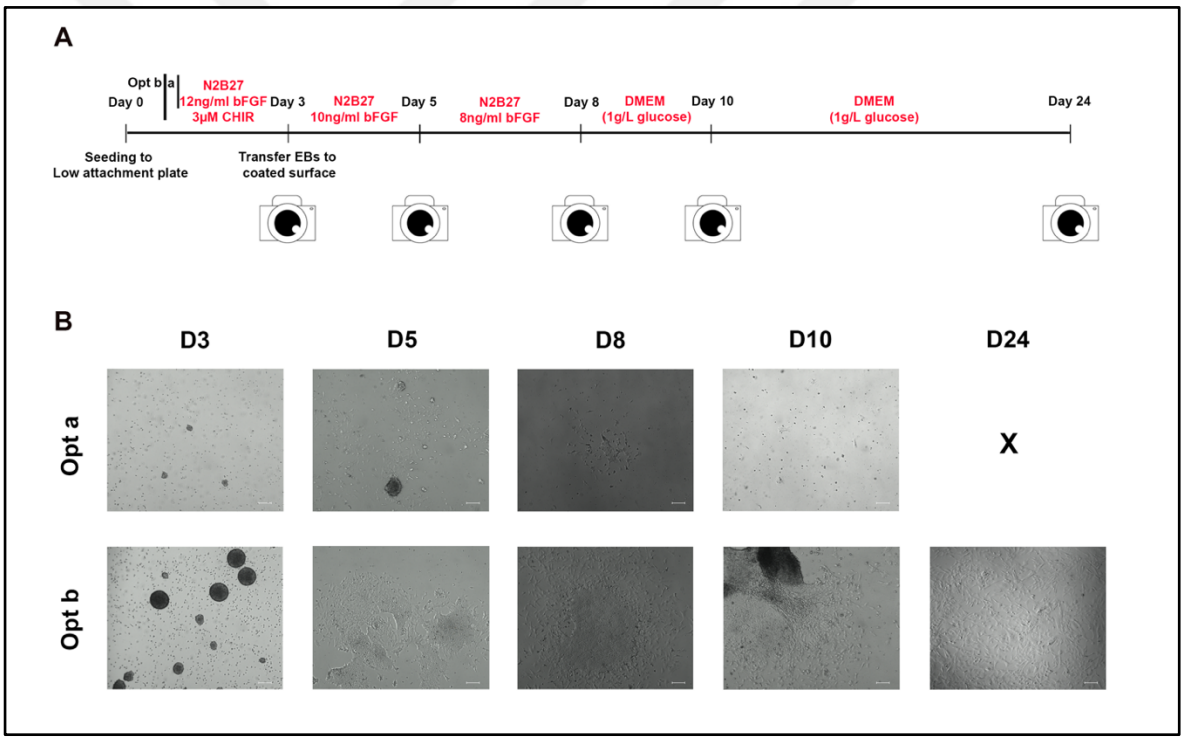


Figure 3.66. Reducing Aplnr Expression in hESC via Media Formulation caused Loss of Viability during MSC Differentiation. A. The 24 days protocol for MSC differentiation from hESC. Media formulation between day 0 and day 3 for Option a and Option b were selected to represent the lowest and the highest amount of Aplnr expressing population, respectively (Figure 3.65). B. Morphological pictures taken at day 3, day 5, day 8, day 10 and day 24 during MSC differentiation of the cells. Scale bar: 200µm.

4. DISCUSSION

4.1. MOUSE ESC-DERIVED MESODERM AND MSCS

Currently, cell-based therapies are focused on using MSCs as a tool to treat degenerative diseases of mesodermal origin. However, considering the limitations, such as obtaining enough cells for treatments, quality, safety, limited lifespan and rapid senescence of the cells, using alternative strategies for the treatments are require. Clinical approaches regarding *in vitro* recapitulation of mesoderm germ layer and derivation of the specific tissues to replace the damaged organ may overcome these obstacles. However, *in vitro* modeling of specified mesoderm from PSCs requires a great understanding of the signaling activities involving various pathways during germ layer formation and cell fate determination. Importance of Aplnr signaling on gastrulation movements, migration and mesoderm cell differentiation were previously reported [106,107,127,129]. However, a better understanding on its regulatory role during mesoderm differentiation is needed. In this study, our group tried to reveal the role of Aplnr signaling during mesoderm cell migration and differentiation from mESCs using *in vitro* EB-based method. In this process, activation of Aplnr signaling was carried out with Apelin-13 peptide and ML233, while silencing involved genetic modifications, including siRNA- and shRNA-mediated silencing as well as CRISPR Cas9 mediated KO of the Aplnr signaling components.

Regarding the migration potential of the EBs during mesoderm differentiation, the results indicated that silencing Apelin or Aplnr reduced total and migration area as wells as migration intensity regardless of the techniques used. However, although the effect was clear at day 3, it couldn't last until day 6 during siRNA mediated silencing of Apelin and Aplnr. Effect of shRNA mediated silencing of Apelin and Aplnr lasted until the end, day 6. Migration area and migration intensity of Apelin KO, Aplnr KO and Elabela KO EBs were far behind the ones of Wild Type cells. Although ML233 helped Apelin KO EBs to regain migration ability a bit, Apelin-13 couldn't do the job. Although ML233 and Apelin-13 significantly enhanced migration ability of the wild type cells, they weren't effective on Aplnr KO and Elabela KO EBs. These results are consistent with previous studies. Deshwar and colleagues reported that Nodal/TGFβ signaling, a key pathway for induction of mesendoderm and migration, is induced by Aplnr during Zebrafish gastrulation [131]. Also,

Aplnr signaling was reported as a positive regulator of cell movement in fibroblast cells [179]. For the Aplnr KO case, it is as expected since the receptor is not working. The case for Ela KO EBs may be that lack of Elabela drove the cells to express Apelin peptide to keep the signaling active. In this case, adding Apelin-13 peptide may induce feedback mechanism to reduce Apelin-13. This can also explain the reduced migration intensity after adding Apelin-13 or ML233. Also, significantly increased gene expression of Apelin at day 6 in Elabela KO EBs and its significant reduction after administration of Apelin-13 support the idea. Moreover, according to LC/MS protein profiling data Apelin-13 treatment enhanced migration related proteins such as Vimentin and integrin signaling proteins.

To generate more Aplnr positive mesoderm cell populations, various media options were tried. Option I and Option III media applied EBs formed neural rosette structure at the core with growing out neurites and highly expressed neural rosette markers, OTX1, Pax3 and ZBTB16. Considering contribution of Wnt/β-catenin pathway on differentiation and patterning of neural development [180,181], it is expected that lack of CHIR, GSK3β inhibitor, in the medium caused constant Wnt activity, which induced neural differentiation in Option I and Option III media treated cells. Among the others, the cells in Option IV media expressed Pax3, paraxial mesoderm marker, generated more Aplnr+ cells compared to others and possessed mesoderm morphology. Also, Option IV media led to the largest core area among the others and high core intensity, indicating high proliferation rate. Moreover, migration intensity and migration area was also quite high at Option IV media treated EBs, indicating migration promoting role of Option IV media.

During the assessment of the effect of Aplnr signaling on mesoderm differentiation, expression of Flk1 [170], a lateral mesoderm marker, Pdgfrα, Bra, Meox1 and Pax1 [170], paraxial mesoderm markers, Sox2 and Nestin, ectoderm and early neural markers [182,183], Sox17, Cxcr4 and Foxa2, endoderm markers, Apelin, Aplnr and FGF signaling pathway components were taken into consideration. Activating Aplnr signaling via small molecules led to increased expression of some mesoderm markers and reduced expression endoderm markers in EBs at day 6. Expression of Cxcr4 [184,185], Sox17 [186] and Foxa2 [187] in mesoderm cells were also reported in previous studies. It was suggested that Cxcr4 is expressed in migrating mesoderm and definitive endoderm in early development of mouse [185]. Sox17 was found to be required for cardiac mesoderm formation and specification during mammalian embryogenesis [186]. Finally, Foxa2 was specified as a marker of early

mesodermal commitment [187]. Sox2 expression reduced at protein level in Apelin-13 treated group at day 3 and its expression was not observed at mRNA level in both control and Apelin-13 treated groups at day 6. Previous studies also reported expression of Aplnr in lateral plate mesoderm, paraxial mesoderm and intermediate mesoderm [188–190]. Moreover, deletion of Aplnr in Zebrafish embryo was reported to cause disruption of mesoderm formation [131,189]. Silencing Apelin or Aplnr via siRNA or shRNA, led to increase of ectoderm marker, Sox2, expression. Expression of lateral mesoderm marker, Flk1, reduced in shApelin and shAplnr treated EBs. Previous reports stated that Akt and MAPK signaling are induced during mesoderm differentiation and Akt signaling is required for neural crest differentiation [191,192]. Interestingly, Akt expression reduced with Aplnr signaling activation and it was enhanced when Aplnr signaling components were silenced according to day 3 IF data. On the other hand, MEK and ERK1/2 protein expression was enhanced after Aplnr signaling was induced with Apelin-13 or ML233 in Wild Type cells. Furthermore, according to protein profiling data, FGF/MAPK signaling pathway proteins were enhanced after induction of Aplnr signaling activity via Apelin-13 addition and antibody array data demonstrated increased expression of LIF with Apelin-13 treatment. These results suggest that Aplnr acts on FGF/MAPK signaling to induce mesoderm differentiation of the EBs.

Finally, MSCs were generated at day 10 from the mesoderm cells at day 6. By administering Apelin-13 between day 2 and day 3, their proliferation, survival and MSC differentiation ability were improved. mRNA and protein expression data as well as morphological analyses indicated that Aplnr signaling improves survival, proliferation, mesoderm and MSC differentiation of mESCs. MSCs, generated in the presence of Apelin-13, possessed higher expression of MSC positive markers and were more negative for hematopoietic markers compared to the control group. Interestingly, CD45 expression was observed in both control and Apelin-13 treated cells but, its expression was reduced in Apelin-13 treated group compared to control MSCs. Although positive expression of CD45 in MSC is an uncommon situation, Kaiser et al. showed that a small fraction of bone marrow derived MSCs originated from CD45+ and CD34+ population [193]. Also, silencing or knocking out any of the components of Aplnr signaling resulted in significantly reduced expression of MSC markers. Vodyanik and colleagues also showed that hESC-derived Aplnr+ mesodermal populations give rise to MSCs [143,194]. Moreover, activation of Aplnr signaling by addition of Apelin-

13, Option IV, improved osteogenic, adipogenic and chondrogenic differentiation of the MSCs. These results indicate the importance of Aplnr signaling as an indispensable player during MSC differentiation from mesoderm. Protein profiling data also supported the role of Aplnr signaling on survival, proliferation, differentiation and adherence.

In summary, Aplnr signaling promotes migration during germ layer formation and is an essential part of the signaling events during mesoderm differentiation from mESCs. Furthermore, Aplnr signaling positively regulates MSC differentiation from mesoderm tissue, most likely via FGF/MAPK pathway, and improves survival and proliferation of the cells.

Although mesoderm formation and tissue specification involves gradient activity of a complex signaling events, tissue his study will provide a steppingstone to find an efficient and a safe protocol to generate mesoderm tissue from PSCs with the aim of clinical use to treat degenerative diseases.

4.2. HUMAN ESC-DERIVED MESODERM AND MSCS

PSCs are able to proliferate indefinitely [195] and desired number of cells can be generated by obtaining mesoderm or MSCs from PSCs. MSCs hold a great promise for treatment of various injuries and its therapeutic applications accelerated in the last decade. However, to increase effect and sustainability of therapies for widely use, problems including limited lifespan, rapid senescence, insufficient cell number for treatment, functional decline and heterogeneity need to be solved. Generation of MSCs from indefinitely proliferating cells, such as PSCs, may be a way to get rid of most of these restraints. So, we revealed that activation of Aplnr signaling during generation of MSCs from PSC-derived mesoderm cells, which is considered as the major source of MSCs, enhanced viability, proliferation and differentiation capacity of the MSCs.

During mammalian embryonic development, lineage specification and early cell fate decision are mainly determined by gastrulation, which give rise to three germ layers [19]. In the course of gastrulation, mesoderm layer emanates by migration of epiblast cells, which undergo epithelial to mesenchymal transition (EMT), to primitive groove to form a new layer between hypoblast and epiblast [20,196]. Mesoderm layer give rise to various tissues,

including genital and urinary system [33], heart, blood vessels, endothelial cells, skeleton, somites, dermis, skeletal muscle, connective tissue [27,197], myocardium, hemangioblast and mesenchyme [32].

In this study, we investigated role of Aplnr signaling during MSC differentiation of hPSCs via mesoderm generation. Migration data revealed positive effect of Aplnr signaling on migration area and migration intensity of hESC-derived EBs on Matrigel-Gelatin coated plates during mesoderm differentiation. Our data was consistent with the previous studies, which emphasized the role of Aplnr signaling on gastrulation movements [107] and mesoderm cell migration during gastrulation of Zebrafish [129].

Antibody array data of hESC-derived mesoderm cells revealed that, activation of Aplnr signaling by Apelin-13 enhanced early mesodermal marker, PDGFRα [170,171], and mesoderm differentiation promoting proteins, including Activin proteins, TGF-beta 1, TGF-beta 3 [172,174,175], Cryptic [176], BMP proteins [177,178]. Co-expression of PDGFRα and Aplnr was also reported in mESC and hESC derived mesoderm cells [132,198,199]. Additionally, Deshwar and colleagues reported that Aplnr induces Nodal/TGF-beta signaling during gastrulation, which is required for mesoderm induction and migration [131]. Moreover, Frizzled 7 protein, a Wnt receptor, which was reported as a regulator of gastrulation movements, mesoderm induction as well as morphogenetic events [127,172,173], were also enhanced with Apelin-13 addition. This indicates the relationship between Aplnr signaling and Wnt pathway. Zhang and colleagues also previously reported Aplnr as Wnt target during hindgut differentiation of ESCs and suggested that Wnt-mediated expression of Aplnr is important for mesendodermal differentiation [127]. Moreover, as BMP proteins act through T/Bra and play role in determination of mesodermal cell [177,178], our PCR data showed that Apelin-13 and ML233 enhanced T/Bra expression and silencing Apelin or Aplnr led to downregulation of T/Bra. Furthermore, increased expression of mesoderm markers, Flk1, and reduced expression of neural marker, Sox2, even at day 3 with Aplnr signaling activity indicates early effect of Aplnr signaling in modulating signaling cascade in favor of mesoderm differentiation. Enrichment analysis of mRNA and miRNA sequencing for hESC-derived mesoderm cells also indicated that the proteins involved in developmental processes were enhanced with Aplnr signaling activation. Additionally, protein profiling data from LC/MS analysis targeted enhanced activity of EGFR and TGF-beta signaling pathways when Aplnr signaling was activated by Apelin-13.

Previous reports also mentioned that TGF-beta/Activin/Nodal signaling, Wnt signaling, FGF signaling and BMP signaling work together to induce mesoderm differentiation [48,49]. All these results consistently indicated that Aplnr signaling promotes mesoderm commitment of hESC-derived EBs by possibly through EGFR and TGF-beta signaling.

Since neural crest and mesoderm are the major source of MSCs [80,200,201], and MSCs were obtained from Aplnr+ precursor cells in bFGF (FGF2) dependent manner during differentiation from hESCs [142,143], we tried to obtain MSCs from hESC through bFGF dependent mesoderm differentiation. Our group and Wang et al. also previously successfully obtained MSC populations from hESCs [139,202]. In this report, hESCs were differentiated to MSCs through mesodermal progenitors and effect of Aplnr signaling was investigated in the process. Activation of Aplnr signaling by Apelin-13 during MSC differentiation led to increased expression of MSC markers in PCR and flow cytometry analysis. Interestingly overexpression of Apelin and Aplnr components led to downregulation of some MSC markers, including CD44, CD105 and CD166, together with hematopoietic markers. Since developmental process is complicated with various signaling oscillations, continuously over activating Aplnr signaling may affect the organization of other signaling pathways and result in differentiation to other cell types. Also, Elabela overexpression led to downregulation of all MSC and hematopoietic markers on mRNA level. Elabela originally expressed during gastrulation, and later restricted to notochord, mesoderm and endoderm [107]. Although, its expression was later detected in kidney, prostate and PSCs [108,203], it basically has role in early development and it is plausible that overexpression of Elabela during MSC differentiation from hPSCs failed the process. Proliferation and viability analysis showed that activation of Aplnr or overexpression of Aplnr components increased proliferation and viability, while reducing doubling time of the cells. Consistently, silencing or knocking out Aplnr components, reduced proliferation and viability of the cells, while increasing cell doubling time. Moreover, when low Aplnr expressing population was generated to differentiate MSCs, the cell couldn't proliferate and died long before completing the protocol for MSC differentiation. These data matches with previous reports stating role of Aplnr signaling in MSC proliferation, survival [144]. Furthermore, differentiation capacity of the cells was determined with multiple differentiation, including osteogenic, chondrogenic, adipogenic, odontogenic, myogenic, neurogenic, epithelial and endothelial differentiations. hPSC derived MSCs differentiated much better compared to characterized MSCs. Moreover,

activating Aplnr or overexpressing Aplnr components improved osteogenic, chondrogenic, adipogenic, odontogenic, endothelial and myogenic differentiation of the cells, while knocking out or silencing Aplnr components hindered osteogenic, chondrogenic, adipogenic, odontogenic and myogenic differentiation of the cells according to gene and protein expression data. On the other hand, while neurogenic differentiation was not significantly affected by Aplnr signaling activation, epithelial differentiation reduced when Aplnr components were overexpressed or repressed. Hang and colleagues also revealed that Aplnr signaling improved osteogenic differentiation of MSCs via Wnt signaling pathway *in vitro* [146]. Another report stated that Apelin contributes proliferation and neural differentiation of neural stem cell [147]. Also, knock down of Aplnr led to decreased cardiomyocyte differentiation from hESC and had detrimental effect on the contractility in 3D engineered heart tissues [204]. In addition to these data, protein profiling and mRNA analysis indicated that various signaling pathways, including EGFR, TGF-beta, Wnt, PDGF and FGF signaling pathways, were affected by Aplnr signaling during MSC differentiation.

In this study, we successfully obtained mesoderm and MSCs from hPSCs. Although generation of MSCs from indefinitely proliferating ESCs allow us to produce unlimited number of MSCs for therapeutic usage, our method has some limitations, including functional decline after freeze/thaw, heterogeneity, limited lifespan and rapid senescence. On the other hand, PSC-derived MSCs or mesoderm cells suits personalized cell therapy. Using patients own PSCs to generate MSCs or other specific cells get rid of the potential failure due to person-to-person differences, minimize the risk of adverse effects and enhances the therapeutic potential for the cell therapy. Our study revealed that Aplnr signaling positively regulates not only migration of mesoderm but also viability, proliferation and differentiation capacity of MSCs. Aplnr signaling might be a significant target for MSC-based or mesoderm-based cell therapy.

5. CONCLUSION

MSCs are invaluable resources for personalized medicine to treat the patients with the highest efficiency by using patient-specific cells. Aplnr signaling was reported to be involved in various biological events, including initiation of gastrulation, mesoderm cell migration, proliferation and differentiation of MSCs. However, our knowledge about the exact role and mechanism of Aplnr signaling during mesoderm and MSCs differentiation is still primitive. The goal of this study is generate mesodermal tissue, as a major source of MSCs, and MSCs from mESCs and hESCs with a high proliferation and differentiation capacity. Another purpose of this work is unveiling the role of Aplnr signaling during mesoderm and MSC differentiation from ESCs by using peptide/small molecule activation, overexpression, siRNA and shRNA mediated knock down or CRISPR Cas9 mediated knock out of the pathway components.

Overall data suggest that Aplnr signaling promote mesoderm commitment possibly via EGFR and TGF-beta signaling pathways and enhances migration of mESC- and hESC-derived EBs during mesoderm differentiation. Secondly, Aplnr signaling enhances MSCs differentiation from ESCs and increases cell viability, proliferation, MSC characteristics and differentiation capacity of MSCs by regulating various pathways, such as EGFR, TGF-beta, Wnt, PDGF and FGF signaling pathways. Moreover, osteogenic, chondrogenic, adipogenic and myogenic differentiations of MSCs were significantly enhanced with Aplnr signaling activity. Considering these findings, Aplnr signaling can be offered as a target to support derivation of MSCs from PSCs and its maintenance for cell therapy and regenerative medicine. This is the first study in the literature that uses Apelin-13 peptide during MSCs derivation from PSCs.

The methods and formulations used for generation of MSCs from PSCs were developed by our group and on the process of patenting (Application Number: 2022/003554).

REFERENCES

1. Lin NH, Gronthos S, Bartold PM. Stem cells and periodontal regeneration. Aust Dent J. 2008;53(2):108–21.

2. Mossahebi-Mohammadi M, Quan M, Zhang JS, Li X. FGF Signaling Pathway: A Key Regulator of Stem Cell Pluripotency. Frontiers in Cell and Developmental Biology. 2020.

3. Munsie MJ, Michalska AE, O'Brien CM, Trounson AO, Pera MF, Mountford PS. Isolation of pluripotent embryonic stem cells from reprogrammed adult mouse somatic cell nuclei. Curr Biol. 2000;

4. Reubinoff BE, Pera MF, Fong CY, Trounson A, Bongso A. Embryonic stem cell lines from human blastocysts: Somatic differentiation in vitro. Nat Biotechnol. 2000;

5. Smith A. Cell therapy: In search of pluripotency. Curr Biol. 1998;

6. Thomson JA, Itskovitz-eldor J, Shapiro SS, Michelle A, Swiergiel JJ, Marshall VS, et al. Embryonic Stem Cell Lines Derived from Human Blastocysts Published by : American Association for the Advancement of Science Stable URL : http://www.jstor.org/stable/2897366 Linked references are available on JSTOR for this article : Embryonic Stem Cell Li. Science (80-). 1998;282(5391):1145–7.

7. Takahashi K, Yamanaka S. Induction of Pluripotent Stem Cells from Mouse Embryonic and Adult Fibroblast Cultures by Defined Factors. Cell. 2006;

8. Takahashi K, Tanabe K, Ohnuki M, Narita M, Ichisaka T, Tomoda K, et al. Induction of Pluripotent Stem Cells from Adult Human Fibroblasts by Defined Factors. Cell. 2007;

9. Narsinh KH, Sun N, Sanchez-freire V, Lee AS, Almeida P, Hu S, et al. Single cell transcriptional profiling reveals heterogeneity of human induced pluripotent stem cells. J Clin Invest. 2011;121(3).

10. Zakrzewski W, Dobrzyński M, Szymonowicz M, Rybak Z. Stem cells: Past, present, and future. Stem Cell Research and Therapy. 2019.

11. Bartold M, Gronthos S, Haynes D, Ivanovski S. Mesenchymal stem cells and biologic factors leading to bone formation. J Clin Periodontol. 2019;

12. Bianco P, Robey PG, Simmons PJ. Mesenchymal Stem Cells: Revisiting History, Concepts, and Assays. Cell Stem Cell. 2008.

13. Dennis JE, Charbord P. Origin and Differentiation of Human and Murine Stroma. Stem Cells. 2002;20(3):205–14.

14. Prockop DJ. Marrow stromal cells as stem cells for nonhematopoietic tissues. Science. 1997.

15. Gronthos S, Mankani M, Brahim J, Robey PG, Shi S. Postnatal human dental pulp stem cells (DPSCs) in vitro and in vivo. Proc Natl Acad Sci U S A. 2000;97(25):13625–30.

16. Wagner W, Wein F, Seckinger A, Frankhauser M, Wirkner U, Krause U, et al. Comparative characteristics of mesenchymal stem cells from human bone marrow, adipose tissue, and umbilical cord blood. Exp Hematol. 2005;

17. Ng AP, Alexander WS. Haematopoietic stem cells: Past, present and future. Cell Death Discovery. 2017.

18. Şişli HB, Hayal TB, Seçkin S, Şenkal S, Kıratlı B, Şahin F, et al. Gene Editing in Human Pluripotent Stem Cells: Recent Advances for Clinical Therapies. Vol. 1237, Advances in Experimental Medicine and Biology. 2020.

19. Stern CD. Gastrulation: From Cells To Embryo [Internet]. 2004 [cited 2020 Jun 15]. Available from: http://www.gastrulation.org/

20. Antin PB, Kaur S, Stanislaw S, Davey S, Konieczka JH, Yatskievych TA, et al. Gallus expression in situ hybridization analysis: A chicken embryo gene expression database. In: Poultry Science. 2007.

21. Bachvarova RF, Skromne I, Stern CD. Induction of primitive streak and Hensen's node by the posterior marginal zone in the early chick embryo. Development. 1998;

22. Ferrer-Vaquer A, Viotti M, Hadjantonakis AK. Transitions between epithelial and mesenchymal states and the morphogenesis of the early mouse embryo. Cell

Adhesion and Migration. 2010.

23. Ferro V, Chuai M, McGloin D, Weijer CJ. Measurement of junctional tension in epithelial cells at the onset of primitive streak formation in the chick embryo via non-destructive optical manipulation. Dev. 2020;

24. Sumi T, Tsuneyoshi N, Nakatsuji N, Suemori H. Defining early lineage specification of human embryonic stem cells by the orchestrated balance canonical Wnt/β-catenin, activin/Nodal and BMP signaling. Development. 2008;

25. Kinder SJ, Tsang TE, Quinlan GA, Hadjantonakis AK, Nagy A, Tam PPL. The orderly allocation of mesodermal cells to the extraembryonic structures and the anteroposterior axis during gastrulation of the mouse embryo. Development. 1999;

26. Tam PPL, Loebel DAF. Gene function in mouse embryogenesis: Get set for gastrulation. Nature Reviews Genetics. 2007.

27. Keith L. Moore. Before We Are Born [Internet]. 2015. 1–1023 p. Available from: papers3://publication/uuid/5EA1AA7A-8B6E-424A-B367-0DC1E86B0C47

28. Grapin-Botton A. Endoderm specification. StemBook. 2008;

29. Kwon GS, Viotti M, Hadjantonakis AK. The Endoderm of the Mouse Embryo Arises by Dynamic Widespread Intercalation of Embryonic and Extraembryonic Lineages. Dev Cell. 2008;

30. Lu CC, Brennan J, Robertson EJ. From fertilization to gastrulation: Axis formation in the mouse embryo. Current Opinion in Genetics and Development. 2001.

31. Carlson BM. Patten's foundations of embryology / Bruce M. Carlson. - Version details - Trove [Internet]. New York: McGraw-Hill. 1996 [cited 2020 Jun 15]. p. 34–5. Available from: https://trove.nla.gov.au/work/9914277?q&sort=holdings+desc&_=1592248243671&versionId=46514389

32. Sharon Nadav BN. Mesodermal Differentiation. Stem Cells and Revascularization Therapies. 2007. 129–148 p.

33. Beddington RSP. An autoradiographic analysis of the potency of embryonic ectoderm

in the 8th day postimplantation mouse embryo. J Embryol Exp Morphol. 1981;

34. Arnold SJ, Robertson EJ. Making a commitment: Cell lineage allocation and axis patterning in the early mouse embryo. Nature Reviews Molecular Cell Biology. 2009.

35. Conlon FL, Lyons KM, Takaesu N, Barth KS, Kispert A, Herrmann B, et al. A primary requirement for nodal in the formation and maintenance of the primitive streak in the mouse. Development. 1994;

36. Mishina Y, Suzuki A, Ueno N, Behringer RR. Bmpr encodes a type I bone morphogenetic protein receptor that is essential for gastrulation during mouse embryogenesis. Genes Dev. 1995;9(24):3027–37.

37. Tremblay KD, Dunn NR, Robertson EJ. Mouse embryos lacking Smad1 signals display defects in extra-embryonic tissues and germ cell formation. Development. 2001;

38. Winnier G, Blessing M, Labosky PA, Hogan BLM. Bone morphogenetic protein-4 is required for mesoderm formation and patterning in the mouse. Genes Dev. 1995;

39. Imai KS, Hikawa H, Kobayashi K, Satou Y. Tfap2 and Sox1/2/3 cooperatively specify ectodermal fates in ascidian embryos. Dev. 2017;

40. Muñoz-Sanjuán I, Brivanlou AH. Neural induction, the default model and embryonic stem cells. Nat Rev Neurosci. 2002;

41. Nowotschin S, Hadjantonakis AK, Campbell K. The endoderm: A divergent cell lineage with many commonalities. Development (Cambridge). 2019.

42. Ferrer-Vaquer A, Hadjantonakis AK. Birth defects associated with perturbations in preimplantation, gastrulation, and axis extension: From conjoined twinning to caudal dysgenesis. Wiley Interdiscip Rev Dev Biol. 2013;

43. Liu P, Wakamiya M, Shea MJ, Albrecht U, Behringer RR, Bradley A. Requirement for Wnt3 in vertebrate axis formation. Nat Genet. 1999;

44. Martyn I, Kanno TY, Ruzo A, Siggia ED, Brivanlou AH. Self-organization of a human organizer by combined Wnt and Nodal signaling. Nature. 2018;

45. Kispert A, Herrmann BG. Immunohistochemical analysis of the Brachyury protein in wild-type and mutant mouse embryos. Vol. 161, Developmental Biology. 1994. p. 179–93.

46. Martin BL, Kimelman D. Regulation of Canonical Wnt Signaling by Brachyury Is Essential for Posterior Mesoderm Formation. Dev Cell. 2008;

47. Raab S, Klingenstein M, Möller A, Illing A, Tosic J, Breunig M, et al. Reprogramming to pluripotency does not require transition through a primitive streak-like state. Sci Rep. 2017;

48. Cheung C, Bernardo AS, Trotter MWB, Pedersen RA, Sinha S. Generation of human vascular smooth muscle subtypes provides insight into embryological origing-dependent disease susceptibility. Nat Biotechnol. 2012;

49. Gertow K, Hirst CE, Yu QC, Ng ES, Pereira LA, Davis RP, et al. WNT3A promotes hematopoietic or mesenchymal differentiation from hESCs depending on the time of exposure. Stem Cell Reports. 2013;

50. Dunty WC, Biris KK, Chalamalasetty RB, Taketo MM, Lewandoski M, Yamaguchi TP. Wnt3a/β-catenin signaling controls posterior body development by coordinating mesoderm formation and segmentation. Development. 2008;

51. Herrmann BG. Expression pattern of the Brachyury gene in whole-mount T(Wis)/T(Wis) mutant embryos. Development. 1991;

52. Wilkinson DG, Bhatt S, Herrmann BG. Expression pattern of the mouse T gene and its role in mesoderm formation. Nature. 1990;37(4):395–401.

53. Herrmann Bernhard G., Labeit Siegfried, Poustka Annemarie, King Thomas R. LH. Cloning of the T gene required in mesoderm formation in the mouse. Nature. 1990;343:617–22.

54. Arnold SJ, Stappert J, Bauer A, Kispert A, Herrmann BG, Kemler R. Brachyury is a target gene of the Wnt/β-catenin signaling pathway. Mech Dev. 2000 Mar 1;91(1–2):249–58.

55. Hofmann M, Schuster-Gossler K, Watabe- M. WNT signaling, in synergy with

T/TBX6, controls Notch signaling by regulating Dll1. Genes & Dev [Internet]. 2004;2712–7. Available from: http://genesdev.cshlp.org/cgi/content/abstract/18/22/2712

56. Yamaguchi TP, Takada S, Yoshikawa Y, Wu N, McMahon AP. T (Brachyury) is a direct target of Wnt3a during paraxial mesoderm specification. Genes Dev. 1999;

57. Faial T, Bernardo AS, Mendjan S, Diamanti E, Ortmann D, Gentsch GE, et al. Brachyury and SMAD signalling collaboratively orchestrate distinct mesoderm and endoderm gene regulatory networks in differentiating human embryonic stem cells. Dev. 2015;

58. Bernardo AS, Faial T, Gardner L, Niakan KK, Ortmann D, Senner CE, et al. BRACHYURY and CDX2 mediate BMP-induced differentiation of human and mouse pluripotent stem cells into embryonic and extraembryonic lineages. Cell Stem Cell. 2011;

59. Efthymiou AG, Chen G, Rao M, Chen G, Boehm M. Self-renewal and cell lineage differentiation strategies in human embryonic stem cells and induced pluripotent stem cells. Expert Opin Biol Ther. 2014;14(9):1333–44.

60. Sakurai H, Sakaguchi Y, Shoji E, Nishino T, Maki I, Sakai H, et al. In Vitro Modeling of Paraxial Mesodermal Progenitors Derived from Induced Pluripotent Stem Cells. PLoS One. 2012;

61. Kaufman DS, Hanson ET, Lewis RL, Auerbach R, Thomson JA. Hematopoietic colony-forming cells derived from human embryonic stem cells. Proc Natl Acad Sci U S A. 2001;

62. Odorico JS, Kaufman DS, Thomson JA. Multilineage Differentiation from Human Embryonic Stem Cell Lines. Stem Cells. 2001;19:193–204.

63. Shu J, Deng H. Lineage Specifiers: New Players in the Induction of Pluripotency. Genomics, Proteomics and Bioinformatics. 2013.

64. Sato N, Meijer L, Skaltsounis L, Greengard P, Brivanlou AH. Maintenance of pluripotency in human and mouse embryonic stem cells through activation of Wnt signaling by a pharmacological GSK-3-specific inhibitor. Nat Med. 2004;

65. Donai K, Inagaki A, So KH, Kuroda K, Sone H, Kobayashi M, et al. Low-molecular-weight inhibitors of cell differentiation enable efficient growth of mouse iPS cells under feeder-free conditions. Cytotechnology. 2015;

66. Yoda K, Ohnuki Y, Kurosawa H. Optimization of the treatment conditions with glycogen synthase kinase-3 inhibitor towards enhancing the proliferation of human induced pluripotent stem cells while maintaining an undifferentiated state under feeder-free conditions. J Biosci Bioeng. 2019;

67. Borowiak M, Maehr R, Chen S, Chen AE, Tang W, Fox JL, et al. Small Molecules Efficiently Direct Endodermal Differentiation of Mouse and Human Embryonic Stem Cells. Cell Stem Cell. 2009;

68. Zhu S, Wurdak H, Wang J, Lyssiotis CA, Peters EC, Cho CY, et al. A Small Molecule Primes Embryonic Stem Cells for Differentiation. Cell Stem Cell [Internet]. 2009;4(5):416–26. Available from: http://dx.doi.org/10.1016/j.stem.2009.04.001

69. Ye S, Tan L, Yang R, Fang B, Qu S, Schulze EN, et al. Pleiotropy of glycogen synthase kinase-3 inhibition by CHIR99021 promotes self-renewal of embryonic stem cells from refractory mouse strains. PLoS One. 2012;

70. Lian X, Bao X, Al-Ahmad A, Liu J, Wu Y, Dong W, et al. Efficient differentiation of human pluripotent stem cells to endothelial progenitors via small-molecule activation of WNT signaling. Stem Cell Reports [Internet]. 2014;3(5):804–16. Available from: http://dx.doi.org/10.1016/j.stemcr.2014.09.005

71. Davis LA, Zur Nieden NI. Mesodermal fate decisions of a stem cell: The Wnt switch. Cellular and Molecular Life Sciences. 2008.

72. Kanke K, Masaki H, Saito T, Komiyama Y, Hojo H, Nakauchi H, et al. Stepwise differentiation of pluripotent stem cells into osteoblasts using four small molecules under serum-free and feeder-free conditions. Stem Cell Reports. 2014;

73. Sudheer S, Liu J, Marks M, Koch F, Anurin A, Scholze M, et al. Different Concentrations of FGF Ligands, FGF2 or FGF8 Determine Distinct States of WNT-Induced Presomitic Mesoderm. Stem Cells. 2016;

74. Loh KMM, Chen A, Koh PWW, Deng TZZ, Sinha R, Tsai JMM, et al. Mapping the

Pairwise Choices Leading from Pluripotency to Human Bone, Heart, and Other Mesoderm Cell Types. Cell. 2016;

75. Xie W, Schultz MD, Lister R, Hou Z, Rajagopal N, Ray P, et al. Epigenomic analysis of multilineage differentiation of human embryonic stem cells. Cell. 2013;

76. Yu P, Pan G, Yu J, Thomson JA. FGF2 sustains NANOG and switches the outcome of BMP4-induced human embryonic stem cell differentiation. Cell Stem Cell [Internet]. 2011;8(3):326–34. Available from: http://dx.doi.org/10.1016/j.stem.2011.01.001

77. Yu Y, Deng P, Yu B, Szymanski JM, Aghaloo T, Hong C, et al. Inhibition of EZH2 Promotes Human Embryonic Stem Cell Differentiation into Mesoderm by Reducing H3K27me3. Stem Cell Reports. 2017;9(3):752–61.

78. Andrzejewska A, Lukomska B, Janowski M. Concise Review: Mesenchymal Stem Cells: From Roots to Boost. Stem Cells [Internet]. 2019 Jul 1 [cited 2020 Jun 15];37(7):855–64. Available from: http://doi.wiley.com/10.1002/stem.3016

79. Caplan AI. Mesenchymal stem cells. J Orthop Res. 1991;

80. Takashima Y, Era T, Nakao K, Kondo S, Kasuga M, Smith AG, et al. Neuroepithelial Cells Supply an Initial Transient Wave of MSC Differentiation. Cell. 2007;

81. Isern J, García-García A, Martín AM, Arranz L, Martín-Pérez D, Torroja C, et al. The neural crest is a source of mesenchymal stem cells with specialized hematopoietic stem cell niche function. Elife. 2014;

82. Agha-Hosseini F, Jahani MA, Jahani M, Mirzaii-Dizgah I, Ali-Moghaddam K. In vitro isolation of stem cells derived from human dental pulp. Clin Transplant. 2010;24(2):23–8.

83. Girdlestone J, Limbani VA, Cutler AJ, Navarrete C V. Efficient expansion of mesenchymal stromal cells from umbilical cord under low serum conditions. Cytotherapy [Internet]. 2009;11(6):738–48. Available from: http://dx.doi.org/10.3109/14653240903079401

84. Katz AJ, Tholpady A, Tholpady SS, Shang H, Ogle RC. Cell Surface and

Transcriptional Characterization of Human Adipose-Derived Adherent Stromal (hADAS) Cells. Stem Cells. 2005;

85. Miao Z, Jin J, Chen L, Zhu J, Huang W, Zhao J, et al. Isolation of mesenchymal stem cells from human placenta: Comparison with human bone marrow mesenchymal stem cells. Cell Biol Int. 2006;

86. Pittenger MF, Mackay AM, Beck SC, Jaiswal RK, Douglas R, Mosca JD, et al. Multilineage potential of adult human mesenchymal stem cells. Science (80-). 1999;

87. Hass R, Kasper C, Böhm S, Jacobs R. Different populations and sources of human mesenchymal stem cells (MSC): A comparison of adult and neonatal tissue-derived MSC. Cell Communication and Signaling. 2011.

88. Heo JS, Choi Y, Kim HS, Kim HO. Comparison of molecular profiles of human mesenchymal stem cells derived from bone marrow, umbilical cord blood, placenta and adipose tissue. Int J Mol Med. 2016;

89. Barberi T, Willis LM, Socci ND, Studer L. Derivation of multipotent mesenchymal precursors from human embryonic stem cells. PLoS Med. 2005;

90. Stavropoulos ME, Mengarelli I, Barberi T. Differentiation of Multipotent Mesenchymal Precursors and Skeletal Myoblasts from Human Embryonic Stem Cells. Curr Protoc Stem Cell Biol. 2009;

91. Karlsson C, Emanuelsson K, Wessberg F, Kajic K, Axell MZ, Eriksson PS, et al. Human embryonic stem cell-derived mesenchymal progenitors-Potential in regenerative medicine. Stem Cell Res. 2009;

92. Luzzani CD, Miriuka SG. Pluripotent Stem Cells as a Robust Source of Mesenchymal Stem Cells. Stem Cell Rev Reports [Internet]. 2017;13(1):68–78. Available from: http://dx.doi.org/10.1007/s12015-016-9695-z

93. Wu R, Gu B, Zhao X, Tan Z, Chen L, Zhu J, et al. Derivation of multipotent nestin+/CD271-/STRO-1- mesenchymal-like precursors from human embryonic stem cells in chemically defined conditions. Hum Cell. 2013;

94. O'Dowd BF, Heiber M, Chan A, Heng HHQ, Tsui LC, Kennedy JL, et al. A human

gene that shows identity with the gene encoding the angiotensin receptor is located on chromosome 11. Gene. 1993;

95. Tatemoto K, Hosoya M, Habata Y, Fujii R, Kakegawa T, Zou MX, et al. Isolation and characterization of a novel endogenous peptide ligand for the human APJ receptor. Biochem Biophys Res Commun. 1998;

96. Mesmin C, Fenaille F, Becher F, Tabet JC, Ezan E. Identification and characterization of apelin peptides in bovine colostrum and milk by liquid chromatography-Mass spectrometry. J Proteome Res. 2011;

97. Boucher J, Masri B, Daviaud D, Gesta S, Guigné C, Mazzucotelli A, et al. Apelin, a newly identified adipokine up-regulated by insulin and obesity. Endocrinology. 2005;

98. Hosoya M, Kawamata Y, Fukusumi S, Fujii R, Habata Y, Hinumat S, et al. Molecular and functional characteristics of APJ: Tissue distribution of mRNA and interaction with the endogenous ligand apelin. J Biol Chem. 2000;

99. Katugampola SD, Maguire JJ, Matthewson SR, Davenport AP. [125I]-(Pyr1)Apelin-13 is a novel radioligand for localizing the APJ orphan receptor in human and rat tissues with evidence for a vasoconstrictor role in man. Br J Pharmacol. 2001;

100. Kleinz MJ, Davenport AP. Immunocytochemical localization of the endogenous vasoactive peptide apelin to human vascular and endocardial endothelial cells. Regul Pept. 2004;

101. Kuba K, Sato T, Imai Y, Yamaguchi T. Apelin and Elabela/Toddler; double ligands for APJ/Apelin receptor in heart development, physiology, and pathology. Peptides. 2019.

102. Medhurst AD, Jennings CA, Robbins MJ, Davis RP, Ellis C, Winborn KY, et al. Pharmacological and immunohistochemical characterization of the APJ receptor and its endogenous ligand apelin. J Neurochem. 2003;

103. Mlyczyńska E, Kurowska P, Drwal E, Opydo-Chanek M, Tworzydło W, Kotula-Balak M, et al. Apelin and apelin receptor in human placenta: Expression, signalling pathway and regulation of trophoblast JEG-3 and BeWo cells proliferation and cell cycle. Int J Mol Med. 2020;

104. O'Carroll AM, Selby TL, Palkovits M, Lolait SJ. Distribution of mRNA encoding B78/apj, the rat homologue of the human APJ receptor, and its endogenous ligand apelin in brain and peripheral tissues. Biochim Biophys Acta - Gene Struct Expr. 2000;

105. Pope GR, Roberts EM, Lolait SJ, O'Carroll AM. Central and peripheral apelin receptor distribution in the mouse: Species differences with rat. Peptides. 2012;

106. Chng SC, Ho L, Tian J, Reversade B. ELABELA: A hormone essential for heart development signals via the apelin receptor. Dev Cell. 2013;

107. Pauli A, Norris ML, Valen E, Chew GL, Gagnon JA, Zimmerman S, et al. Toddler: An embryonic signal that promotes cell movement via apelin receptors. Science (80-). 2014;

108. Wang Z, Yu D, Wang M, Wang Q, Kouznetsova J, Yang R, et al. Elabela-Apelin Receptor Signaling Pathway is Functional in Mammalian Systems. Sci Rep. 2015;5:1–8.

109. Atluri P, Morine KJ, Liao GP, Panlilio CM, Berry MF, Hsu VM, et al. Ischemic heart failure enhances endogenous myocardial apelin and APJ receptor expression. Cell Mol Biol Lett. 2007;12(1):127–38.

110. Brailoiu GC, Dun SL, Yang J, Ohsawa M, Chang JK, Dun NJ. Apelin-immunoreactivity in the rat hypothalamus and pituitary. Neurosci Lett. 2002;

111. De Mota N, Reaux-Le Goazigo A, El Messari S, Chartrel N, Roesch D, Dujardin C, et al. Apelin, a potent diuretic neuropeptide counteracting vasopressin actions through inhibition of vasopressin neuron activity and vasopressin release. Proc Natl Acad Sci U S A. 2004;

112. Dray C, Knauf C, Daviaud D, Waget A, Boucher J, Buléon M, et al. Apelin Stimulates Glucose Utilization in Normal and Obese Insulin-Resistant Mice. Cell Metab. 2008;8(5):437–45.

113. Kasai A, Shintani N, Oda M, Kakuda M, Hashimoto H, Matsuda T, et al. Apelin is a novel angiogenic factor in retinal endothelial cells. Biochem Biophys Res Commun. 2004;

114. Kidoya H, Takakura N. Biology of the apelin-APJ axis in vascular formation. Journal of Biochemistry. 2012.

115. O'Carroll AM, Lolait SJ, Harris LE, Pope GR. The apelin receptor APJ: Journey from an orphan to a multifaceted regulator of homeostasis. J Endocrinol. 2013;

116. Sorli SC, Le Gonidec S, Knibiehler B, Audigier Y. Apelin is a potent activator of tumour neoangiogenesis. Oncogene. 2007;

117. Szokodi I, Tavi P, Földes G, Voutilainen-Myllylä S, Ilves M, Tokola H, et al. Apelin, the novel endogenous ligand of the orphan receptor APJ, regulates cardiac contractility. Circ Res. 2002;91(5):434–40.

118. Winzell MS, Magnusson C, Ahrén B. The apj receptor is expressed in pancreatic islets and its ligand, apelin, inhibits insulin secretion in mice. Regul Pept. 2005;

119. Charo DN, Ho M, Fajardo G, Kawana M, Kundu RK, Sheikh AY, et al. Endogenous regulation of cardiovascular function by apelin-APJ. Am J Physiol - Hear Circ Physiol. 2009;

120. Ho L, Van Dijk M, Chye STJ, Messerschmidt DM, Chng SC, Ong S, et al. ELABELA deficiency promotes preeclampsia and cardiovascular malformations in mice. Science (80-). 2017;

121. Sato T, Sato C, Kadowaki A, Watanabe H, Ho L, Ishida J. ELABELA – APJ axis protects from pressure overload heart failure and Angiotensin II-induced cardiac damage . 2016;

122. Miura T, Luo Y, Khrebtukova I, Brandenberger R, Zhou D, Thies RS, et al. Monitoring early differentiation events in human embryonic stem cells by massively parallel signature sequencing and expressed sequence tag scan. Stem Cells Dev. 2004;

123. Pritchard N, Kaitu'u-Lino TJ, Gong S, Dopierala J, Smith GCS, Charnock-Jones DS, et al. ELABELA/APELA Levels Are Not Decreased in the Maternal Circulation or Placenta among Women with Preeclampsia. Am J Pathol. 2018;

124. Chaves-Almagro C, Castan-Laurell I, Dray C, Knauf C, Valet P, Masri B. Apelin receptors: From signaling to antidiabetic strategy. Eur J Pharmacol [Internet].

2015;763:149–59. Available from: http://dx.doi.org/10.1016/j.ejphar.2015.05.017

125. Hamada J, Kimura J, Ishida J, Kohda T, Morishita S, Ichihara S, et al. Evaluation of novel cyclic analogues of apelin. Int J Mol Med. 2008;

126. Masri B, Knibiehler B, Audigier Y, Lahlou H, Mazarguil H. Apelin (65-77) activates extracellular signal-regulated kinases via a PTX-sensitive G protein. Biochem Biophys Res Commun. 2002;

127. Zhang X, Chen Y, Ye Y, Wang J, Wang H, Yuan G, et al. Wnt signaling promotes hindgut fate commitment through regulating multi-lineage genes during hESC differentiation. Cell Signal [Internet]. 2017;29:12–22. Available from: http://dx.doi.org/10.1016/j.cellsig.2016.09.009

128. D'Aniello C, Lonardo E, Iaconis S, Guardiola O, Liguoro AM, Liguori GL, et al. G protein-coupled receptor APJ and its ligand apelin act downstream of cripto to specify embryonic stem cells toward the cardiac lineage through extracellular signal-regulated kinase/p70S6 kinase signaling pathway. Circ Res. 2009;

129. Norris ML, Pauli A, Gagnon JA, Lord ND, Rogers KW, Mosimann C, et al. Toddler signaling regulates mesodermal cell migration downstream of nodal signaling. Elife. 2017;

130. Zeng XXI, Wilm TP, Sepich DS, Solnica-Krezel L. Apelin and Its Receptor Control Heart Field Formation during Zebrafish Gastrulation. Dev Cell. 2007;

131. Deshwar AR, Chng SC, Ho L, Reversade B, Scott IC. The Apelin receptor enhances Nodal/TGFβ signaling to ensure proper cardiac development. Elife. 2016;

132. Yu QC, Hirst CE, Costa M, Ng ES, Schiesser J V., Gertow K, et al. APELIN promotes hematopoiesis from human embryonic stem cells. Blood. 2012;

133. Kikuchi T, Morizane A, Doi D, Magotani H, Onoe H, Hayashi T, et al. Human iPS cell-derived dopaminergic neurons function in a primate Parkinson's disease model. Nature [Internet]. 2017;548(7669):592–6. Available from: http://dx.doi.org/10.1038/nature23664

134. Sougawa N, Miyagawa S, Fukushima S, Kawamura A, Yokoyama J, Ito E, et al.

Immunologic targeting of CD30 eliminates tumourigenic human pluripotent stem cells, allowing safer clinical application of hiPSC-based cell therapy. Sci Rep [Internet]. 2018;8(1):1–12. Available from: http://dx.doi.org/10.1038/s41598-018-21923-8

135. Yamanaka S. Pluripotent Stem Cell-Based Cell Therapy—Promise and Challenges. Cell Stem Cell [Internet]. 2020;27(4):523–31. Available from: https://doi.org/10.1016/j.stem.2020.09.014

136. Prockop DJ. Marrow stromal cells as stem cells for nonhematopoietic tissues. Science (80-). 1997;276(5309):71–4.

137. Thompson M, Mei SHJ, Wolfe D, Champagne J, Fergusson D, Stewart DJ, et al. Cell therapy with intravascular administration of mesenchymal stromal cells continues to appear safe: An updated systematic review and meta-analysis. EClinicalMedicine. 2020;19.

138. Renesme L, Cobey KD, Le M, Lalu MM, Thebaud B. Establishment of a consensus definition for mesenchymal stromal cells (MSC) and reporting guidelines for clinical trials of MSC therapy: A modified Delphi study protocol. BMJ Open. 2021;11(10):1–5.

139. Şenkal S, Hayal TB, Sağraç D, Şişli HB, Asutay AB, Kıratlı B, et al. Human ESC-derived Neuromesodermal Progenitors (NMPs) Successfully Differentiate into Mesenchymal Stem Cells (MSCs). Stem Cell Rev Reports [Internet]. 2022;18(1):278–93. Available from: https://doi.org/10.1007/s12015-021-10281-0

140. Phinney DG. Functional heterogeneity of mesenchymal stem cells: Implications for cell therapy. J Cell Biochem. 2012;113(9):2806–12.

141. Peng KY, Lee YW, Hsu PJ, Wang HH, Wang Y, Liou JY, et al. Human pluripotent stem cell (PSC)-derived mesenchymal stem cells (MSCs) show potent neurogenic capacity which is enhanced with cytoskeletal rearrangement. Oncotarget. 2016;7(28):43949–59.

142. Vodyanik MA, Yu J, Zhang X, Tian S, Stewart R, Thomson JA, et al. A mesoderm-derived precursor for mesenchymal stem and endothelial cells. Cell Stem Cell

[Internet]. 2010;7(6):718–29. Available from: http://dx.doi.org/10.1016/j.stem.2010.11.011

143. Slukvin II, Vodyanik M. Endothelial origin of mesenchymal stem cells. Cell Cycle. 2011;10(9):1370–3.

144. Liang D, Han D, Fan W, Zhang R, Qiao H, Fan M, et al. Therapeutic efficacy of apelin on transplanted mesenchymal stem cells in hindlimb ischemic mice via regulation of autophagy. Sci Rep. 2016;6(September 2015):1–14.

145. Chen G, Liang X, Han Q, Mai C, Shi L, Shao Z, et al. Apelin-13 Pretreatment Promotes the Cardioprotective Effect of Mesenchymal Stem Cells against Myocardial Infarction by Improving Their Survival. Stem Cells Int. 2022;2022(Mi).

146. Hang K, Ye C, Xu J, Chen E, Wang C, Zhang W, et al. Apelin enhances the osteogenic differentiation of human bone marrow mesenchymal stem cells partly through Wnt/β-catenin signaling pathway. Stem Cell Res Ther. 2019;10(1):1–10.

147. Liu Q, Zhou S, Wang X, Gu C, Guo Q, Li X, et al. Apelin alleviated neuroinflammation and promoted endogenous neural stem cell proliferation and differentiation after spinal cord injury in rats. J Neuroinflammation [Internet]. 2022;19(1):1–18. Available from: https://doi.org/10.1186/s12974-022-02518-7

148. Şişli HB, Şenkal S, Sağraç D, Hayal TB, Ayşegül D. Feeder-Dependent / Independent Mouse Embryonic Stem Cell Culture Protocol ¸ is. Methods Mol Biol. 2021;2520:101–15.

149. Sağraç D, Şenkal S, Hayal TB, Şahin F, Çobandede Z, Doğan A. Surface coating materials regulates the attachment and differentiation of mouse embryonic stem cell derived embryoid bodies into mesoderm at culture conditions. Cytotechnology [Internet]. 2022;74(2):293–307. Available from: https://doi.org/10.1007/s10616-022-00529-z

150. Sakuma T, Nishikawa A, Kume S, Chayama K, Yamamoto T. Multiplex genome engineering in human cells using all-in-one CRISPR/Cas9 vector system. Sci Rep. 2014;

151. Hayal TB, Doğan A, Şişli HB, Kiratli B, Şahin F. Ubiquitin-specific protease 7

downregulation suppresses breast cancer in vitro. Turkish J Biol. 2020;44(4):145–57.

152. Schneider CA, Rasband WS, Eliceiri KW. NIH Image to ImageJ: 25 years of image analysis. Nat Methods. 2012;9(7):671–5.

153. Sağraç D, Şenkal S, Hayal TB, Demirci S, Şişli HB, Asutay AB, et al. Protective role of Cytoglobin and Neuroglobin against the Lipopolysaccharide (LPS)-induced inflammation in Leydig cells ex vivo. Reprod Biol. 2022;22(1).

154. Akpinar G, Yoneten KK, Kasap M, Karaoz E. Search for Novel Plasma Membrane Proteins as Potential Biomarkers in Human Mesenchymal Stem Cells Derived from Dental Pulp, Adipose Tissue, Bone Marrow, and Hair Follicle. J Membr Biol [Internet]. 2021;254(4):409–22. Available from: https://doi.org/10.1007/s00232-021-00190-1

155. Doğan A, Demirci S, Şahin F. In vitro differentiation of human tooth germ stem cells into endothelial- and epithelial-like cells. Cell Biol Int. 2015;39(1):94–103.

156. Şişli HB, Hayal TB, Şenkal S, Kıratlı B, Sağraç D, Seçkin S, et al. Apelin Receptor Signaling Protects GT1-7 GnRH Neurons Against Oxidative Stress In Vitro. Cell Mol Neurobiol [Internet]. 2022;42(3):753–75. Available from: https://doi.org/10.1007/s10571-020-00968-2

157. Metsalu T, Vilo J. ClustVis: A web tool for visualizing clustering of multivariate data using Principal Component Analysis and heatmap. Nucleic Acids Res. 2015;43(W1):W566–70.

158. Tyanova S, Temu T, Sinitcyn P, Carlson A, Hein MY, Geiger T, et al. The Perseus computational platform for comprehensive analysis of (prote)omics data. Nat Methods. 2016;13(9):731–40.

159. Szklarczyk D, Gable AL, Lyon D, Junge A, Wyder S, Huerta-Cepas J, et al. STRING v11: Protein-protein association networks with increased coverage, supporting functional discovery in genome-wide experimental datasets. Nucleic Acids Res. 2019;47(D1):D607–13.

160. Thomas PD, Campbell MJ, Kejariwal A, Mi H, Karlak B, Daverman R, et al. PANTHER: A library of protein families and subfamilies indexed by function.

Genome Res. 2003;13(9):2129–41.

161. Mi H, Muruganujan A, Huang X, Ebert D, Mills C, Guo X, et al. Protocol Update for large-scale genome and gene function analysis with the PANTHER classification system (v.14.0). Nat Protoc [Internet]. 2019;14(3):703–21. Available from: http://dx.doi.org/10.1038/s41596-019-0128-8

162. Mi H, Ebert D, Muruganujan A, Mills C, Albou LP, Mushayamaha T, et al. PANTHER version 16: A revised family classification, tree-based classification tool, enhancer regions and extensive API. Nucleic Acids Res. 2021;49(D1):D394–403.

163. Demirci S, Kaya MS, Doğan A, Kalay Ş, Altin NÖ, Yarat A, et al. Antibacterial and cytotoxic properties of boron-containing dental composite. Turkish J Biol. 2015;39(3):417–26.

164. Taşlı PN, Doğan A, Demirci S, Şahin F. Myogenic and neurogenic differentiation of human tooth germ stem cells (hTGSCs) are regulated by pluronic block copolymers. Cytotechnology. 2016;68(2):319–29.

165. Taşlı PN, Doğan A, Demirci S, Şahin F. Boron enhances odontogenic and osteogenic differentiation of human tooth germ stem cells (hTGSCs) in vitro. Biol Trace Elem Res. 2013;153(1–3):419–27.

166. Demirci S, Hayal TB, Kıratlı B, Şişli HB, Demirci S, Şahin F, et al. Design and synthesis of phenylpiperazine derivatives as potent anticancer agents for prostate cancer. Chem Biol Drug Des. 2019;94(3).

167. Sakuma T, Nishikawa A, Kume S, Chayama K, Yamamoto T. Multiplex genome engineering in human cells using all-in-one CRISPR/Cas9 vector system. Sci Rep. 2014;4:4–9.

168. Bourillot PY, Aksoy I, Schreiber V, Wianny F, Schulz H, Hummel O, et al. Novel STAT3 target genes exert distinct roles in the inhibition of mesoderm and endoderm differentiation in cooperation with Nanog. Stem Cells. 2009;27(8):1760–71.

169. He Z, Li JJ, Zhen CH, Feng LY, Ding XY. Effect of leukemia inhibitory factor on embryonic stem cell differentiation: Implications for supporting neuronal differentiation. Acta Pharmacol Sin. 2006;27(1):80–90.

170. Sakurai H, Okawa Y, Inami Y, Nishio N, Isobe K ichi. Paraxial Mesodermal Progenitors Derived from Mouse Embryonic Stem Cells Contribute to Muscle Regeneration via Differentiation into Muscle Satellite Cells. Stem Cells. 2008;26(7):1865–73.

171. Ding G, Tanaka Y, Hayashi M, Nishikawa SI, Kataoka H. PDGF Receptor Alpha+ Mesoderm Contributes to Endothelial and Hematopoietic Cells in Mice. Dev Dyn. 2013;242(3):254–68.

172. Gadue P, Huber TL, Paddison PJ, Keller GM. Wnt and TGF-β signaling are required for the induction of an in vitro model of primitive streak formation using embryonic stem cells. Proc Natl Acad Sci U S A. 2006;103(45):16806–11.

173. Grunz H, Scheer A wilhelm, Kruppke H, Heib R. The Vertebrate Orginizer [Internet]. Springer Berlin Heidelberg; 2004. Available from: http://download.springer.com/static/pdf/185/bfm%253A978-3-642-56668-4%252F1.pdf?auth66=1401995374_4d363c462609ae19e3de18b0ee51ef07&ext=.pdf

174. Dale L, Matthews G, Colman A. Secretion and mesoderm-inducing activity of the TGF-β-related domain of Xenopus Vg1. EMBO J. 1993;12(12):4471–80.

175. Bai H, Xie YL, Gao YX, Cheng T, Wang ZZ. The balance of positive and negative effects of TGF-β signaling regulates the development of hematopoietic and endothelial progenitors in human pluripotent stem cells. Stem Cells Dev. 2013;22(20):2765–76.

176. Zinski J, Tajer B, Mullins MC. TGF-β family signaling in early vertebrate development. Cold Spring Harb Perspect Biol. 2018;10(6).

177. James RG, Schultheiss TM. Bmp signaling promotes intermediate mesoderm gene expression in a dose-dependent, cell-autonomous and translation-dependent manner. Dev Biol. 2005;288(1):113–25.

178. Sharma R, Shafer MER, Bareke E, Tremblay M, Majewski J, Bouchard M. Bmp signaling maintains a mesoderm progenitor cell state in the mouse tailbud. J Cell Sci. 2017;130(17):2982–93.

179. Doğan A. Apelin receptor (Aplnr) signaling promotes fibroblast migration. Tissue Cell. 2019;56(January):98–106.

180. Westphal M, Panza P, Kastenhuber E, Wehrle J, Driever W. Wnt/β-catenin signaling promotes neurogenesis in the diencephalospinal dopaminergic system of embryonic zebrafish. Sci Rep [Internet]. 2022;12(1):1–19. Available from: https://doi.org/10.1038/s41598-022-04833-8

181. Patapoutian A, Reichardt LF. Roles of Wnt proteins in neural development and maintenance. Curr Opin Neurobiol. 2000;10(3):392–9.

182. Kishi M, Mizuseki K, Sasai N, Yamazaki H, Shiota K, Nakanishi S, et al. Requirement of Sox2-mediated signaling for differentiation of early Xenopus neuroectoderm. Development. 2000;127(4):791–800.

183. Roellig D, Tan-Cabugao J, Esaian S, Bronner ME. Dynamic transcriptional signature and cell fate analysis reveals plasticity of individual neural plate border cells. Elife. 2017;6:1–24.

184. Norrman K, Strömbeck A, Semb H, Ståhlberg A. Distinct gene expression signatures in human embryonic stem cells differentiated towards definitive endoderm at single-cell level. Methods [Internet]. 2013;59(1):59–70. Available from: http://dx.doi.org/10.1016/j.ymeth.2012.03.030

185. McGrath KE, Koniski AD, Maltby KM, McGann JK, Palis J. Embryonic expression and function of the chemokine SDF-1 and its receptor, CXCR4. Dev Biol. 1999;213(2):442–56.

186. Liu Y, Kaneda R, Leja TW, Subkhankulova T, Tolmachov O, Minchiotti G, et al. Hhex and cer1 mediate the Sox17 pathway for cardiac mesoderm formation in embryonic stem cells. Stem Cells. 2014;32(6):1515–26.

187. Howard L, Mackenzie RM, Pchelintsev NA, McBryan T, McClure JD, McBride MW, et al. Profiling of transcriptional and epigenetic changes during directed endothelial differentiation of human embryonic stem cells identifies FOXA2 as a marker of early mesoderm commitment. Stem Cell Res Ther. 2013;4(2):2–8.

188. Inui M, Fukui A, Ito Y, Asashima M. Xapelin and Xmsr are required for

cardiovascular development in Xenopus laevis. Dev Biol. 2006;298(1):188–200.

189. Sağraç D, Şişli HB, Doğan A. Apelin receptor signaling during mesoderm development. Vol. 1298, Advances in Experimental Medicine and Biology. 2020.

190. Zeng XXI, Wilm TP, Sepich DS, Solnica-Krezel L. Apelin and Its Receptor Control Heart Field Formation during Zebrafish Gastrulation. Dev Cell. 2007;12(3):391–402.

191. Geary L, Labonne C. FGF mediated mapk and pi3k/akt signals make distinct contributions to pluripotency and the establishment of neural crest. Elife. 2018;7:1–20.

192. Sittewelle M, Monsoro-Burq AH. AKT signaling displays multifaceted functions in neural crest development. Dev Biol [Internet]. 2018;444(May):S144–55. Available from: https://doi.org/10.1016/j.ydbio.2018.05.023

193. Kaiser S, Hackanson B, Follo M, Mehlhorn A, Geiger K, Ihorst G, et al. BM cells giving rise to MSC in culture have a heterogeneous CD34 and CD45 phenotype. Cytotherapy [Internet]. 2007;9(5):439–50. Available from: http://dx.doi.org/10.1080/14653240701358445

194. Vodyanik MA, Yu J, Zhang X, Tian S, Stewart R, Thomson JA, et al. A mesoderm-derived precursor for mesenchymal stem and endothelial cells. Cell Stem Cell [Internet]. 2010;7(6):718–29. Available from: http://dx.doi.org/10.1016/j.stem.2010.11.011

195. Mohr JC, de Pablo JJ, Palecek SP. 3-D microwell culture of human embryonic stem cells. Biomaterials. 2006;27(36):6032–42.

196. Arnold SJ, Robertson EJ. Making a commitment: Cell lineage allocation and axis patterning in the early mouse embryo. Nat Rev Mol Cell Biol. 2009;10(2):91–103.

197. Tani S, Chung U il, Ohba S, Hojo H. Understanding paraxial mesoderm development and sclerotome specification for skeletal repair. Exp Mol Med [Internet]. 2020;52(8):1166–77. Available from: http://dx.doi.org/10.1038/s12276-020-0482-1

198. Slukvin II, Kumar A. The mesenchymoangioblast, mesodermal precursor for mesenchymal and endothelial cells. Cell Mol Life Sci [Internet]. 2018;75(19):3507–

20. Available from: https://doi.org/10.1007/s00018-018-2871-3

199. Jackson M, Fidanza A, Taylor AH, Rybtsov S, Axton R, Kydonaki M, et al. Modulation of APLNR Signaling Is Required during the Development and Maintenance of the Hematopoietic System. Stem Cell Reports [Internet]. 2021;16(4):727–40. Available from: https://doi.org/10.1016/j.stemcr.2021.02.003

200. Morikawa S, Mabuchi Y, Niibe K, Suzuki S, Nagoshi N, Sunabori T, et al. Development of mesenchymal stem cells partially originate from the neural crest. Biochem Biophys Res Commun [Internet]. 2009;379(4):1114–9. Available from: http://dx.doi.org/10.1016/j.bbrc.2009.01.031

201. Olsen BR, Reginato AM, Wang W. Bone Development. Annu Rev Cell Dev. 2000;16:191–220.

202. Wang H, Li D, Zhai Z, Zhang X, Huang W, Chen X, et al. Characterization and therapeutic application of mesenchymal stem cells with neuromesodermal origin from human pluripotent stem cells. Theranostics. 2019;9(6):1683–97.

203. Chng SC, Ho L, Tian J, Reversade B. ELABELA: A hormone essential for heart development signals via the apelin receptor. Dev Cell [Internet]. 2013;27(6):672–80. Available from: http://dx.doi.org/10.1016/j.devcel.2013.11.002

204. Macrae RGC, Colzani MT, Williams TL, Bayraktar S, Kuc RE, Pullinger AL, et al. Inducible apelin receptor knockdown reduces differentiation efficiency and contractility of hESC-derived cardiomyocytes. Cardiovasc Res. 2022;1–12.